

Copyright
By
Jeremiah David Fasl
2008

The Influence of Overhang Construction on Girder Design

by

Jeremiah David Fasl, B.S.C.E

Thesis

Presented to the Faculty of the Graduate School of

The University of Texas at Austin

in Partial Fulfillment

of the Requirements

for the Degree of

Master of Science in Engineering

The University of Texas at Austin

August 2008

The Influence of Overhang Construction on Girder Design

**APPROVED BY
SUPERVISING COMMITTEE:**

Todd A. Helwig, Supervisor

Michael D. Engelhardt

Dedication

To Dad, Mom, Travis, Kati, Thomas, Jasmin, Matthew,
Anna, Mikayla, and the rest of my family

Acknowledgements

First, I would like to thank the Texas Department of Transportation for providing the funding for my project and master's education. Both have been very rewarding.

The professors and staff at Ferguson Laboratory are awesome. They combine to create a team-oriented atmosphere and have made my master's time truly special. In particular, I want to thank the professors on my project, Todd Helwig, Mike Engelhardt, and Richard Klingner. All have contributed significantly to the progress and success of this project, for which I appreciate. In addition, I would like to extend a special thank you to Karl Frank and Todd Helwig. Dr. Frank was an amazing resource over the course of the research, despite not being on the project, and a good source of encouragement. Dr. Helwig assisted with this thesis and made numerous contributions to the project over the past two years. Yet, his greatest impact to me was through the friendship, the humor, and the energy he brought to the research. Dr. Engelhardt was terrific as my second reader and a wonderful professor. Barbara Howard was tremendous, as she was always there to answer my questions on trip logistics and project purchases. Also, the project benefited many times from the instrumentation expertise of Eric Shell.

I have enjoyed working with the many great students at Ferguson, in both the laboratory and in the field. I was especially privileged to work with such talented students on the many field studies, from Austin to Lubbock to San Angelo to Dallas. Thanks to each of you for all of your help! Seong Yang, PhD student on this project, thank you for all of the help and hard work you put into our research.

It is difficult to condense my family's encouragement into only a few words. So, I will simply state that their love and support have made me who I am today... thank you for always being there!

August 14, 2008

The Influence of Overhang Construction on Girder Design

Jeremiah David Fasl, M.S.E.

The University of Texas at Austin, 2008

SUPERVISOR: Todd Helwig

Overhangs on bridges result from economical constraints to use as few girders as possible across the bridge width. While designers commonly employ rules of thumb to define overhang geometry, the rules generally lead to unbalanced loading that is not considered in the design. The overhang brackets are connected to the top of the fascia girder and react against the side of these girders. Due to the eccentricity of the overhang, a torsional load is applied to the fascia girder. The torsional load causes the girders to twist and can affect both the global and local stability of the girders. The deformational behavior of the girders is generally not well understood and is sensitive to the construction details. Depending on the geometry, the overhangs can lead to stability problems in both steel and concrete girder systems. To improve the understanding of overhang behavior, three Texas bridges were monitored during the concrete deck construction to collect data for validation of a 3-D finite element model. The results of the field monitoring are presented in this thesis.

Table of Contents

CHAPTER 1 INTRODUCTION	1
1.1 Overview	1
1.2 Scope of Study	2
1.3 Thesis Overview	3
CHAPTER 2 BACKGROUND	5
2.1 Motivation for Study	5
2.1.1 Overhang Equilibrium	6
2.1.2 Deformation Modes	7
2.1.3 Details for Restraining Twist of Concrete Girders	9
2.1.4 Representative Case Studies	13
2.2 Literature Review	19
2.2.1 Overhang Construction	19
2.2.2 Department of Transportation (DOT) Guidelines	21
2.3 Typical Overhang Construction	24
2.4 Typical Overhang Bracket Geometrical Configurations	25
CHAPTER 3 INSTRUMENTATION	29
3.1 Prestressed Concrete Bridge (SH 71-SH 130)	29
3.1.1 Instrumentation Plan for Prestressed Concrete Bridge	31
3.1.1.1 Vertical Deflections	32
3.1.1.2 Torsional Rotations	37
3.1.1.3 Strain in Top Bracing Bars	40
3.2 Steel Bridge with Skewed Supports (US 82-19th Street Bridge)	47
3.2.1 Instrumentation Plan for Skewed Steel Bridge	48

3.2.1.1	Vertical Deflections	48
3.2.1.2	Torsional Rotations.....	50
3.2.1.3	Web Imperfections.....	52
3.3	Curved Steel Bridge (SH 71-SH 130).....	55
3.3.1	Instrumentation Plan for Curved Steel Bridge.....	56
3.3.1.1	Torsional Rotations.....	56
3.3.1.2	Web Imperfections.....	57
3.4	Data Acquisition System.....	59
3.4.1	Strain Gages	60
3.4.2	Tilt Sensors	60
3.4.3	Linear Potentiometer.....	63
CHAPTER 4 RESULTS		65
4.1	Prestressed Concrete Bridge (SH 71-SH 130).....	65
4.1.1	Vertical Deflections	66
4.1.2	Torsional Rotations.....	69
4.1.3	Strain in Top Bracing Bar	74
4.2	Steel Bridge with Skewed Supports (US 82-19th Street Bridge)	81
4.2.1	Vertical Deflections	82
4.2.2	Torsional Rotations.....	85
4.2.3	Web Imperfections.....	92
4.3	Curved Steel Bridge (SH 71-SH 130).....	100
4.3.1	Torsional Rotations.....	101
4.3.2	Web Imperfections.....	109

CHAPTER 5 SUMMARY AND CONCLUSIONS	117
5.1 Summary of Research Problem	117
5.2 Summary of Results	118
5.2.1 Prestressed Concrete Bridge (SH 71-SH 130)	118
5.2.2 Steel Bridge with Skewed Supports (US 82 - 19 th Street Bridge)	119
5.2.3 Curved Steel Bridge (SH 71-SH 130)	120
5.3 Recommendations & Future Work	121
APPENDIX A 19TH STREET BRIDGE WEB IMPERFECTIONS: FASCIA GIRDER	123
APPENDIX B 19TH STREET BRIDGE WEB IMPERFECTIONS: INTERIOR GIRDER	135
APPENDIX C SH 71-SH 130 (SPAN 14): FASCIA GIRDER	146
APPENDIX D SH 71-SH 130 (SPAN 14): INTERIOR GIRDER	154
References	162
Vita	165

List of Tables

Table 2-1 Maine DOT Overhang Guidelines (2003).....	22
Table 2-2 South Carolina DOT Overhang Guidelines (2006).....	22
Table 2-3 DOT Guidelines.....	23
Table 4-1 Deflection Measurements at SH 71-SH 130	69
Table 4-2 Deflection Measurements During Deck Pour at 19th Street Bridge	84
Table 4-3 Torsional Rotation at Bearing Pads.....	92
Table 4-4 Accuracy of Linear Displacement Potentiometer Gauge	94
Table 4-5 Summary of Shapes at 19th Street Bridge.....	100
Table 4-6 Torsional Rotation at the Fifth Bracing Line Due to Deck Pour.....	108
Table 4-7 Torsional Rotation at the Fifth Bracing Line (Only Spans 15 and 16 Poured).....	109
Table 4-8 Summary of Shapes at SH 71-SH 130, Span 14	116

List of Figures

Figure 1-1 Bridge Deck Overhang.....	1
Figure 2-1 Idealized Free Body Diagram of Bridge Overhang	6
Figure 2-2 Effect of Rigid and Flexible Supports on Eccentricity	9
Figure 2-3 Progression of Bracing Details.....	10
Figure 2-4 Top Bracing Bar After Panel Installation.....	12
Figure 2-5: Effect of Twist on Timber Blocking	13
Figure 2-7 Twin Girder Widening with Excessive Girder Twist	15
Figure 2-6 Differences in Torsion for New & Bridge Widening Projects.....	15
Figure 2-8 Girder Twist	16
Figure 2-9 Fabrica Pad Lift-Off.....	16
Figure 2-10 Girder Rotates off Bearing Pad.....	17
Figure 2-11 Large Rotations of Prestressed, Fascia Girder at Bridge 1	18
Figure 2-12 Measured Rotations of Bridge 1	18
Figure 2-13 Typical Deck Construction	24
Figure 2-14 Overhang Brackets Used at SH 71-130 Bridge.....	26
Figure 2-15 Overhang Brackets Transiting Between Concrete and Steel Girders	27
Figure 2-16 Overhang Bracket Geometry at US 82-19th Street Bridge.....	28
Figure 2-17 Connection of Overhang Bracket to Steel Beam	28
Figure 3-1 Slab Reinforcement at Overhang	30
Figure 3-2 Overhang Brackets Used at SH 71-SH 130 Bridge	31

Figure 3-3 Instrumentation Plan for SH 71-SH 130 (Span 22)	32
Figure 3-4 Idealized Deflection Measurement Setup	33
Figure 3-5 Hole for Isolated Base of Deflection Measurement	34
Figure 3-6 Mixing Hydro-Stone for Isolated Base	35
Figure 3-7 Spray-Painted Spot for Deflection Measurements	35
Figure 3-8 Deflection Laser Measurement from Isolated Base	36
Figure 3-9 Vertical Deflection Measurement Locations at SH 71-SH 130	37
Figure 3-10 Tilt Sensor Attached to Steel Plate.....	38
Figure 3-11 Locations of Tilt Sensors on SH 130-71 (Span 22)	39
Figure 3-12 Timber Blocking of Concrete Girders.....	40
Figure 3-13 Top Bracing Bar Before PCP Installation.....	41
Figure 3-14 Top Bracing Bar After PCP Installation	42
Figure 3-15 Weld of Top Bracing Bar to R-Bar of Girder	42
Figure 3-16 Location of Top Bracing Bars After PCP Installation	43
Figure 3-17 Location of Top Bracing Bar Strain Gages.....	44
Figure 3-18 Strain Gages Installed at Mid-Length and at Ends of Bar	44
Figure 3-19 Idealized Correction of Stress in Bar Due to Bending.....	45
Figure 3-20 Installed Strain Gage on Top Bracing Bar	46
Figure 3-21 Heating Protective Tape on Top Bracing Bar	46
Figure 3-22 Silicone Applied as Moisture Protection to Top Bracing Bar.....	47
Figure 3-23 Instrumentation Plan for 19th Street Bridge over US 82	48
Figure 3-24 Vertical Deflection Measurement at 19th Street Bridge	49

Figure 3-25 Vertical Deflection Measurement Locations at 19th Street Bridge ...	50
Figure 3-26 Locations of Tilt Sensors at 19th Street Bridge	51
Figure 3-27 Control Rotation Measurement at Support of 19th Street Bridge.....	52
Figure 3-28 Difference in Location of Overhang Bracket.....	53
Figure 3-29 Example of Correcting Data from Potentiometer Displacement Gauge	54
Figure 3-30 19th Street Bridge Web Imperfection Plan	55
Figure 3-31 Instrumentation Plan for SH 71-SH 130 (Span 14)	56
Figure 3-32 Location of Tilt Sensors at SH 71-SH 130 (Span 14).....	57
Figure 3-33 Web Imperfection Plan at SH 71-SH 130 (Span 14)	58
Figure 3-34 Tilt Sensor to Datalogger Wire Diagram	62
Figure 3-35 Tilt Sensor to Multiplexer to Datalogger Wire Diagram	63
Figure 3-36 Linear Potentiometer	64
Figure 4-1 Timeline For Deck Pour at SH 71-SH 130 (Span 22).....	66
Figure 4-2 Vertical Deflection Due to Deck Pour	67
Figure 4-3 Typical Cross Section of Bridge	68
Figure 4-4 Sign Convention of Rotations	70
Figure 4-5 Torsional Rotation of Fascia Girder After Deck Pour	72
Figure 4-6 Torsional Rotation of Interior Girder After Deck Pour	73
Figure 4-7 Torsional Rotation Along Girder Due to Deck Pour	74
Figure 4-8 Stress of Bars on East Side of Bridge During Pour	76
Figure 4-9 Stress of Bars on West Side of Bridge During Deck Pour.....	77

Figure 4-10 Behavior of Strain Gages on West Side of Bridge After Deck Pour	.78
Figure 4-11 Behavior of Bars on West Side of Bridge After Deck Pour79
Figure 4-12 Strain At End and Middle of Bar on West Side of Bridge (Location 1).....	80
Figure 4-13 Strain At End and Middle of Bar on West Side of Bridge (Location 4).....	80
Figure 4-14 Timeline For Deck Pour at US 82-19th Street Bridge82
Figure 4-15 Vertical Deflection of Fascia Girder Due to Deck Pour83
Figure 4-16 Vertical Deflection Along Fifth Intermediate Bracing Line84
Figure 4-17 Sign Convention of Rotations86
Figure 4-18 Torsional Rotation Along Span 1 of Girders 3-6 Relative to Girder 6.....	87
Figure 4-19 Change in Torsional Rotation After Deck Pour (TS-G3-1)88
Figure 4-20 Change in Torsional Rotation After Deck Pour (Location 1)89
Figure 4-21 Change in Torsional Rotation After Deck Pour (Location 2)89
Figure 4-22 Change in Torsional Rotation After Deck Pour (Location 3)90
Figure 4-23 Change in Torsional Rotation After Deck Pour (Location 4)91
Figure 4-24 Sign Convention & Typical Web Imperfection at 19th Street Bridge.....	93
Figure 4-25 Typical Relative Web Imperfection Due to Deck Pour93
Figure 4-26 Maximum Relative Imperfection of Fascia Girder95
Figure 4-27 Relative Imperfection of Fascia Girder at Location 1.....	96
Figure 4-28 Imperfection of Fascia Girder at Location 6.....	97
Figure 4-29 Imperfection of Fascia Girder at Location 12.....	98

Figure 4-30 Relative Imperfection of Fascia Girder at Cross Frame Locations....	99
Figure 4-31 Timeline For Deck Pour at SH 71-SH 130 (Span 14).....	101
Figure 4-32 Sign Convention for Rotations at Span 14.....	102
Figure 4-33 Example of TS-G1-1 Temperature Voltage at Span 14.....	104
Figure 4-34 Change in Torsional Rotation After Deck Pour (Span 14, Location 1).....	105
Figure 4-35 Change in Torsional Rotation After Deck Pour (Span 14, Location 2).....	106
Figure 4-36 Change in Torsional Rotation After Deck Pour (Span 14, Location 3).....	106
Figure 4-37 Change in Torsional Rotation After Deck Pour (Span 14, Location 4).....	107
Figure 4-38 Summary of Measurements After Deck Pour	108
Figure 4-39 Maximum Relative Imperfection of Fascia Girder (Span 14)	111
Figure 4-40 Imperfection of Fascia Girder at Location 12 (Span 14)	112
Figure 4-41 Imperfection of Fascia Girder at Location 33 (Span 14)	113
Figure 4-42 Imperfection of Fascia Girder at Location 32 (Span 14)	114

CHAPTER 1

Introduction

1.1 OVERVIEW

Overhangs on bridges result from economical constraints to use as few girders as possible across the bridge width. As seen in Figure 1-1, the overhang cantilevers out from the fascia girder, extending the roadway to support both traffic and the concrete barrier. Designers typically proportion overhangs so that the same girder sections are used for both interior and fascia girders. Most designers employ common rules of thumb with regard to the geometry; however, these rules of thumb usually lead to unbalanced torsional loading on the girder system that is not considered in the design. With no research justification for these rules of thumb, influences such as girder span or configuration of the overhang brackets relative to the girder geometry are not given proper consideration and have led to problems during bridge construction. In some cases excessive girder twist has resulted in bridges that were dangerously close to failure.



Figure 1-1 Bridge Deck Overhang

The main issue of overhangs is the unbalanced loading, which is the product of current construction practice. The deck over the overhang is usually formed by plywood forms supported by brackets intermittently spaced along the length of the bridge. The overhang brackets are connected to the top of the fascia girder and react against the side of these girders. Due to the eccentricity of the overhang, a torsional load is applied to the fascia girder. The torsional load causes the girders to twist and can affect both the global and local stability of the girders. The deformational behavior of the girders is sensitive to the construction details and not well understood. Depending on the geometry, the overhangs can lead to stability problems in both steel and concrete girder systems.

Even though practices based upon common rules of thumb have been followed, normal and large overhangs have caused fascia beams to rotate during construction. This rotation can cause potential safety and maintenance issues. The safety issues linked to overhang behavior include both excessive deformations as well as stability concerns. Excessive girder deformations can lead to hazardous conditions for the construction personnel since large rotations could potentially drop segments of the stay-in-place forms through the girder system. The stability concerns can lead to bridge failures in both steel and concrete bridge systems, as will be discussed in Chapter 2. The potential maintenance issues can occur if the girder rotations lead to shifts in the deck steel reinforcement, which can compromise the concrete cover and lead to long-term corrosion in the deck steel as well as premature deck cracking.

1.2 SCOPE OF STUDY

The results presented in this thesis were part of TxDOT research study 0-5706, Impact of Overhang Construction on Girder Design. The primary goals of the research project included improving the understanding of the behavior of girders subject to overhang forces, identifying system geometries that may lead to problems, and developing improved details for overhang construction. The following items were identified by TxDOT as suggested items to study.

- Slab and overhang placement bracing requirements, particularly with flexible girders and narrow beam spacings such as those frequently encountered on bridge widenings, which are particularly susceptible to global stability concerns.
- The effect of adjacent beam spacing on maximum overhang dimensions.
- The effect of bearing pad rotational stiffness on slab and overhang construction.
- The effect of girder (steel and prestressed concrete) stiffness in torsion and bending on overhang construction.

The project includes field monitoring, laboratory testing, and parametric finite element modeling. This thesis focuses on results from the field monitoring. Three bridges were monitored during construction to collect data that could be used to validate a finite element analysis computer model. The finite element model will be used to conduct parametric analyses to improve the understanding of girder behavior and identify problematic geometries for overhang construction. It is anticipated that this project will culminate in a set of recommendations for engineers to use in determining overhang dimensions and their effect on prestressed concrete and steel girder design. In particular, current rules of thumb will be evaluated to develop rules based upon research results. In addition, critical overhang and bracing geometries will be identified that can result in poor behavior. Based upon the findings, recommendations will be developed for the bracing or support conditions that can be utilized to avoid problems.

1.3 THESIS OVERVIEW

The thesis consists of five chapters. Following this introductory chapter, Chapter 2 provides a discussion of the background information relevant to bridge overhangs. In particular, the motivation for a study of overhangs, the results of a literature review, and a discussion of typical overhang construction are presented.

In Chapter 3, the specifics of the three bridges monitored during construction are identified. The studies were conducted on one prestressed concrete girder bridge and two

steel girder bridges. There is a discussion of the methods of evaluating strains in key structural members, vertical deflections, and torsional rotations in the girder systems. In addition, an overview of the method used to evaluate imperfections in the steel girder webs is provided. Finally, there is a brief overview of the data acquisition system used.

The results and observations from each of the three bridges are presented in Chapter 4. A discussion of the results in terms of vertical deflections, lateral rotations, rebar strain, and web imperfections, due to the construction loading of the concrete deck pour is provided. The final chapter of the thesis provides a summary of the experimental investigation and the resulting conclusions.

CHAPTER 2

Background

A discussion of the background information relevant to bridge overhangs is provided in this chapter. In particular, the motivation for a study of overhangs, the results of a review of the literature, and an overview of typical overhang construction details are presented.

2.1 MOTIVATION FOR STUDY

Overhangs on bridges result from economical constraints to use as few girders as possible across the bridge width. While designers commonly employ rules of thumb with regard to the geometry of the overhang, the actual behavior of the girder system is not well understood due to unbalanced loading conditions. The overhang brackets are connected to the top of the fascia girder and react against the side of these girders. Due to the eccentricity of the overhang, a torsional load is applied to the fascia girder, causing the girders to twist, and thereby affecting both the global and local stability of concrete and steel bridge girders. In some bridge widening projects, the torsional loading from the brackets coupled with the relatively large length-to-width ratio of the widening have led to systems that were dangerously close to failure.

The main goal of this research project was to understand the behavior of girders subjected to overhang forces. As is outlined in Section 2.2.2, the Department of Transportation (DOT) from various states generally handle overhangs differently due to little research justification. This lack of understanding has led to many bridges that have failed or have been close to failure. To understand overhangs construction, it is beneficial to look at the equilibrium of the girder system, possible deformation modes, and some representative case studies.

2.1.1 Overhang Equilibrium

Overhangs influence the stability of the bridge system due to the induced torsion, which is a result of the technique for forming the concrete bridge deck. The torsional load is idealized by the free body diagram of the system in Figure 2-1. Once the concrete has cured, the concrete deck overhang has sufficient strength to cantilever from the edge of the fascia girder. However, while the concrete is still fluid, the overhang portion of the deck must be supported by overhang brackets. The resultant force from the overhang weight, W_o , acts at an eccentricity, e_o , from the edge of the fascia girder. If the overhang load and eccentricity are large enough, the system can become unstable and rotate about the point referred to as the “point of rotation.” For a beam with a rigid support, the point of rotation is the edge of the beam or end of the rigid support, whichever is closest to the centerline of the beam. The stability of the system can be evaluated by summing the moments about the point of rotation as given in Equation 2-1 and Equation 2-2.

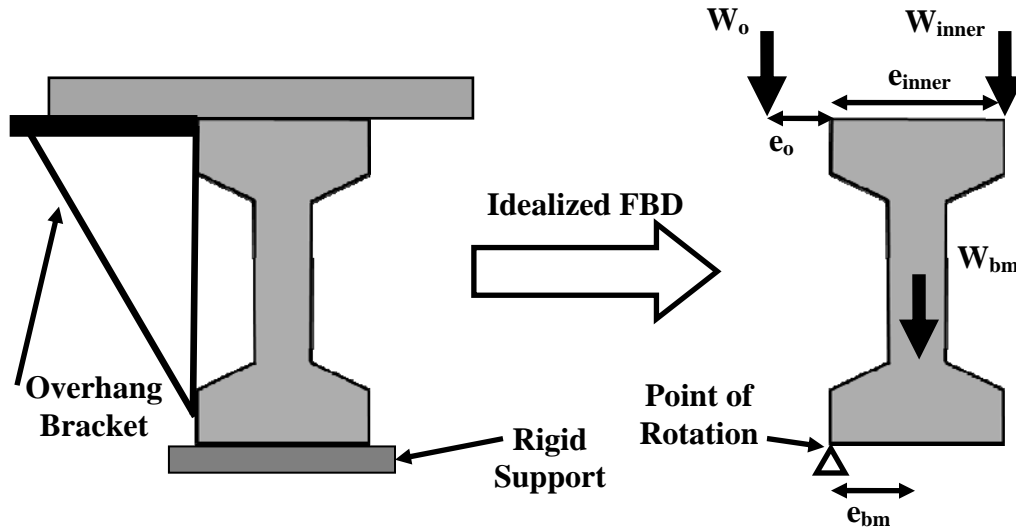


Figure 2-1 Idealized Free Body Diagram of Bridge Overhang

$$\Sigma M_{corner} = W_{bm} * e_{bm} + W_{inner} * e_{inner} - W_o * e_o = 0 \quad \text{Equation 2-1}$$

W_{bm} = Weight of beam and concrete deck over beam

$W_o = \text{Weight of concrete deck from overhang}$

$W_{inner} = \text{Weight of concrete deck from interior span}$

$e_{bm} = \text{Eccentricity from } W_{bm} \text{ to point of rotation}$

$e_o = \text{Eccentricity from } W_o \text{ to point of rotation}$

$e_{inner} = \text{Eccentricity from } W_{inner} \text{ to point of rotation}$

Stable for: $W_{bm} * e_{bm} + W_{inner} * e_{inner} \geq W_o * e_o$ **Equation 2-2**

For the system idealized in Figure 2-1, the self weight of the fascia girder as well as the reaction from the weight of the concrete deck on the inside of the fascia girder, W_{inner} (Equation 2-2), provide a stabilizing effect to the torsional load from the overhang. Thus, simple ways to have a stable system are to reduce the weight from the overhang or use a heavier girder. If a large overhang is required on a concrete girder system, bracing along the length of a girder can be added to prevent instability. A variety of different solutions are used, depending on the state's standard practices and guidelines.

For steel girder systems, the cross frames that are used for stability bracing help to resist the torsion from the overhang. The cross-frame locations are commonly treated as brace points for lateral-torsional buckling. However, in cases where only a few girders are used, such as in bridge widenings, a system mode of buckling is possible that is not sensitive to the spacing between cross frames or diaphragms (Yura, 2008). In those systems, the torsion from the overhang system intensifies the system mode of buckling.

2.1.2 Deformation Modes

The forces from the overhang brackets can cause girder deformations that are not well understood in both concrete and steel bridge systems. In concrete girder systems, the overhangs often cause rotation in the fascia girders that are locked into the bridge system once the concrete bridge deck cures. In addition to locking this undesirable

rotation into the girders, there are safety concerns with regard to the potential for dropping the formwork between the adjacent girders due to excessive twist of the fascia girder. In steel girder systems, the overhang brackets can cause problems with the local and global stability of the girders. The deformational behavior of both concrete and steel bridge systems are discussed in the remainder of this sub-section.

Two sources of deformations arise for prestressed concrete bridges loaded by overhangs: torsional deformations and rigid body rotation from flexible bearings. Due to the eccentricity of the overhang, torsion develops in the fascia girder that reduces the flexural capacity of the girder. Rather than specifically design for the torsion, many designers control the problem by limiting the overhang dimension based upon rules of thumb. The torsional rigidity of most prestressed concrete bridge girders is very large due to the thick flanges and web, making most torsional deformations small enough to neglect. Nonetheless, torsional deformations do contribute to the overall deformed shape of the girder. Flexible bearings, the other source of deformations, are important components of the structural system that allow the bridge to expand and contract due to changes in the thermal environment throughout the year. Although the flexibility of the bearing is helpful in accommodating the thermal expansion and contraction, the flexibility is detrimental to the torsional deformations from the overhang. The high compressibility of the bearings moves the point of rotation inward toward the center of the girder, which can lead to large rigid body rotations (Figure 2-2). Moving the point of rotation inward increases the eccentricity of the overhang load and thereby decreases the stability of the bridge. The torsional stiffness of the concrete girder system is sensitive to the details that are used to restrain girder twist. These details have changed dramatically over the past 20 years, as is discussed in the next subsection.

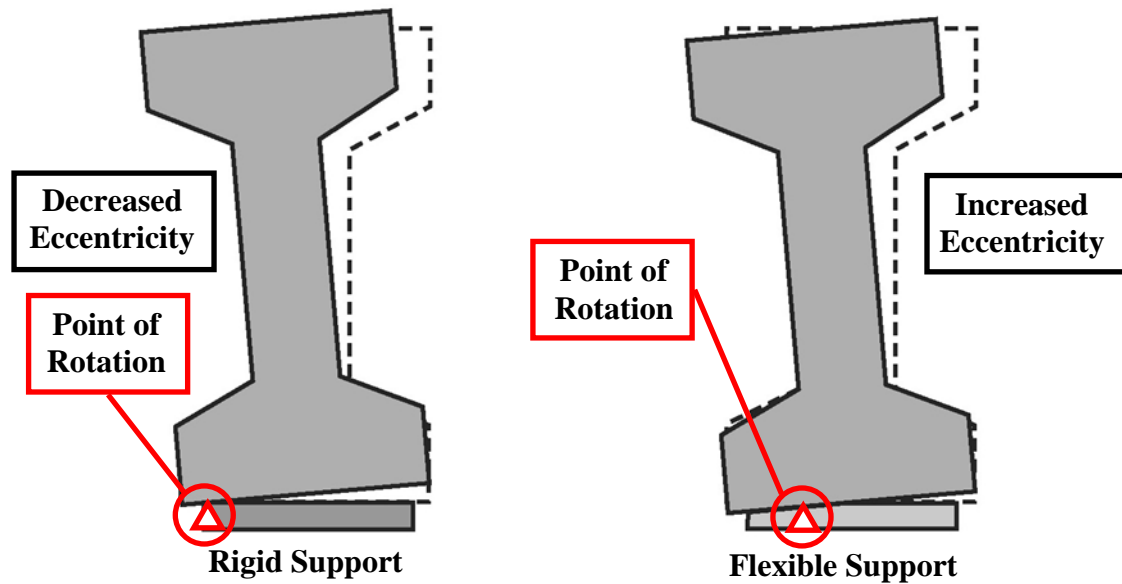


Figure 2-2 Effect of Rigid and Flexible Supports on Eccentricity

For steel girder bridges, both global and local deformations can occur as a result of the overhang loads. The global deformation issues are the same as for the prestressed concrete bridges: torsional deformations and rigid body rotation due to flexible bearings. As compared to concrete girders, steel girders are more susceptible to torsional deformations due to the thinner flanges. However, the thinner flanges are generally compensated by deeper webs, thereby increasing the distance between flanges and minimizing torsional deformations. In addition, the torsional stiffness of the fascia girder is aided by the use of intermediate cross-frames spaced along the length of the bridge. The local deformation problem arises from the positioning of the strut from overhang brackets. In many situations the overhang brackets exert large concentrated forces on portions of the web in compression. The forces can distort the web, leading to local instabilities or large web imperfections that can get locked into the girders once the deck cures.

2.1.3 Details for Restraining Twist of Concrete Girders

The details to resist twist of the concrete girder systems have changed dramatically over the past 20 years. As outlined above, cross-frames or diaphragms are

commonly used with steel girders to improve the torsional stiffness of the girder system. Similar details were used in the past with concrete bridges; however these braces were eliminated to improve the economy of the bridge system. Figure 2-3 shows pictures of concrete girder bridges constructed in the 1970's alongside a concrete bridge completed in 2006. In the 1970's, removable forms were commonly used for both the overhang and the interior bridge deck. A cast-in-place concrete diaphragm was used at the middle of the simply supported girders, while a smaller concrete diaphragm was employed at the support above the abutment. In addition to restraining girder twist, the concrete diaphragms also provided lateral bracing against wind loads during construction.

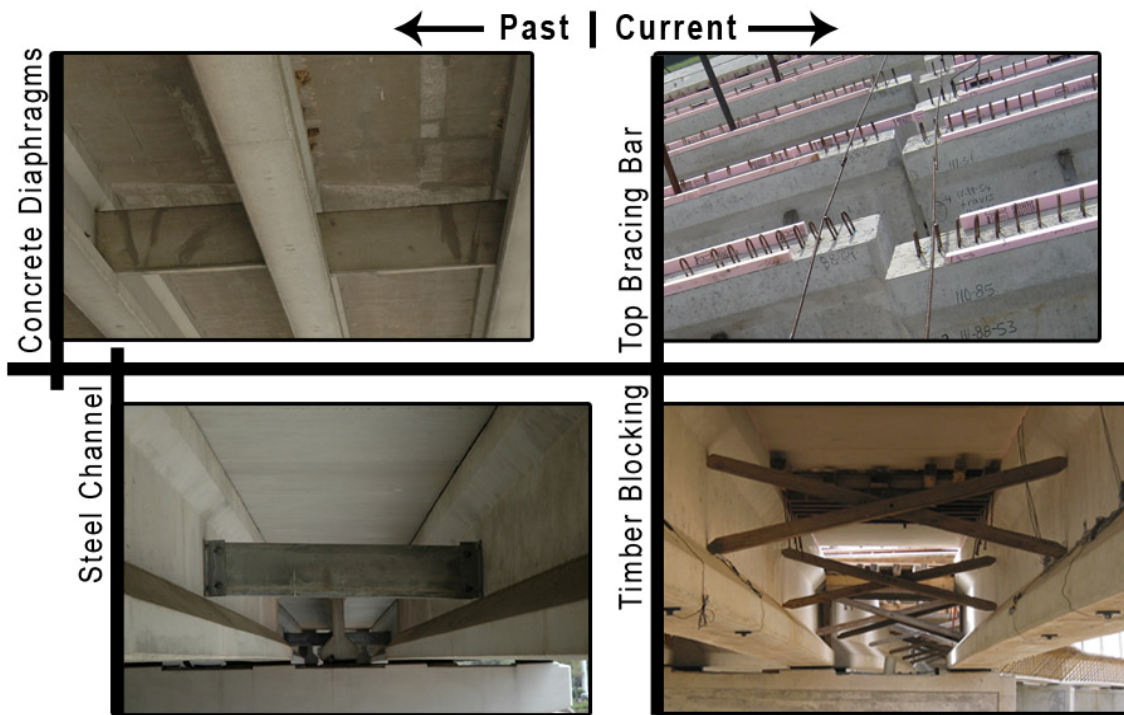


Figure 2-3 Progression of Bracing Details

Cast-in-place diaphragms were expensive and took a large amount of time to form and cast. As a result, simpler types of diaphragms were also used. While precast concrete diaphragms were sometimes used, many applications utilized steel channel diaphragms. The diaphragms were connected to an angle that was bolted to the webs of the concrete girders.

In recent years, permanent diaphragms are rarely used on prestressed concrete bridges. In current Texas practice, the bracing requirements of prestressed concrete girders are governed by standard sheet MEBR(C)-1, “Minimum Erection and Bracing Requirements.” During construction, lateral bracing is mainly provided with the use of 4-inch square timbers. The lateral bracing from the timbers is achieved with the use of a combination of X’s and lateral struts positioned near the bottom flange. In addition, the top bracing bar shown in the top right picture of Figure 2-3 is used to provide additional restraint to twist of the fascia girder. This restraint is accomplished by welding the bracing bar directly to the R-bars that extend from the top of the precast girders. There are two different stages that the top bracing bar is used, one before and one after the precast concrete panels (PCP) are installed. Prior to PCP installation, #5 reinforcement are welded to adjacent bars and to the R-bar from one side of the bridge to the other. This detail requires a line of bars to be placed at each end and at mid-span of the bridge. The bracing bar shown in Figure 2-3 is the bar installed prior to PCP installation.

After the PCP are installed on the bridge, the detail of the top bracing bar changes. Instead of welding #5 bars in series, one #5 bar is used between each adjacent girder. Due to the height of the panels, the #5 bars are bent around the panels and welded to the R-bar (Figure 2-4). Whereas the bracing bars prior to PCP installation are usually only positioned at the ends and middle of the girders, after the deck panels are installed, the bracing bars are spaced at approximately 15 feet increments along the girder length.

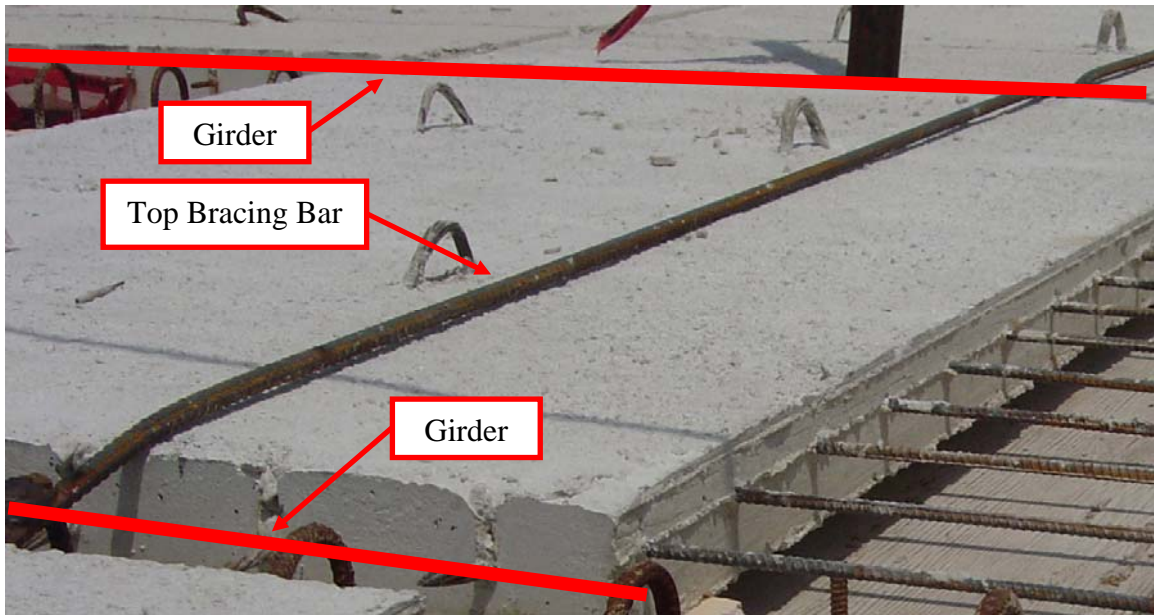


Figure 2-4 Top Bracing Bar After Panel Installation

The importance of effective bracing details, before, during, and after construction, can be illustrated for both steel and concrete bridges around the country. In particular, a recent collapse in Arizona highlights the potential for stability problems in concrete girder systems during construction. Nine of the eleven 114 feet prestressed concrete girders collapsed on August 9, 2007 (Illia, 2007). The bridge was located in Mesa, Arizona, along the Loop 202 Red Mountain Highway, just east of Power Road. The girders fell from the pier caps three weeks after being placed. However, at the time, the final bracing, in the form of precast concrete diaphragms, was not installed when the incident occurred. It is important to note that the detail used in Arizona differs from the current detail used in Texas.

In Texas, the effectiveness of the current 4-inch timbers and top bracing bars are of interest. Current 4-inch timbers used to transmit lateral wind loads between adjacent girders are limited in their ability to restrain girder twist during construction. The timbers serve as compression members and only are effective if there is a positive connection between the timbers and the concrete girders. For wind loads, there is generally not a problem with the connection. However, when a torsional load causes the girder to twist,

many of the timbers may become dislodged during deck construction as shown in Figure 2-5. In addition, as seen in Figure 2-4, the top bracing bar is very flexible and located above the top flange of the beam, making it inefficient.



Figure 2-5 Effect of Twist on Timber Blocking

2.1.4 Representative Case Studies

There are three Texas bridges that spurred much of the motivation for this research project. The first bridge was a widening project that utilized steel girders. The other two bridges consisted of prestressed concrete girders that experienced excessive rotation during construction of the concrete bridge deck. The following two sub-sections provide an overview of these girder systems.

2.1.4.1 Steel Bridge Widening

This section provides an overview of a problem that occurred during a bridge widening that was made by adding two steel girders to an existing bridge. In typical widening projects, a few girders are utilized to increase the width of an existing bridge. The widening is usually isolated from the existing bridge so that the added girders are free to displace during casting of the concrete slab, thereby resulting in a relatively flat bridge deck. As a result, the geometry of the addition often has a relatively large span-to-width ratio, which makes it susceptible to a “system mode” of buckling that is relatively insensitive to the spacing or size of the intermediate cross-frames. The system mode of

buckling is a mode in which the girders are tied together and buckle as a unit in a half sine curve along the length. Several cases have been reported involving the system buckling mode. A discussion of the phenomenon as well as design equations are presented in Yura et al. (2008). Structural systems with several girders spaced across the width have a large combined stiffness and are not generally susceptible to the system mode of buckling.

Before the specifics of the problematic bridge are outlined, the static differences of new construction versus a bridge widening should be discussed. In new construction, the overhangs on the two edges of the bridge are often similar in geometry such that the two overhangs counterbalance each other (Figure 2-6). In such a girder system, the overhang may cause local torsional distortions in the fascia girders. In a bridge widening, the overhang only exists on one side leading to an unbalanced load that must be fully resisted by the torsional stiffness of the girder system. Since many bridge widening projects only consist of a few girders, the combined torsional stiffness may be relatively low and such girder systems are highly susceptible to the system mode of buckling outlined above. In the case of the steel girder system used in the bridge widening, the torsional deformations were aggravated due to the unbalanced load from the overhang.

Figure 2-7 shows the twin girder system used in a bridge widening that had problems related to the system mode of buckling. Although several intermediate cross-frames were used, the system suffered a significant twist as shown in Figure 2-7. The twist of the girders is indicated in Figure 2-8 by the 10 inch offset of the bottom flange measured from a plumb line dropped from the top flange.

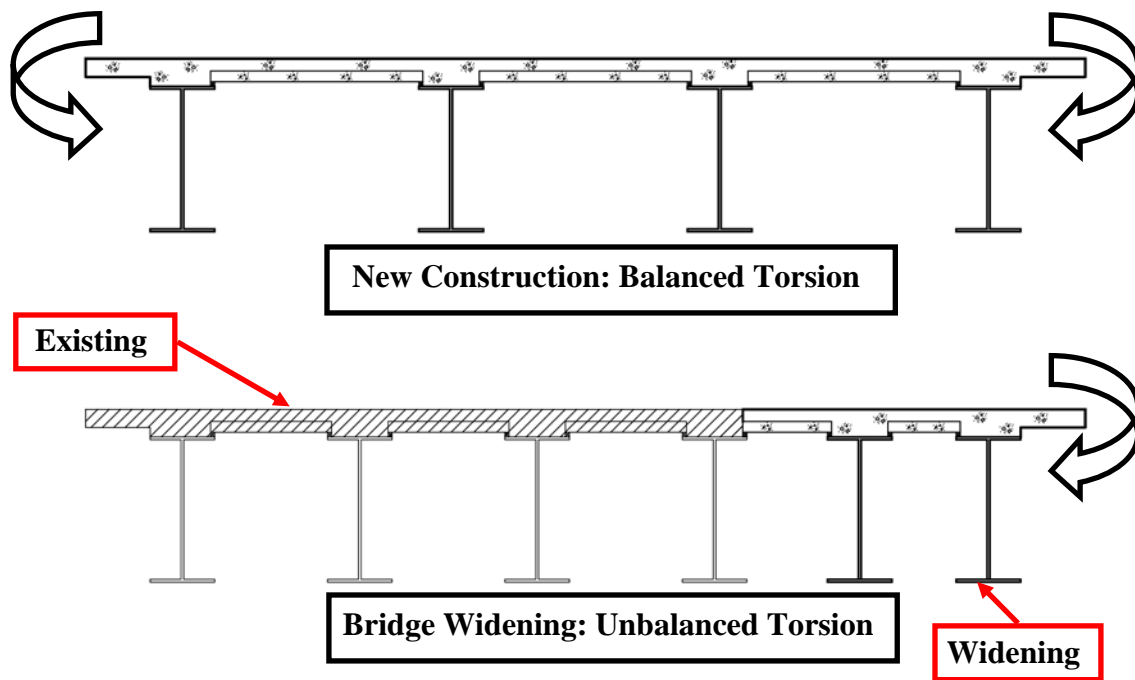


Figure 2-6 Differences in Torsion for New & Bridge Widening Projects



Figure 2-7 Twin Girder Widening with Excessive Girder Twist

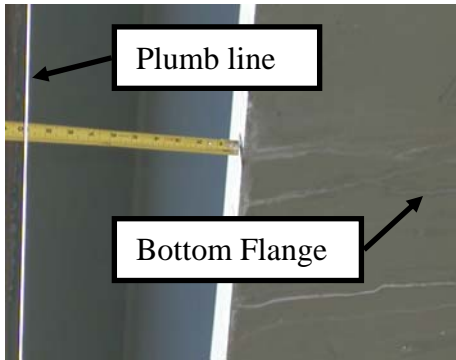


Figure 2-8 Girder Twist

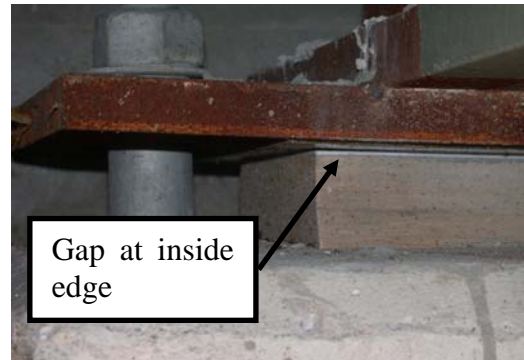


Figure 2-9 Fabric Pad Lift-Off

The system buckling mode was amplified by the torque from the overhang. Figure 2-9, shows a close up of the support deformations from the bridge. The overhang twisted the girder outwards causing a separation between the sole plate and the fabric pads at the interior edge. Though the (approximately) 1/16 inch gap does not seem too large in this case, the resulting rotation in the girder cross-section can be quite large. For example, assuming a rigid cross-section, if the 1/16 inch gap occurred over a 12 inch wide bottom flange, the lateral deformation at the top flange of a 60 inch deep girder would be on the order of 5/16 inches. This is a relatively large rigid body twist in the girder that can be intensified by a distributed twist along the bridge length.

2.1.4.2 Prestressed Concrete Bridges with Excessive Girder Rotation

The two prestressed concrete bridges discussed in this section experienced excessive girder rotation during the casting of the concrete bridge deck. For the purposes of referencing, the two bridges are referred to as Bridge 1 and Bridge 2. Both bridges were constructed in accordance with typical Texas practices and feature Type B prestressed girders, 36 inches deep with 18 inch wide flanges. The overhang dimension was 30 inches, measured from the center line of the beam to the edge of the bridge. In terms of bracing, standard sheet MEBR(C)-1 was used. Both bridges were reported to have large rotations shortly after the deck pour, as noticed by the girder lifting off the bearing pad (Figure 2-10).



Figure 2-10 Girder Rotates off Bearing Pad

To determine the extent of rotations, a site visit was conducted in November 2006. Both bridges were investigated and found to have significant rotations, as evidenced in Figure 2-11. The rotation of the girders was determined by measuring the difference in elevation of the flange ends with a level and dial caliper. On Bridge 1, three measurements were made on the north fascia girder at approximately the mid span, quarter point, and support. As can be seen from Figure 2-12, the rotations are approximately the same along the length and ranged from 2° to 3°. On Bridge 2, the rotations of the two fascia girders at the supports were found to be 2.8° and 2.3°.



Figure 2-11 Large Rotations of Prestressed, Fascia Girder at Bridge 1

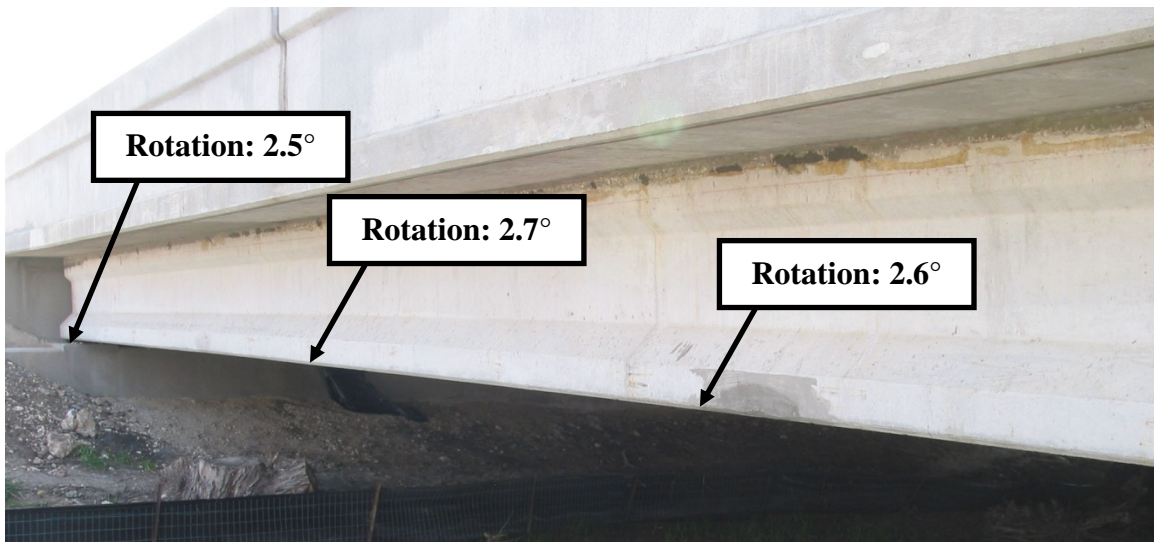


Figure 2-12 Measured Rotations of Bridge 1

A couple observations can be made from the data. First, the controlling deformation mode for the fascia girder was rigid body rotation due to flexible bearings. This deformation mode is evident from the similar rotations found across the length of

the girder at the Bridge 1. If torsional deformations were critical, there would have been a larger difference between the rotations near the support and at mid span. The second observation was that current bracing details are inefficient in preventing large rotations. Ranging from 2° to 3°, the girders rotated noticeably under the concrete deck loading. For the shallow girder and long overhang properties given, the combination of timber blocks and top bracing bars were inefficient in limiting girder rotation.

2.2 LITERATURE REVIEW

A literature review regarding overhangs was conducted prior to the field studies. In particular, literature related to overhang construction and current Department of Transportation (DOT) Guidelines were found. The below sections discuss past rules of thumb, current directions in overhang research, and the range of guidelines from various State DOTs.

2.2.1 Overhang Construction

Although the actual impact of overhang details are generally not well understood, designers have developed a number of rules of thumb in an effort to reduce potential problems. The Texas Department of Transportation (TxDOT) Load and Resistance Factor Design (LRFD) Bridge Design Manual prescribes a maximum overhang dimension of 1.3 times the girder depth. Other engineers sometimes limit the overhang to half of the spacing between adjacent girders. The National Steel Bridge Alliance (NSBA) discusses the economical side of defining the overhang width. The following was taken from Chapter 8: Stringer Bridges – Making the Right Choices, of the Steel Bridge Design Handbook (NSBA, 2006):

When establishing the girder spacing, it is important to balance the moments in the girders with the appropriate deck overhang width beyond the fascia girder. If the overhang is too large, the exterior girders will carry significantly higher forces than the interior girders due to the cantilever effect of the deck beyond the fascia. A small deck overhang results in lower forces in the exterior girders than in the

interior girders. Refined analyses have shown that the forces in the exterior and interior girders will be reasonably balanced when the deck overhang is around 30% to 32% of the girder spacing. This allows similar sections to be used for the interior and exterior girders, thereby allowing greater fabrication economy due to repetition.

While the applications of rules of thumb provide some basic guidelines for overhang design, such methods generally do not have research justification. As such, the effects of torsion on the fascia girder are not properly addressed. In addition, these rules do not consider some important factors that can have a dramatic effect on the deformational behavior of the bridge, such as the span of the girders or the configuration of the overhang brackets relative to the girder geometry.

In 1990, the American Institute of Steel Construction (AISC) developed one of the first reports addressing loads from overhangs (Grubb, 1990). That report used a single-span flexure analogy to calculate overhang loads. This approach assumed that the flanges of the girder act independently under torsion. As such, the flanges are modeled as single spans loaded laterally by a horizontal couple that is statically equivalent to the torsion imposed by the overhang brackets. Due to the assumptions in the model, the accuracy of the method may not be as accurate as desired.

A study at The University of Kansas by Roddis et al (1999) furthered the direction of the AISC report. The study examined assumptions of the AISC report to develop a more accurate model. The culmination of that study was the creation of a torsional analysis program for Kansas Department of Transportation (KDOT), which was called “Torsional Analysis for Exterior Girders (TAEG).” The design program was later modified in 2005, addressing previous issues and adding new capabilities for KDOT. However, it was found that “data obtained in field tests is in poor agreement with results calculated by TAEG. This is due to uncertainties in load conditions and to unaccounted lateral support provided by falsework, etc. (Roddis, 1999).” Thus, a better understanding of the bridge behavior is needed for a more accurate model.

For concrete girders, overhang brackets are usually attached through hangers embedded to the top flange of the fascia girder. Due to a current design trend toward thinner flanges in concrete girders, the embedment area of the hangers has decreased. Two studies were recently completed to examine the performance of hangers in thin concrete flanges under overhang loads. The first was performed at North Carolina State University and determined that the ultimate load of the two hanger types tested did not reach the ultimate strength provided by the manufacturer (Ariyasajjakorn, 2006).

The other study, performed at The University of Texas at Austin (Clifton, 2008), was an experimental investigation of current bridge deck overhang construction practice as it relates to the use of the new Texas I-girders (Tx girders). The primary objectives of that study were to examine the performance of commercially available overhang form products and provide recommendations for their use with Tx Girders. At the completion of the testing, a new concept was developed to use a precast overhang as an alternate solution to create the finished bridge deck overhang.

TxDOT has also recently funded another study at Texas A&M University to investigate the development of precast overhangs. Although the use of precast overhangs can minimize some construction problems caused by the brackets, the use of precast overhangs can have a number of uncertainties in girder stability due to construction loads from the screed and other concrete placement equipment. Since current construction details for prestressed concrete girder systems derive their stability primarily from the large gravity forces from self-weight reacting on the flexible bearing pad, the torsional performance of the girders can be unpredictable. Timber bridging between the girders helps distribute lateral wind loads between the girders. Yet, this bridging is relatively ineffective in bracing the girders against twist, due to the lack of a positive connection with the girders.

2.2.2 Department of Transportation (DOT) Guidelines

To determine the range of different overhang requirements, the overhang guidelines for each Department of Transportation (DOT) were reviewed. Maine and

South Carolina are two states with a set of specific limits, which varies based on beam spacing and/or depth. Table 2-1 and Table 2-2 list the specific overhang guidelines for these states. As of Fall 2006, it was found that less than 50% of the states have specific guidelines and as can be seen from Table 2-3, there is a great deal of variability in the guidelines from state to state. Only the states that provided some guidelines on overhang construction are listed in Table 2-3.

Table 2-1 Maine DOT Overhang Guidelines (2003)

Type of Beam	Beam Spacing	Maximum Deck Overhang
Structural Steel	Less than 9'-0"	3'-0" or depth of beam
	9'-0" to 10'-6"	1/3 of the beam spacing or depth of beam
	Greater than 10'-6"	3'-6" or depth of beam
Concrete	All	2'-0"

Table 2-2 South Carolina DOT Overhang Guidelines (2006)

Type of Beam	Depth of Beam	Maximum Deck Overhang
Prestressed Concrete	<54"	42"
	54" - 63"	48"
	> 63"	54"
Structural Steel	< 36"	Depth of beam
	36" - 48"	42"
	> 48"	45"

Table 2-3 DOT Guidelines

Number	State	Code
1	California	For Composite Box Girders, 60 percent of the average distance center-to-center of flanges of adjacent boxes, but shall in no case exceed 6 feet (2004)
2	Colorado	For Precast concrete and Steel I-Girders, use maximum of center-to-center spacing/3 or flange/web distance + 12" For Steel Box Girders, use center-to-center spacing/3 Overhang criteria may be exceeded with approval from Staff Bridge Engineer (1991)
3	Connecticut	Minimum of four feet or depth of the member (2003)
4	Delaware	Normal overhang is 2'-6." Maximum overhang is half the beam spacing or 4'-0," whichever is less (2005)
5	Florida	User empirical design method for overhangs less than 6'-0" and traditional design method for total deck overhang is less than 6'-0" (2008)
6	Kansas	Use TAEG to determine torsional loads (2006)
7	Maine	See Table 2-1
8	Michigan	Follow typical details, maximum overhang = 2'-6" (2001)
9	Montana	For steel giders, the overhang width restrictions (more strict of): 1. not more than 0.30 to 0.35 times the beam spacing to balance moments in interior and ext. beams 2. not more than the depth of the beam, or 3. not more than 1200 mm For prestressed concrete beams, the overhang dimensions are standardized (2002)
10	Nebraska	Max overhang=4'-6" For up to 5-girder bridges, minimize overhang and if the exterior girder controls, use exterior girder design for all girders. For more than 5-girder bridges, minimize the overhang and use the interior girder design for the entire bridge (2006).
11	Nevada	Deck overhangs shall be considered as falsework and designed as such (2001)
12	New York	The recommended maximum overhang of a concrete deck slab beyond the centerline of the steel fascia I-girder is 4 ft. In addition, the maximum overhang for steel fascia I-girders less than 5 ft in depth should be limited to 3 ft. The use of an overhang greater than 3 ft. with steel fascia I-girders less than 5 ft. in depth requires a detailed analysis (2008).
13	Ohio	In order to facilitate forming, deck slab overhangs should not exceed 4'-0" (2004)
14	Oregon	Deck overhangs should be no more than one-half the span length (2004)
15	South Carolina	Deck overhang shall be designed in accordance with Section 13 of the LRFD Specifications - see Table 2-2 (2006)
16	Texas	Maximum overhang is lesser of 3'-11" or 1.3 times depth of girder from centerline of beam (2001)
17	West Virginia	For bridges with structurally continuous concrete barriers, the minimum total overhang width shall be 3.0 times the depth of the deck, measured from the center of the exterior girder (AASHTO 9.7.2.4). The maximum total overhang width shall be the smaller of 0.625 times the girder spacing and 6 feet (2004).

2.3 TYPICAL OVERHANG CONSTRUCTION

Many of the problems that develop with overhangs occur due to the bridge construction process. Thus, it is useful to look at this process. After the girders have been lifted into place, formwork is placed to shape the deck. Between interior girders, the deck is typically formed by a stay-in-place (SIP) deck form, such as precast concrete panels or metal decks. At the fascia girder, the overhang is formed by wooden forms, which are supported by the overhang brackets. The wooden forms extend to support a rail for the screed and walking path for construction workers. If deck steel is needed, it is placed before the concrete deck is poured. The concrete is properly vibrated by construction workers before the screed creates a level roadway. Figure 2-13 depicts the typical cross section during a deck pour.

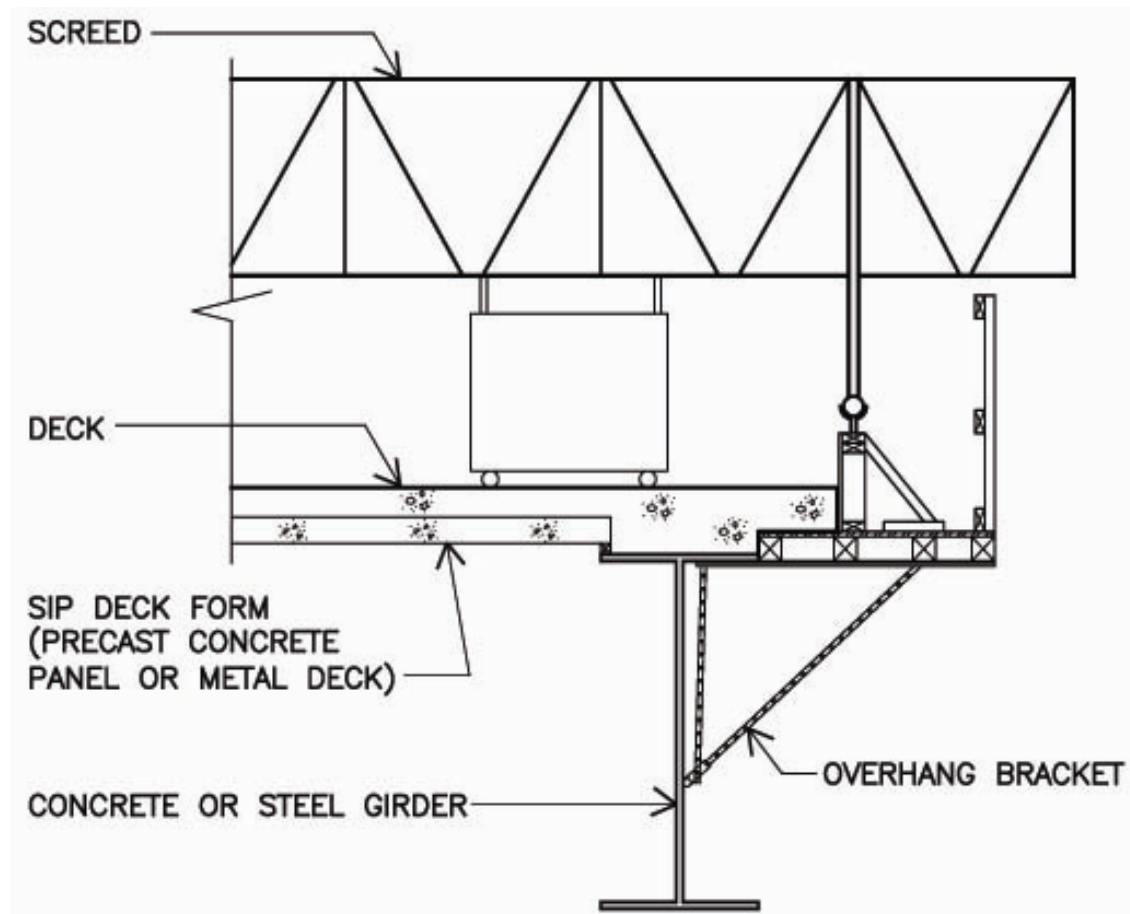


Figure 2-13 Typical Deck Construction

When the deck is cast, there are many different sources of loads applied to the bridge including the weights of the wet concrete, deck forms, construction equipment, and construction personnel. The wet concrete and construction equipment add the most load to the structure. Most overhang decks are at least 8 inches thick, while the screed weight can vary by manufacturer and model. For example at the two field sites outlined in this thesis, there was a significant difference in the screed weight. At the SH 71-SH 130 and US 82-19th Street Bridges the screed weights were 13 kips and 16.7 kips. Another source of load from construction equipment are the finishing bridges, which varied from 4 kips to 8 kips at the various field sites.

2.4 TYPICAL OVERHANG BRACKET GEOMETRICAL CONFIGURATIONS

Texas limits the overhang, as measured from the centerline of the beam, to 3 feet-11 inches or 1.3 times the depth of the girder, whichever is the lesser of the two limits. Overhang brackets come in all shapes and sizes, as can be seen in Figure 2-14 and Figure 2-16. The heights of the overhang brackets can be altered at the jobsite to fit most girder configurations. For instance, some of the brackets listed on the Meadow Burke website can be fitted for bracket heights between 30 and 50 inches, while others fit heights between 50 and 70 inches. In addition, Meadow Burke's standard brackets could support up to a 3 feet overhang, while the heavy duty brackets could be custom made for overhang lengths of 14 feet. Figure 2-14 shows the typical overhang brackets used at the interchange between SH 71 and SH 130.



Figure 2-14 Overhang Brackets Used at SH 71-130 Bridge

A possible problem develops when the same overhang bracket is used interchangeably on both the steel and concrete girders, which is a very common practice. In Figure 2-14, the overhang bracket can be seen as bearing on the bottom flange of the concrete girder. However, when the same bracket is used on steel girders without adjustment, a different scenario arises: one in which the bracket can bear in the middle of the steel web, as seen in Figure 2-15. Ideally, the overhang brackets should be positioned to react close to the girder flanges where the web plate will be the stiffest. Yet, in many instances on steel girder applications, the brackets react near the mid depth of the web or may even react in the compression portion of the web. Both of these instances can cause lateral deformations in the web plate that can be locked into the web once the concrete deck cures and affect the local stability of the web plates.



Figure 2-15 Overhang Brackets Transiting Between Concrete and Steel Girders

Figure 2-16 shows the typical overhang brackets used at the 19th Street Bridge over US 82 in Lubbock, Texas. As can be seen, the brackets are much different from the girder and brackets shown in Figure 2-14. The brackets in Lubbock are the heavy-duty type and bear near the bottom flange. Two adjacent brackets are connected to create a platform to form the overhang, support the screed rail, and create a path for the construction workers.

Overhang brackets are connected to the concrete or steel girder by a hanger. For concrete girders, the hanger is generally embedded into the top flange, during either the cast or as a post-process installation. For steel girders, the hanger is welded to both sides of the top flange of the beam, as seen in Figure 2-17.



Figure 2-16 Overhang Bracket Geometry at US 82-19th Street Bridge



Figure 2-17 Connection of Overhang Bracket to Steel Beam

CHAPTER 3

Instrumentation

Three Texas bridges were identified for monitoring the effects of overhang construction on girder behavior during construction. Two of the bridges are in Austin, while the third is in Lubbock. The two Austin bridges are located at the interchange between State Highway (SH) 71 and SH 130, and consist of a prestressed concrete girder bridge and a curved steel girder bridge. The bridge in Lubbock is a straight steel girder bridge with significant support skew. The geometry and instrumentation of these bridges is discussed below. In addition, discussion of the data acquisition system used at all the sites is provided in Section 3.4.

3.1 PRESTRESSED CONCRETE BRIDGE (SH 71-SH 130)

State Highway (SH) 130 is a Texas Department of Transportation (TxDOT) sponsored toll-road to “improve mobility and relieve congestion on I-35 and other major transportation facilities within the Austin-San Antonio corridor (CTTS, 2007).” The 49-mile toll-road runs from Interstate 35 north of Georgetown to US 183 southeast of Austin and includes both steel and prestressed concrete bridge segments. With the approval of TxDOT and the contractor, Lone Star Infrastructure, the SH 71 eastbound to SH 130 northbound direct connector was chosen for instrumentation. The connector contains a total of 23 spans consisting of 13 prestressed concrete beam units and 10 spans of horizontally curved steel plate girders units.

The prestressed concrete bridge unit that was monitored was labeled Span 22 on the direct connector between eastbound SH 71 to northbound SH 130. The simply-supported bridge features seven prestressed concrete girders spaced 7.25 feet on-center with a 120 foot span. The girders are typical American Association of State Highway and Transportation Officials (AASHTO) Type IV beams, 54 inches deep with 26 inch flange widths. Between interior girders, the 8-inch thick concrete deck consists of

precast deck panels (approximately 4 inches thick) with 4 inches of cast in-place concrete. At the overhangs, standard plywood forms were used as shown in Figure 3-1. The overhang dimension is 3 feet from the center of the exterior beams. The total width of the bridge is 50 feet.

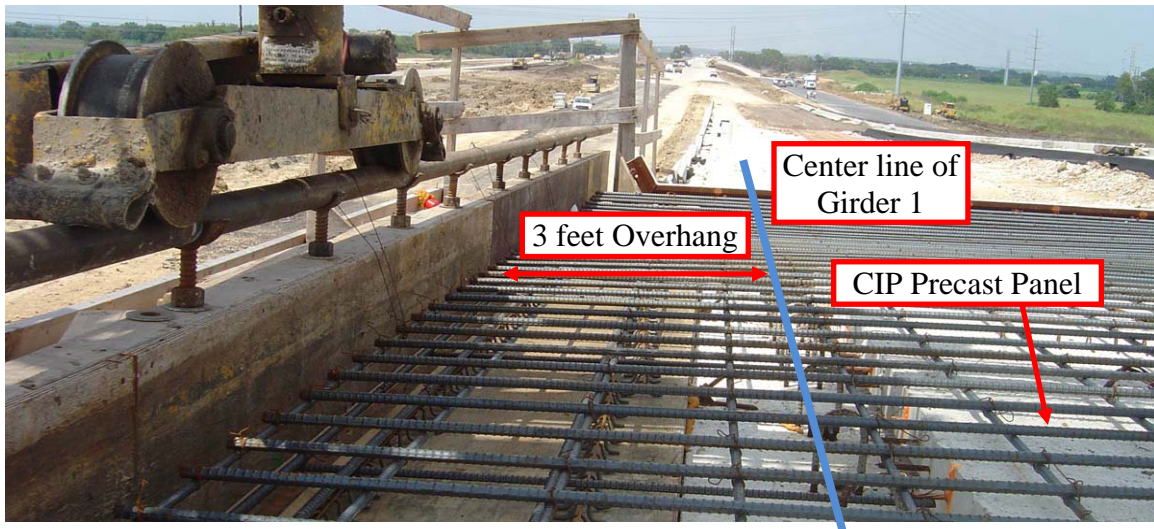


Figure 3-1 Slab Reinforcement at Overhang

The weight of the wood forms, the fluid concrete of the deck overhang, and the finishing machine is supported using cantilever overhang brackets as shown in Figure 3-2. The brackets are supported at the top with a tension tie that is typically welded to an insert at the top of the girders. The bottom of the bracket reacts on the edge of the bottom girder flange.



Figure 3-2 Overhang Brackets Used at SH 71-SH 130 Bridge

3.1.1 Instrumentation Plan for Prestressed Concrete Bridge

The type of data collected at each site is related to the anticipated deformations that were discussed in Section 2.1.2. For concrete girders, torsional deformations along the girder length can affect the global stability of the girders. Thus, the instrumentation of Span 22 focused on monitoring twist of the girders and the effectiveness of the top bracing bars during concrete placement. In addition vertical deflections of both exterior and interior girders were measured at stations along the girder length. An overall instrumentation plan is shown in Figure 3-3. The specifics of monitoring vertical deflections, torsional rotations, and strain in the top bracing bar at SH 71-SH 130 are discussed in the next three sections.

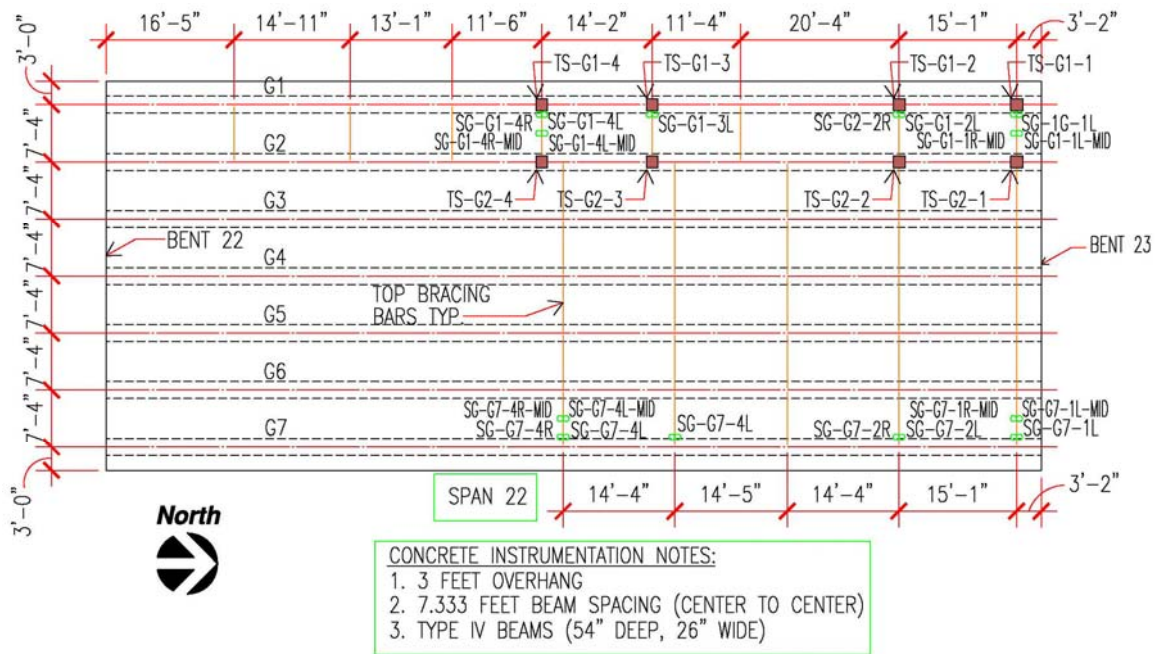


Figure 3-3 Instrumentation Plan for SH 71-SH 130 (Span 22)

3.1.1.1 Vertical Deflections

Vertical deflections were found using a laser distance meter to measure changes in girder elevations before and after construction activity. The Hilti® PD-32 was chosen as the laser distance meter to monitor vertical deformations during construction. The resolution of the instrument was 1/16th of an inch. Conceptually, the vertical deflection due to the deck pour was taken as the difference in elevation of the girders before and after the concrete deck was poured. Elevations were determined using a setup that is idealized in Figure 3-4.

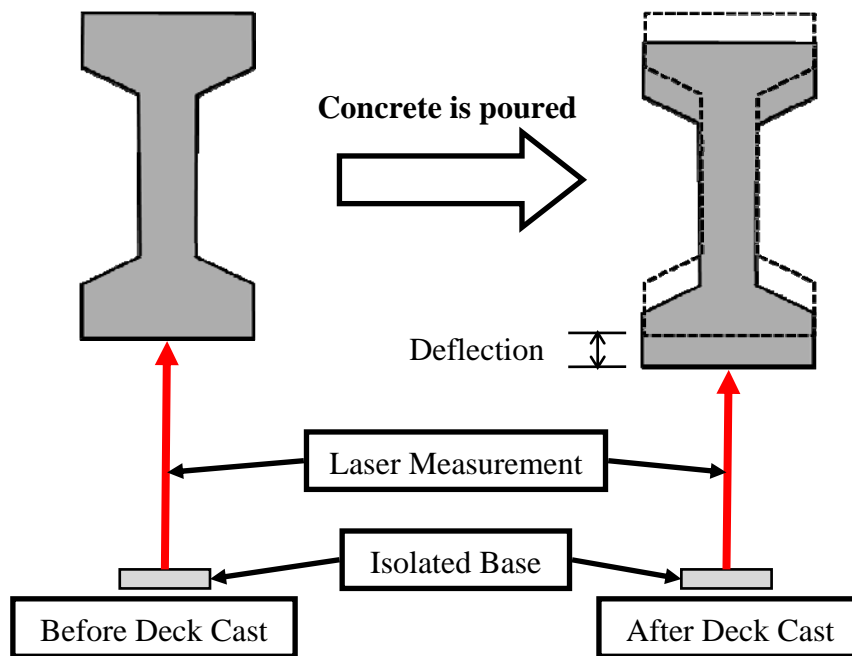


Figure 3-4 Idealized Deflection Measurement Setup

A concern for nearly any test setup is how to take measurements accurately and consistently. For this site, the concern was related to the reference point of the measurements. An important aspect of the accuracy of the measurements was to place the instrument in the same position and to have a solid foundation at the measurement locations. For instance, if the soil is used as the reference point, changes in the top soil conditions between the initial and final measurements from concrete trucks or other construction equipment in the area was a major concern. As such, an isolated base was created for each deflection measurement location to minimize local movements. Below each deflection location, a hole was dug 6 to 8 inches deep, as shown in Figure 3-5. Figure 3-6 shows the mixing process for the Hydro-Stone® that was used to fill the hole. The set time for Hydro-Stone is relatively short, thereby quickly providing an isolated base for the laser measurements (Figure 3-6). The laser distance meter was aimed at a target mark located on the bottom side of the girder, as shown in Figure 3-7. Figure 3-8 shows that a nail was placed in the Hydro-Stone base points to ensure that the distance meter was placed at the same location for each reading. The corner of the laser distance meter was placed over the nail each time to ensure that repeatable results could be

obtained. The nail also provided a high point that provided support to the distance meter at its base so that the spirit level on top of the instrument could be used to level the meter and allow the laser to hit the target on the bottom of the girder and obtain consistent readings.



Figure 3-5 Hole for Isolated Base of Deflection Measurement



Figure 3-6 Mixing Hydro-Stone for Isolated Base

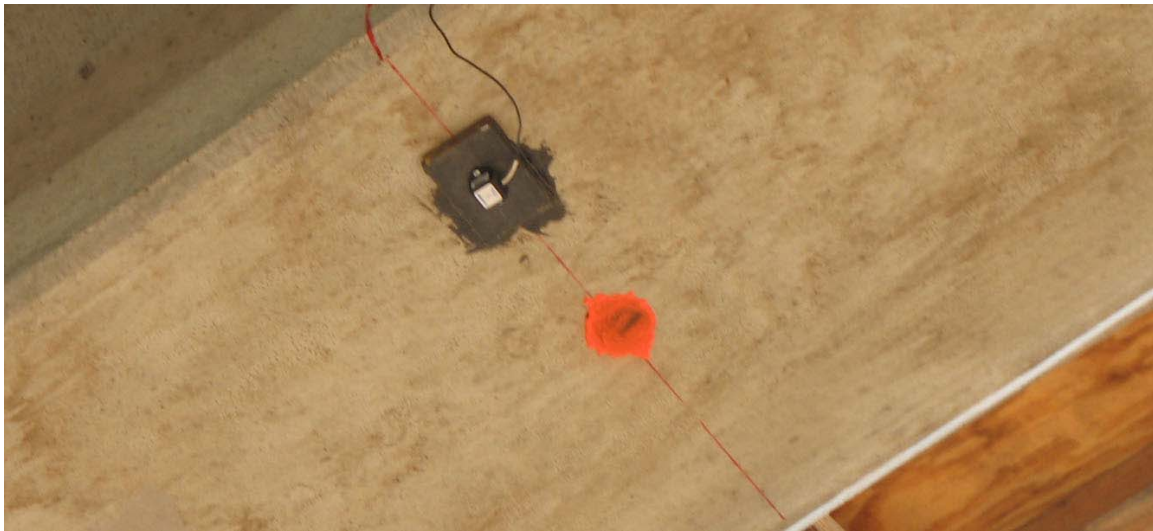


Figure 3-7 Spray-Painted Spot for Deflection Measurements



Figure 3-8 Deflection Laser Measurement from Isolated Base

A total of seven locations were chosen for vertical deflection measurements. As can be seen in Figure 3-9, three readings were taken on the fascia girder (girder 1) and first interior girder (girder 2) at three stations along the girder length. The final location was a point on the pier to be used as a control measurement. Due to the stiffness of the pier and the symmetric loading, the deflection of the pier will not likely register on the laser distance meter. If significant deflection was recorded, it could be attributed to movement of the isolated base. Thus, the pier location was chosen to determine if the isolated bases moved, as well as to confirm that the pier did not deflect.

To establish confidence in the deflection measurement setup, several readings were taken throughout a day when no construction activity was taking place on the bridge. It was found that the data was very repeatable throughout the day, within the precision, 1/16th of an inch, of the laser distance meter. During the deck pour, three readings were taken in succession to obtain the deflection at a given location. The deflection was taken as the average of the three readings. As will be noticed in Chapter

4, most readings were the same for a given set, while those with differences were within the precision of the laser distance meter.

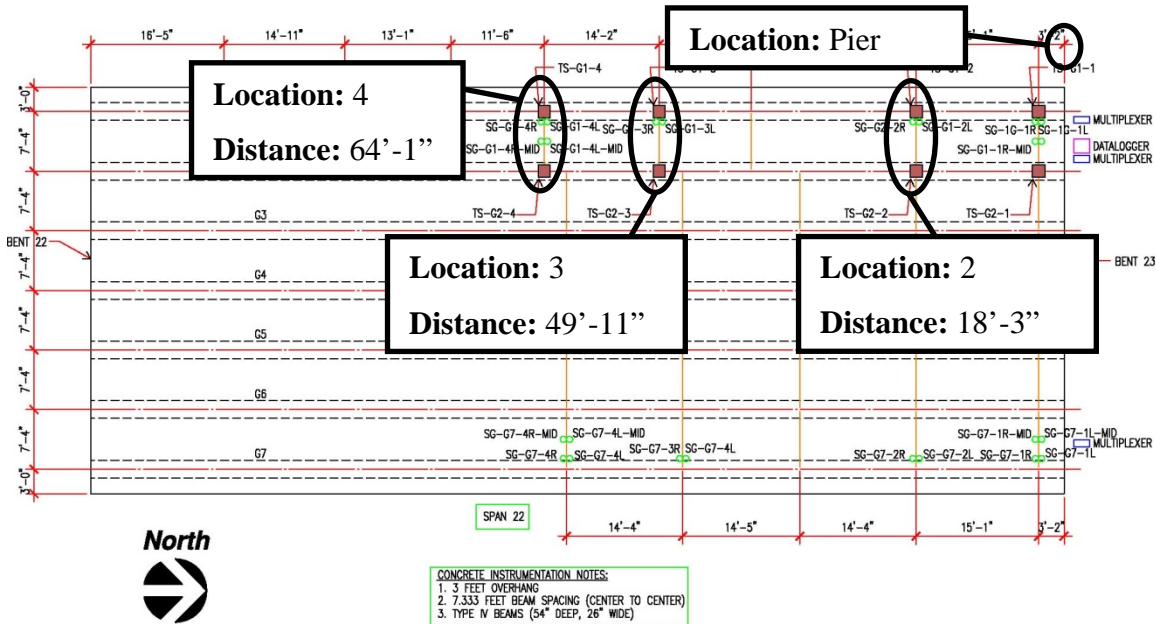


Figure 3-9 Vertical Deflection Measurement Locations at SH 71-SH 130

3.1.1.2 Torsional Rotations

The twist of the girders was determined by tilt sensors (CXTLA-01-T) manufactured by Crossbow Technology, Inc. The electronic side of the tilt sensors is discussed in Section 3.4.2. In the field, the tilt sensors were attached to steel plates before being installed on the underside of the girders, as seen in Figure 3-10. The tilt sensors were planned to be used on multiple projects over a series of months. Thus, steel plates were used, as compared to wood, because long term stability was a concern. To install on the underside of the girder, a 5-minute metal/concrete epoxy from Loctite was used. Bar clamps were used to hold the steel plate to the concrete surface while the epoxy cured.



Figure 3-10 Tilt Sensor Attached to Steel Plate

Four tilt sensors were placed along the lengths of both Girders 1 and 2. Girder 1 was denoted as the fascia girder on the west side of the bridge, while Girder 2 was denoted as the adjacent interior girder. Figure 3-11 details the locations of the tilt sensors along each girder. The distances were measured relative to the end of beam at Bent 23, which is located on the north end of the bridge. Tilt sensors are denoted by the abbreviation TS, girder number, and location number. Thus, the third tilt sensor on Girder 2 is labeled: TS-G2-3.

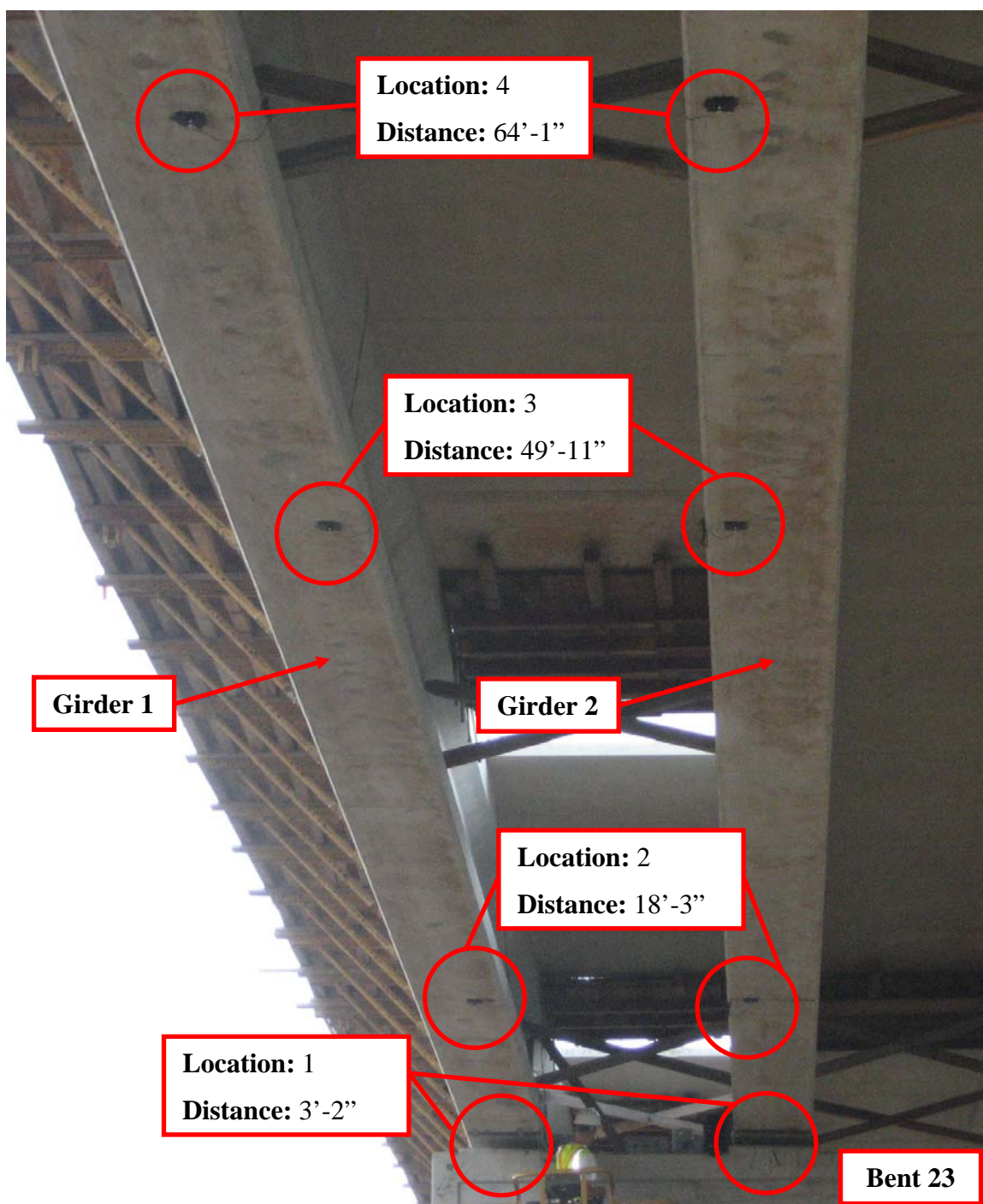


Figure 3-11 Locations of Tilt Sensors on SH 130-71 (Span 22)

3.1.1.3 Strain in Top Bracing Bars

The bracing details for prestressed concrete girders have changed over the years. In the 1970's, cast-in-place concrete diaphragms were often used at the middle of the simply supported girders, while smaller concrete diaphragms were employed at the supports above the abutment. In addition to restraining girder twist, the concrete diaphragms provided lateral bracing against wind loads during construction. Due to the cost of forming the diaphragms, a steel channel was also employed to brace the girders. However, in recent years, permanent diaphragms are rarely utilized. Current practice often relies on lateral bracing by square timbers forming an X as shown in Figure 3-12. Another detail that is combined with the square timbers is the use of “top bracing bars.”



Figure 3-12 Timber Blocking of Concrete Girders

There are two different stages that the top bracing bar is used, one before and one after the precast concrete panels (PCP) are installed. Figure 3-13 shows the type of detail used before the panels are installed. The #5 reinforcement are welded to adjacent bars and to the R-bar—hoop coming out of the prestressed concrete girder—from one side of the bridge to the other. This detail requires a line of bars to be placed at each end and at mid-span of the bridge. As seen in Figure 3-13, the line of bars seems to be relatively flexible.

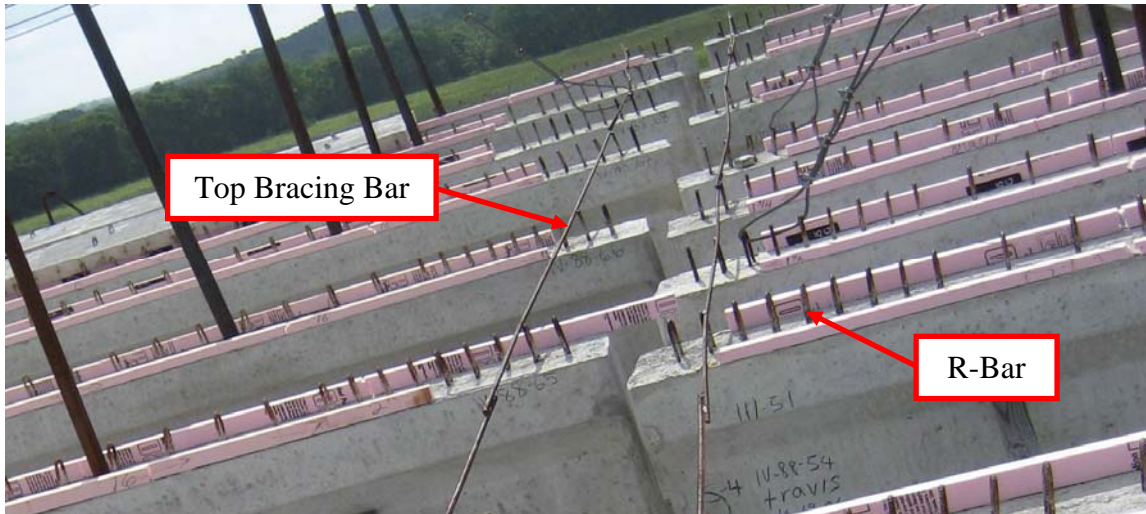


Figure 3-13 Top Bracing Bar Before PCP Installation

After the deck panels are installed on the bridge, the detail of the top bracing bar changes. Instead of welding #5 bars in series, one #5 bar is used between each adjacent girder, as seen in Figure 3-14. Due to the height of the panels, the #5 bars are bent around the panels and welded to the R-bar (Figure 3-15). It should be noted that the bracing bars come into contact with the edge of the panels. As such, friction can be transferred from the bars to the panels. Whereas the bracing bars prior to PCP installation are usually only positioned at the ends and middle of the girders, after the deck panels are installed, the bracing bars are spaced at approximately 15 feet increments along the girder length. Figure 3-16 details the frequency of bars across the north half of the bridge. Near the north end of the girder, the bars are in a continuous line from one end of the bridge to the other. However, after the second line of bars, the line becomes discontinuous at the west exterior girder (Girder 1). The bracing line is discontinuous due to the presence of a drain at approximately 31 feet from Bent 23. Since wooden forms were used to form the deck around the drain, rather than PCP, the top bracing bars were offset to the next PCP.

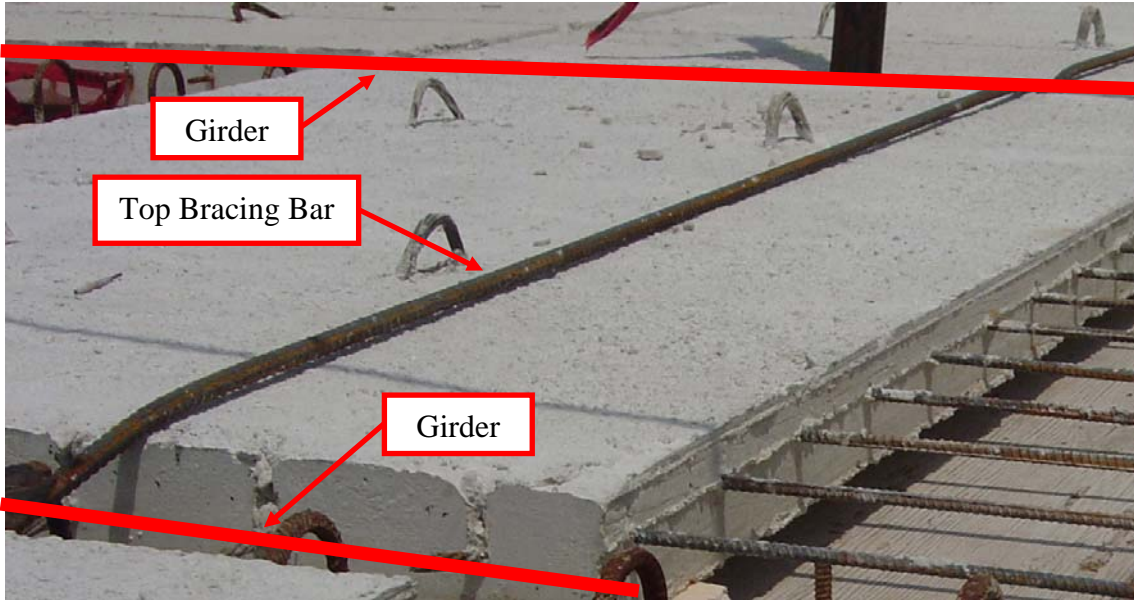


Figure 3-14 Top Bracing Bar After PCP Installation

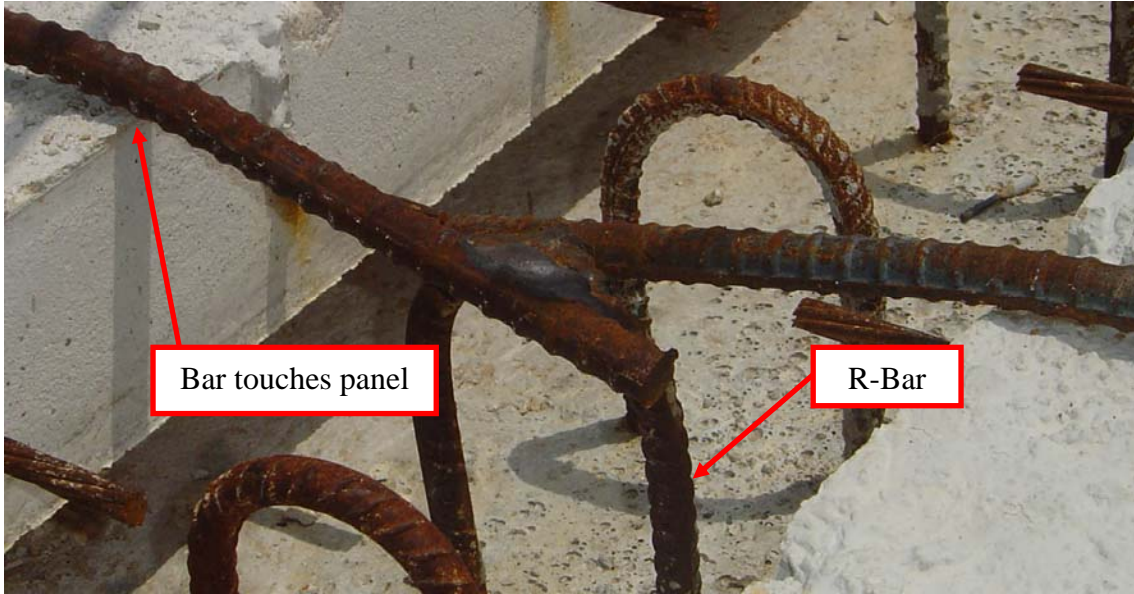


Figure 3-15 Weld of Top Bracing Bar to R-Bar of Girder

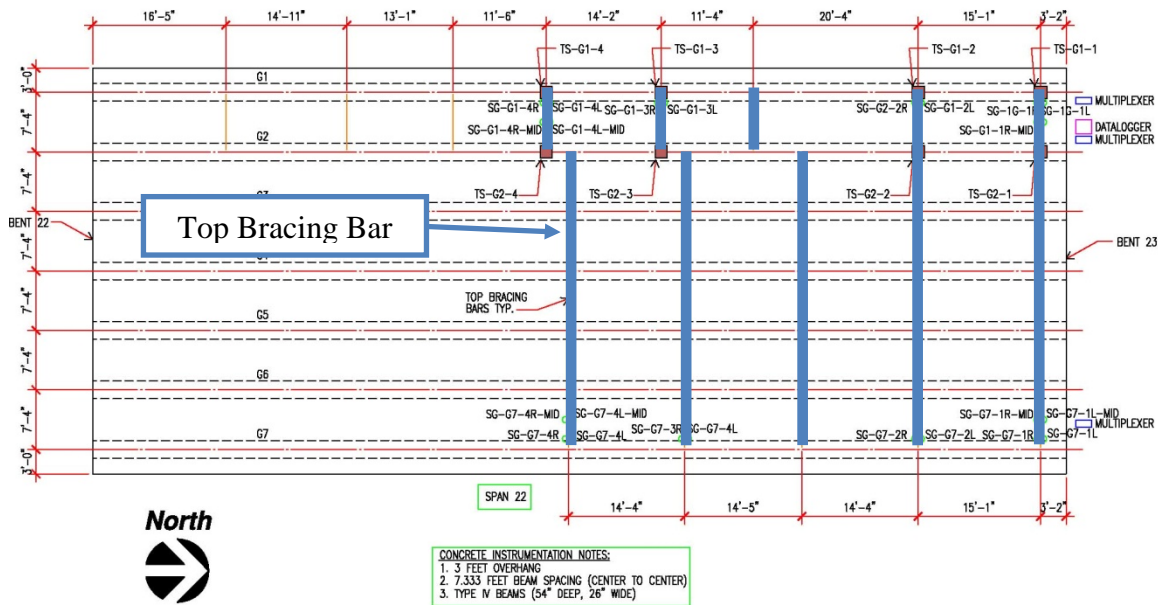


Figure 3-16 Location of Top Bracing Bars After PCP Installation

Strain gages were installed on some of the bracing bars to monitor the forces that developed in the bars during concrete placement. A total of 24 strain gages were applied along 8 bars throughout the north half of the bridge. As can be seen from Figure 3-17, the strain gages are installed on bars spanning between the exterior and interior girders on the east and west sides of the bridge. Two-thirds of the strain gages were applied at the ends of the bars, near the weld at the exterior beam. The remaining gages were installed at mid-length of the bars to determine if there was a different stress value between the ends and mid-length of the bars (Figure 3-18). The mid-length strain gages were placed on bars near the support (Location 1) and mid-span (Location 4) on both the east and west sides of the bridge. The distances were measured from the end of the beam at Bent 23. The locations of the individual bars are also sequentially numbered from Bent 23.

Strain gages are denoted by the abbreviation SG, girder number, location number, and orientation. Thus, the strain gage oriented on the left side of the bar at the third location on Girder 7 (east side) is labeled: SG-G7-3L. Left and right were defined from the orientation given in Figure 3-16. Therefore gages designated on the left were on the side of the bar closest to Bent 23, while gages designated right were on the side of the bar

closest to Bent 22. If the strain gage is located at mid-length of the bar, then a -MID is added to the end of the label (i.e. SG-G1-4L-MID).

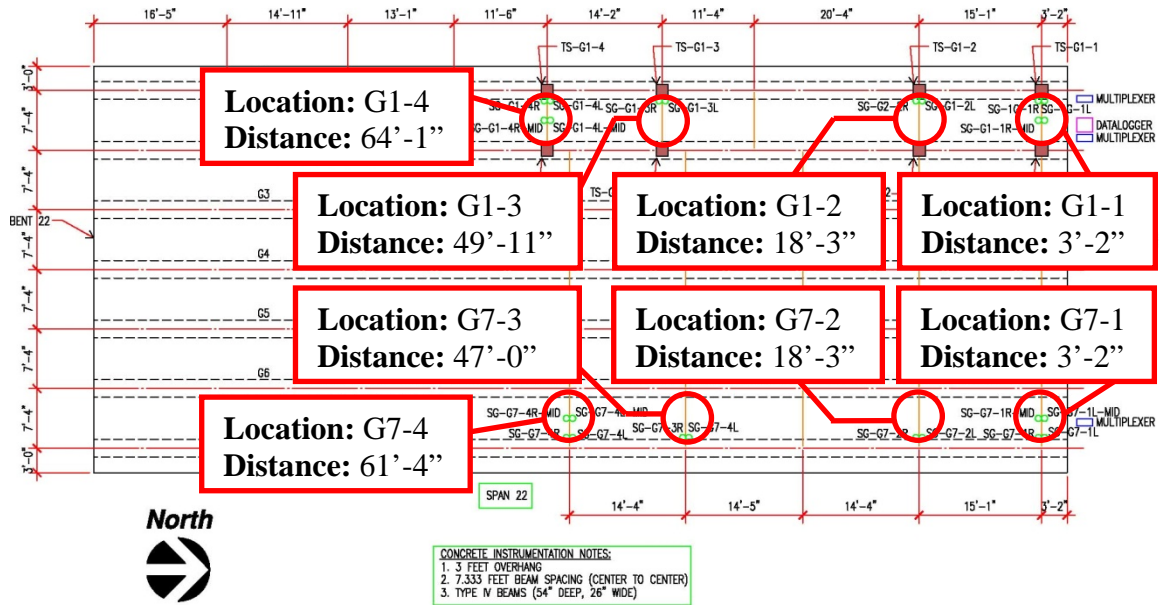


Figure 3-17 Location of Top Bracing Bar Strain Gages

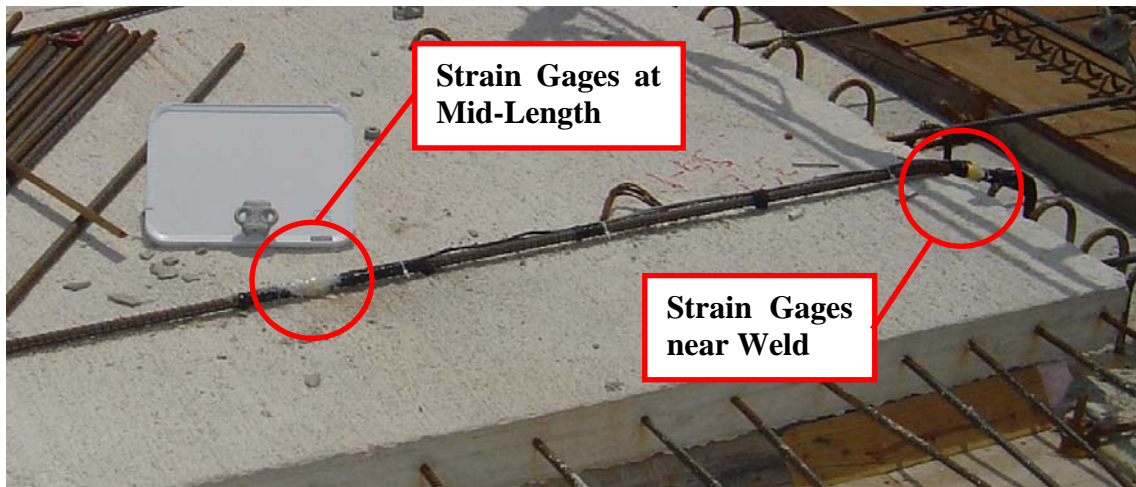


Figure 3-18 Strain Gages Installed at Mid-Length and at Ends of Bar

As noted above, strain gages were placed on both the right and left sides of each bar. Two gages were installed at each specific location to eliminate the error due to bending of the bars. This correction is highlighted in Figure 3-19. Assuming a

distribution of stress, which is derived from the strain readings, of 2 ksi on one end and 1 ksi on the other, the effective axial stress in the bar is 1.5 ksi. This value is calculated by subtracting off the bending component. Therefore, the axial stress is simply the average stress of the right and left strain gages.

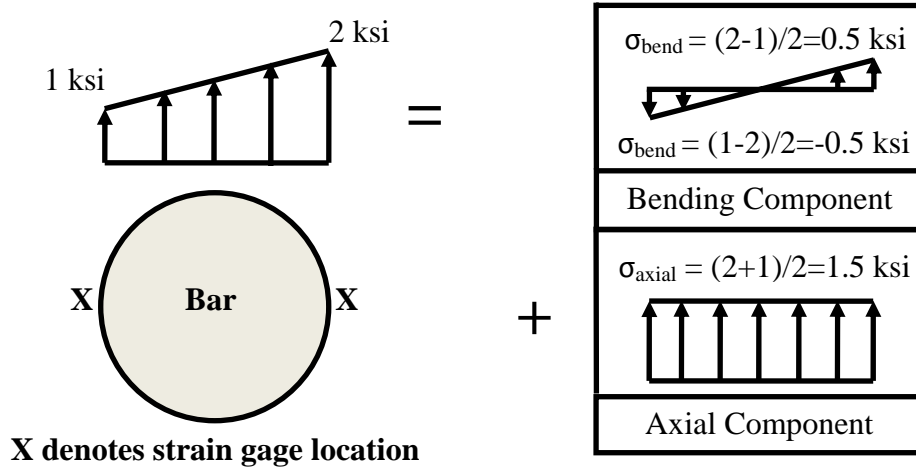


Figure 3-19 Idealized Correction of Stress in Bar Due to Bending

The installation of strain gages to the top bracing bars is discussed below. The strain gages were traditional foil backed gages obtained from Texas Measurement (Gage Factor = 2.12). Specific details on the strain gages are provided in Section 3.4.1. A strain gage installed on a top bracing bar is shown in Figure 3-20. The strain gages were placed on the bars by first sanding the surface smooth and then cleaning with acetone. A two-part adhesive was then used to bond the gage to the steel bars.

Field sites are harsh environments that create additional complications for instrumentation as compared to laboratory instrumentation. Thus, two levels of protection were used for to guard against moisture and mechanical damage. The first protection level consisted of a shrink-wrap coating tape from Texas Measurement, type CT-D10, as shown in Figure 3-21. After placing the tape over the strain gage, the tape was heated to shrink around the gage surface, thereby providing some moisture and mechanical protection. A second level of protection provided was from a silicone adhesive, which gave mechanical protection once it hardened (Figure 3-22). The silicone

is a special formulation (Dow Corning® 3145) obtained from Vishay that will not react with the strain gage adhesive.



Figure 3-20 Installed Strain Gage on Top Bracing Bar



Figure 3-21 Heating Protective Tape on Top Bracing Bar

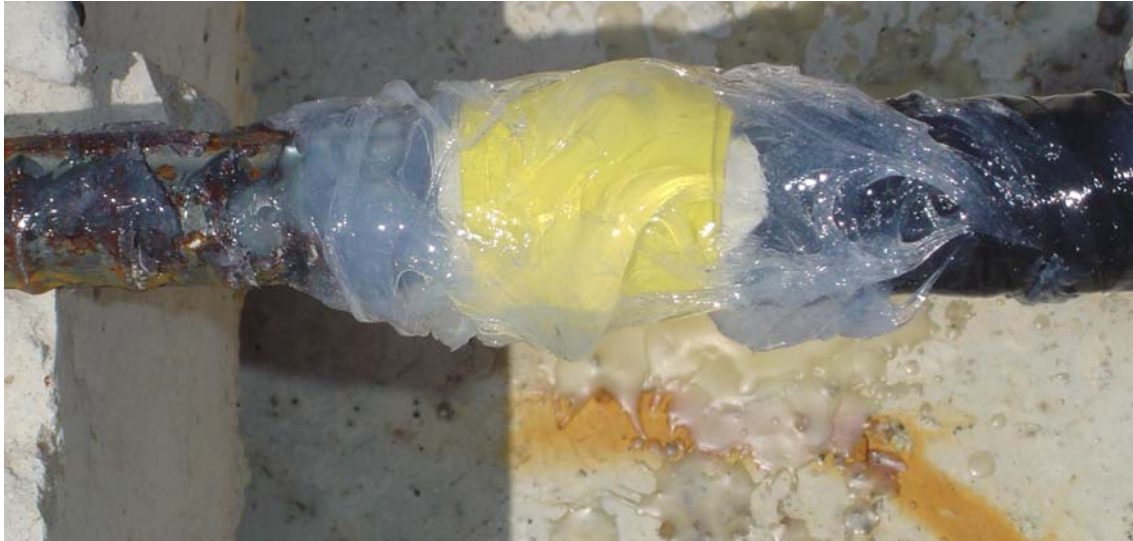


Figure 3-22 Silicone Applied as Moisture Protection to Top Bracing Bar

3.2 STEEL BRIDGE WITH SKEWED SUPPORTS (US 82-19TH STREET BRIDGE)

The 19th Street Bridge over US 82 Highway in Lubbock, Texas, is a steel plate girder bridge with skewed supports of approximately 60°. In addition to the study on overhang construction documented in this thesis, two other TxDOT sponsored research studies obtained data from this bridge. These other two projects include TxDOT project 5-1772 Implementation of Lean-On Bracing technique and study 0-5701 Cross-Frame and Diaphragm Layout and Connection Details.

The instrumented bridge is a two-span continuous system with six steel plate girders. The overall span of the individual girders in the bridge is 289.5 feet, with a length of 150.5 feet for Span 1. The steel plate girders are 54 inches deep with 18 inch wide flanges and are spaced at 8.2 feet on-center. The 8.5-inch deck was formed by permanent metal deck form (PMDF) between interior girders and wooden forms over the overhangs. The overall width of the bridge is 41 feet with overhangs of 3 feet measured from the middle of the top flange of the fascia girder.

3.2.1 Instrumentation Plan for Skewed Steel Bridge

Due to the contractor's lifting sequence, the girders along Span 1 were the focus for the instrumentation at 19th Street Bridge. The instrumentation plan for the bridge is shown in Figure 3-23. The goal of the project was to monitor the local and global deformations of the bridge. The overhang brackets can cause large local forces in the webs of the girders and cause out-of-plane plate deformations. For local deformations, a method developed by Mercan (2005) was used to measure web imperfections. In addition to local deformations, the large skew angle can result in significant interaction between adjacent girders. In terms of global deformations, vertical deflection and torsional twist of the girders due to the deck pour were measured both across the width and along the length of the bridge. A live load test was also conducted at the bridge in conjunction with the other two projects. Yet, the results from the live load test are not presented in this thesis.

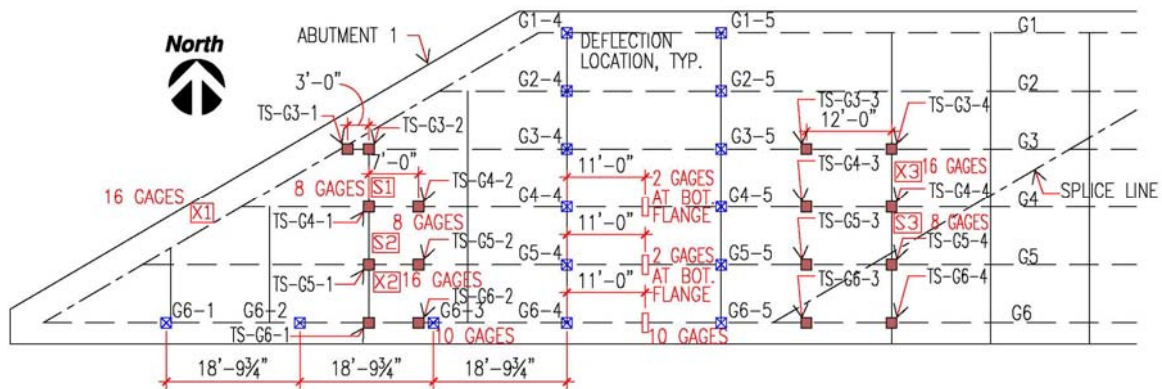


Figure 3-23 Instrumentation Plan for 19th Street Bridge over US 82

3.2.1.1 Vertical Deflections

The same method as described in Section 3.1.1.1 for the prestressed concrete girder bridge in Austin was used in Lubbock to measure vertical deflections. Due to the soil and field conditions on the day of the deck pour, a different isolated base was used in Lubbock than in Austin. Before the deck pour, an isolated base was created using a cement paste. However, as shown in Figure 3-24, excessive rain water collected below

the bridge the week before the deck pour and an alternate base was necessary. The new isolated base took the form of CMU blocks embedded in the soil. Placing the CMU blocks directly on the ground provided a stable foundation for the readings because the soil below the bridge was very hard so that soil settlement due to vibration would be very small. To ensure uniformity and repeatability in readings at each location, the laser was placed along a corner of the CMU block and aligned in the same orientation each time. The CMU blocks were tested as the isolated bases before the deck pour and it was found that the girder elevations were very repeatable.



Figure 3-24 Vertical Deflection Measurement at 19th Street Bridge

A total of fifteen locations were chosen for deflection measurement, as detailed in Figure 3-23. During the deck pour, only nine locations were chosen for deflection measurement (Figure 3-25). A series of live load tests were performed approximately a month later, in which the final six locations were used for deflection measurements. Of the nine measurements, four were taken at Girder 6 (exterior girder), while one measurement was taken at each of the other five girders. Location 4 is the reading at each of the girders, which corresponds to a bracing line that is measured 76.75 feet from

the end of Girder 6 at Abutment 1. Deflection measurements are labeled as girder number and location. Thus, the deflection of Girder 3 at location 4 is denoted G3-4.

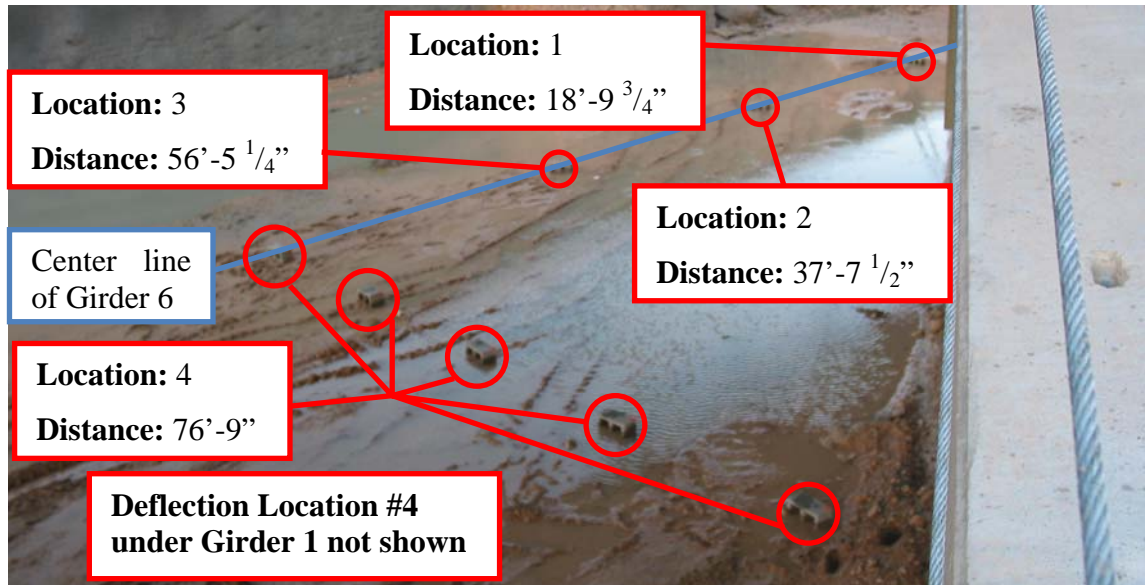


Figure 3-25 Vertical Deflection Measurement Locations at 19th Street Bridge

3.2.1.2 Torsional Rotations

The twist of the girders was determined using the same tilt sensors (Crossbow CXTLA-01-T) used at the prestressed concrete bridge in Austin. The tilt sensors were attached to wooden mounting boards, which were installed on the underside of the girders using C-clamps. Long-term distortions of the boards were not a concern since the tilt sensors were not scheduled to be attached to the girders for more than two weeks.

Sixteen tilt sensors were installed on the 19th Street Bridge. Twelve of the tilt sensors were placed along three interior girders and four along Girder 6, which was a fascia girder on the south side of the bridge. The three interior girders with tilt sensors were Girders 3, 4, and 5. The locations of the tilt sensors are indicated on Figure 3-26. The locations are numbered from Abutment 1 (east side of bridge), while the distances shown are referenced from the east end of Girder 6. The tilt sensor at location 1 on Girder 4 malfunctioned during the pour and is not shown. Also, the numbering scheme for locations 1 and 2 along Girder 3 is slightly different than along the other girders. The

difference is noted in Figure 3-26. Tilt sensors are denoted by the abbreviation TS, girder number, and location number. Thus, the third tilt sensor on Girder 5 is labeled: TS-G5-3.

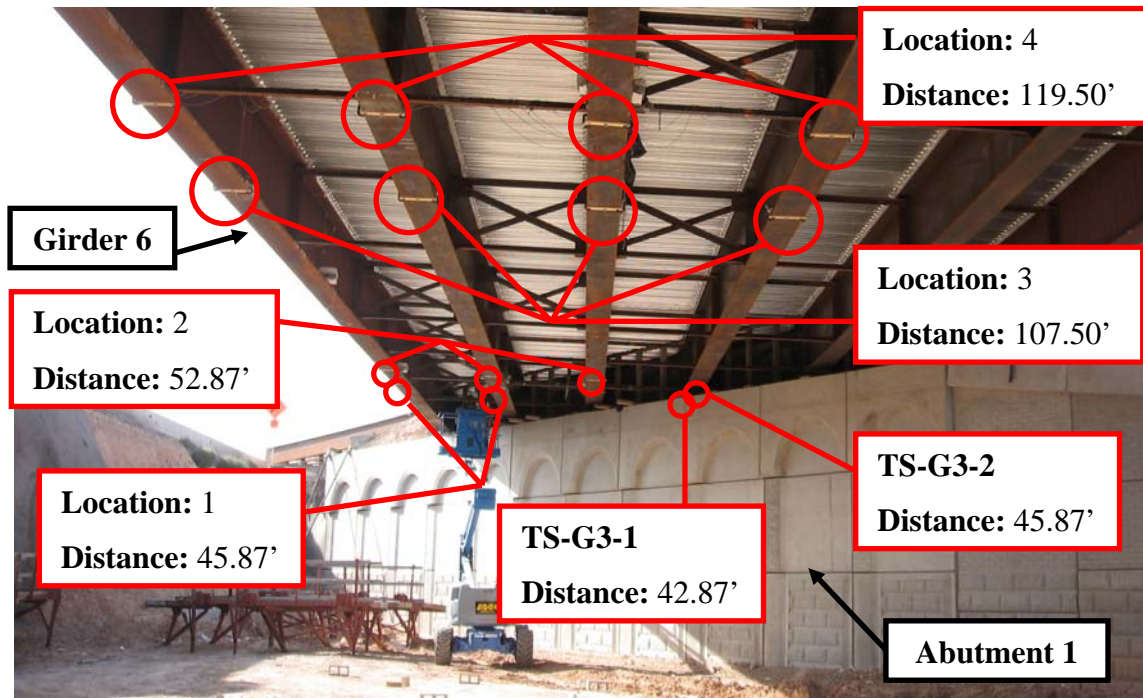


Figure 3-26 Locations of Tilt Sensors at 19th Street Bridge

At the 19th Street Bridge, another method was used to measure rotations at the abutments on the east and west ends. This method was considered a control measurement and is demonstrated by Figure 3-27. A vertical plumb line was created by adding weight to a string. A block of wood was clamped to the bearing stiffener at the support to provide a reference point that could be measured before and after the concrete placement. Figure 3-27 shows the initial measurement being taken prior to the deck pour. A similar measurement was taken at another reference point near the top of the girder. The amount of girder twist was calculated by comparing the deformations that occurred at the two reference points during the concrete placement divided by the distance between the reference points. The control measurement was taken at an exterior (Girder 6) and interior girder (Girder 5) for both Abutment 1 (east end) and Abutment 3 (west end).



Figure 3-27 Control Rotation Measurement at Support of 19th Street Bridge

3.2.1.3 Web Imperfections

The final type of data obtained at the 19th Street Bridge were local plate deformations in steel girder webs due to loading from the overhang brackets. Overhang brackets typically react directly on the web resulting in a large concentrated force that bends the plate. Since steel plate girders typically have relatively thin webs, the forces can distort the web, thereby leading to local instabilities or large web imperfections that get locked into the girders once the deck cures. Since the brackets in Lubbock are the heavy-duty type, the brackets are spaced further apart and apply larger forces at the web. However, this force is compensated by the position of the brackets, which bear near the bottom of the web. The difference in position of the overhang brackets for the 19th Street Bridge and Span 14 of SH 71-SH 130 can be seen in Figure 3-28. For the 19th Street Bridge, the impact of plate bending in the web is expected to be less than at the Span 14 Bridge due to the position of the bracket.



Figure 3-28 Difference in Location of Overhang Bracket

Web imperfections were measured using a potentiometer displacement gauge (PDG), which was developed by Mercan (2005). The PDG consists of an aluminum channel with 5 linear potentiometers equally spaced across the channel. The system measures the profile and magnitude of the imperfections in a plate. Readings from the potentiometers are recorded by a Campbell Scientific CR5000 Datalogger, which is equipped with a switch for PDG measurements.

Web imperfections are determined by comparing measurements in the field to a flat reference. In Mercan's research, the reference was a "zero-bar" that was calibrated to a machinist's lathe. To eliminate the need to calibrate all of the PDG to a machinist's lathe each time a test occurred, Mercan used a calibrated zero-bar. However, since only two different web depths were evaluated in this project, the zero-bar was not used. Instead, the positions of the potentiometers were determined relative to a milling table, which represents a flat surface. Since the potentiometers were not removed from the

PDG between tests, the position of the potentiometers remained constant from one test to the next. Thus, the imperfection in the webs was found by subtracting the position of the potentiometers relative to the milling table from the field readings. An example of the correction is shown in Figure 3-29. Additional details of the web imperfection readings can be found in Mercan's (2005).

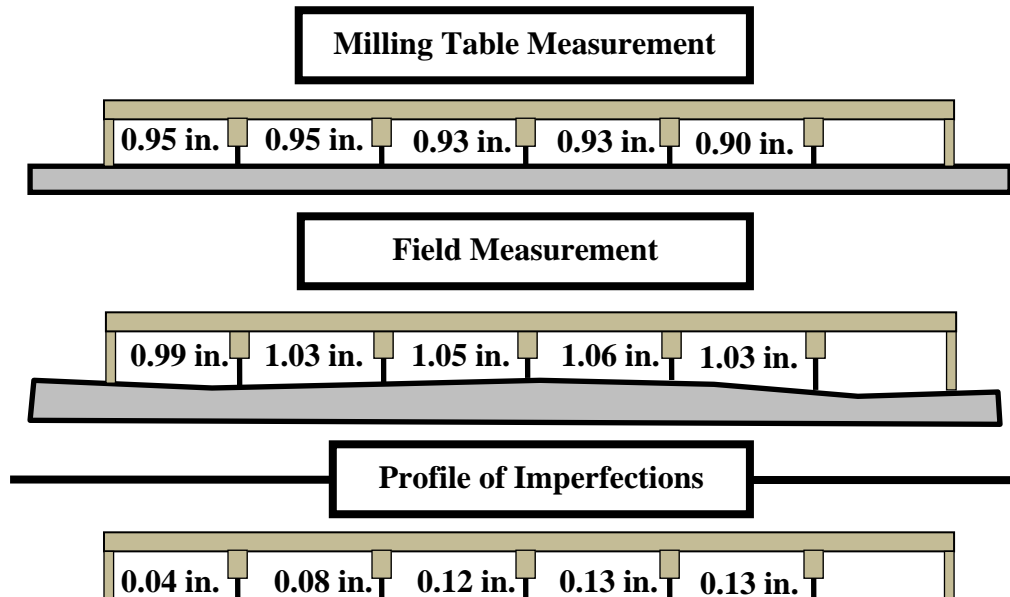


Figure 3-29 Example of Correcting Data from Potentiometer Displacement Gauge

The stations of measured web imperfections are indicated in the plan view shown in Figure 3-30. The measurements were taken along Girder 6 (exterior) and Girder 5 (interior). Defining the portion of the web between two adjacent lateral bracing lines (i.e. locations of cross frames or struts) as a panel, measurements were taken at three locations, equally spaced along the panel as well as at each panel end (Figure 3-30).

Three phases during construction were identified as important for measuring web imperfections. The first period is soon after the girders are lifted into position to get a baseline imperfection reading. The next phase is after the deck has been poured to record imperfections due to the presence of the additional load. Finally, the last period is after the overhang brackets have been removed from the bridge to determine if there is any recovery. A total of three readings were taken at each station to ensure accurate

measurements. If a potentiometer was noticed not to return to its original position, an additional reading was taken at the same location.

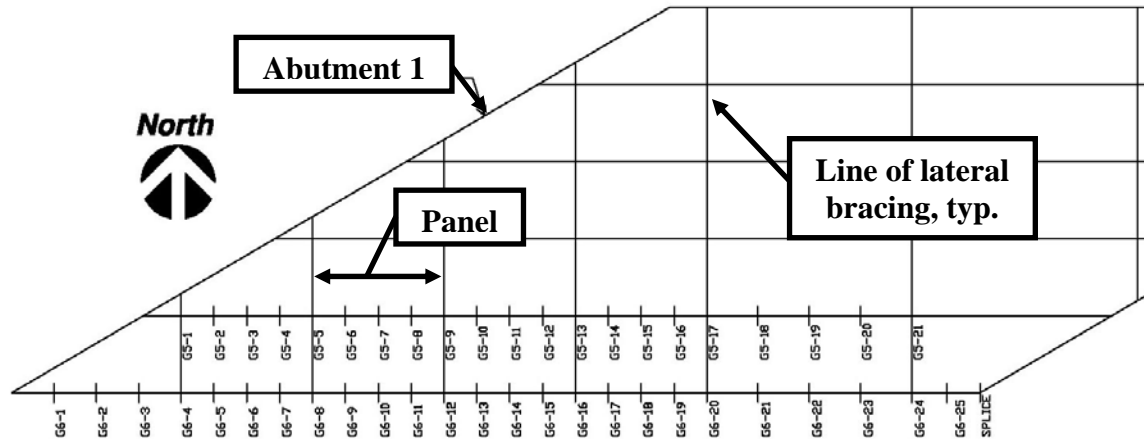


Figure 3-30 19th Street Bridge Web Imperfection Plan

3.3 CURVED STEEL BRIDGE (SH 71-SH 130)

A curved steel bridge at the SH 71 eastbound to SH 130 northbound direct connector was chosen for instrumentation. The study related to overhangs was performed in conjunction with research for another TxDOT sponsored project, 0-5574 Curved Plate Girder Design for Safe and Economical Construction.

The bridge investigated was a three-span continuous curved steel system at the interchange between SH 71 and SH 130. The total bridge length was nearly 550 feet with individual span lengths of 185 feet (Span 14), 205 feet (Span 15), and 158.5 feet (Span 16). The radius of curvature along the center line of the bridge is approximately 1,220 feet. Four plate girders with 84 inch deep webs and 24 inch wide flanges were spaced at 10.33 feet on-center. The overall bridge width was 38 feet due to overhangs of 3.5 feet, measured from the middle of the top flange of the fascia girder to the edge of the bridge. The bridge features an 8.5-inch concrete deck formed by permanent metal deck form (PMDF) between interior girders and wooden forms over the overhangs.

3.3.1 Instrumentation Plan for Curved Steel Bridge

Girder 3 and Girder 4 along Span 14 of the curved steel girder system were instrumented and monitored for local and global deformations from girder erection to the concrete deck pour. Strain gages were installed at three locations along each girder and two cross frames (Figure 3-31). Data from the strain gages during these periods were reported by Schuh (2008). The location of the overhang reaction was shown in Figure 3-28. Local deformations were monitored using the PDG method outlined in Section 3.2.1.3 that was developed by Mercan (2005). In addition, vertical and torsional deformations of the girders during the deck pour were measured at multiple locations across the width and along the length of the bridge. Though the girders and cross frames were instrumented and erected in March 2007, the concrete deck pour of Span 14 did not occur until April 2008 due to a delay in the construction schedule. Meanwhile, a frontage road under Span 14 was opened in September 2007 to allow operation of SH 130, which greatly reduced access to the equipment on the bridge.

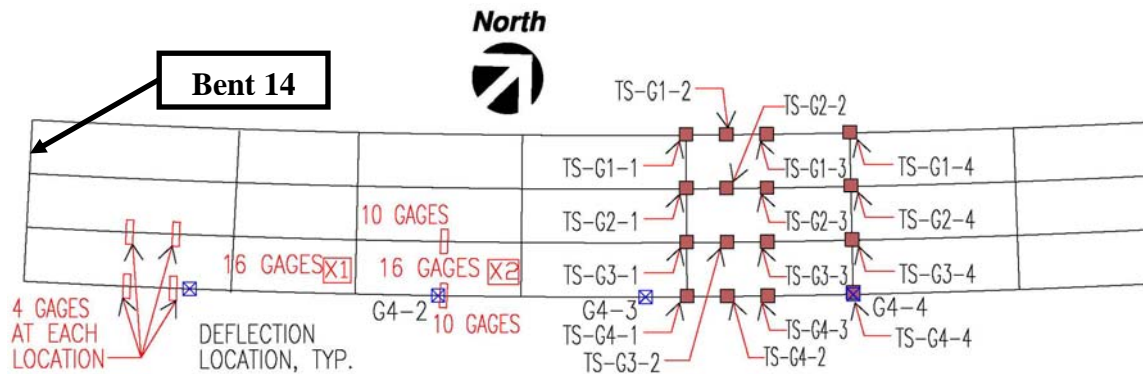


Figure 3-31 Instrumentation Plan for SH 71-SH 130 (Span 14)

3.3.1.1 Torsional Rotations

Sixteen of the Crossbow CXTLA-01-T tilt sensors were used to measure twist of the four girders. The tilt sensors were attached to steel plates and installed on the underside of the girders using C-clamps. Though plywood was considered for the mounting plates used to attach the tilt sensors to the girders, steel plates were used since

long-term distortions of the mounting plates were a concern due to the long period between instrumentation and deck pour.

As depicted in Figure 3-31, the tilt sensors were installed on each girder in the fifth panel measured from Bent 14. A panel is defined as the region between two adjacent cross frame lines. Tilt sensors were installed at each end (Location 1 and 4), near the panel's first quarter point (Location 2), and near the panel's midpoint (Location 3). A picture of the instrumented panels is shown in Figure 3-32. The locations are numbered from Bent 14, while the distances shown are referenced from the Bent 14 end of each girder. Tilt sensors are denoted by the abbreviation TS, girder number, and location number. Thus, the third tilt sensor on Girder 2 is labeled: TS-G2-3.

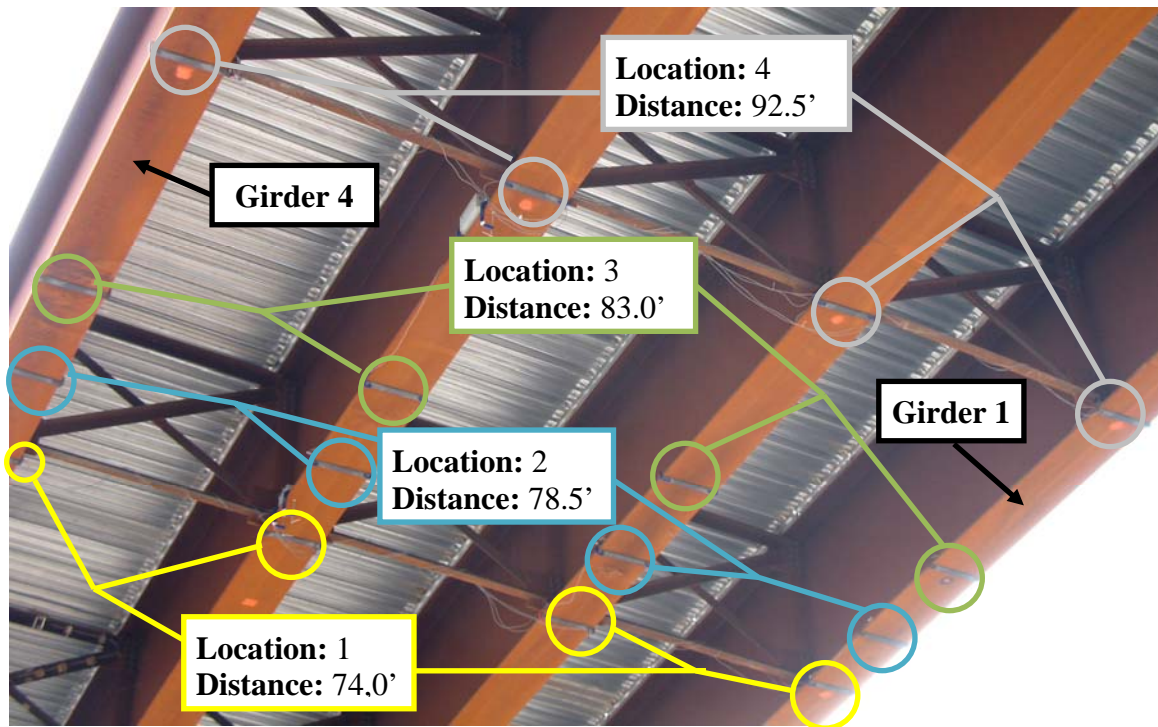


Figure 3-32 Location of Tilt Sensors at SH 71-SH 130 (Span 14)

3.3.1.2 Web Imperfections

A similar procedure as described in Section 3.2.1.3 to monitor local plate deformations was used in Span 14. A large number of stations (74) were laid out to measure local deformations since the combination of a deep web and position of the

overhang brackets at mid depth was expected to have a significant influence on deformations (Figure 3-28). The stations of measured web imperfections are indicated in the plan view of Span 14 shown in Figure 3-33. The measurements were taken along Girder 4 (fascia) and Girder 3 (interior). Following the information in Section 3.2.1.3, measurements were taken at three phases during construction. Panels of the webs were defined by the web stiffener locations. For the baseline imperfection readings, measurements were taken at panel ends and at three locations equally spaced at Panels 1, 2, 5, and 6. At Panels 3 and 4, measurements were taken at 2 foot intervals to better capture the variations in web deformations along the panel length (Figure 3-33). These panels were heavily investigated to track global deformation trends in the panels. However, due to the time constraints involved with traffic under the bridge, only 32 locations, at Panels 2, 3, and 6, were chosen for the “after the deck pour” measurement. After the overhang brackets had been removed, the number of locations was further reduced to six due to constraints from the contractor. In addition, as will be shown from the results presented in Section 4.3.2, the sample of the magnitudes of the deformations did not warrant extensive measurements. A total of three readings were taken at each station to ensure accurate measurements. If a potentiometer was noticed not to return to its original position, an additional reading was taken at the same location.

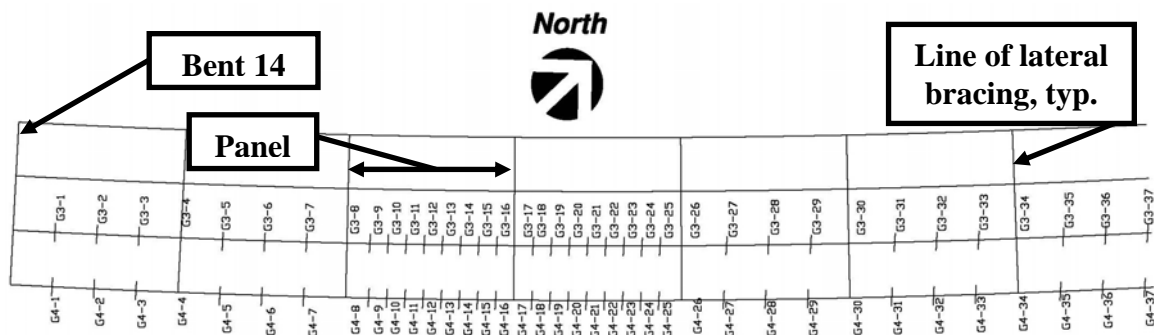


Figure 3-33 Web Imperfection Plan at SH 71-SH 130 (Span 14)

3.4 DATA ACQUISITION SYSTEM

For each of the sites, a data acquisition system manufactured by Campbell Scientific, Inc. was used. The system consisted of a CR5000 Datalogger combined with AM416 Multiplexers. Both instruments in the system provide precision measurement capabilities with the benefits of being versatile, portable, and durable.

By itself, the CR5000 is limited to monitoring 40 single-ended sensors or 20 differential sensors at a time. However, with the addition of multiplexers, the data acquisition system can quickly monitor additional sensors. A multiplexer acts like a router in a network, thereby expanding the available resources of the system. A multiplexer can allow up to 32 single-ended sensors that do not require excitation and up to 16 single-ended or differential sensors that do require excitation (full bridge measurements).

Electronic signals are naturally variable due to electronic noise and interference; thus, care was taken when choosing scanning properties for the data acquisition system. In particular, controlling settling time, integration time, and excitation reversal properties with the CR5000 has an impact on the precision of the system. Because dynamic testing was not a concern in the tests, the properties could be optimized. The settling time refers to the time between when an excitation voltage is applied to when the datalogger actually starts recording a value. Allowing a longer settling time prevents the influence of “lag,” which is the time it takes the sensor to represent actual measurement in the system. The integration value represents the time the datalogger integrates a channel being measured. Choosing a longer integration time allows noise to be filtered out of the measurement. Finally, by turning on excitation reversal, the inputs are reversed and a second measurement is made. The two measurements are then averaged and recorded for each reading. This feature removes any voltage offset errors due to the datalogger measurement circuitry, including common mode errors (Campbell, 2001).

A variety of sensors, strain gages, tilt sensors, and linear potentiometers, were used with the data acquisition systems for each of the sites. Those sensors are discussed in the sections below.

3.4.1 Strain Gages

Strain gages from Texas Measurement, type FLA-6-350-11-3LT, were used. This sensor is a general purpose uniaxial gage, 6 millimeters long with a resistance of 350 ohms. The strain gage is temperature-compensated for mild carbon steel and has three parallel lead wires. All strain gage wires were spliced to a thicker gage wire so that the wire was insulated and shielded from possible electrical interference that may be present in the field.

On the datalogger side, strain gages operate as a differential sensor through a full bridge system. Campbell Scientific 4WFB350 4 Wire Full Bridge Terminal Input Modules were used to complete the full bridge of the strain gage. Strain gages generally respond very quickly to excitation, thereby eliminating long lag periods. Therefore, the settling time was set to 3,000 milliseconds for each reading. In addition, an integration value of 16,667 milliseconds was used, which helps filter noise on the 50 hertz level. Finally, the excitation reversal option was turned on, allowing for the average of two measurements to be used for each reading.

3.4.2 Tilt Sensors

The CXTLA series of tilt sensors were used to monitor girder twist in the field. According to the datasheet for these sensors (Crossbow, 2006), inclination of the sensor relative to gravity is measured using a micro-machined acceleration sensing element with a direct-current response. The CXTLA01 is a single-axis tilt sensor, while the CXTLA02 is a dual-axis tilt sensor. The sensors have a $\pm 20^\circ$ range and have a relatively small profile with a width of 1.07 inches and a length of 1.75 inches. The angular resolution of the CXTLA01 is 0.03° with a cross-axis error of less than 5%. All CXTLA01 tilt sensors are calibrated at 25°C by Crossbow before being shipped. As such, all the sensors are

slightly different. A “T” at the end of CXTLA01 represents that the sensor has a temperature channel.

The tilt sensors are shipped with approximately two feet of wire, which is generally not sufficient for most field applications. As such, each sensor was equipped with a female “Switchcraft Inline Connector (#20, 6-pin)” connection before being installed in the field. The sensor is then connected to a shielded extension wire with a male “Switchcraft Inline Connector (#20, 6-pin)” connection, which connects to the data acquisition system. Using the “Switchcraft” connections ensures a good splice between the tilt sensor and extension wire, as well as enabling easy installation and removal so that sensors can be shared on multiple projects.

The tilt sensors can function as either single ended or differential sensors on the CR5000 Datalogger and AM416 Multiplexer data acquisition system. The sensors are powered through the Continuous Analog Output (CAO) ports on the CR5000. Single ended measurements are taken by determining the voltage difference of the sensor’s output signal relative to the ground. Differential measurements are measured by the voltage difference between the high and low inputs of a differential channel, which improves the accuracy of the measurement compared to single ended measurements. All tilt sensors in this study were connected and used as differential type measurements.

It is rarely practical to use a single datalogger only for tilt sensors; thus, the tilt sensors were often mixed with other sensors (i.e. strain gages, multiplexers, etc.). Two possible ways to mix different sensors are discussed below. The first is to mix the sensors on the datalogger side, in which differential sensors (i.e. strain gages, multiplexers, etc.) use up the first few appropriate channels and then tilt sensors are installed on the remaining channels. For instance, if three multiplexers and six CXTLA01-T sensors are used for a project, then differential channels 1-3 can be used for the three multiplexers and differential channels 7-18 (two channels per sensor due to the angle and temperature channels) are available for the tilt sensors. Another way to mix sensors is to use an AM416 multiplexer. Up to eight tilt sensors (due to the angle and temperature channels) can be installed on each multiplexer. A multiplexer can be used to

increase the number of tilt sensors each datalogger can hold as well as decrease the total required amount of wire.

The requirements for wiring the tilt sensors to the CR5000 datalogger and/or AM416 multiplexer are discussed in the following two paragraphs. If the tilt sensor is connected directly to a CR5000 datalogger, the wiring is as follows (see Figure 3-34):

- Red wire goes to excitation channel (i.e., COA1 or COA2)
- White wire goes to H input on differential angle channel
- Brown wire goes L input on differential angle channel
- Black wire goes to GND input on differential angle channel
- Green wire goes to H differential temperature channel
- Add a wire that goes from L input on angle channel to L input on temperature channel
- Add a wire from GND input on angle channel to GND input on temperature channel
- Exposed bare wire goes to any ground channel on the datalogger

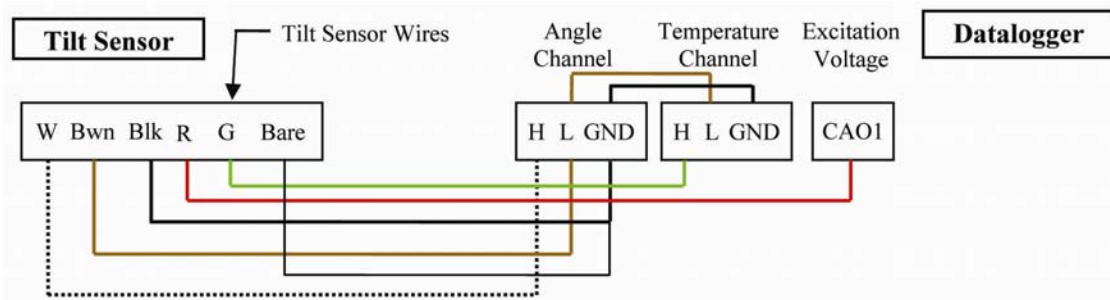


Figure 3-34 Tilt Sensor to Datalogger Wire Diagram

If the tilt sensor is connected to an AM416 multiplexer, the wiring is as follows (see Figure 3-35):

- Red wire goes to L2 of angle (1st) channel of multiplexer
- Black wire goes to H2 of angle (1st) channel of multiplexer
- White wire (angle voltage) goes to H1 of angle (1st) channel of multiplexer
- Brown wire goes to L1 of angle (1st) channel of multiplexer

- Green wire (temperature voltage) goes to H1 of temperature (2nd) channel of multiplexer
- Add a wire that goes from L1 input on angle channel to L1 input on temperature channel
- Add a wire from H2 input on angle channel to H2 input on temperature channel
- Add a wire from L2 input on angle channel to L2 input on temperature channel
- The wiring from a multiplexer to a datalogger is shown below.

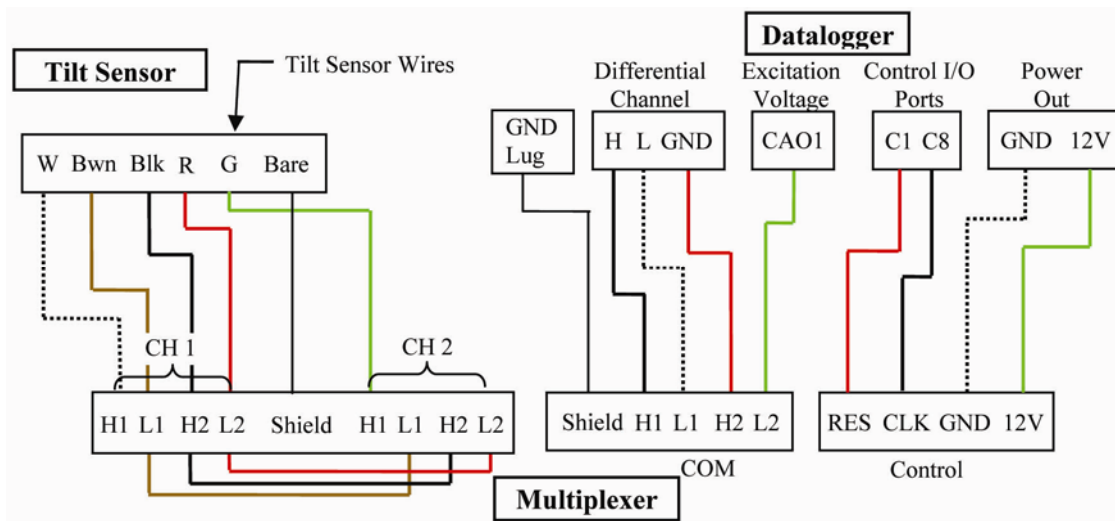


Figure 3-35 Tilt Sensor to Multiplexer to Datalogger Wire Diagram

To ensure accurate measurements at each reading, settling time, integration time, and excitation reversal options were optimized for this instrumentation. Since the tilt sensors electronic response is slightly slower than strain gages, a settling time of 50,000 milliseconds was allowed. For an integration value, 20,000 milliseconds was used to filter noise on the 60 hertz level. Finally, the excitation reversal option was turned on, allowing for the average of two measurements to be used for each reading.

3.4.3 Linear Potentiometer

Linear potentiometers were used to measure plate imperfections by tracking changes in the deformation in the web plates. The potentiometer, when excited by a voltage, produces a resistance output proportional to its displacement. Potentiometers

with a 2-inch stroke were used with the PDG. The stroke is the maximum measurable deflection of the potentiometer. The tip of the potentiometer plunger is slightly rounded to ensure the plunger does not bend.

The linear potentiometers used with the PDG are from ETI Systems, model LCP12-S. For these potentiometers, the red wire represents the signal, the white wire represents the power, and the black wire represents the ground (see Figure 3-36). Potentiometer measurements are recorded using single ended channels on the datalogger. Thus, the wiring should be as seen in Figure 3-36.

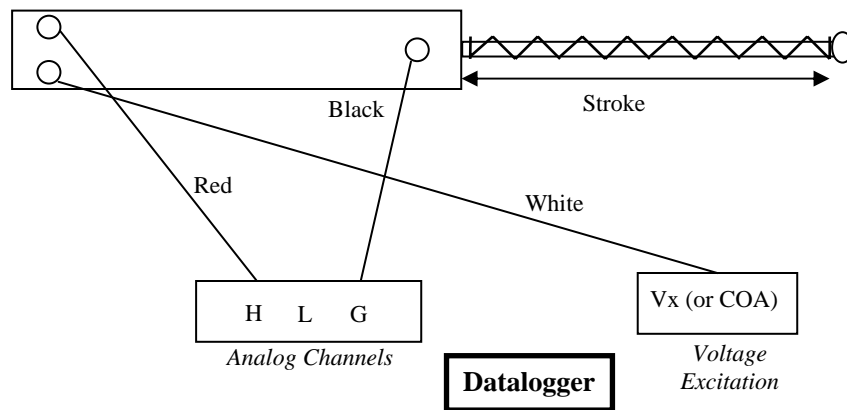


Figure 3-36 Linear Potentiometer

CHAPTER 4

Results

Results are presented in this chapter from the field investigations at the three bridges identified in Chapter 3. The investigations tracked the behavior of the bridges, in terms of vertical deflections, lateral rotations, rebar strain, and web imperfections, due to the construction loading of the concrete deck pour. The field studies and results in this report represent the experimental phase of Texas Department of Transportation Project 0-5706, Impact of Overhang Construction on Girder Design. The results from these investigations were used in the analytical portion of Project 0-5706 to validate a finite element analysis (FEA) computer model that was used to run parametric studies.

4.1 PRESTRESSED CONCRETE BRIDGE (SH 71-SH 130)

Data was gathered during the deck pour on Span 22 of the direct connector of SH 71-SH 130. The data includes strain from some of the key bracing components of the bridge system as well as girder deformations. The strain gages were applied to some of the bracing bars that are welded to the R-bars that protrude from the top of the beams and are provided to help control girder twist from the overhang load. The unit weight of the concrete deck was determined by casting five 6 inch by 12 inch cylinders. The self-weight of the concrete was necessary to obtain an accurate measure of the loading during construction. The concrete cylinders were weighed and the unit weight of the concrete was found to be 148 pounds per cubic foot. By finding the actual unit weight, the error from assuming a concrete unit weight in a computer model is minimized.

The concrete deck for Span 22 was poured on September 19, 2007. Figure 4-1 highlights the timeline for the deck pour. The deck pour started at approximately 4:00am; however, since the contractor was pouring three spans (Spans 21 through 23) that morning, the first two hours did not affect the instrumentation on Span 22. The contractor poured the three decks in reverse order, starting with Span 23 and ending with

Span 21. Pier 23 represents the start of concrete placement on the instrumented span. With a total volume of nearly 400 cubic yards of concrete poured, it took almost 6 hours for the contractor to finish all three spans. The contractor used one screed and two finishing bridges during the deck pour. The screed weighed approximately 13 kips, while both finishing bridges weighed nearly 4 kips each.

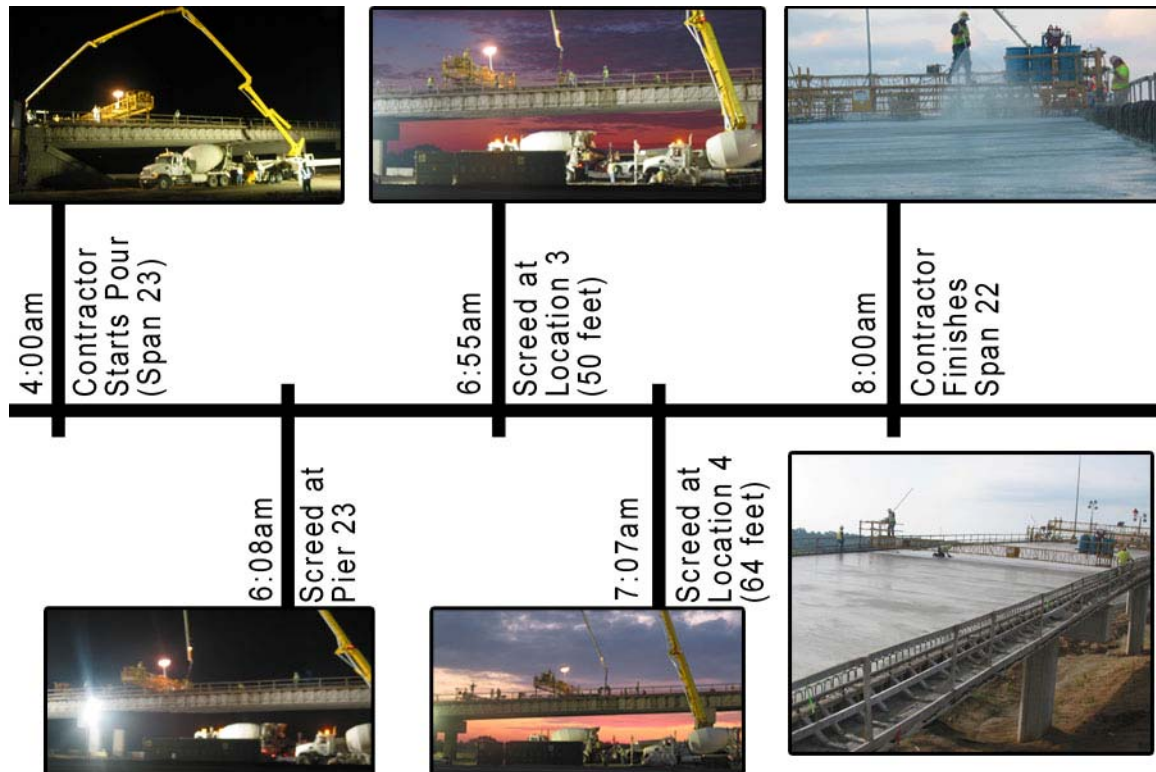


Figure 4-1 Timeline For Deck Pour at SH 71-SH 130 (Span 22)

4.1.1 Vertical Deflections

The vertical deflections were measured using the procedure described in Section 3.1.1.1. The initial measurements were taken the morning of the deck pour when the construction equipment—one screed and two finishing bridges—was located on Span 23 and no concrete had been placed on Span 22. As noticed in Figure 4-2, the fascia girder deflected more than the interior girder, which can be attributed to the distribution of the applied loading during concrete placement. The deflections that were measured represent

the deformations that occurred during the placement of the wet concrete; however the thickness of the fresh concrete differs due to the forming systems that are used across the bridge width. Between interior girders, the deck is formed by precast concrete panels, as shown in Figure 4-3. The precast panels contribute to the deck height, thereby partially loading the girders when the initial measurements were taken. For instance, if a 4-inch thick panel is used and an 8-inch deck is specified, only 4 inches of additional concrete is needed for the deck. In contrast, the full deck height of concrete is poured at the overhangs of fascia girders since removable wooden forms are used in these regions. Therefore, the wet concrete load is often higher on the fascia girders as compared to the interior girders since the interior girders have already deflected due to the precast forms. As a result, the larger amount of wet concrete load on the fascia girders during the deck pour caused more deflection than the interior girders as shown in Figure 4-2.

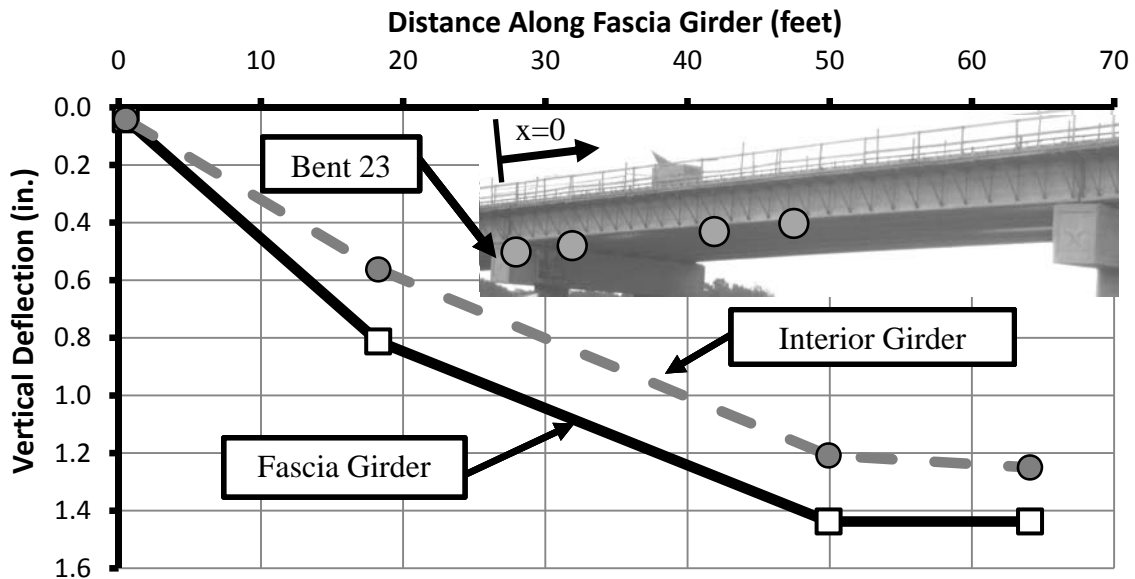


Figure 4-2 Vertical Deflection Due to Deck Pour



Figure 4-3 Typical Cross Section of Bridge

Table 4-1 details the laser distance measurements recorded during the deck pour. The final measurements were determined at approximately 9:30am, when one of the finishing bridges (4 kips) was located near the midpoint of Span 22. The three measurements were averaged and the deflection was calculated by subtracting the final measurement from the initial and rounding to the nearest 16th of an inch. As can be seen from the data, at least two measurements from each set of readings were identical, with the third being within the error (1/16 of an inch) of the laser distance meter. The only exception is G2-3, where the difference between the first and second readings was 3/16 inches. As such, a fourth reading was taken, which was the same as the first reading. The pier was not noticed to move during the deck pour, as seen from the average recorded deflection of 1/32 inch. Thus, error from axial shortening of the piers can be neglected.

Table 4-1 Deflection Measurements at SH 71-SH 130

Location	Initial Measurement	Final Measurement	Deflection
Pier	1.) 16'-9 ⁵ / ₈ " 2.) 16'-9 ⁵ / ₈ " 3.) 16'-9 ⁵ / ₈ " Average: 16'-9 ⁵ / ₈ "	1.) 16'-9 ⁹ / ₁₆ " 2.) 16'-9 ⁹ / ₁₆ " 3.) 16'-9 ⁵ / ₈ " Average: 16'-9 ¹⁹ / ₃₂ "	1 ¹ / ₃₂ "
G1-2	1.) 21'-7 ³ / ₈ " 2.) 21'-7 ¹ / ₂ " 3.) 21'-7 ¹ / ₂ " Average: 21'-7 ¹⁷ / ₃₂ "	1.) 21'-6 ⁵ / ₈ " 2.) 21'-6 ¹¹ / ₁₆ " 3.) 21'-6 ⁵ / ₈ " Average: 21'-6 ²¹ / ₃₂ "	1 ³ / ₁₆ "
G1-3	1.) 23'-0 ⁵ / ₈ " 2.) 23'-0 ⁹ / ₁₆ " 3.) 23'-0 ⁵ / ₈ " Average: 23'-0 ¹⁹ / ₃₂ "	1.) 22'-11 ³ / ₁₆ " 2.) 22'-11 ¹ / ₈ " 3.) 22'-11 ³ / ₁₆ " Average: 22'-11 ⁵ / ₃₂ "	1 ⁷ / ₁₆ "
G1-4	1.) 23'-7 ¹ / ₁₆ " 2.) 23'-7" 3.) 23'-7 ¹ / ₁₆ " Average: 23'-7 ¹ / ₃₂ "	1.) 23'-5 ⁹ / ₁₆ " 2.) 23'-5 ⁵ / ₈ " 3.) 23'-5 ⁵ / ₈ " Average: 23'-5 ¹⁹ / ₃₂ "	1 ⁷ / ₁₆ "
G2-2	1.) 23'-5 ⁵ / ₁₆ " 2.) 23'-5 ⁵ / ₁₆ " 3.) 23'-5 ³ / ₈ " Average: 23'-5 ¹¹ / ₃₂ "	1.) 23'-4 ³ / ₄ " 2.) 23'-4 ³ / ₄ " 3.) 23'-4 ¹³ / ₁₆ " Average: 23'-4 ²⁵ / ₃₂ "	9 ¹ / ₁₆ "
G2-3	1.) 25'-2" 2.) 25'-1 ¹³ / ₁₆ " 3.) 25'-1 ¹⁵ / ₁₆ " (23'-2") Average: 23'-1 ²⁹ / ₃₂ "	1.) 25'-0 ¹³ / ₁₆ " 2.) 25'-0 ³ / ₄ " 3.) 25'-0 ³ / ₄ " Average: 25'-0 ²⁵ / ₃₂ "	1 ³ / ₁₆ "
G2-4	1.) 25'-9 ³ / ₄ " 2.) 25'-9 ⁵ / ₈ " 3.) 25'-9 ⁵ / ₈ " Average: 25'-9 ²¹ / ₃₂ "	1.) 25'-8 ⁷ / ₁₆ " 2.) 25'-8 ³ / ₈ " 3.) 25'-8 ⁷ / ₁₆ " Average: 25'-8 ¹³ / ₃₂ "	1 ¹ / ₄ "

4.1.2 Torsional Rotations

The Crossbow tilt sensors are relatively sensitive to temperature variations. Thus, except to get trends, it is not very useful to analyze changes in the data over time periods with significant changes in the temperature. Major shifts in temperature generally occur during the daytime hours when the ambient temperature changes and direct solar radiation heats the bridge up. More reliable results can be obtained by evaluating the sensors during nighttime hours when the bridge temperature has stabilized. Good

consistency can be obtained by comparing data from the early morning hours before and the day after the concrete has been placed. By comparing rotations from the morning before the deck pour to a morning after the deck pour, a change can be determined which represents the effect of the deck pour. Figure 4-4 shows the sign convention of rotations used at the SH 71-SH 130 Bridge, in which rotations toward the middle of the bridge were considered positive. Therefore, with an orientation from Bent 22 towards Bent 23, a counterclockwise rotation is defined as positive at Girders 1 (fascia) and Girder 2 (interior). The overhang bracket creates a force couple such that the bottom of the overhang pushes inward and the top pulls outward; thus, inward movement is positive because it is the direction expected from the overhang load.

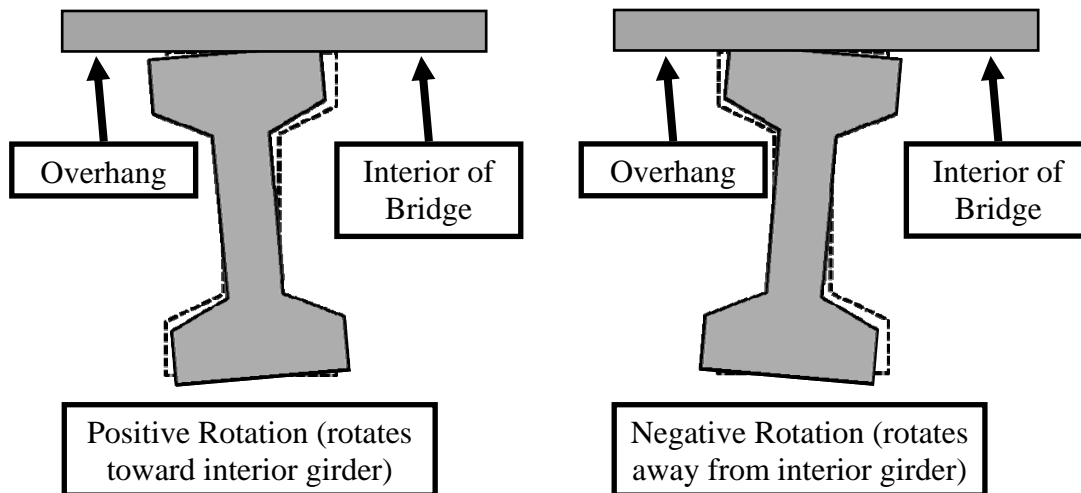


Figure 4-4 Sign Convention of Rotations

To determine the effect of the deck pour, the measured rotation of the tilt sensors relative to a zero value was plotted for three mornings after the deck pour. The zero value was the average of 25 readings taken between 3:45am and 5:45am, at 5-minute intervals, the morning of the deck pour. During that period, the Span 23 deck was being poured and no load was on Span 22. On the mornings following the deck pour, the datalogger recorded readings at 30 minute intervals. The reported values shown in the graphs are relative to the zero value and averaged over four readings from 7:00am to

8:30am on 9/19/2007, seven readings from 5:30am to 8:30am on 9/20/2007, and five readings from 2:00am to 4:00am on 9/21/2007.

The boxed rotation values in Figure 4-5 and Figure 4-6 are the average rotations from the tilt sensors for all three mornings (9/19/2007 through 9/21/2007) and represent the induced rotation from the deck pour. Readings at different times for each morning were used so as to match the temperature channel of the tilt sensors on the morning of the deck pour as closely as possible. By matching the voltages on the temperature channels of the tilt sensors from morning to morning, the error from sensor drift due to temperature fluctuations is minimized. Looking at the graphs, it can be noticed that all data points for a given sensor, except G1-1, are within the precision of the instrumentation, 0.03° . As such, the data from each morning was averaged to determine the boxed rotation values.

Figure 4-5 shows the distribution of twist for the fascia girder, Girder 1, at each tilt sensor for the three mornings after the deck pour. As can be seen from the data, Location 1 (TS-G1-1) recorded a relatively small rotation (0.05°) on the first two mornings, which is approximately half the magnitude of the measurements at the other three locations. The other three locations had recorded rotations of 0.10° , 0.10° , and 0.11° along the length. Comparing the rotation along the length, the rotations did not seem to be a rigid body rotation phenomenon, as was seen at the US 79 bridges near SH 130 in Hutto. Instead, the girders at Span 22 seemed to rotate as a function of the torsion from the overhang.

The measured rotations follow the expected behavior of a girder loaded in torsion. Since the bridge is simply-supported, only positive rotations were expected, which was confirmed by the data. Also, since the bottom flange is constrained at the ends, little to no rotation was expected in that region. In contrast, the maximum rotation is expected in the middle of the bridge, which is seen by the higher rotation at Location 4.

On the third morning, the recorded rotation for Location 1 (TS-G1-1) jumped to 0.12° . If the first two mornings are ignored, the rotation at Location 1 is within the precision of the tilt sensors at the other three locations. Thus, all four locations would have similar rotations, which is a rigid body deformation mode. Due to the high torsional

stiffness of the girders, rigid body deformation dominating the twist is logical. However, the first two mornings might be correct if the sensor malfunctioned on the third morning.

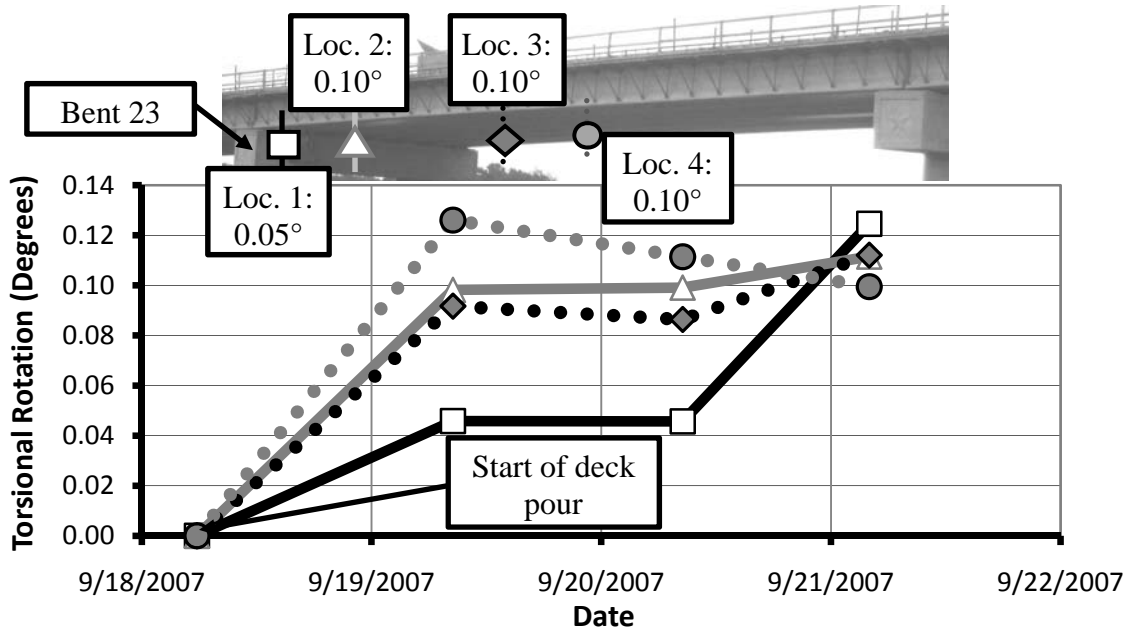


Figure 4-5 Torsional Rotation of Fascia Girder After Deck Pour

Looking at Figure 4-6, there is a different trend for the interior Girder 2 rotations as compared to the fascia girder. As can be seen, the rotations enclosed in the boxes are relatively small with values less than 0.04° . Due to a sensor resolution of 0.03° , most of the average values show negligible rotations along Girder 2. As such, the interior girder essentially did not rotate during the deck pour. Little to no rotation was expected in the interior girders since the torsional load is negligible due to symmetric loading.

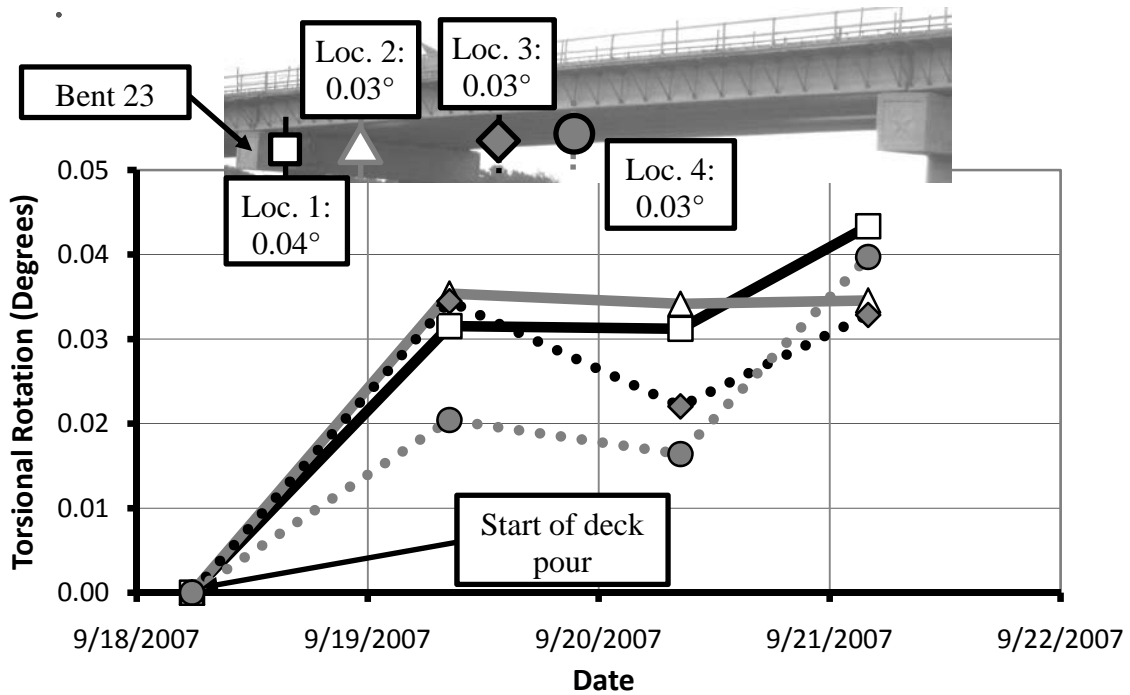


Figure 4-6 Torsional Rotation of Interior Girder After Deck Pour

Figure 4-7 shows the variation of rotation along each girder. This graph consists of the boxed twists reported on Figure 4-5 and Figure 4-6. Both girders behaved in a similar fashion at the support, with very little rotation. However, away from the supports, the behavior of the girders differed, with more rotation occurring at the fascia girder. The error bars on the graph represent the resolution (0.03°) of the tilt sensors. From the graph, the error of the tilt sensors is close to zero rotation for the interior girders. At the fascia girder rotations were on the order of 0.10° . However, the rotation at SH 71-SH 130 was very small when compared to the US 79 bridges around SH 130 in Hutto, which rotated nearly 3° .

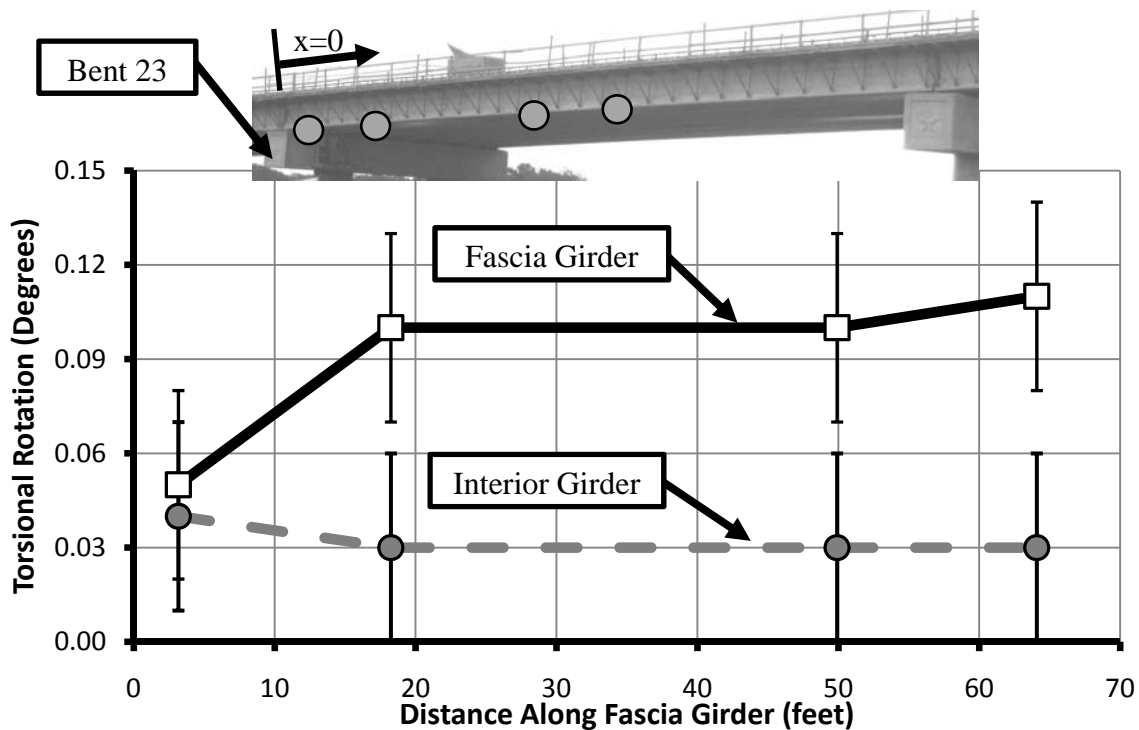


Figure 4-7 Torsional Rotation Along Girder Due to Deck Pour

4.1.3 Strain in Top Bracing Bar

A total of 24 strain gages were installed on the top bracing rebar of Span 22. However, a portion of the strain gages malfunctioned during the deck pour. The gages were likely damaged by the vibrators that were used to consolidate the concrete during deck placement. .

The data acquisition system recorded the strain gage readings every 5 minutes during the pour. The strain was converted to stress by multiplying by the typical modulus of elasticity for steel, which is 29,000 kips per square inch (ksi). To correct for any bending of bracing rebar, the stress in each bar was calculated by averaging the readings of the two strain gage installed at each instrumentation location (see Section 3.1.1.3). Since temperature-compensated gages are not sensitive to dynamic loading or temperature swings, the gages can be monitored with time. Though the strain gages are temperature-compensated for mild steel, the compensation is not perfect, especially at the

temperatures that occurred during the deck pour. Depending on the temperature level, an additional correction can be made to improve the accuracy of the strain gages. However, for the data presented in this thesis, no additional correction for temperature level was made to the strain values. A sign convention was used for this bridge site that considered positive strain/stress values tensile and negative values compressive.

Figure 4-8 and Figure 4-9 show the distribution of stress in the top bracing bars from the start of the data acquisition system to the end of the deck pour at Span 22 (~9:45am). The readings were zeroed relative to the initial strain reading from the datalogger. As discussed in Section 3.1.1.3, two strain gages at each location are needed to correct for any bending in the top bracing bar. On the East side of the bridge (Figure 4-8), only two locations had both strain gages intact after the deck pour. In contrast, strain gages at all four locations on the West side of the bridge were still functioning (Figure 4-9).

Though only two locations (Location 1 and 2) had both strain gages intact on the east side, one of the strain gages at Location 4 is graphed with the Location 1 and 2 gages on Figure 4-8. As seen from the figure, the values from 4:00am to 6:00am are not shown for Locations 2 and 4, as the values fluctuated out-of-range during this time frame when no construction activity was present on the span. The data acquisition system recorded out-of-range values, which tends to represent gages that are no longer bonded to the bars. However, once load was applied to the bridge, the strain gages seemed to stabilize. The strain gages at Location 1 seemed to drift, with two distinct drops at 4:20am and 6:00am, when no load was applied to the bridge. Thereafter, the gages stayed at the same strain level. Location 2 was a spot where the strain gages did not record significant changes. At Location 4, the data is characterized by only one strain gage since the second strain gage malfunctioned. The gage results were graphed because it recorded the highest stress change for a single gage, on the order of 5 ksi. However, it should be noted a portion of that 5 ksi is due to bending in the bar. Looking at the bars from the West side of the bridge, the bending was found to be significant. Thus, it is expected that the axial stress at Location 4 would be lower than 5 ksi.

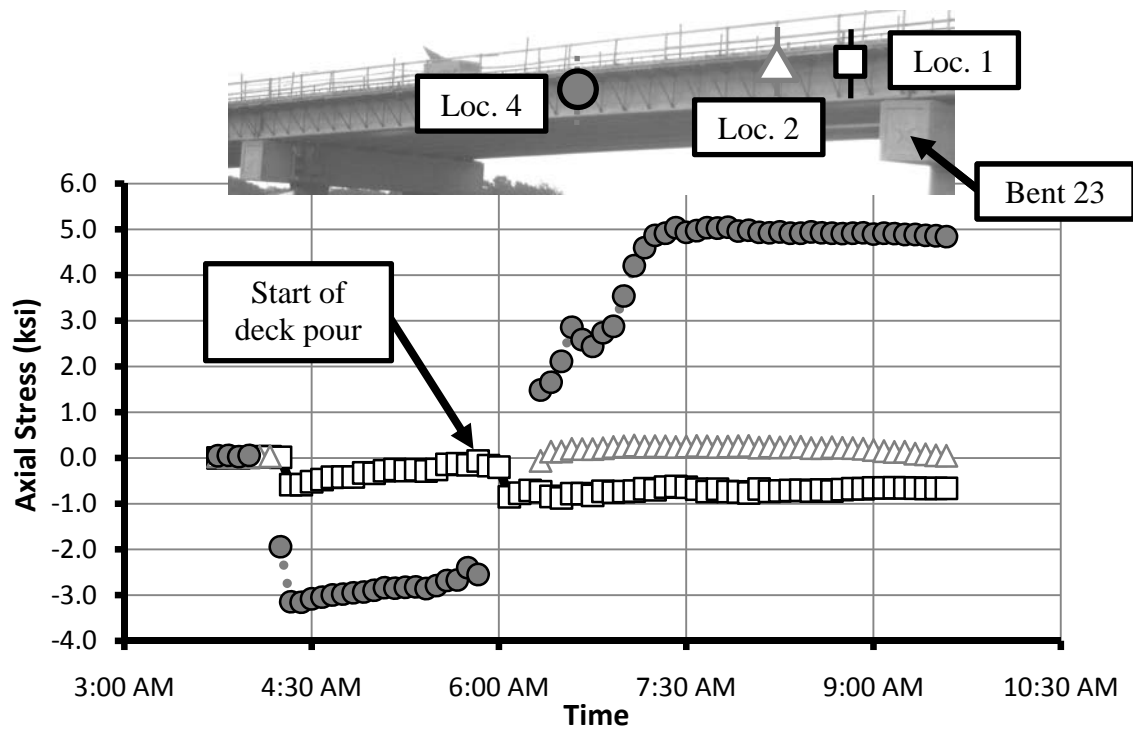


Figure 4-8 Stress of Bars on East Side of Bridge During Pour

Initially, all of the strain gages on the West side of the bridge behaved as expected since the values are near zero stress from 3:40am until 5:45am (Figure 4-9). During this time, no load was present on Span 22 since all the construction equipment was on Span 23. Gages at Locations 1 and 2 on the West side had gage readings similar in magnitude to those on the East side of the bridge, with just the opposite sign. Location 3 indicated tension at the beginning of the pour, yet near the time when the concrete was poured over the gages and the screed passed over Location 3, the gages switched to compression. A peak in the data can be noticed at Location 4 around 7:15am, which corresponds to when the screed passed over Location 4. On the West side of the bridge, the highest stresses, 0.7-0.9 ksi, are at Locations 1 and 4. Considering that #5 rebar were used for the bracing bars, the bar at Location 4 provided about 300 pounds of restraint, which is a small amount.

Theoretically, the fascia girders are expected to twist outward causing a tensile force to develop in the top bracing rebar. In addition, it would be expected that with

larger rotations, the bars are engaged and caused a larger stress to develop. Location 4 followed these expected trends with a tensile stress and was the highest since the most rotation occurred at Location 4. However, one of the highest stress levels was recorded at Location 1, which experienced the smallest amount of rotation recorded directly after concrete placement. This discrepancy could be attributed to the presence of the timber blocking, which tends to complicate the behavior of the bridge. Finally, it is possible that the timber blocking can lead to compressive forces developing in the top bracing bars. This aspect of the research will be analyzed in the parametric study FEA portion of the study that is being completed by another student.

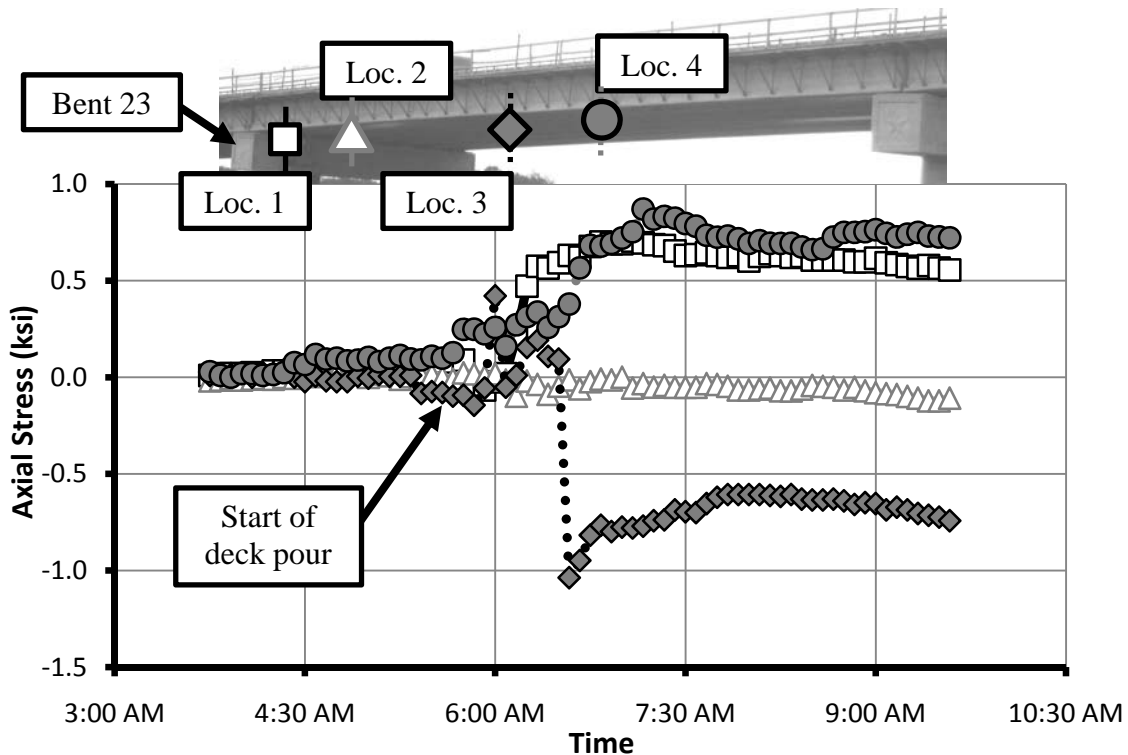


Figure 4-9 Stress of Bars on West Side of Bridge During Deck Pour

The behavior of the strain gages after the deck pour is more complicated, as noticed in Figure 4-10 and Figure 4-11. There was a discontinuity in the data from 9:35am until 11:00am, when the data acquisition system was turned off to download data. After measuring the vertical deflections, the system was turned back on to scan the

instrumentation at 30 minute intervals. Once turned on, as seen in Figure 4-10, all of the gages recorded a drop in stress of approximately 0.5 ksi and the trend continued throughout the day. Through the process of the concrete cooling and drying, the deck will shrink. The shrinking of the concrete will provide a compressive stress, negative value, to the bars, which is seen in the data (Figure 4-10). At about 1:00pm, the data starts to stabilize a little before decreasing again.

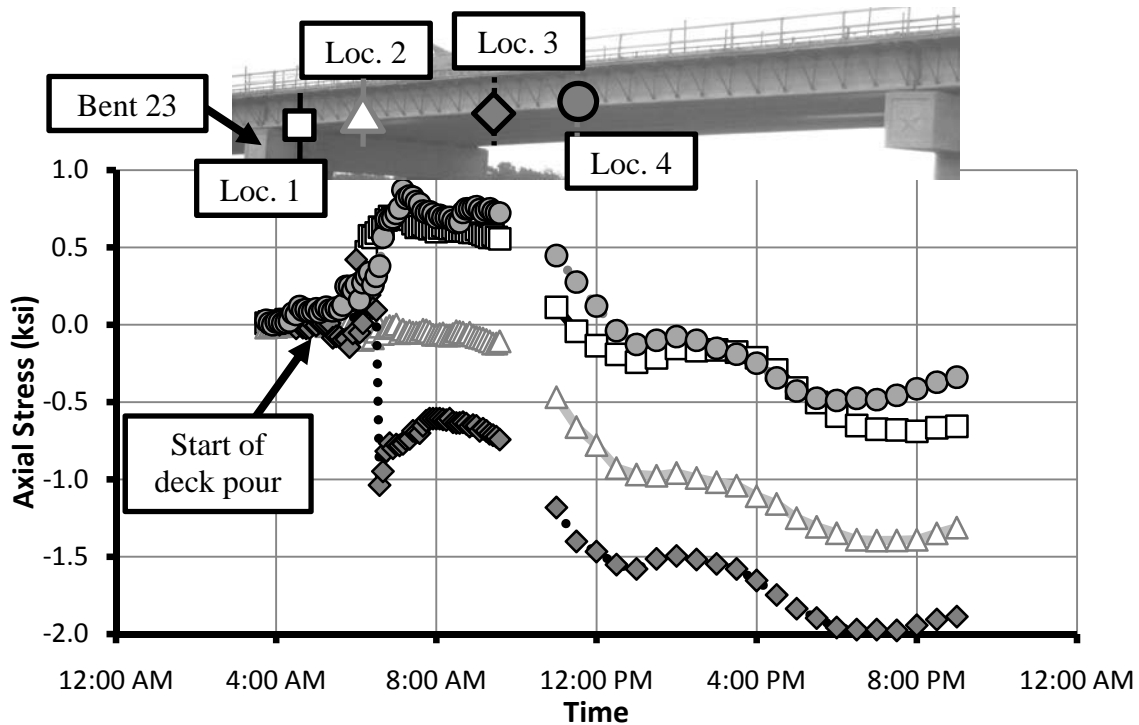


Figure 4-10 Behavior of Strain Gages on West Side of Bridge After Deck Pour

After the concrete sets, two additional trends can be seen in the behavior of the deck after the concrete pour. Looking at Figure 4-11, a line could be added to the graph, as seen at Location 2, which shows a trend of the data increasing with each passing day. Though the datalogger was stopped on the third day (9/21/2007), it seems that the data had started to level off around that time, especially at Location 1. As can be noticed, the values on the third morning (9/21/2007) had nearly reached the levels achieved the morning of the deck pour before the concrete had set. This upward trend was likely due to relaxation of the concrete, which would apply a tensile stress in the bars. The second

trend involves the behavior of the bars from day to day. As noticed, the stress cycles around the line added to Figure 4-11. This cyclic behavior can be attributed to deck expansion and contraction, which comes from daily temperature swings.

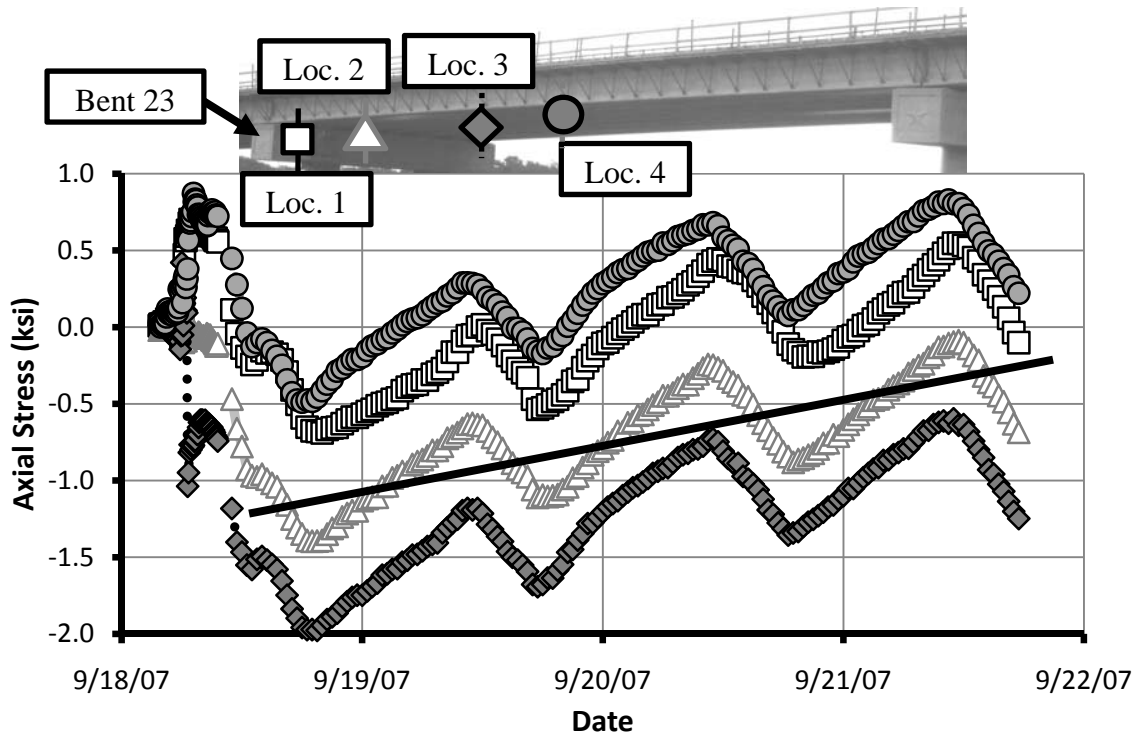


Figure 4-11 Behavior of Bars on West Side of Bridge After Deck Pour

At four locations on the bridge, strain gages were placed at the ends of the bars and the middle of the bars. Nonetheless, some of the gages were destroyed in the deck pour as a result of the pumping and consolidation of the concrete. Since the strain gages at the middle of the bar are more exposed than at the end, a majority of the middle strain gages were lost during the deck pour. One of the west end strain gages at Location 1, near Bent 23, survived the construction process and is plotted with the strain gages at the ends for Location 1. As can be seen from Figure 4-12, the solid lines tracked each other very well. Unfortunately, the second strain gage was destroyed; thus, a comparison of the average stress in the middle and end of bar cannot be evaluated. If the bar is in tension from the overhangs on either side of the bridge, the two locations should have the same stress level.

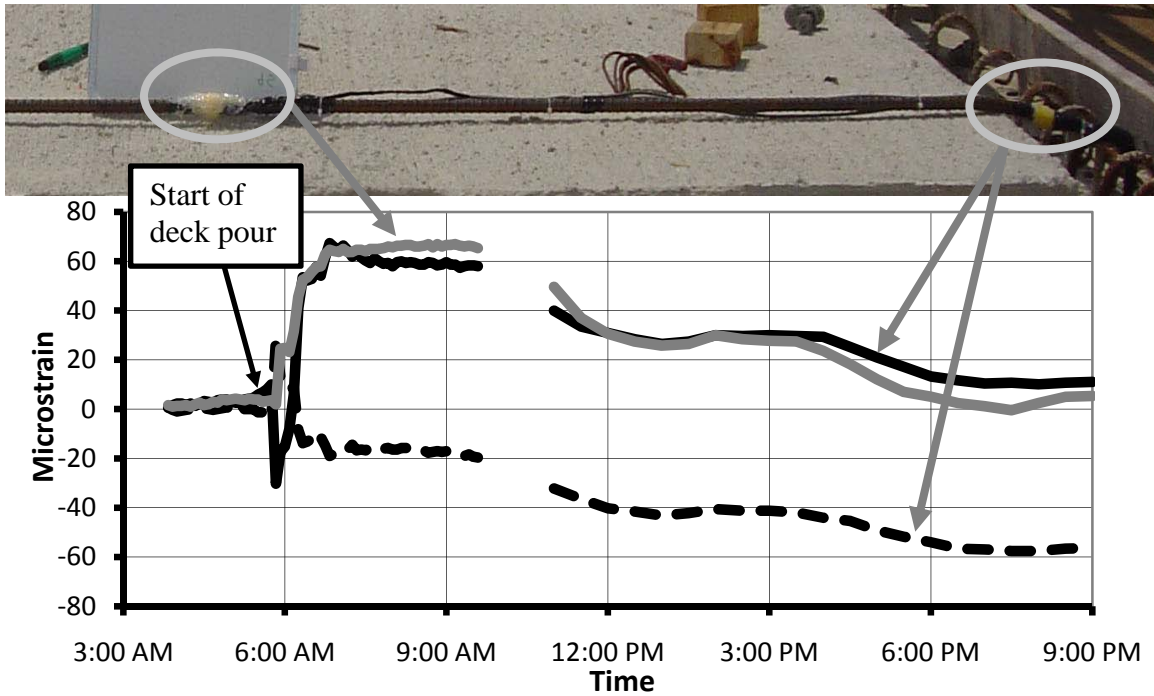


Figure 4-12 Strain At End and Middle of Bar on West Side of Bridge (Location 1)

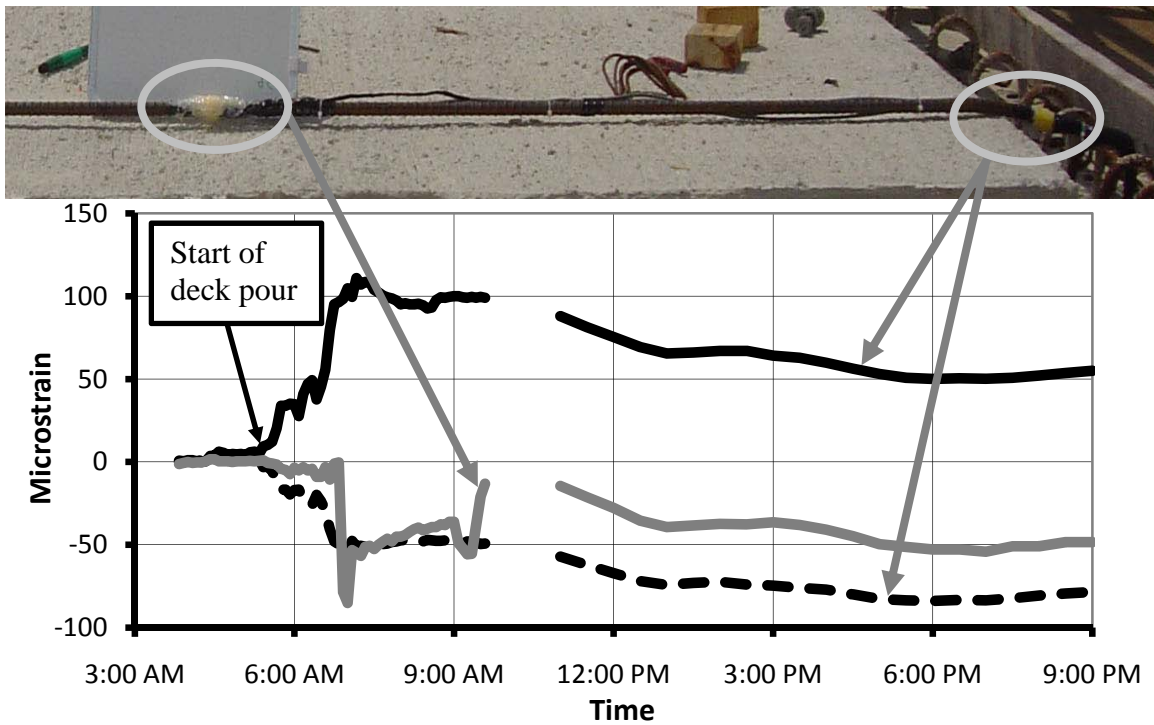


Figure 4-13 Strain At End and Middle of Bar on West Side of Bridge (Location 4)

Figure 4-13 shows the comparison of strain at Location 4 (west end) for gages at the end compared to one gage in the middle of the bar. The agreement between the strain gages located at the middle and end at Location 4 were not as good as observed at Location 1. A difference could arise if friction exists in the bar, such as at the panel-bracing bar interface. Since the second strain gage in the middle of the bar at Location 4 was destroyed, a comparison between the stress in the middle and end of the bar cannot be made.

4.2 STEEL BRIDGE WITH SKEWED SUPPORTS (US 82-19TH STREET BRIDGE)

At the US 82-19th Street Bridge in Lubbock, vertical deflections, torsional rotations, and web imperfections were monitored along a fascia girder and interior girders of Span 1 during the deck pour to determine the impact of the overhang loads. As with the SH 71-SH 130 Bridge in Austin, the unit weight of the concrete was determined for the 19th Street Bridge. Using four 6 inch diameter cylinders that were 12 inches high, the concrete unit weight was found to be 144 pounds per cubic foot.

The concrete deck for the 19th Street Bridge over US 82 was poured on October 4, 2007. Figure 4-14 highlights the timeline for the deck pour. The deck pour started with the west approach at approximately 2:25am. At approximately 5:30am, the screed was positioned over Abutment 1 and started loading Span 1. The contractor continued at a constant pace until 8:15am when work was suspended, at approximately 105 feet from Abutment 1 along Girder 6. The stoppage in concrete placement was done to pre-load Span 2 near Abutment 3 to minimize vertical movement of the bridge during the pour. Since the bridge is continuous, loading the bridge on one span can lead to large movements on the opposite span. Thus, concrete was placed near Abutment 3 to cause a downward deflection, which counteracts the upward movement at Abutment 3 caused by the screed moving towards the middle support. However, because the concrete trucks were delayed, work did not restart until more than 30 minutes later. Around 11:15am, problems were noted with the deck at Span 2. As a result of the delay, the preloaded concrete had started to bond and was therefore no longer plastic before being finished.

Despite the problems, the contractor kept pouring the deck. The total volume of concrete was approximately 570 cubic yards. It took almost 12 hours for the contractor to finish the west approach and the two bridge spans. During the deck pour, one screed and two finishing bridge were used. The screed and one of the finishing bridges weighed approximately 16.7 and 8 kips, respectively, in part because they were oriented parallel to the skew of the bridge. The second finishing bridge weighed 4 kips since it was oriented perpendicular to the bridge width.

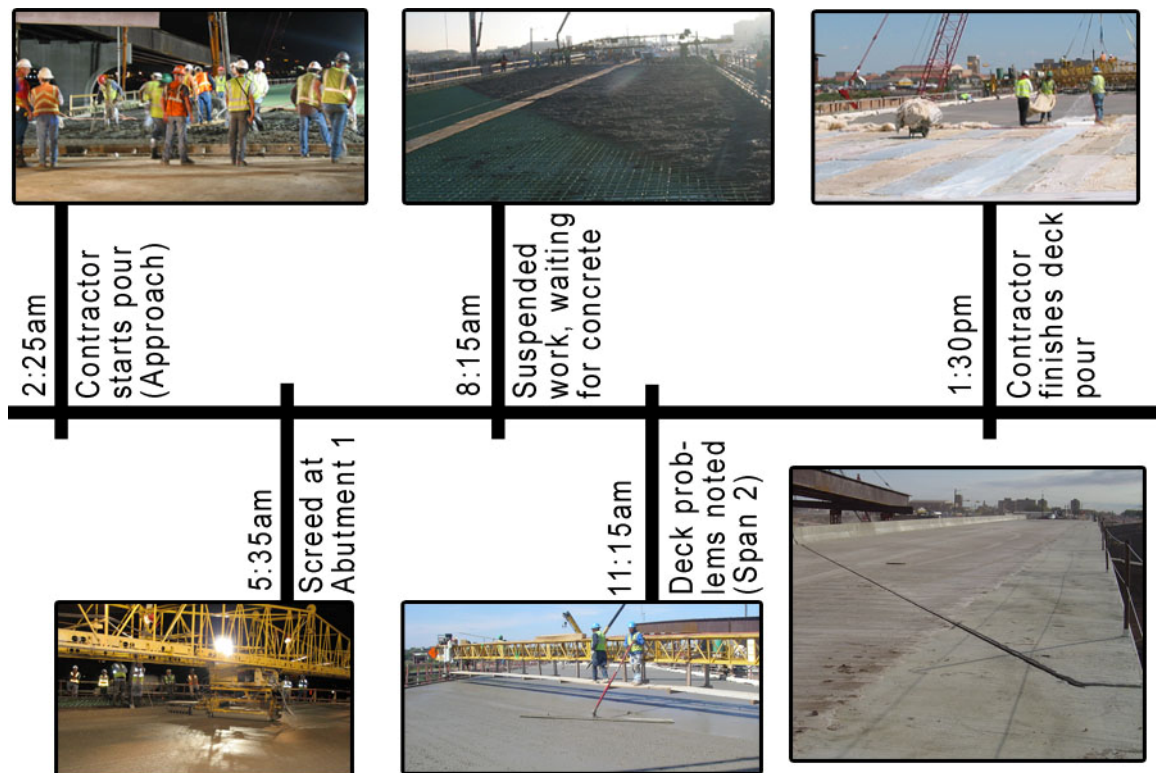


Figure 4-14 Timeline For Deck Pour at US 82-19th Street Bridge

4.2.1 Vertical Deflections

The vertical deflections were measured using the procedure described in Chapter 3.2.1.1. The initial measurements were taken the morning of the deck pour when the construction equipment was located at the approach and no concrete had been placed on

the bridge. Figure 4-15 shows the deflection of the fascia girder due to the deck construction.



Figure 4-15 Vertical Deflection of Fascia Girder Due to Deck Pour

Table 4-2 details the measurements recorded during the deck pour for the fascia girder (Girder 6). The final measurements were recorded at approximately 12:30pm when the last finishing bridge (4 kips) on Span 1, was within 25 feet of Bent 2 as measured along Girder 6. As seen from the table, all three readings from most of the locations were identical. For the locations where all three readings were not identical, two readings were the same with the third reading being within the error (1/16 of an inch) of the laser distance meter. Thus, the procedure was very repeatable.

Figure 4-16 shows the vertical deflection across the bridge for a bracing line located ~77 feet along Girder 6 (measured from the end abutment). This line is the fifth intermediate (not counting the bent plate diaphragm at the support) bracing line along Girder 6. As can be seen from the graph, the girders deflected together, in almost a straight line. Due to the relative location along each girder, Girder 6 was expected to deflect the most and Girder 1 (bracing line is located ~77 feet along Girder 6 and ~7 feet along Girder 1) the least, which is seen from the data. Thus, trends in the deflection measurements recorded from the bridge were as expected.

Table 4-2 Deflection Measurements During Deck Pour at 19th Street Bridge

Location	Initial Measurement	Final Measurement	Deflection
G6-1 (20'-3 3/4" along G6)	1.) 21'-10 15/16" 2.) 21'-10 15/16" 3.) 21'-10 15/16" Average: 21'-10 15/16"	1.) 21'-9 7/16" 2.) 21'-9 7/16" 3.) 21'-9 7/16" Average: 21'-9 7/16"	1 1/2"
G6-2 (39'-1 1/2" along G6)	1.) 22'-1 1/4" 2.) 22'-1 3/16" 3.) 22'-1 3/16" Average: 22'-1 7/32"	1.) 21'-10 11/16" 2.) 21'-10 11/16" 3.) 21'-10 5/8" Average: 21'-10 21/32"	2 9/16"
G6-3 (57'-11 1/4" along G6)	1.) 22'-1 7/8" 2.) 22'-1 7/8" 3.) 22'-1 7/8" Average: 22'-1 7/8"	1.) 21'-10 13/16" 2.) 21'-10 13/16" 3.) 21'-10 13/16" Average: 21'-10 13/16"	3 1/16"
G6-4 (76'-9" along G6)	1.) 22'-1 5/8" 2.) 22'-1 5/8" 3.) 22'-1 5/8" Average: 22'-1 5/8"	1.) 21'-10 11/16" 2.) 21'-10 11/16" 3.) 21'-10 11/16" Average: 21'-10 11/16"	2 15/16"

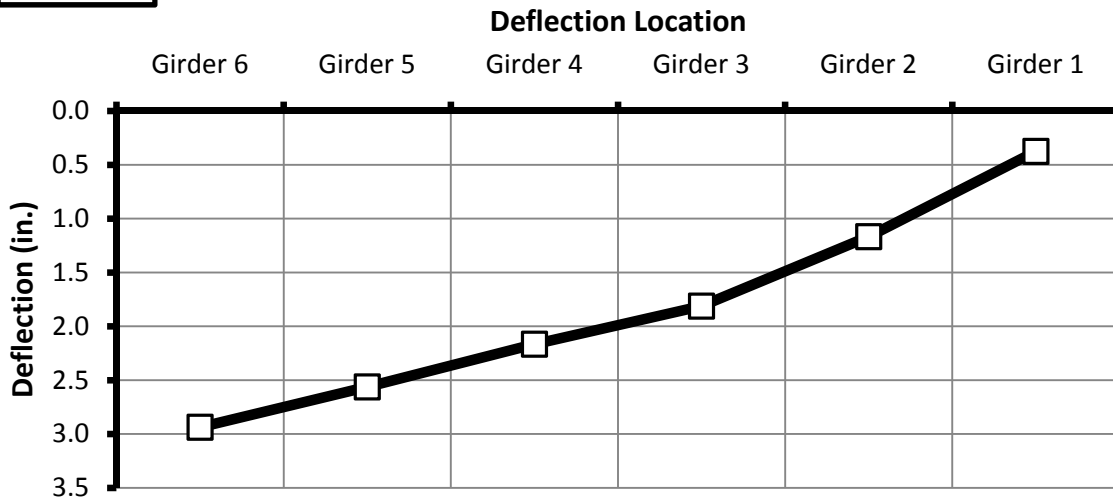
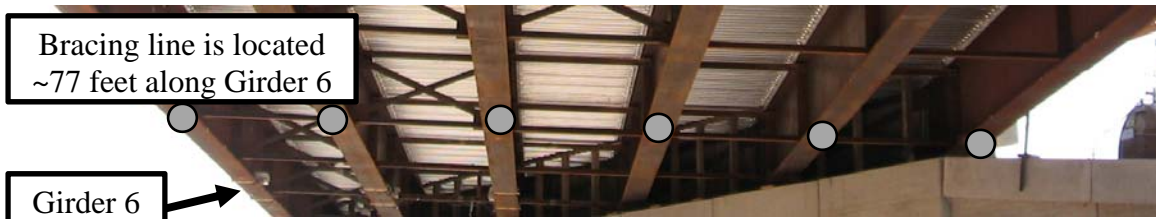


Figure 4-16 Vertical Deflection Along Fifth Intermediate Bracing Line

4.2.2 Torsional Rotations

As noted in earlier sections, the Crossbow tilt sensors are very sensitive to temperature changes. Prior to the bridge construction in Lubbock, multiple tests were performed in the laboratory to determine the relationship between the temperature and angle channels on the tilt sensors. The tests revealed that the variation of the temperature channel with the angle channel was not linear and that all of the tilt sensors have a unique temperature-to-angle channel relationship. Rather than correct the drift in the angle channels when the temperature changed, only data during a time when the temperature was reasonably constant, such as the early morning, was used. In addition, the times were chosen when the temperature reading was close to the recorded temperature from the morning of the deck pour. Following this procedure minimized the error from signal drift resulting from temperature fluctuations.

Though data was recorded at 10 minute intervals during the 19th Street Bridge deck pour, the rotations were found by comparing data at similar ambient air temperatures during the early morning hours. That change comes from analyzing values from morning to morning after the deck pour, when the temperature is nearly constant. During the time after the deck pour, the data acquisition was programmed to record readings every 30 minutes.

The reported values shown in the following section were determined by averaging rotations over the first two days after the deck pour and zeroing to a time before load was applied to the bridge. The zero value was the average of thirteen data points from 1:00am to 3:00am the morning of the cast (10/04/2007), when no load was on the bridge. For the two days after the deck pour, data points were found by matching similar temperature readings after the deck pour to the temperature values immediately prior to deck placement. On the morning after the deck pour (10/05/2007), five readings were averaged from 4:30am to 6:30am. Two days after the deck pour (10/06/2007), seven readings were averaged from 1:00am to 4:00am. Readings from subsequent days were neglected, as the temperature readings were not similar to the deck pour.

A similar sign convention as used with the concrete girders was used for the steel girders and can be seen in Figure 4-17. Looking back-station, or from Abutment 3 towards Abutment 1, counterclockwise rotation is considered positive for Girders 3 through 6.

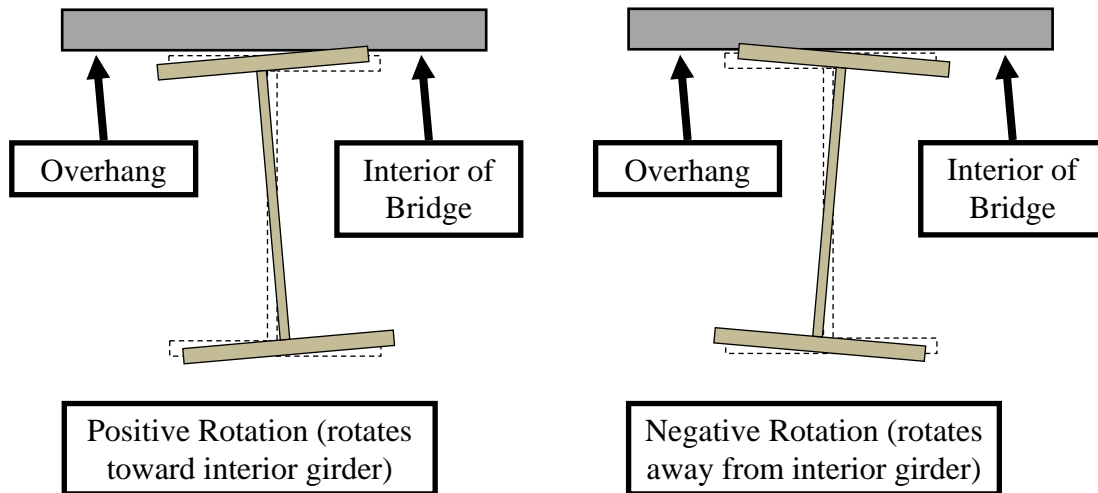


Figure 4-17 Sign Convention of Rotations

Figure 4-18 shows the variation of rotation for Girders 3 through 6, which used rotations derived from Figure 4-19 through Figure 4-23. As can be seen from Figure 4-18, rotations of nearly 0.50° were recorded during the deck pour. Due to the skew of the bridge, the relative location of the tilt sensor along the fascia Girder (Girder 6) is used as the reference point so that twists at the same cross frame or strut could be examined. If the data was plotted relative to its position on each girder, then, due to the skew of the bridge, the lines would be out of phase. From Figure 4-18, the interior and fascia girders behave similarly at each tilt sensor locations, with twists of approximately the same magnitude. This result reinforces what was seen with the vertical deflections in Figure 4-16: the individual girders are moving together as a unit due to the distribution of cross frames and struts throughout the bridge.

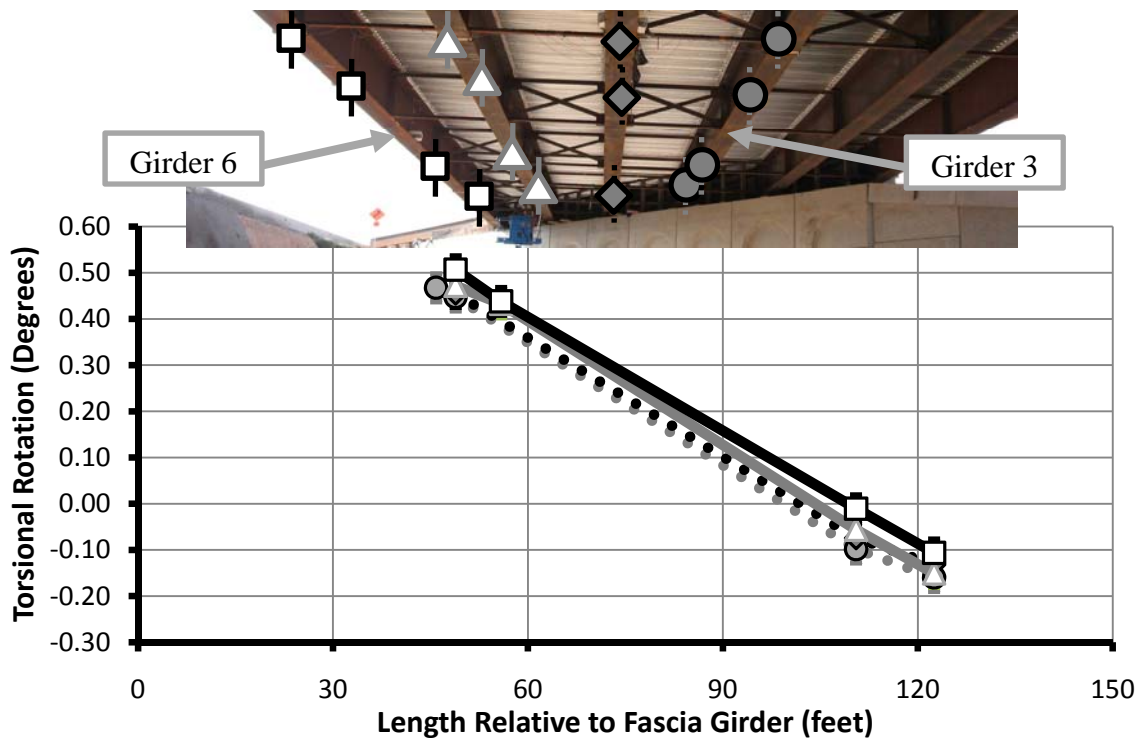


Figure 4-18 Torsional Rotation Along Span 1 of Girders 3-6 Relative to Girder 6

To show the effect of temperature on the tilt sensor, Figure 4-19 details the distribution of rotation of TS-G3-1 throughout many days after the deck pour. Starting with three days after the pour (10/07/2007), the data points shown below were determined by averaging 5 readings from 1:00am to 3:00am every morning. The first few data points shown on the graph were determined by matching temperature readings, as discussed at the beginning of this section. In addition to the rotation data, the temperature of the datalogger at 3:00am each morning is plotted on a secondary axis.

As seen on Figure 4-19, the data varies from as little as 0.45° to as much as 0.65° . Once the deck cures, the steel girders and concrete act compositely and little rotation is expected since any applied torsion is resisted by the entire bridge. As a result, in the early morning, when the temperature is relatively constant for the day—no large temperature differential with time—no net rotation on the bridge is expected. For the difference of 0.20° from minimum to maximum rotation in Figure 4-19, the temperature channel of the tilt sensor recorded a difference of nearly 300 millivolts. If that is

contrasted to a difference of 0.003° (10/11/2007 versus 10/12/2007) from a 0.1 millivolt change on the temperature channel, it can be seen that error is minimized when the values from the temperature channels are matched. By using data from 10/05/2007 and 10/06/2007, an average rotation of 0.47° was determined at TS-G3-1. TS-G3-1 is located approximately 1 foot along Girder 3 which corresponds to a distance of 42.87 feet from the abutment on Girder 6 (the approximate beginning of the bridge).

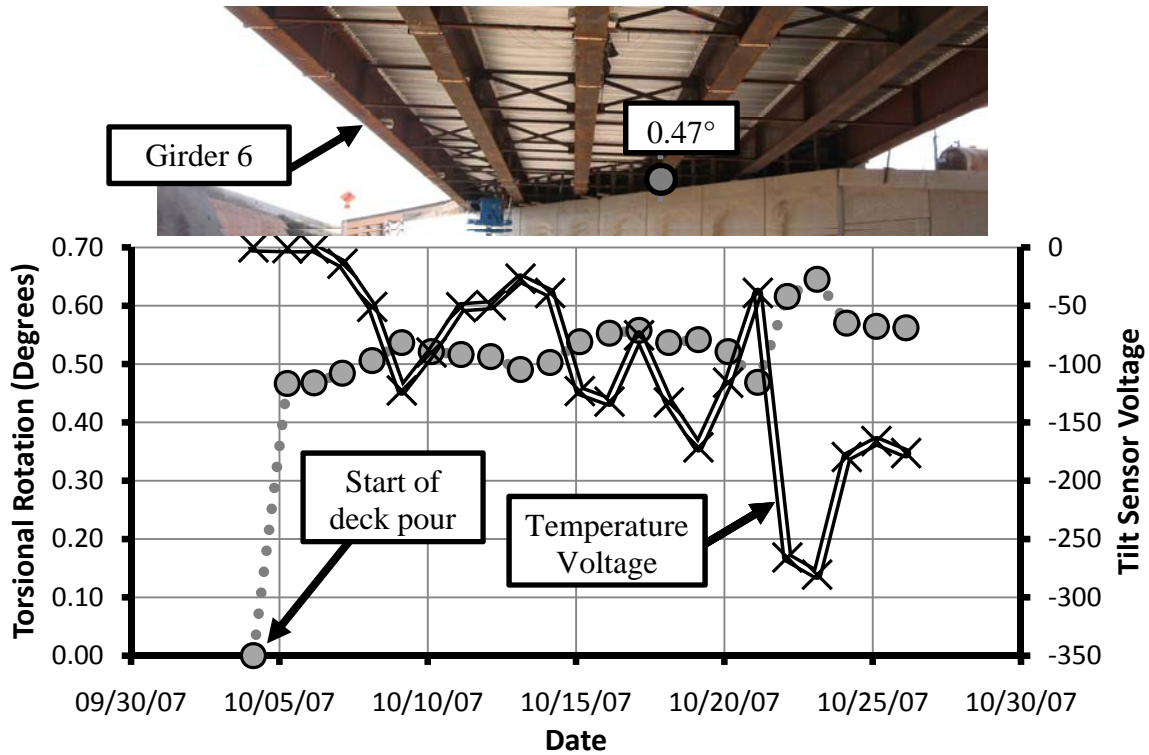


Figure 4-19 Change in Torsional Rotation After Deck Pour (TS-G3-1)

The next two figures show the rotation of the girders at a line of bracing (Figure 4-20) and at approximately the midpoint of the fourth panel (Figure 4-21). The tilt sensors at Location 1 are at a line of cross frames or struts, which measured approximately 49 feet along Girder 6. Location 2, near the panel midpoint, was located approximately 56 feet along Girder 6. As seen in Figure 4-20, there was slightly more rotation at the exterior girder than at the interior girders, 0.51° compared to $\sim 0.46^\circ$. In addition, all of the interior girders are within the resolution of the tilt sensor of each other.

Due to a malfunction of one of the tilt sensors, only two tilt sensors are shown at Location 2. At Figure 4-21, the rotations are essentially the same for the exterior girder and the interior girder.

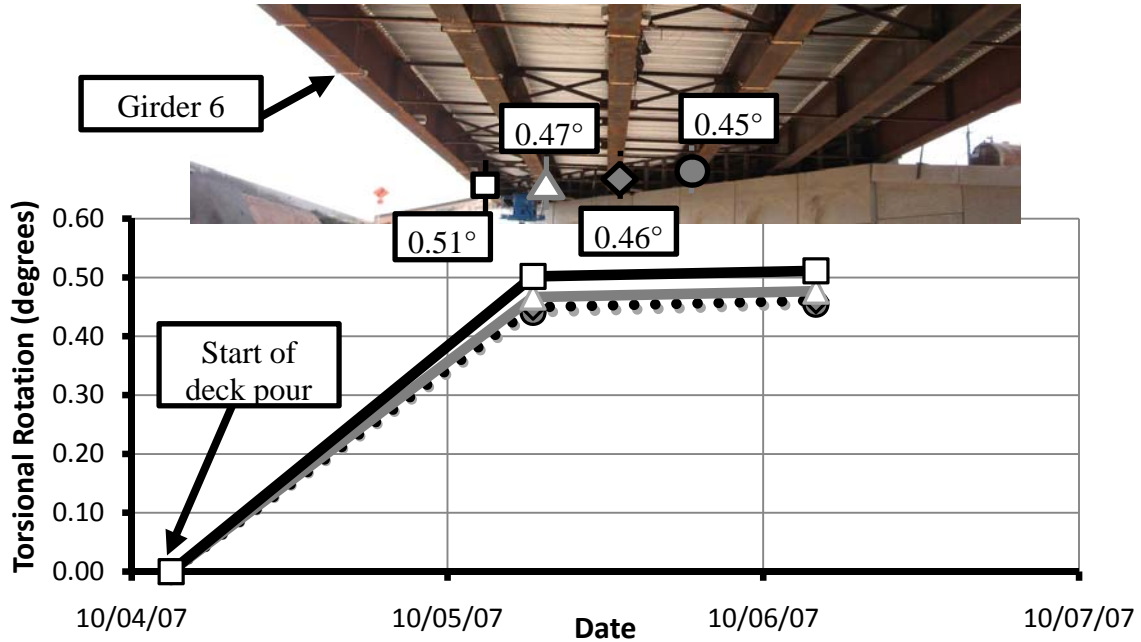


Figure 4-20 Change in Torsional Rotation After Deck Pour (Location 1)

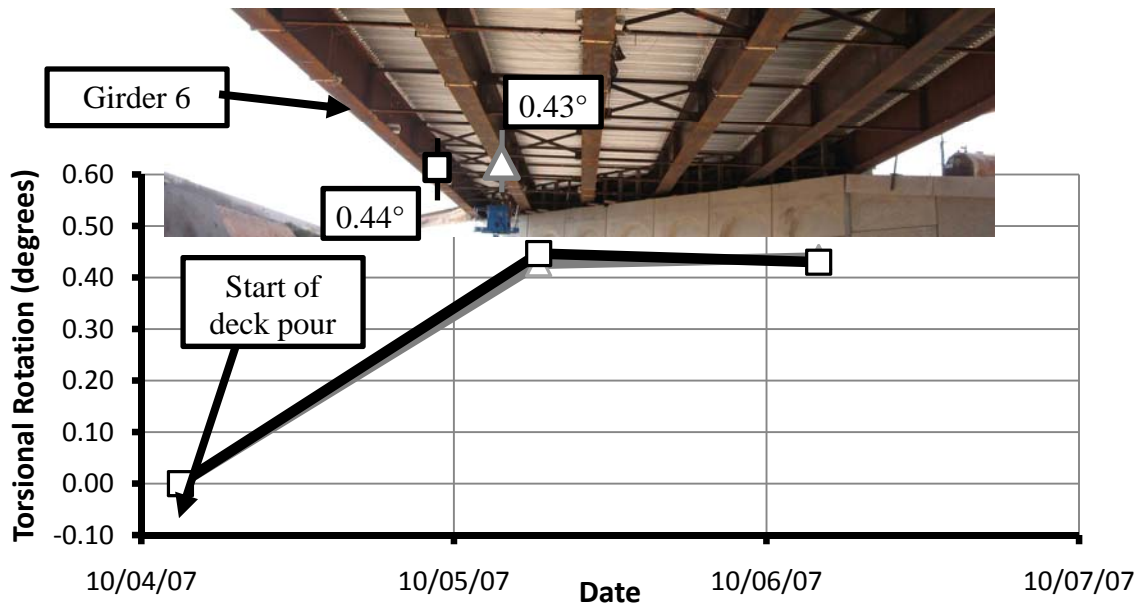


Figure 4-21 Change in Torsional Rotation After Deck Pour (Location 2)

All of the tilt sensors at Location 3 had a negative rotation (Figure 4-22), which looking backstation means the girders rotated clockwise or the bottom of the girder kicked outward from the bridge. From the effect of the overhang load, this type of movement would be counterintuitive for a bridge with normal supports. However, since the bridge is heavily skewed, a negative rotation can occur. As can be seen from Figure 4-22, the exterior girder had less negative rotation than the interior girders. Location 3 was located approximately 110 feet from the end of Girder 6 and is near the midpoint of the seventh panel.

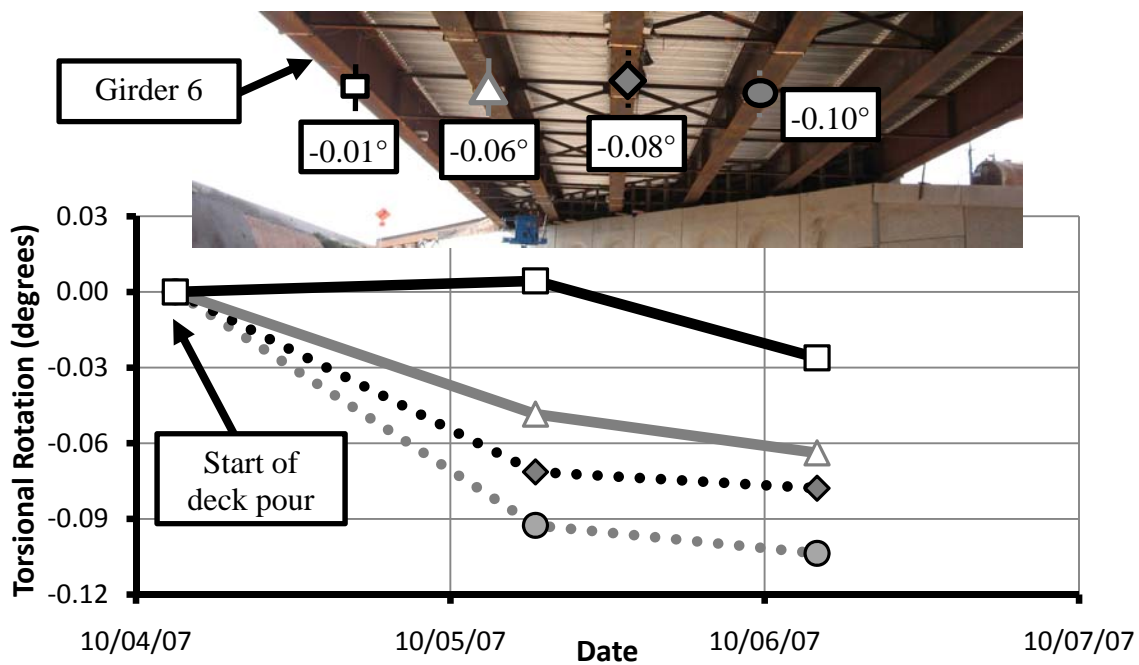


Figure 4-22 Change in Torsional Rotation After Deck Pour (Location 3)

Figure 4-23 shows the distribution of rotation after the deck pour for Location 4, which was at the end of the seventh panel. Location 4 is located approximately 122 feet along Girder 6. The exterior girder rotates slightly less outward than the interior girders. All of the interior girders are within 0.03° of each other. Looking at the rotation data, it can be seen that Girders 3 through 6 experienced larger negative rotations closer to the middle support, which is expected due to the continuous behavior of the skewed bridge.

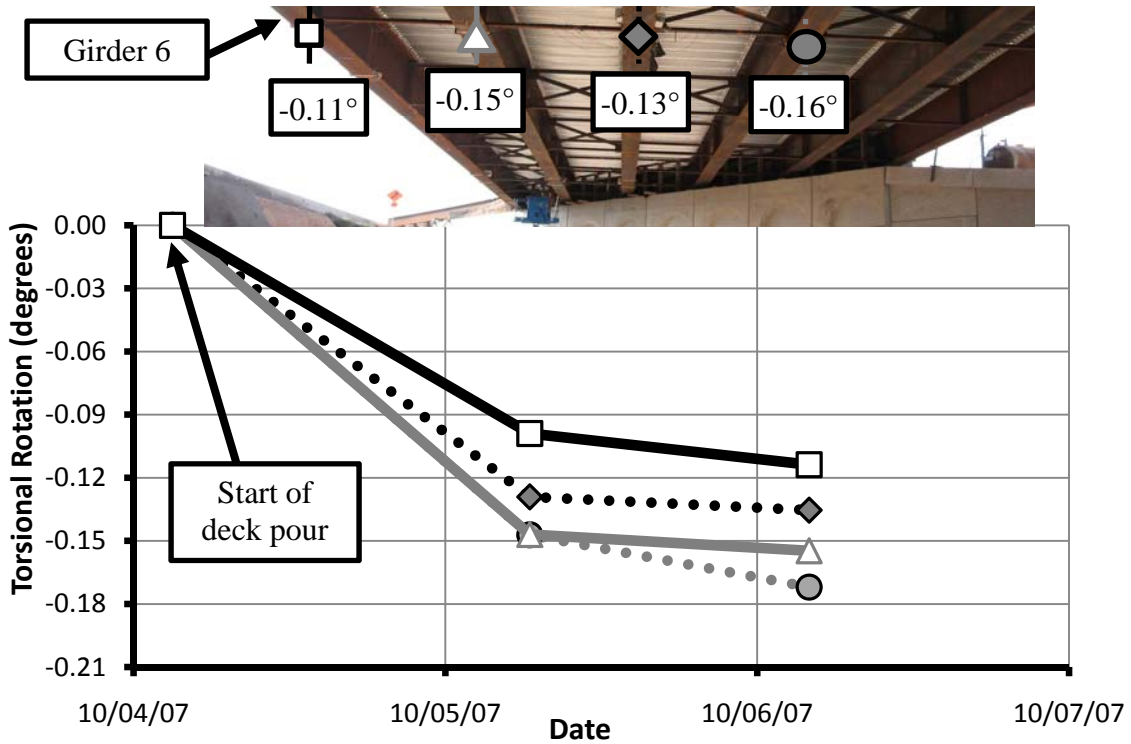


Figure 4-23 Change in Torsional Rotation After Deck Pour (Location 4)

Table 4-3 details the lateral displacement of Girders 5 and 6 at Abutment 1 and Abutment 3, as discussed in Section 3.2.1.3. The lateral displacement is the measurement of the top flange movement relative to a point near the bottom of the flange/stiffener. At Girder 6 of Abutment 1, the top distance was also measured before (3.23”) and after (3.21”) the deck cast, which was found to move a very small amount (0.02”). Though the rotation for Girder 5 and 6 at each abutment was fairly similar, the rotations differed by more than 0.70°. Also, as expected, the rotation at both abutments was larger at the fascia girder (Girder 6) as compared to the interior girder (Girder 5). This is expected behavior because the overhang at Girder 6 should cause additional positive rotation, separate from the global rotation of the bridge.

The lateral displacements at Abutment 1 and Abutment 3 were determined to check the rotations from the tilt sensors. By comparing the rotations from the lateral displacement measurements and the tilt sensor rotations, confidence can be gained in the

measurement techniques used. As seen in the preceding data, the rotations obtained from the tilt sensors matched very well with the rotations from the lateral displacements. For instance, the rotation at Abutment 1, Girder 6, was 0.58°. The rotation at TS-G6-1 (Figure 4-19), which was located approximately 46 feet away from Abutment 1, was 0.51°. From the lateral displacement method, the rotation of an interior girder at Abutment 1 was 0.53°. From a tilt sensor, the rotation at TS-G3-1, approximately 1 foot from Abutment 1, was 0.47°, which is very close to the rotation of 0.53°.

Table 4-3 Torsional Rotation at Bearing Pads

Location	Measurement		Change (in.)	Height (in.)	Rotation
	Initial (in.)	Final (in.)			
Abutment 1, Girder 5	2.75	3.09	0.34	37 1/8	0.53°
Abutment 1, Girder 6	2.77	3.16	0.39	38 3/4	0.58°
Abutment 3, Girder 5	3.27	3.39	0.12	38 1/2	-0.18°
Abutment 3, Girder 6	2.96	3.06	0.10	39 3/8	-0.15°

4.2.3 Web Imperfections

Measurements of web imperfection were taken at a total of 46 locations in three phases: initial (before deck construction), after the deck pour (overhang brackets were still installed), and final (after the overhang brackets were removed). Select results for the 19th Street Bridge are shown in this section to demonstrate the general trends from the data. The remainder of the web imperfection data readings are presented in Appendix A (fascia girder) and Appendix B (interior girder).

The imperfection of the web at each of the phases was determined by correcting the data relative to a zero reading obtained from a flat reference surface in the laboratory, as discussed in Section 3.2.1.3. Figure 4-24 shows the distribution of absolute imperfection of the three phases for a typical location, as well as depicting the sign

convention. For an overhang bracket bearing on the outside of a girder, the load from a deck pour is expected to cause the web to bend inward. Thus, a positive imperfection is in the direction of expected bending.

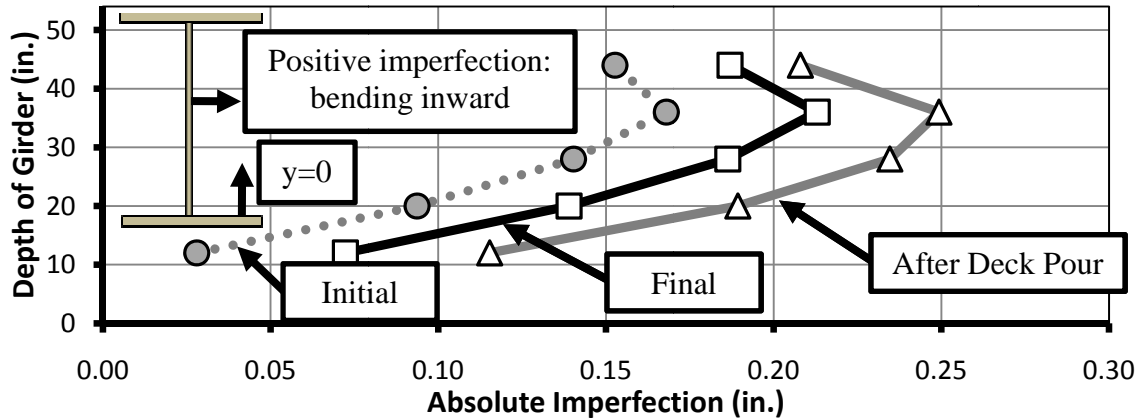


Figure 4-24 Sign Convention & Typical Web Imperfection at 19th Street Bridge

From the absolute imperfection figures, the relative imperfection can be determined and used to analyze the impact of the deck pour. The relative imperfection, as seen in Figure 4-25, is found by subtracting the initial measurement from the later two measurements. For convenience, in subsequent figures of individual locations, the absolute and relative imperfections are plotted side by side.

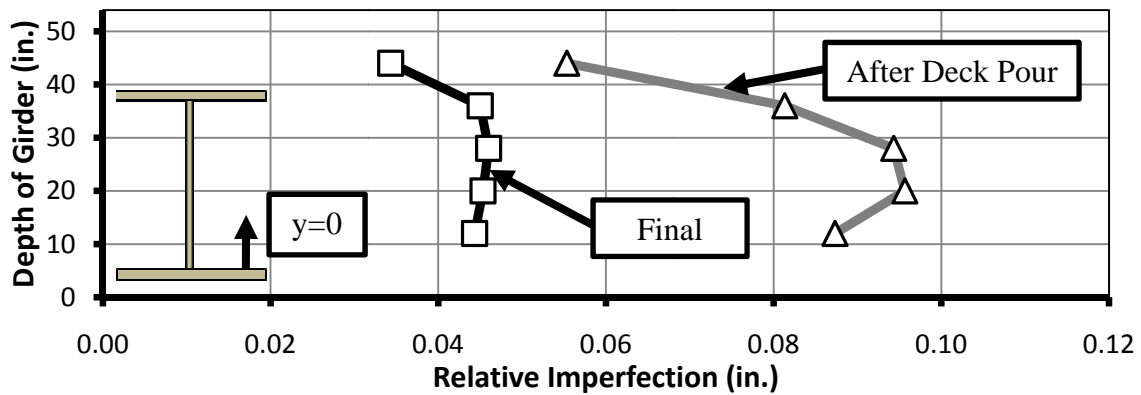


Figure 4-25 Typical Relative Web Imperfection Due to Deck Pour

In the D1.5 code from the American Welding Society (2008), a fabrication imperfection limit of $D/150$ is specified for an unstiffened web. For the webs at 19th

Street Bridge, 0.36 inches of imperfection due to fabrication would therefore be within these limitations. Thus, the webs can be checked for compliance by comparing the initial measurements to the allowed imperfection.

A test was performed to determine the accuracy of the linear displacement potentiometer gauge (LDPG) from day to day. A table in the laboratory with some imperfections was chosen and measured at the same location on two days. The data from that experiment is presented in Table 4-4. The experiment was performed in the same manner as in the field, where three measurements were taken on each day. From this data, it was determined that the LDPG had a resolution of ± 0.02 inches with three measurements. If the number of measurements at each location is increased, the resolution can be reduced to less than ± 0.01 inches. However, more measurements causes more time in the field, which can delay construction or traffic. For the purposes of this research project, a resolution of ± 0.02 inches was deemed sufficiently accurate.

Table 4-4 Accuracy of Linear Displacement Potentiometer Gauge

	Pot 1 (in.)	Pot 2 (in.)	Pot 3 (in.)	Pot 4 (in.)	Pot 5 (in.)
Imperfection on May 22	0.02	0.08	0.10	0.08	0.03
Imperfection on May 27	0.01	0.06	0.08	0.06	0.02
Error	0.01	0.02	0.02	0.02	0.01

Figure 4-26 shows the maximum relative imperfection in the web across the length of the fascia girder. Dashed lines on the graph represent cross frame or strut locations. The figure above the graph is a legend of the girder, in which each line represents a web imperfection measurement location. From the graph, it can be seen that the range of relative imperfections is about 0.2 inches, as the values vary from 0.10 inches to -0.10 inches (D/540). Thus, the change in imperfection due to the deck load is less than 1/8 of an inch for all cases. For a 54 inch deep web, a 1/8 inch imperfection due

to the deck pour is not significant, for it is an imperfection of $D/540$, much less than the $D/150$ limit allowed for fabrication. In fact, the imperfections were so small at fabrication and the deck pour that when added together, the largest absolute imperfection was 0.31 inches, which is still less than the $D/150$ limit of 0.36 inches.

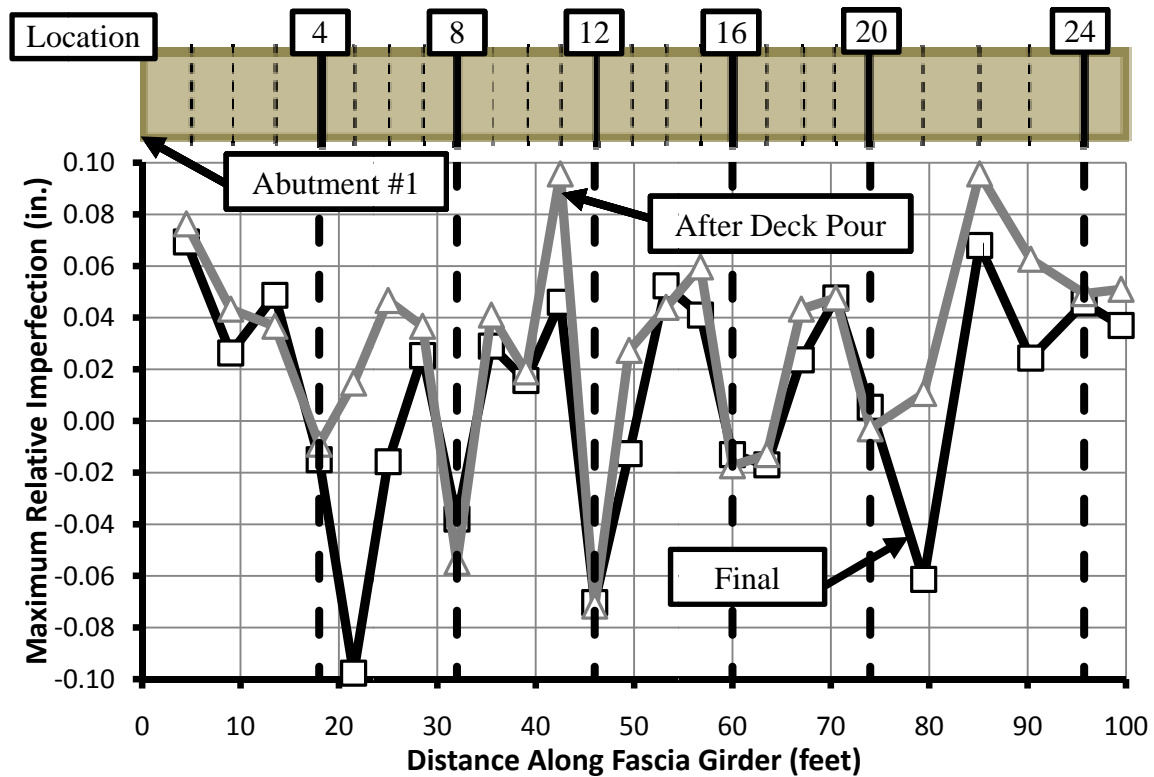


Figure 4-26 Maximum Relative Imperfection of Fascia Girder

At a majority of the locations, the change in imperfection was positive, which means that the imperfections grew inward, as expected, due to the deck pour. Of the eight locations where the change due to the deck pour caused a negative change in imperfection, five of those were at a line of bracing (Locations 4, 8, 12, 16, and 20). Those locations are slightly more complicated, as they feature cross frames and struts, which can push the webs in the opposite direction. Thus, a negative imperfection can occur at cross frame locations due to load distribution from the cross frames.

Figure 4-27 shows the imperfections due to the construction loading of the fascia girder at Location 1. As seen in the graph of absolute imperfection, the imperfection is

negative at the bottom and positive at the top in the initial profile, causing an S-shaped curve. In contrast, when looking at the other two absolute imperfection profiles, after the deck pour and the final reading, the shapes are those of a half-wave shape. Therefore, as seen from the plot of relative imperfections, the web moved inward after the deck pour. With a relative imperfection of nearly 0.08 inches (D/710), this location has one of the higher changes due to the deck pour.

Another interesting aspect of Location 1 is that the imperfections decreased slightly at the final measurement—after the removal of the overhang brackets. However, the recovery was relatively small. The relatively small recover can be attributed to two aspects: 1) the lateral load from the overhang bracket was applied relatively close to the bottom flange, and 2) the stiffened concrete provides some restraint to web recovery. In most cases, the location of maximum imperfection is at either the midpoint of the web or the point above the midpoint. If the lateral load from the bracket had a significant impact, the maximum imperfection should have been located lower on the web due to the position of the bracket and caused a larger recovery when the bracket was removed.

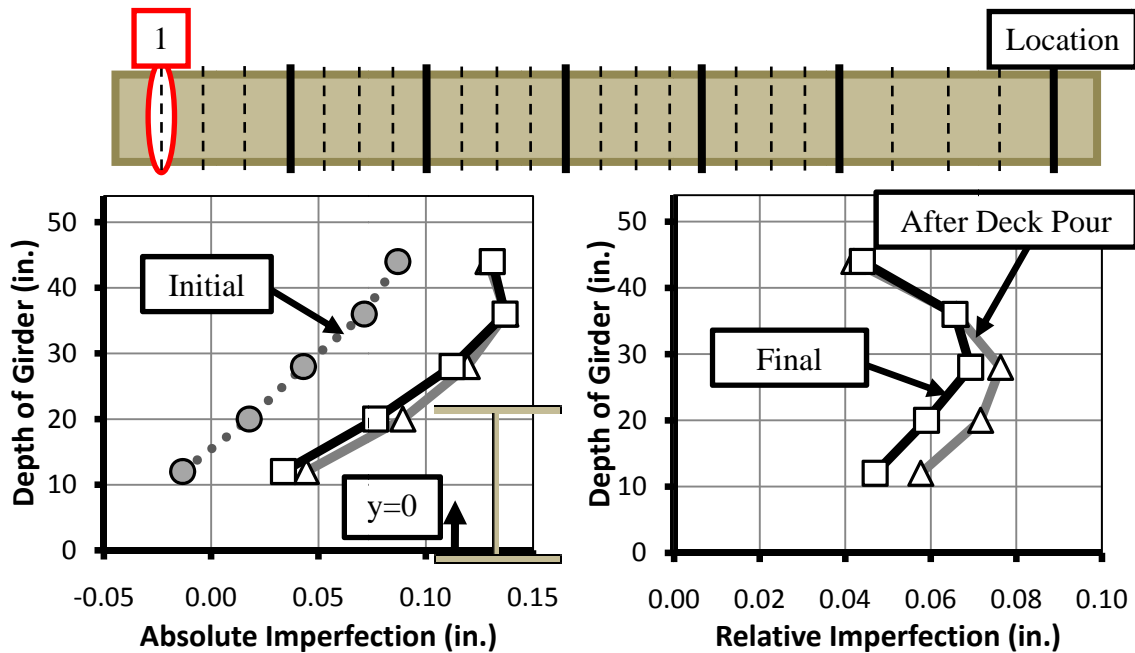


Figure 4-27 Relative Imperfection of Fascia Girder at Location 1

Looking at another location, it can be seen that the deck pour helped to smooth out the profile of the web imperfections. From Figure 4-28, all three web profiles are bending in a half-wave pattern. The initial profile is somewhat jagged, yet when the deck is poured, the half wave becomes smoother. From the relative imperfection figure, it can be noted that an S-shaped curve, one where the bottom bends inward (positive) and the top bends outward (negative), was needed to smooth out the curves. With the imperfections at the bottom increasing (positive value) due to the deck pour, the bottom behaves as expected from applying a concentrated load from the overhang load. After the overhang bracket is removed, the imperfections decrease; thus, there is some recovery after removing the overhang brackets. However, the maximum relative imperfection at this location is on the order of 1/20 of an inch ($D/1150$), which is very small. This small imperfection can be partially attributed to bending in an S-shape.

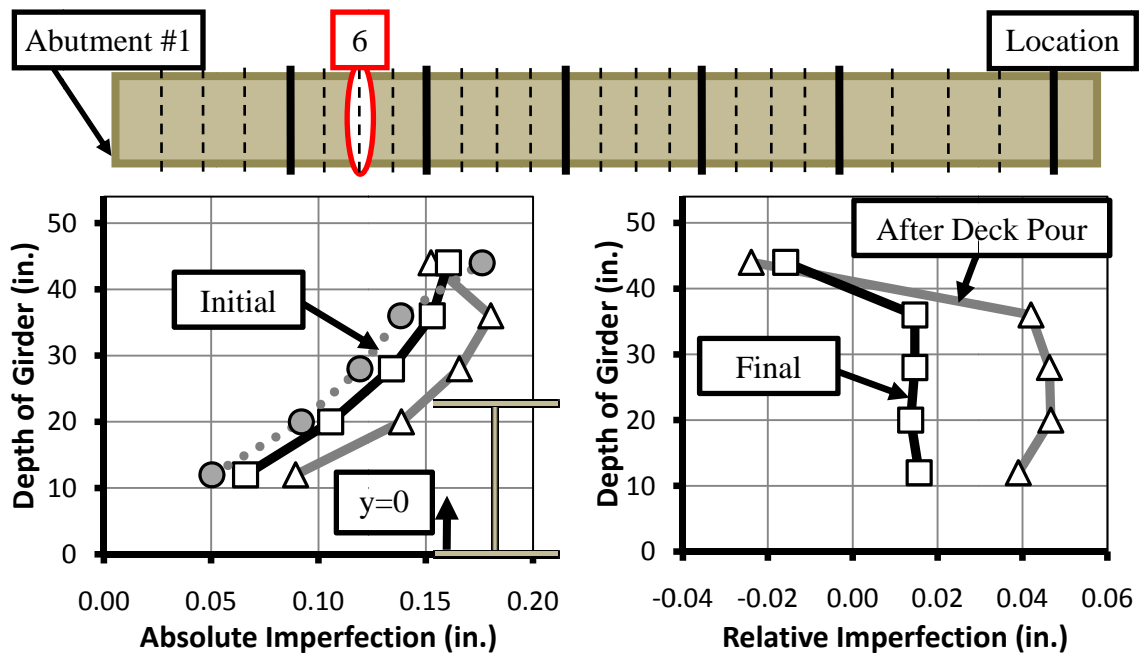


Figure 4-28 Imperfection of Fascia Girder at Location 6

The behavior of imperfections at a bracing line is interesting, as it is different from the majority of the other locations. All “bracing line locations” are actually located within 6 inches of the bracing line to allow for access by the LDPG. All of these locations are near stiffeners, which are needed to connect the braces to the girders and

help reduce imperfections. Location 12 (Figure 4-29) has the largest relative imperfections of the bracing line locations measured. At this location, the relative imperfections are negative, which indicates the web was bending outward. This movement can be seen from the absolute imperfection plot since both lines are to the left of the initial profile. As discussed earlier, the negative imperfections can be due to the force of the brace, which could be greater than the overhang bracket force. When the overhang bracket is removed, the imperfections hardly vary from those measured after the deck pour; thus, there is essentially no measurable recovery after removing the overhang brackets at the stiffener locations. Still, the maximum relative imperfection at this location is just over 1/12 of an inch ($D/750$). Therefore, significant deformation was not found at this location.

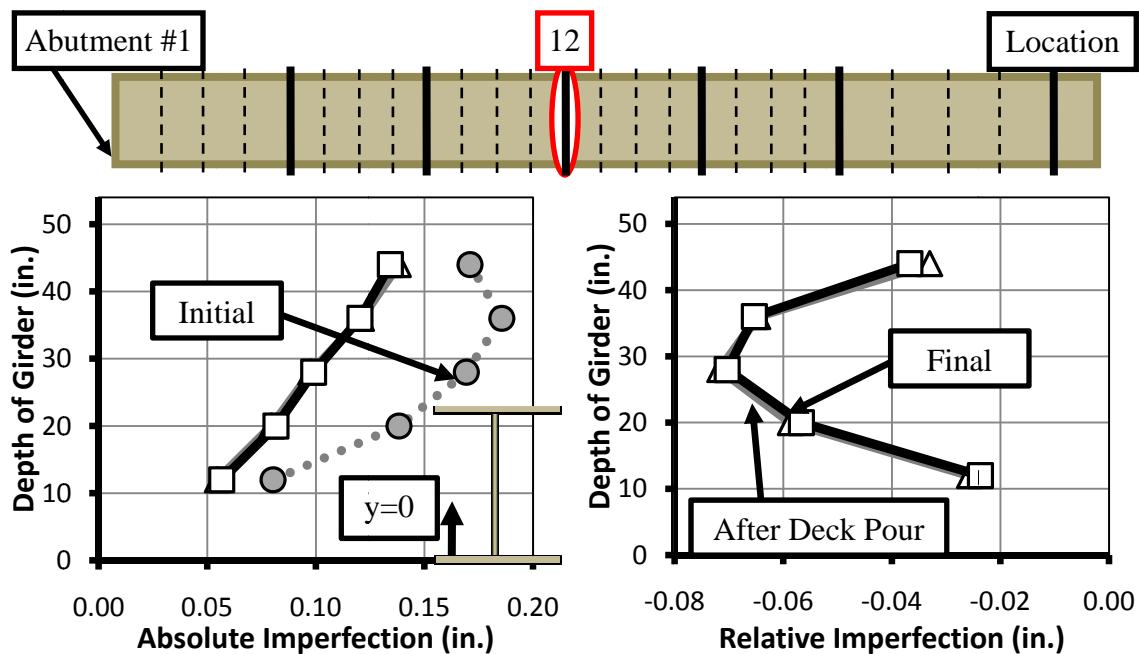


Figure 4-29 Imperfection of Fascia Girder at Location 12

Figure 4-30 shows the relative imperfection of the exterior girder at the cross frame locations. This graph supports the idea that struts/cross frame locations are negative due to the force in the struts/cross frames being larger than the overhang force. According to Wang and Helwig (2005), the brace forces are a function of the moment at the brace location. Thus, the largest brace forces will occur at the regions with the

highest moments. Due to its position on the bridge, Location 12 is expected to have the highest cross frame forces and it has the highest relative imperfection of all of the cross frame/strut locations. Location 24 is expected to have the lowest cross frame/strut forces and it has the lowest relative imperfection of the cross frame/strut locations.

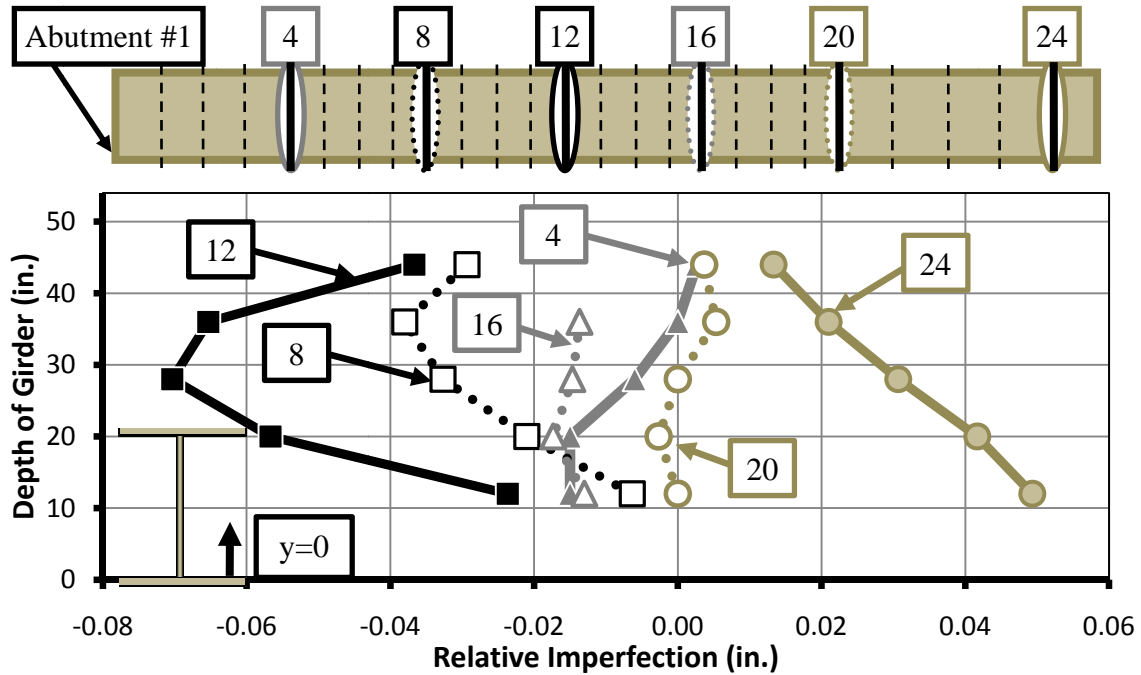
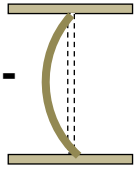

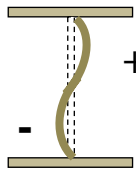
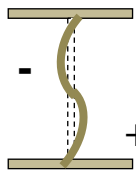


Figure 4-30 Relative Imperfection of Fascia Girder at Cross Frame Locations

The shapes of the webs at the 19th Street Bridge were identified and categorized in Table 4-5 for both a fascia and an interior girder. The table is useful in summarizing the patterns of the data. First, most of the initial and final shapes are half-wave shapes (83%), as opposed to S-shaped waves (17%). Second, the majority of changed shapes for the fascia girder behaved as expected (84%) with either a positive half-wave or an S-shaped wave with positive imperfections at the bottom. For the fascia girder, the final shape of the imperfections changed from the initial shape as a result of the deck pour for only one location, going from a half-wave curve to an S-shaped wave. In contrast, for the interior girder, the shape of the imperfections (positive half-wave shape) changed at two locations from initial to final measurement as a result of the deck pour.

Table 4-5 Summary of Shapes at 19th Street Bridge

Deflected Shape	Initial Shape		Changed Shape		Final Shape	
	Fascia	Interior	Fascia	Interior	Fascia	Interior
	0 (0%)	0 (0%)	3 (12%)	8 (38%)	0 (0%)	0 (0%)
	20 (83%)	20 (95%)	15 (63%)	8 (38%)	21 (87.5%)	20 (95%)
	4 (17%)	1 (5%)	1 (4%)	3 (14%)	3 (12.5%)	0 (0%)
	0 (0%)	0 (0%)	5 (21%)	2 (10%)	0 (0%)	1 (5%)

4.3 CURVED STEEL BRIDGE (SH 71-SH 130)

Torsional rotations and web imperfections were monitored during the deck pour of Span 14 at the direct connector from SH 71 to SH 130 to obtain a measure of the impact from the loading on the overhangs. The concrete deck for Span 14 was poured on April 16, 2008. Figure 4-31 highlights the timeline for the deck pour. The deck pour started at approximately 1:30am and finished nearly 10 hours later. The contractor poured three spans in reverse order, starting with Span 16 and finishing with Span 14. The total volume of concrete needed for the three-span continuous steel bridge was over

650 cubic yards. The contractor used one screed and two finishing bridges during the deck pour. The screed weighed approximately 13 kips, while both finishing bridges weighed nearly 4 kips each. The contractor did not preload any of the sections, as was done on the 19th Street Bridge in Lubbock.

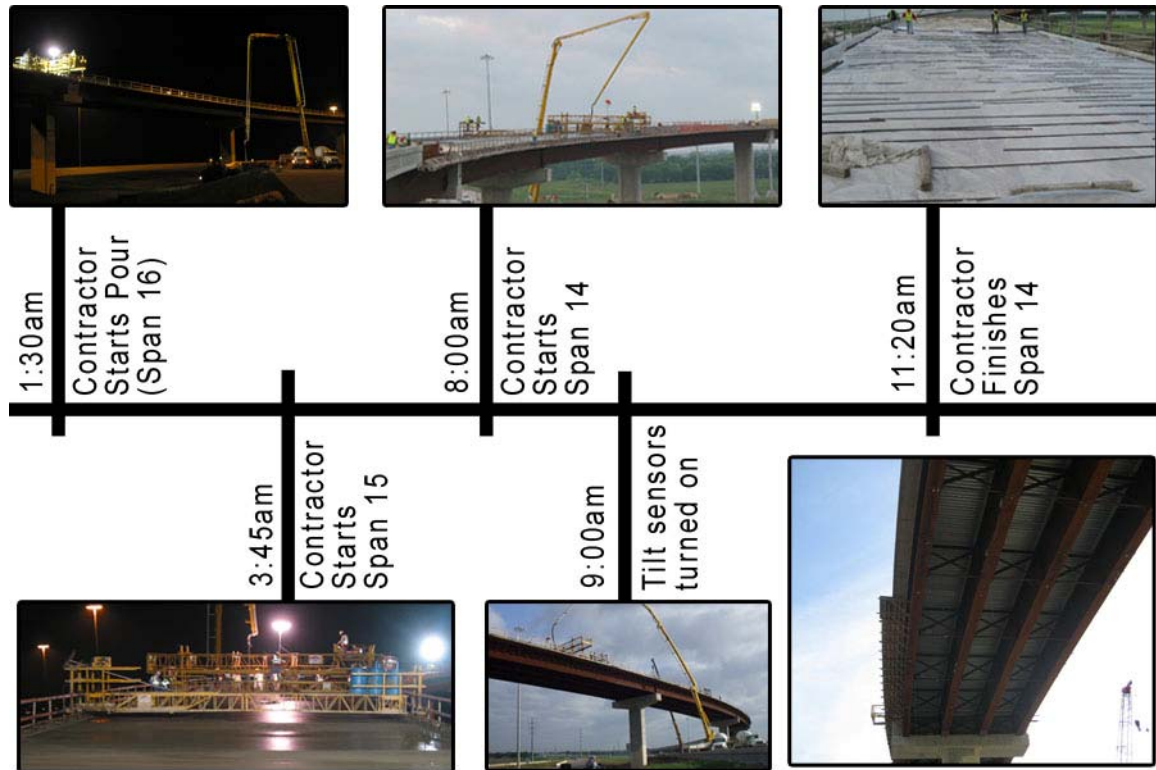


Figure 4-31 Timeline For Deck Pour at SH 71-SH 130 (Span 14)

4.3.1 Torsional Rotations

Sixteen tilt sensors were installed on Panel 5, as described in Section 3.3.1.1. A slightly different rotation sign convention was used at Span 14 since the entire width of the bridge was instrumented. As seen in Figure 4-32, it is revised by defining the direction relative to the entire bridge, rather than just a single overhang. When looking toward Bent 14 (backstation), Girder 4 is located on the left and Girder 1 is on the right. Any twist that causes the girders to rotate counterclockwise is considered positive with this sign convention.

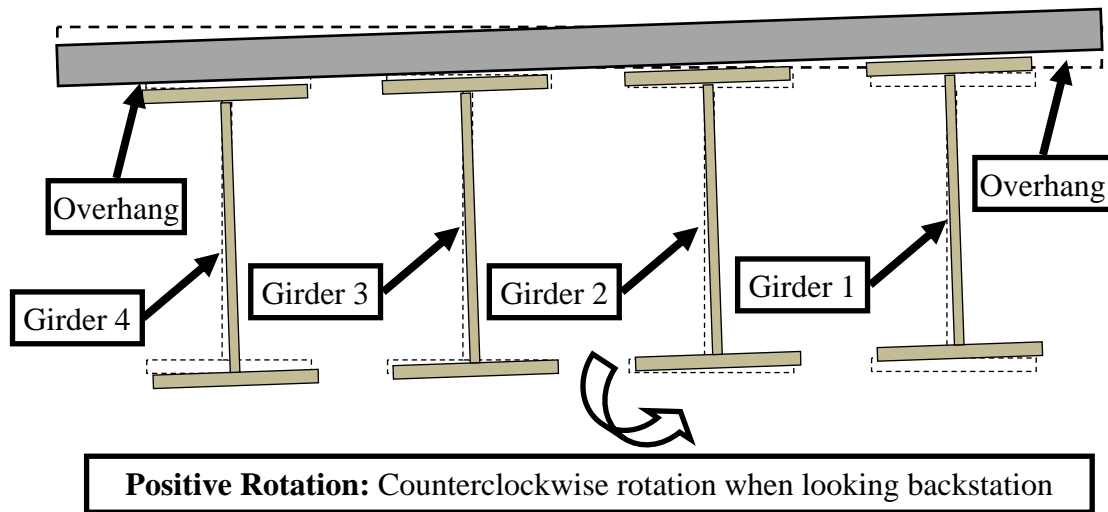


Figure 4-32 Sign Convention for Rotations at Span 14

The construction schedule at Span 14 caused a few complications in determining the rotation for the bridge. In September 2007, the area under Span 14 was opened to traffic, which significantly limited access to the instrumentation at Span 14. In early April, the contractor allowed access to Span 14 to prepare the instrumentation for the deck pour. At that time, all sensors were turned on to record data to prepare for the scheduled deck pour. Unfortunately, a subsequent delay resulted in the datalogger monitoring the tilt sensors being shut down to conserve power.

As outlined in the last section at 19th Street Bridge, the rotation from the deck pour can be determined by averaging tilt sensor values in the mornings after the deck pour and zeroing to a time when no load was applied to the bridge. The values that are used in the mornings after the deck pour must be chosen to match the temperature voltages seen at the “zero point,” thereby minimizing the tilt sensors’ temperature drift issues. After the deck pour was delayed, it made getting an accurate zero point difficult due to the high power consumption of the tilt sensors. To conserve the datalogger’s internal battery, the tilt sensors were turned off on April 8, 2008. Worried about access to the bridge before the deck pour, a switch was installed on the datalogger to turn on the tilt sensors as needed. However, in the hours before the deck pour, the switch was

damaged by construction personnel. Without the switch, the tilt sensors could not be turned on until 9:00am on April 16, 2008; by which time, the contractor was finished with nearly 80 percent of the deck pour.

Since no data was obtained in the hours immediately before the deck pour, the zero point was calculated by using data from the morning of April 8, 2008. The main concern with using a zero point so far back is related to the temperature swings that occurred at the bridge site from week to week. As discussed in Section 4.2.2, the tilt sensors can drift significantly with changes in temperature, which is why matching temperature values to minimize error is so important. Using a zero point eight days prior to the deck pour made it difficult to match temperatures, as the high temperature changed by more than 10°F. A second concern is sensor stability. Most sensors will naturally begin to drift slightly as time elapses over a lengthy period of monitoring. Acknowledging these concerns, six readings from 12:00am to 6:00am on April 8, 2008 were used for the zero point.

Figure 4-33 shows the temperature voltage for TS-G1-1 from April 7, 2008, through April 24, 2008. In analyzing the data, only two mornings were found to be at adequate temperature voltages. In the graph, the mornings are highlighted by the bottom of each dip, at which the temperature is relatively constant. Typically, only data before the sun rises is used since thermal gradients can cause local and global twisting in the girders. On April 17, 2008, four data points were used between 9:00am and 10:30am. Though the sun had risen, the temperature did not change quickly during this time frame. Four days later on April 21, 2008, four data points were used between 12:00am and 1:30am. Looking at the other mornings, data with temperature voltages that matched the zero point could not be found.

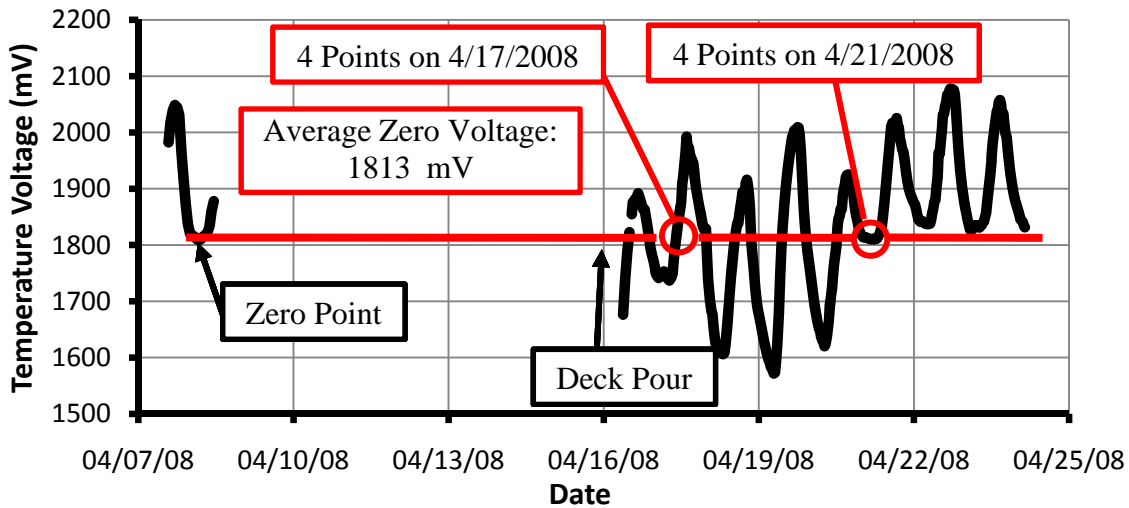


Figure 4-33 Example of TS-G1-1 Temperature Voltage at Span 14

Figure 4-34 through Figure 4-37 show the variation of the tilt sensors with the two days chosen for comparison. Location 1 is positioned at the fourth bracing line from Bent 14 which marks the beginning of the fifth panel, while Locations 2 and 3 are located at the first quarter point and midspan of the fifth panel, respectively. Finally, Location 4 is at the end of the fifth panel, which corresponds to the fifth bracing line. At Location 1, the tilt sensor on Girder 4 (TS-G4-1) malfunctioned; thus, the data is not shown. However, all of the other tilt sensors are within 0.03° of each other, reinforcing the idea that the tilt sensors move together at a bracing line. As seen from Figure 4-34, the rotations vary from each day, yet always within an error of $\pm 0.03^\circ$. Thus, the rotations enclosed in the boxes were calculated by averaging the rotation on April 17, 2008, with the rotation on April 21, 2008.

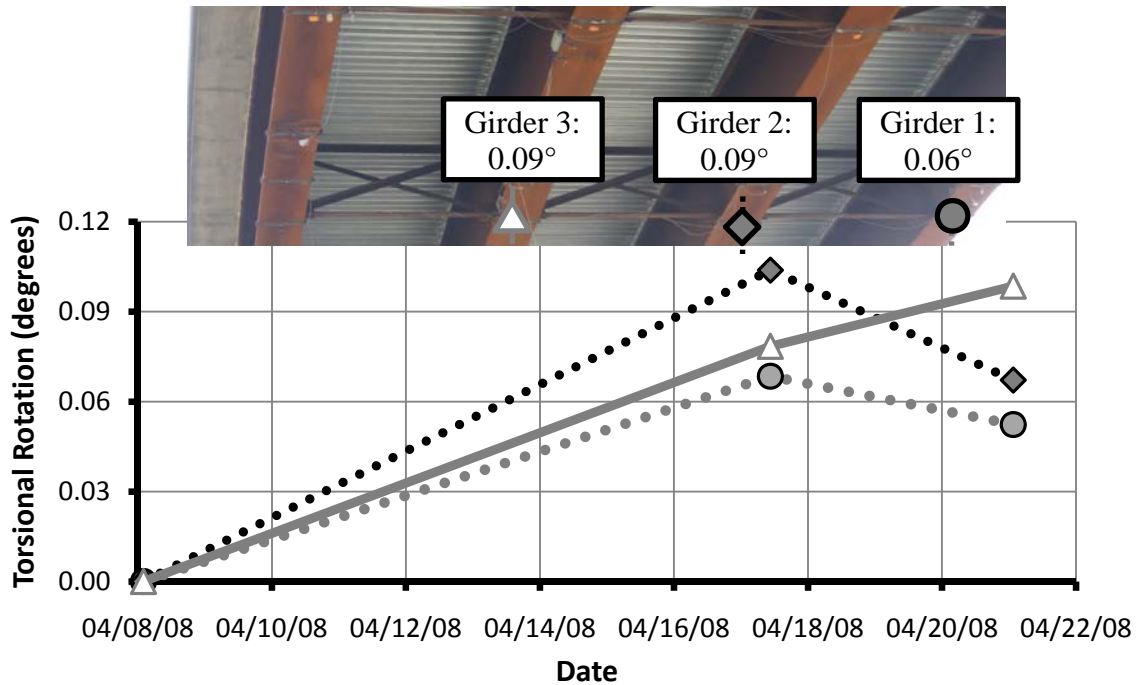


Figure 4-34 Change in Torsional Rotation After Deck Pour (Span 14, Location 1)

Between bracing lines, the rotations at Locations 2 and 3 are not expected to be uniform across the width of the bridge and are expected to be larger than the rotations at adjacent bracing lines. Figure 4-35 shows the rotations at Location 2, which, with the exception of Girder 3, are larger than the rotations at Location 1. Though it is possible that the tilt sensor at Girder 3 drifted, it is within 0.06° of the other locations.

At Location 3, higher maximums were found at the exterior girders, Girders 1 and 4, while the tilt sensor at Girder 3 was near its rotation at Location 1 (Figure 4-36). The tilt sensor at Girder 2 was not reported, as it malfunctioned while on the bridge. Due to the geometry of the system, curved girders naturally want to twist. For locations of positive rotation, an overhang at Girder 4 will amplify the twist as the torsional load acts in the direction of twist. In contrast, Girder 1 should rotate less than Girder 4 at locations of positive rotation, as the overhang at Girder 1 counteracts the twist. In general, it is expected that a fascia girder will twist more than an interior girder due to the torsional load of the overhang.

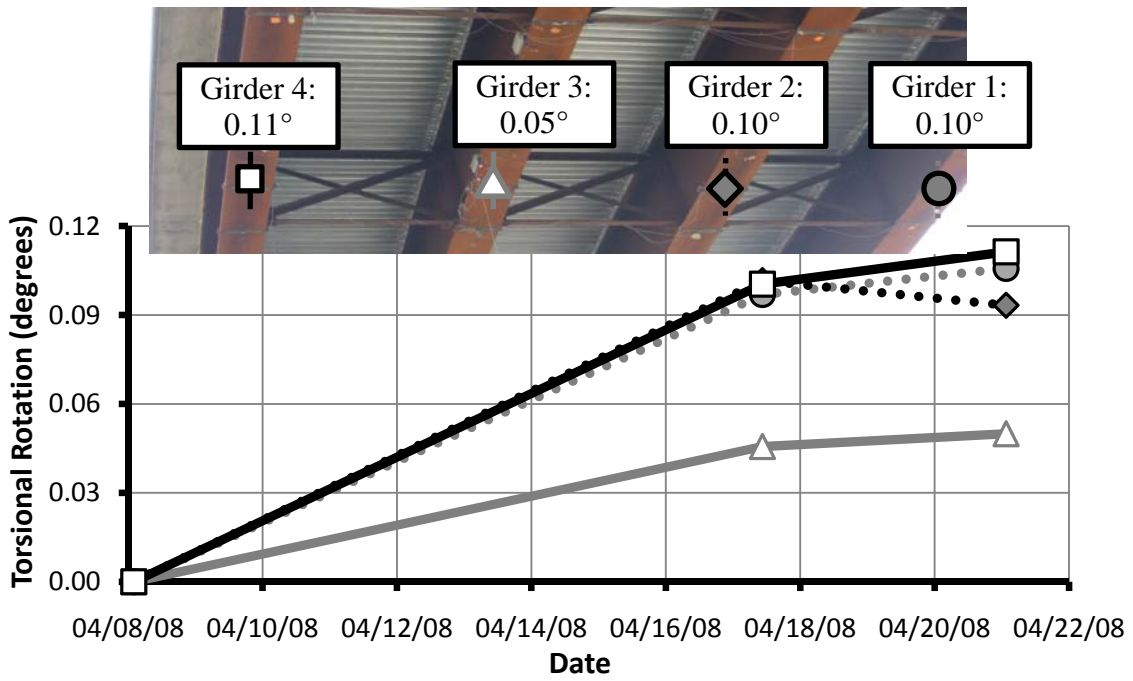


Figure 4-35 Change in Torsional Rotation After Deck Pour (Span 14, Location 2)

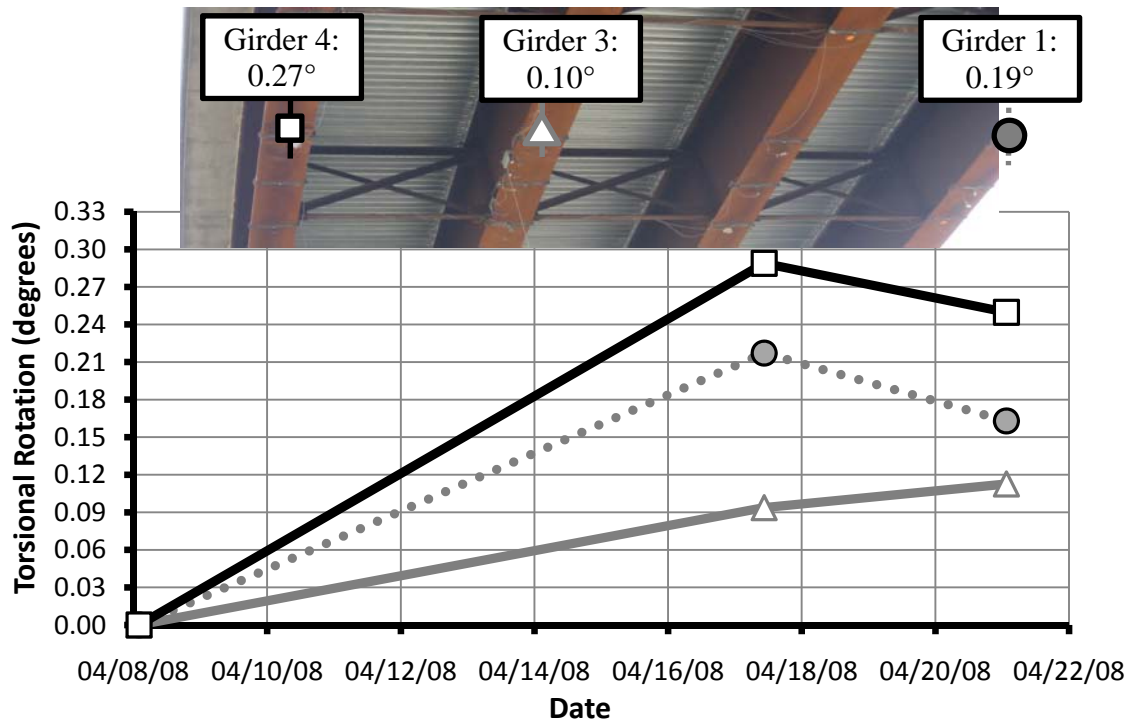


Figure 4-36 Change in Torsional Rotation After Deck Pour (Span 14, Location 3)

The final instrumented location was positioned at the fifth bracing line. The presence of the cross frames should cause the rotations to be fairly uniform across the width. After averaging the data from the two days (April 17 and April 21, 2008), it can be seen from Figure 4-37 that all of the sensors are within an error of $\pm 0.03^\circ$ of each other. Thus, the girders behaved as expected.

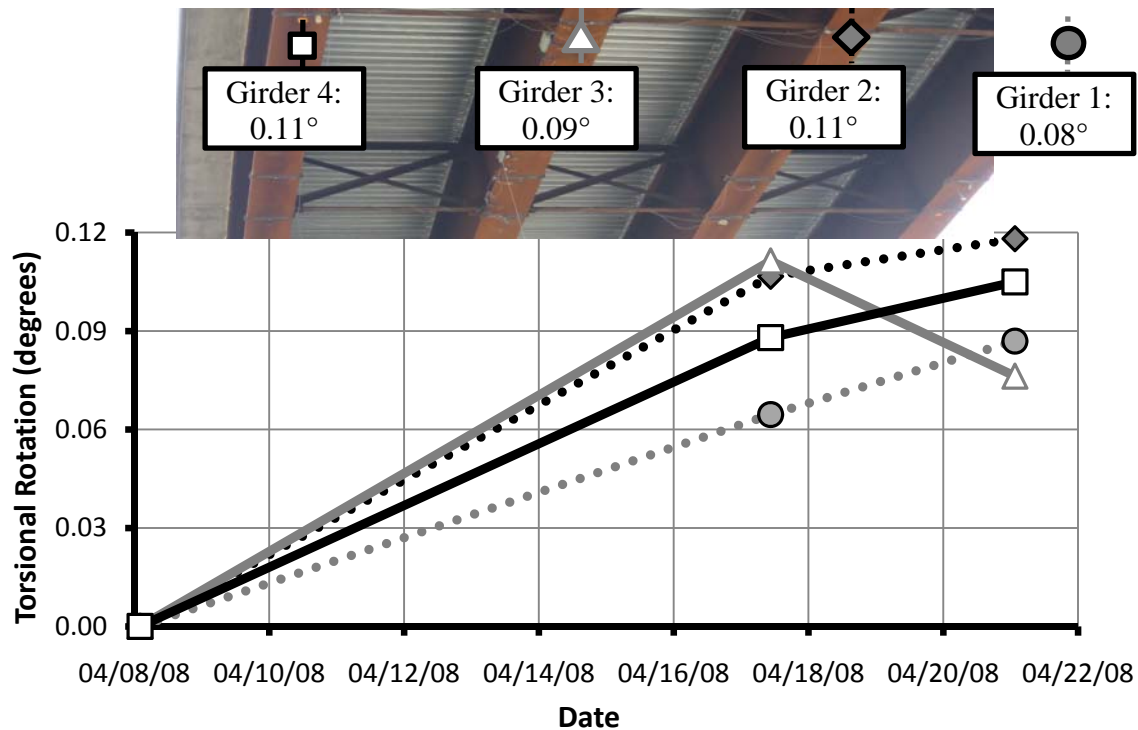


Figure 4-37 Change in Torsional Rotation After Deck Pour (Span 14, Location 4)

Due to the uncertainty of the zero point for the tilt sensors, it is beneficial to determine the validity of the readings. To help in validating future computer models, deflections were measured at ten locations along Span 14. In particular, deflection measurements were determined at the fifth bracing line, which corresponded to Location 4 of the tilt sensors. As seen at the 19th Street Bridge, the rotation at a bracing line is nearly the same for all of the girders due to the presence of cross frames. Therefore, the relative deflection between girders can be used to estimate the twist of the bridge. Table 4-6 shows the deflection for all of the girders at bracing line 5 and the rotation for each relative to Girder 1. With the largest spacing between girders (31 feet) and relative

deflection (0.54 inches), the rotation (0.08°) at Girder 4 is likely the best estimate of the twist of the bridge (Figure 4-38). The error was determined by assuming a 1/16 inch resolution with each measurement. Since the error can occur at each end of the bridge, a maximum error of 1/8 inch is possible. It should be noted that the rotations are an estimate only, as this method does not taken into account any independent twisting of the girders. Comparing the rotation derived from the deflections with the values obtained with the tilt sensors at Location 4, varying from 0.08° to 0.11° , it can be seen that the rotations are very close. Thus, the deflection measurements confirm the procedure used to calculate the tilt sensor rotations.

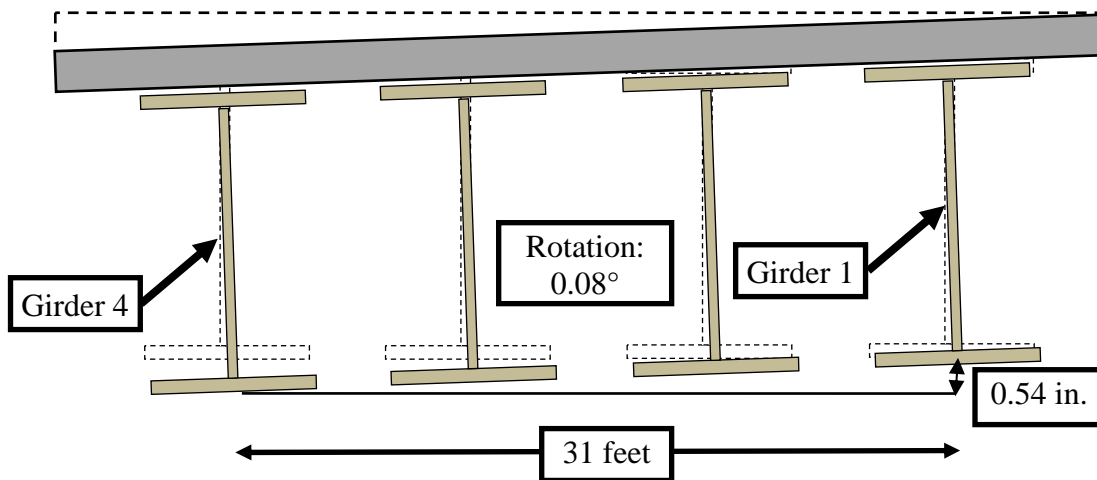


Figure 4-38 Summary of Measurements After Deck Pour

Table 4-6 Torsional Rotation at the Fifth Bracing Line Due to Deck Pour

Location	Deflection (in.)	Rotation (Relative to Girder 1)	Error
Girder 1	2.42 (down)	-	-
Girder 2	2.69 (down)	0.12°	$\pm 0.06^\circ$
Girder 3	2.67 (down)	0.06°	$\pm 0.04^\circ$
Girder 4	2.96 (down)	0.08°	$\pm 0.02^\circ$

Deflection measurements were taken at various times during the deck pour. One of the more interesting times was when only Spans 15 and 16 had been poured. As noted in Table 4-7, all four girders had an upward deflection, making the girders rotate in the opposite direction of when Span 14 had been poured. In addition, the maximum absolute rotation at the fifth bracing line was greater when the spans were partially loaded (0.22°), as opposed to being fully loaded (0.08°).

Table 4-7 Torsional Rotation at the Fifth Bracing Line (Only Spans 15 and 16 Poured)

Location	Deflection (in.)	Rotation (Relative to Girder 1)	Error
Girder 1	0.98 (up)	-	-
Girder 2	1.33 (up)	-0.16°	$\pm 0.06^\circ$
Girder 3	1.96 (up)	-0.23°	$\pm 0.03^\circ$
Girder 4	2.44 (up)	-0.22°	$\pm 0.02^\circ$

4.3.2 Web Imperfections

The combination of a deep web and position of the overhang brackets at mid depth was expected to have a significant influence on deformations at Span 14. Thereby, a total of 74 locations on Girders 3 (interior) and 4 (fascia) were chosen for initial imperfection measurements taken in August 2007. When the concrete deck pour was delayed by more than eight months, a frontage road under Span 14 was opened in September 2007 that reduced access to the underside of the bridge. To account for traffic interruptions, the number of locations was reduced to 32 locations (Panels 2, 3, and 6 for Girders 3 and 4) in April 2008 for the second measurement phase (after the deck was poured). The three panels chosen were those with the largest measured initial imperfections. The 32 locations were further reduced to six locations in May 2008 for the final measurement phase (after the overhang brackets are removed). For the 32 locations where at least the second measurement phase occurred (after deck pour), the

web imperfection data for Span 14 is presented in Appendix C (fascia girder) and Appendix D (interior girder).

The same sign convention as used at the 19th Street Bridge was used at Span 14. As such, since the force from an overhang bracket is expected to cause the web to bend inward, inward movement is considered a positive imperfection. The D/150 fabrication limit allowed for Span 14 is 0.56 inches. In addition, this limit can be used as a benchmark to evaluate the significance of relative changes in the imperfections as a result of the overhang.

Though the position of the overhang bracket was expected to have a larger impact, the range of relative imperfections is only slightly larger than the 19th Street Bridge deformations. As seen from Figure 4-39, the imperfections at the fascia girder vary from 0.15 inches to -0.20 inches. As with the 19th Street Bridge, the figure above the graph is a legend of the girder, in which each line represents a web imperfection measurement location. Correcting for the depths of the girders, 0.15 inches (D/560) of imperfection at Span 14 is approximately equivalent to 0.10 inches (D/540) at 19th Street Bridge. Therefore, despite having worse-positioned brackets at Span 14, the positive imperfection at both sites was nearly the same. The overhang brackets at the 19th Street Bridge were heavy-duty brackets positioned at a more ideal location on the web (near the bottom flange), yet spaced further apart and delivering more force to the web. This higher force could have compensated for the better-positioned brackets, making the imperfections similar to Span 14. Yet, as discussed earlier, since the removal of the brackets did not cause a huge recovery, it is more likely that neither of these webs were critical sections for local web imperfection problems. In terms of the D/150 fabrication limit, four locations (Location 9 on Girder 4 and Locations 14, 15, and 31 on Girder 3) were found during the initial measurements to exceed the allowed 0.56 inches.

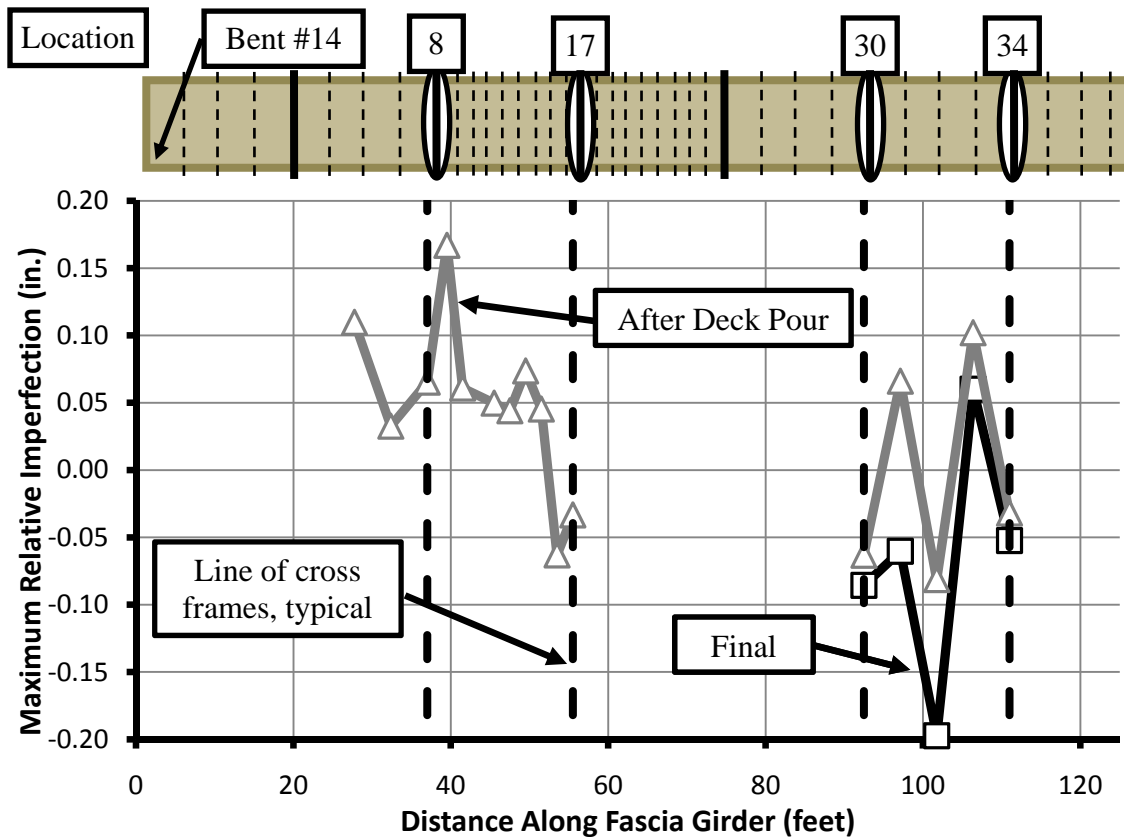


Figure 4-39 Maximum Relative Imperfection of Fascia Girder (Span 14)

At a majority of the locations, the maximum change in imperfection was positive, which means that the imperfections grew inward, as expected, due to the deck pour. For the fascia girder, a pattern developed where based on the initial profile, the changed profile could be determined for most locations. In general, as will be seen later, if the initial shape of the webs was a half-wave shape, whether positive or negative, the relative imperfection shape was an S-shaped curve.

Figure 4-40 shows the imperfections due to the deck pour for Location 12 (fascia girder), which was located near the midpoint of Panel 3. From the absolute imperfection graph, the initial profile was a negative half-wave shape. The change in imperfection from the deck pour caused the web to bend in an S-shaped curve, with positive imperfection at the bottom and negative at the top. Since the overhang bracket was positioned near a height of 40 inches, the bracket seems to act as a brace point, causing

the web to bend around the bracket. Location 13 of the fascia girder had a very similar negative half-wave initial imperfection and behaved in the same manner, with an S-shaped curve change.

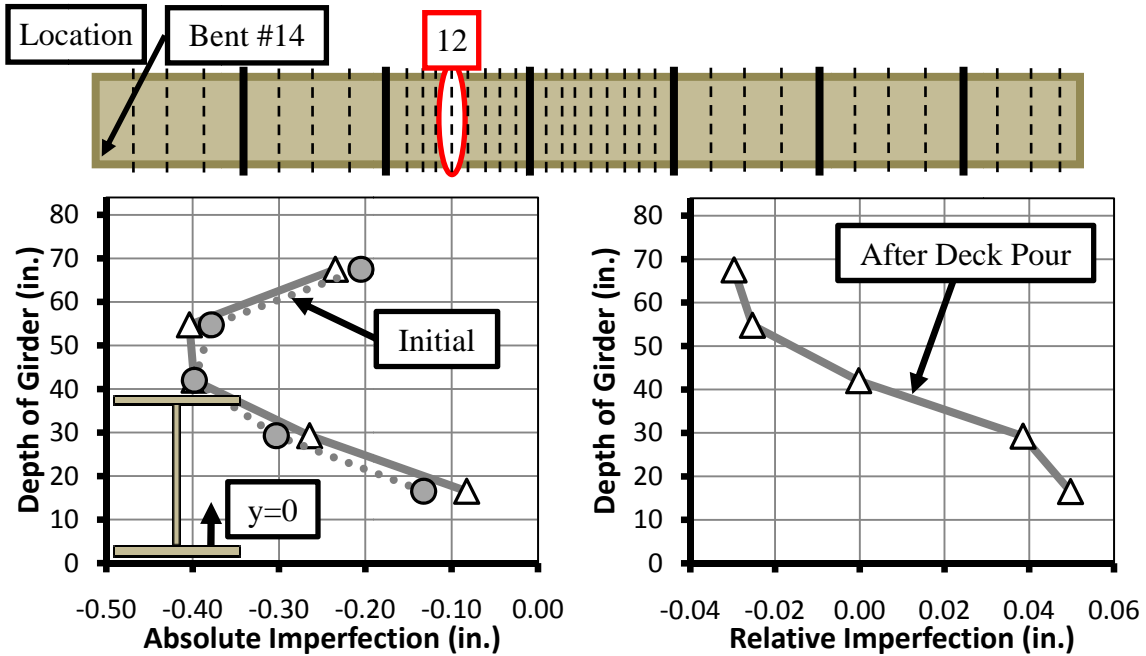


Figure 4-40 Imperfection of Fascia Girder at Location 12 (Span 14)

Ten of the sixteen locations at the fascia girder behaved similarly to Location 33 from initial imperfection profile to relative imperfection shape. Two other locations had a similar initial imperfection profile, yet the change in shape was different, most likely due to the presence of cross frames. As such, Location 33 is an important location because all three measurement phases were performed and it can summarize most of the trends. Figure 4-41 details the shapes of the imperfections in the web. As seen from the absolute imperfection graph, the web had a half-wave shape with positive imperfections. Yet, looking at the relative imperfection profiles, the change in imperfection at the top is positive and negative at the bottom, causing an S-shaped change. The overhang bracket was positioned approximately 40 inches from the bottom of the web, which is where the maximum relative imperfection occurs (0.10 inches). Thus, the overhang bracket appears to have an influence on the shape of the web imperfections at Location 33, causing the

web to move inward. Nonetheless, the relative imperfection is on the order of $D/840$, much smaller than the $D/150$ limit. It should also be noted that when the overhang bracket is removed, the web recovered by 0.04 inches, nearly one half of the original change in imperfection.

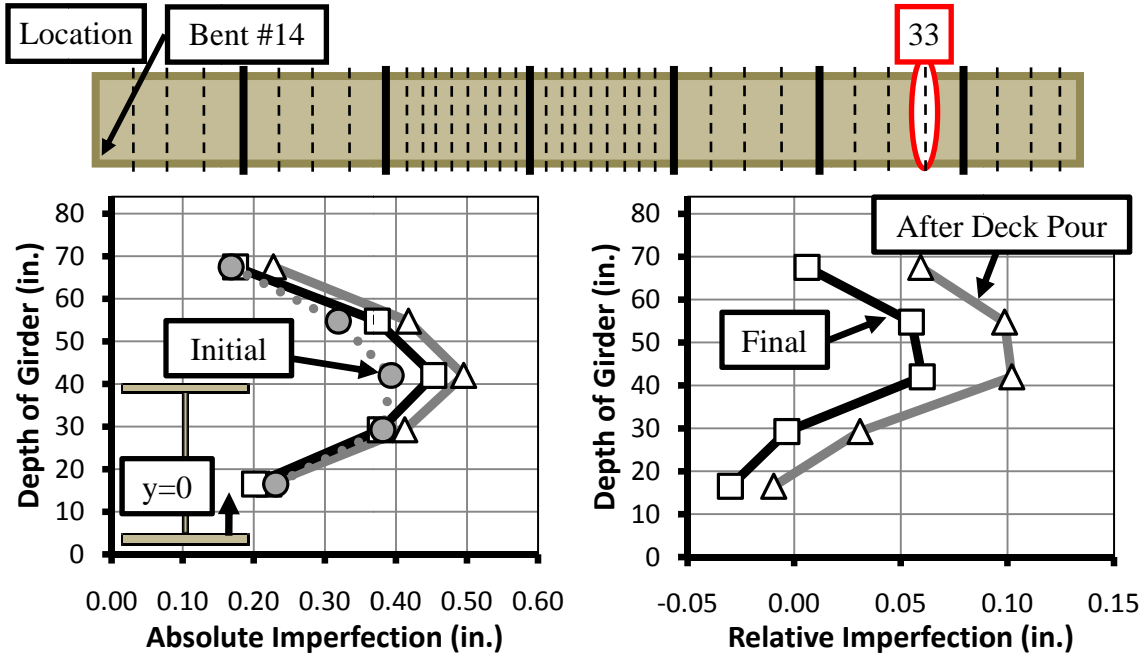


Figure 4-41 Imperfection of Fascia Girder at Location 33 (Span 14)

Figure 4-42 shows Location 32 of the fascia girder, which is an interesting location because the shapes are in the opposite direction as expected. As noticed, the absolute imperfection graphs had half-wave shapes, yet with a negative imperfection. Located in the middle of Panel 6, the impact of the overhang brackets was expected to be the largest since the effect of cross frames forces should be minimized. However, the relative imperfection profile is a negative single-wave shape, the opposite as expected.

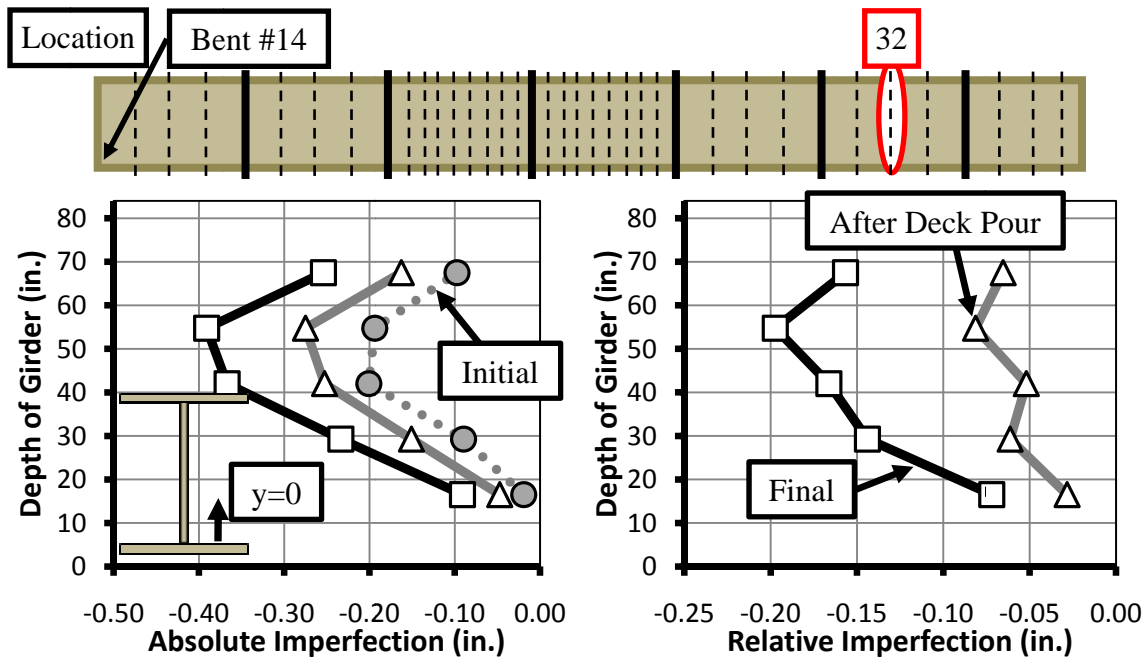




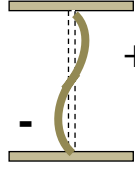
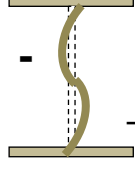
Figure 4-42 Imperfection of Fascia Girder at Location 32 (Span 14)

From the relative imperfection profile at Location 32, the data suggests that web imperfections could be affected by global effects as well. For instance, Location 12 (Figure 4-40) is near the midpoint of the Panel 3 and has a negative initial imperfection, like Location 32. Therefore, if the problem were only a local problem, both locations should have similar figures. Yet, there is a large difference between the relative imperfection graphs, as Location 32 does not have any positive relative imperfections. Locally, the locations have a very similar initial imperfection and relative panel position. Instead, the differences at these locations are of a global nature. For instance, Location 32 was more exposed to thermal changes due to its position along Span 14; Location 32 was oriented along more of an eastern plane than Location 12. An increase in temperature would cause Girder 4 to bend outward, causing higher negative imperfections at Location 32. The stresses at these two locations are also slightly different, which could have affected the imperfections. Finally, the position of the overhang brackets could have influenced the behavior if Location 12 was positioned at a bracket and Location 32 was positioned between adjacent brackets.

The shapes of the webs at Span 14 were identified and categorized in Table 4-8 for both a fascia and interior girder. As discussed earlier, there was a general trend in the profiles from initial to changed shapes for the fascia girder. For Panels 2 and 3, if the initial profile was a negative half-wave shape, the relative change in shape was an S-shaped wave with positive imperfections at the bottom and negative at the top. For Panels 2, 3, and 6, with the exception of Locations 30 and 34 (cross frame locations), if the initial shape was a positive half-wave, the relative change in shape was an S-shaped curve that was positive at the top and negative at the bottom. At Locations 30 and 34, the initial shape was a positive half-wave shape and yet the relative change in shape was a negative half-wave shape. The negative change was likely due to load transferring to the cross frames and counteracting the force from the overhang brackets. Location 16 was unique in that the initial shape was an S-shaped curve and the changed shaped was a negative sine wave. For the fascia girder, the initial and changed shapes were closely related.

Whereas the initial shape at a location gave an indication of the relative change in shape for the fascia girder, the initial shape for the interior girder rarely followed a trend. The majority (75%) of the interior girders had an initial shape consisting of a negative half-wave shape and only a couple with a positive half-wave or S-shaped curves. In contrast, the relative changes in shapes were mainly distributed between a positive half-wave and an S-shaped curve with positive imperfections at the bottom and negative imperfections at the top, with only a few having a negative half-wave shape. Though the shapes for the relative imperfections were more difficult to interpret, the absolute imperfection shapes seemed to get smoother for the interior girder as a result of the deck pour.

Table 4-8 Summary of Shapes at SH 71-SH 130, Span 14

Deflected Shape	Initial Shape		Changed Shape	
	Fascia	Interior	Fascia	Interior
	3 (19%)	12 (75%)	4 (25%)	3 (19%)
	12 (75%)	2 (12.5%)	0 (0%)	5 (31%)
	0 (0%)	2 (12.5%)	10 (63%)	1 (6%)
	1 (6%)	0 (0%)	2 (12%)	7 (44%)

CHAPTER 5

Summary and Conclusions

This thesis is the culmination of the field monitoring portion of TxDOT research study 0-5706. Three bridges were instrumented and monitored during the concrete deck pour to collect data that can be used to validate finite element models of the bridges. A summary of those results, as well as recommendations, are presented in this chapter. For a more detailed discussion of the project and results, see the previous chapters.

5.1 SUMMARY OF RESEARCH PROBLEM

In 2006, TxDOT funded research study 0-5706, Impact of Overhang Construction on Girder Design. The primary goals of the research project included improving the understanding of the behavior of girders subject to overhang forces, identifying system geometries that may lead to problems, and developing improved details for overhang construction.

Overhangs on bridges cantilever from the fascia girder to extend the roadway and support both traffic and the bridge rail. Most designers employ common rules of thumb to define overhang geometry without considering the impact of the overhang load on the girder behavior. The overhang generally leads to unbalanced torsional loading on the girder system that can lead to excessive rotation of the fascia girder as well as global stability issues of the overall system.

The unbalanced loading, the main issue for overhangs, is a product of current construction practice. Typically, the overhang deck is formed by plywood forms that are supported by brackets intermittently spaced along the length of the bridge. The overhang brackets are connected to the top of the fascia girder and react against the side of these girders. Due to the eccentricity of the overhang, a torsional load is applied to the fascia girder. Even if common rules of thumb are followed, the fascia girders can rotate during construction and lead to stability problems in both steel and concrete girder systems. The

stability problems develop because the deformational behavior of the girders is sensitive to the construction details and not well understood.

5.2 SUMMARY OF RESULTS

To evaluate the behavior of overhang construction, three Texas bridges were chosen for field monitoring during construction. Two of the bridges were located in Austin, along the interchange between State Highway (SH) 71 and SH 130, and consist of a prestressed concrete girder bridge and a curved steel plate girder bridge. The third bridge is a straight steel plate girder bridge with a support skew of nearly 60 degrees in Lubbock. The investigations tracked the behavior of the bridges, in terms of vertical deflections, lateral rotations, rebar strain, and web imperfections, due to the construction loading of the concrete deck pour. The highlights of the results are discussed below.

5.2.1 Prestressed Concrete Bridge (SH 71-SH 130)

The prestressed concrete bridge is simply-supported (Span 22) and features seven Type IV girders spanning 120 feet. The concrete deck was poured on September 19, 2007. The following paragraphs summarize the conclusions from the vertical deflections, torsional rotations, and strain in the top bracing bars.

- During the deck pour, the fascia girders deflected more than the interior girders. Due to the presence of precast concrete panels, less concrete is needed to achieve the deck thickness at the interior portions of the bridge as compared to the overhangs where the full deck thickness is poured. If the relative difference in deflection is ignored, more concrete will be added at the overhangs to make the roadway level, thereby increasing the torsional load and decreasing the stability of the system.
- The rotations at the fascia girder of the instrumented span were a function of torsional deformations, with the maximum rotation being 0.11° . The rotations were small due to the large weight and high torsional stiffness of the Type IV girders. With a torsional deformation mode, the bridge

deformed differently than Bridges 1 and 2 that were discussed in Chapter 2. These bridges experienced significant rotations of the fascia girder and lifted off the bearing pads.

- Due to the symmetric loading from the deck pour, the interior girders experienced negligible rotation.
- The stress in the top bracing bars was low, which can be attributed to the small rotations and the flexibility of the connection. It is due to the flexibility of the connection that the bars are not expected to prevent high rotations. For instance, the same bracing bar detail was used at Bridges 1 and 2 (Chapter 2) and allowed rotations that varied from 2° - 3° .

5.2.2 Steel Bridge with Skewed Supports (US 82 - 19th Street Bridge)

The 19th Street Bridge over US 82 Highway in Lubbock, Texas, is a steel plate girder bridge with skewed supports of approximately 60° . The bridge is a two-span continuous system with six steel plate girders that are 54 inches deep. Vertical deflections, torsional rotations, and web imperfections were determined during the concrete deck pour on October 4, 2007. A summary of the results are as follows:

- In general, the bridge rotated and deflected as a unit due to the presence of the cross frames and struts. The fascia girder did rotate slightly more than the interior girders, which represents the effect of the overhang. Yet, the differences in rotations of the interior and exterior girders were small, varying from 0.01° to 0.09° , due to the high torsional stiffness of the steel plate girders.
- Rotations were higher (0.51°) at the 19th Street Bridge than the prestressed concrete bridge. However, most of the rotation seemed to be the result of the skewed supports, for a skewed bridge creates a system that naturally rotates due to the differences in support conditions on the individual girders. The slight differences at the exterior and interior girders were likely driven by the torsion of the overhang.

- The majority of relative imperfection shapes for the fascia girder changed as expected (84%), either as a positive half-wave shape or an S-shaped wave with positive imperfections at the bottom. Thus, the overhang brackets did have a significant impact on the shape of the imperfections.
- The relative imperfections due to the deck pour at the 19th Street Bridge were on the order of $D/540$, which is relatively small to permissible imperfections during fabrication. Though the imperfections were not significant, the deck pour did seem to smooth out the profile of the initial web imperfections. In addition, the absolute imperfections were small, as all of the locations were less than the $D/150$ fabrication limit specified by AWS (2008).
- Placing the heavy duty overhang brackets toward the bottom of the web helped to reduce the effect of the larger force from the brackets.

5.2.3 Curved Steel Bridge (SH 71-SH 130)

A three-span continuous curved steel system, with a center line radius of curvature of approximately 1,220 feet, at the interchange between SH 71 and SH 130 (Span 14), was the final bridge investigated. The bridge has four plate girders with 84 inch deep webs and a total length of nearly 550 feet. On April 16, 2008, the torsional rotations and web imperfections were monitored during the deck pour. The highlights of the results are presented below.

- As with the 19th Street Bridge, the instrumented span rotated as a unit at the bracing line locations. Between the cross frames, the fascia girders had slightly higher rotations, which is expected due to the torsional loading.
- Considering the depths of the girders, the imperfection at Span 14 and the 19th Street Bridge in Lubbock were approximately the same, $D/550$. Therefore, despite having worse-positioned brackets at Span 14, the positive imperfections at both sites were nearly the same. Since the

relative imperfections were not large, it is likely that neither of these webs were critical sections for local web imperfection problems.

- The differences in profile shapes for Locations 12 and 32 along the fascia girder suggest that web imperfections could be affected by global effects in addition to the local effects of the overhang brackets.
- For the fascia girder, the initial profile gave an indication of the relative imperfection profile. In general, the deck pour caused an S-shaped relative change in imperfection profile for the locations measured.
- Where the initial shape at a location gave an indication of the changed shape for the fascia girder, the initial shape for the interior girder rarely followed a trend, which also suggests that imperfections are influenced by global properties, such as temperature and girder stress.

5.3 RECOMMENDATIONS & FUTURE WORK

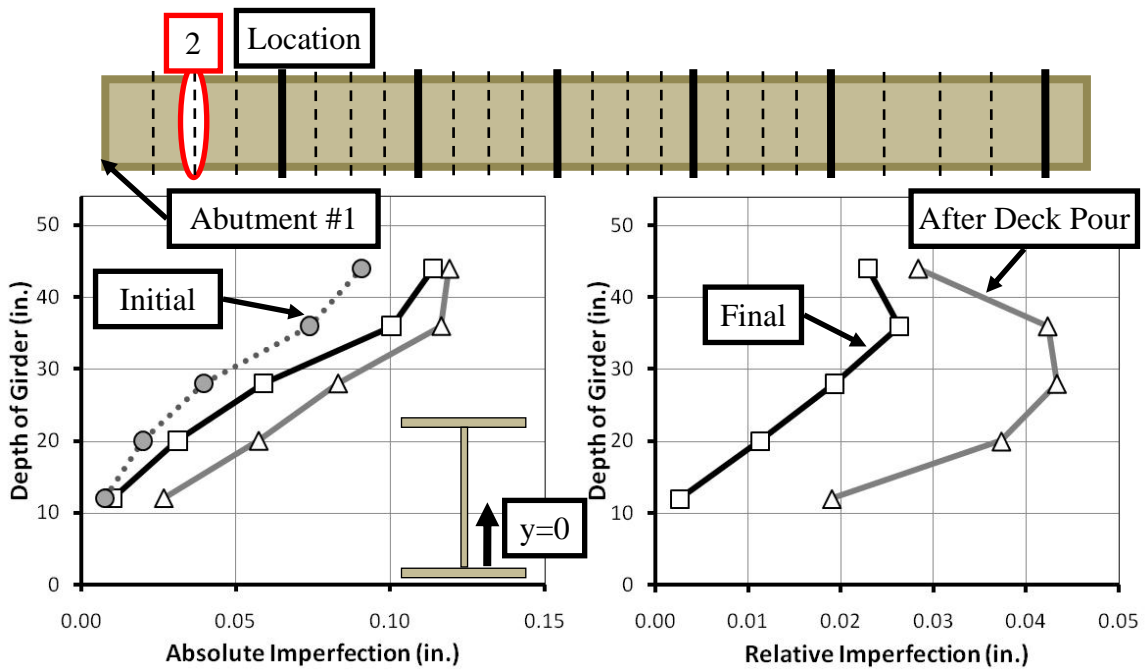
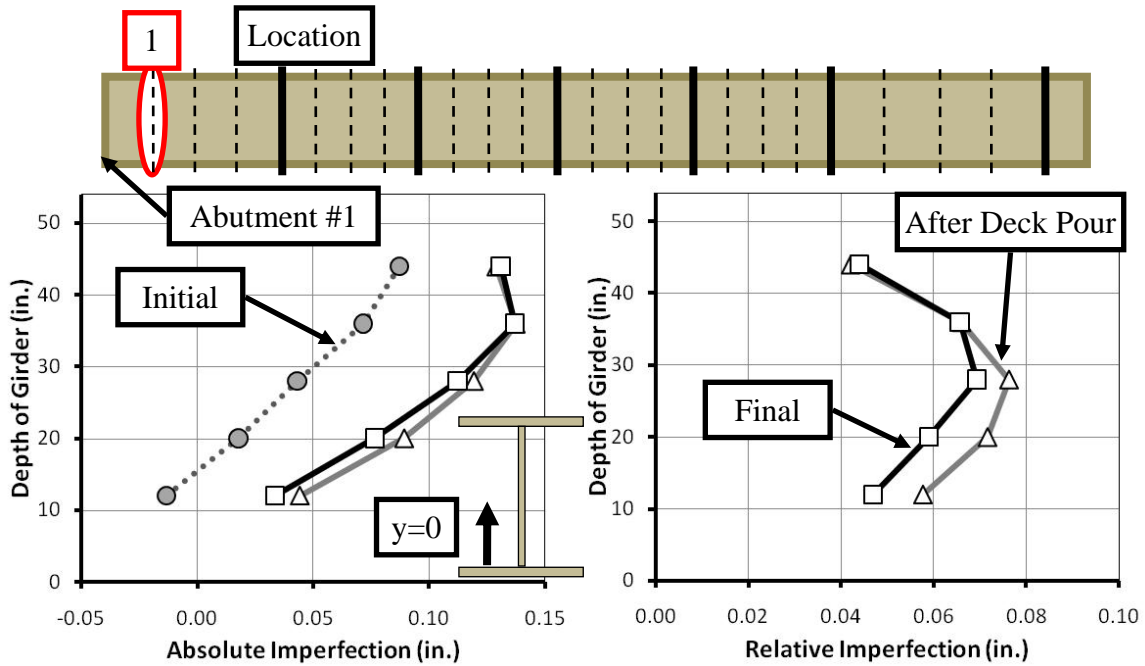
Considering only the results from the field monitoring, the below recommendations can be made. Other recommendations will follow once the laboratory testing and parametric studies are finished. In particular, current rules of thumb will be evaluated to develop rules supported by research observations. In addition, critical overhang and bracing geometries will be identified that can result in poor behavior. Based upon the findings, recommendations will be developed for the bracing or support conditions that can be utilized to avoid problems.

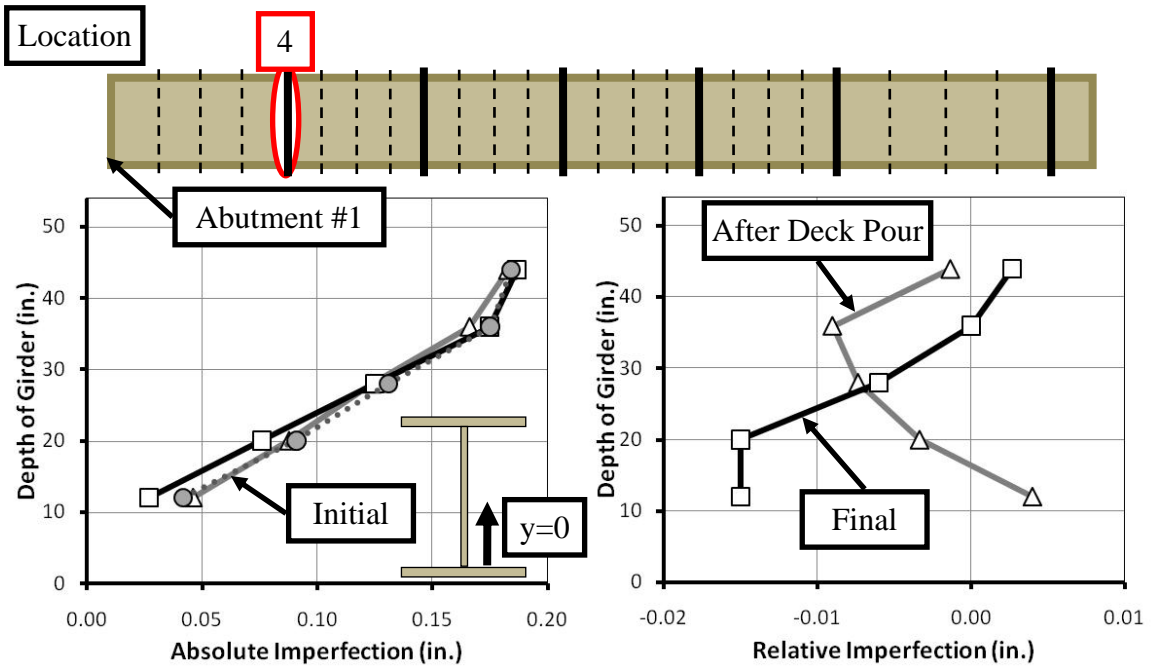
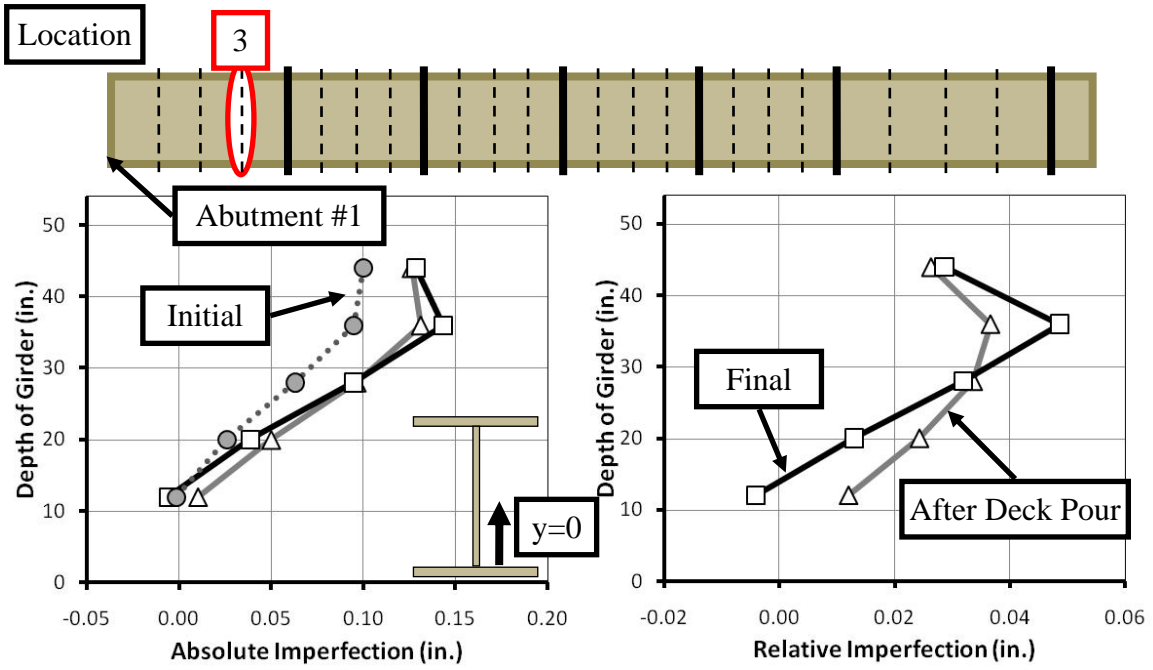
- Limits on the overhangs of bridges will be established based upon the girder sizes. Whether steel or concrete, smaller girders weigh less and have a lower torsional resistance. As discussed in Chapter 2, these girders are less stable and often result in more rotation during construction.
- The influence of overhang brackets on steel webs may cause more significant problems in girders with thinner webs. As such, the overhang brackets should be positioned near the bottom of the web to minimize the impact of the brackets on web imperfection behavior.

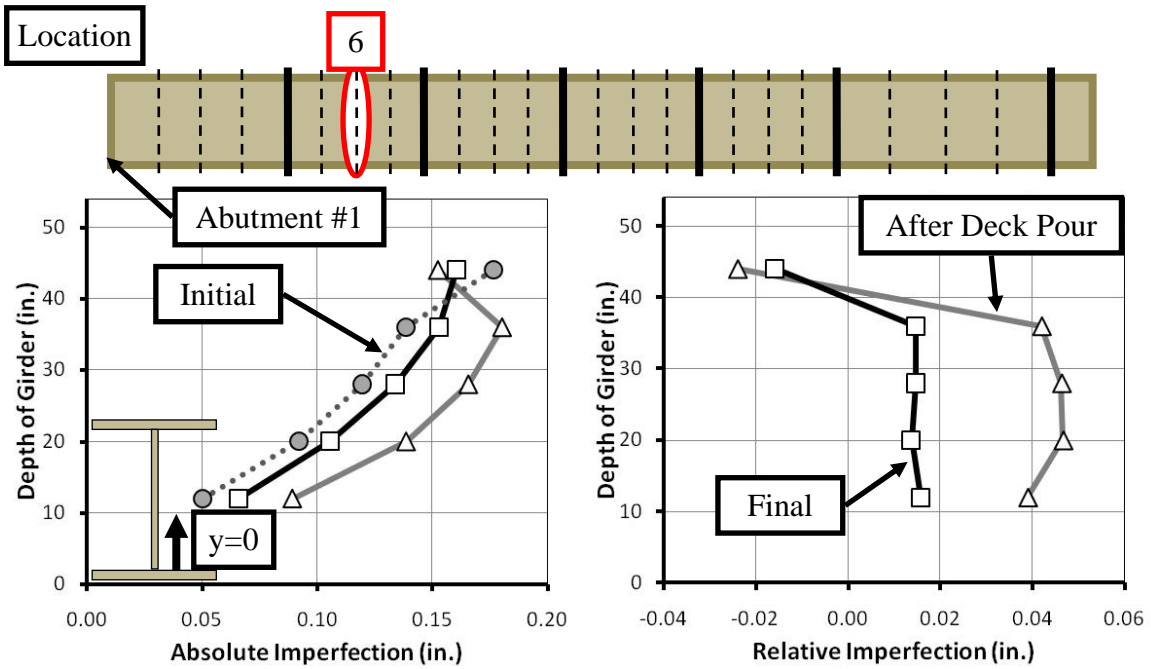
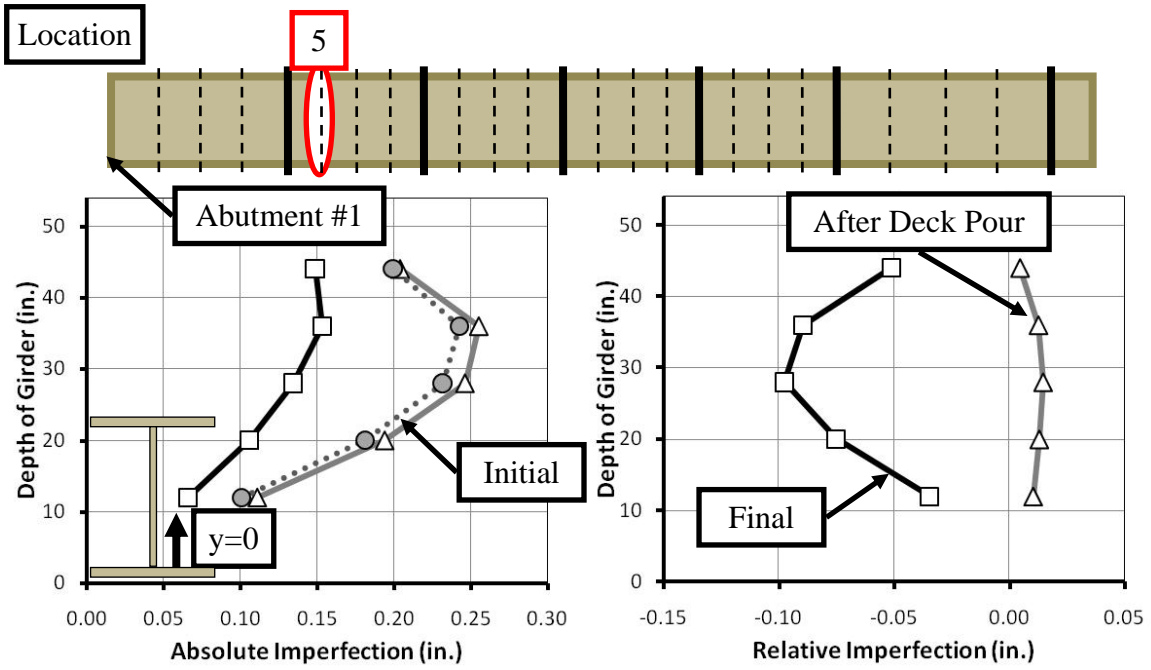
- Current connection details for the top bracing bar lead to ineffective bracing for prestressed concrete girder systems. Improved connection details will be developed based upon laboratory test results and parametrical FEA investigations.

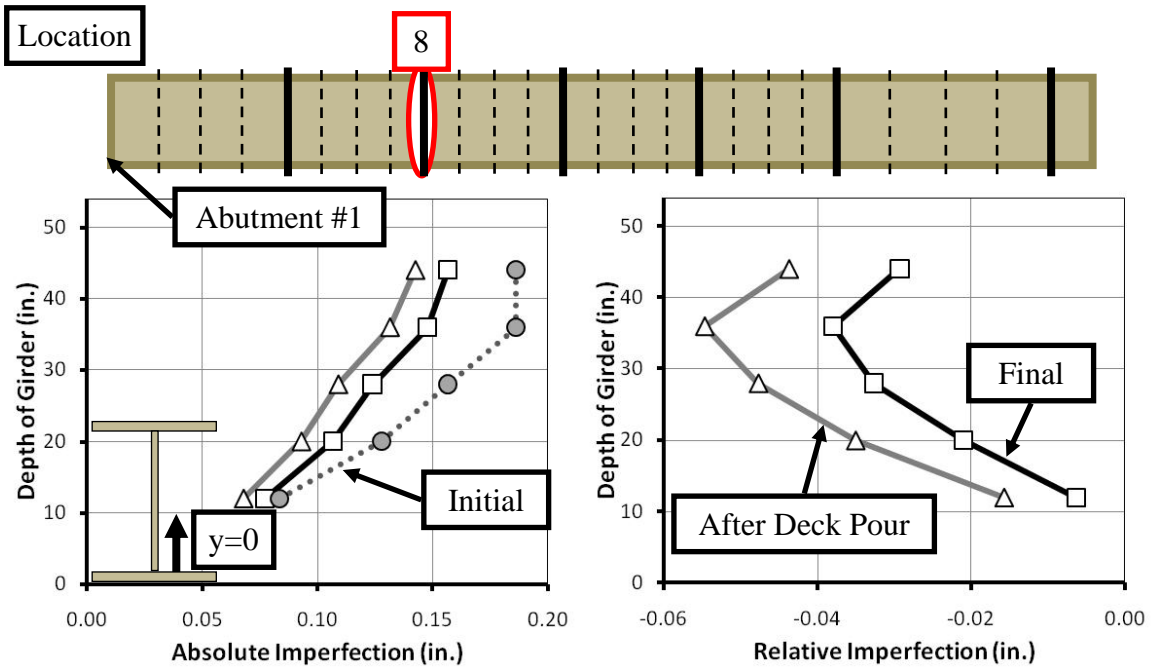
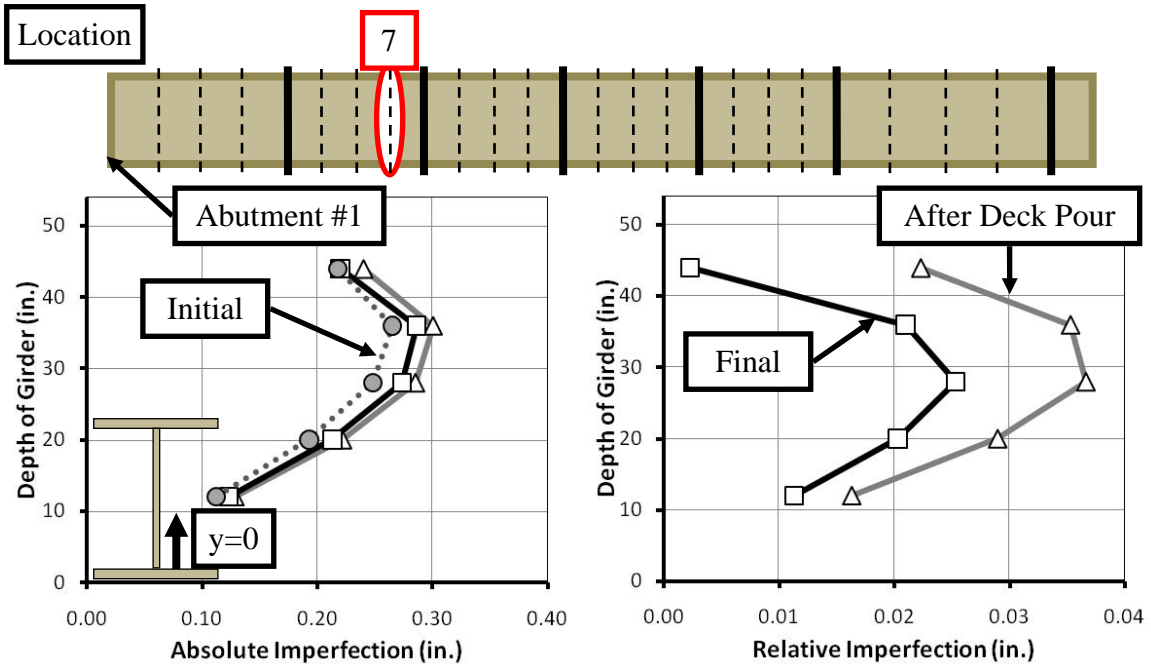
APPENDIX A

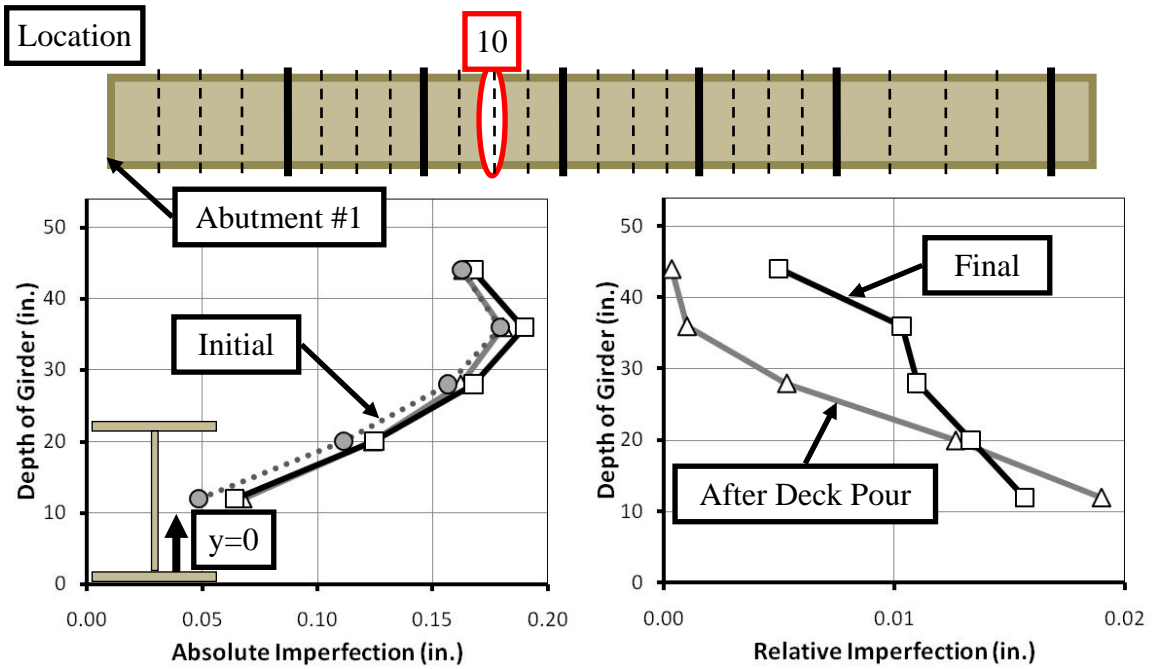
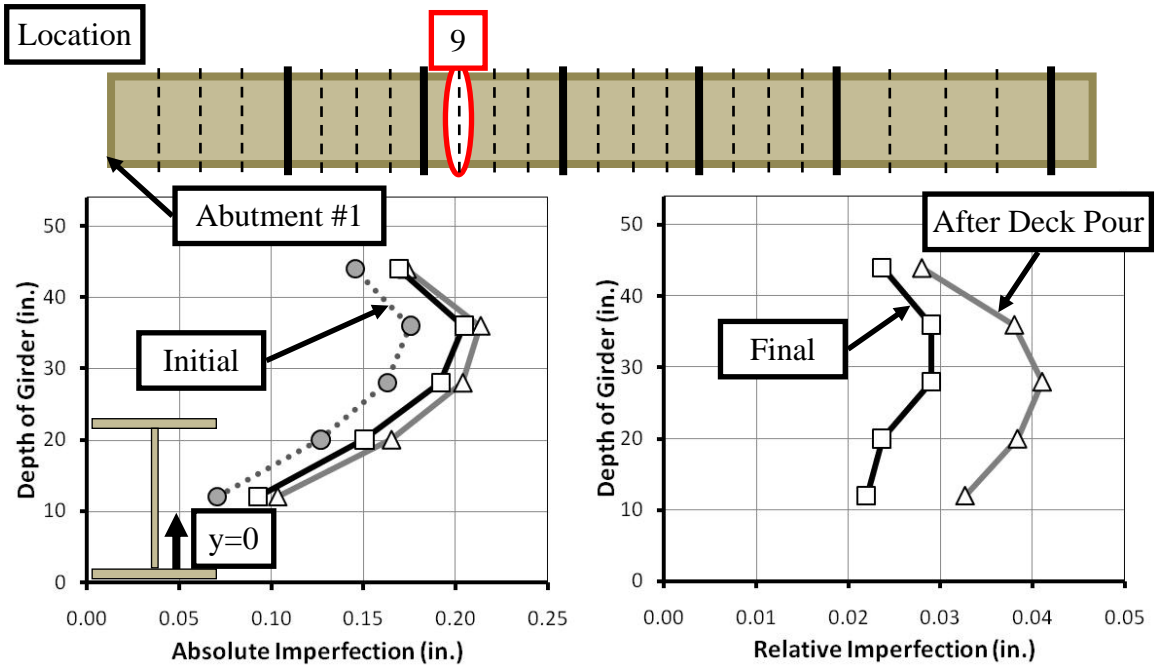
19th Street Bridge Web Imperfections: Fascia Girder

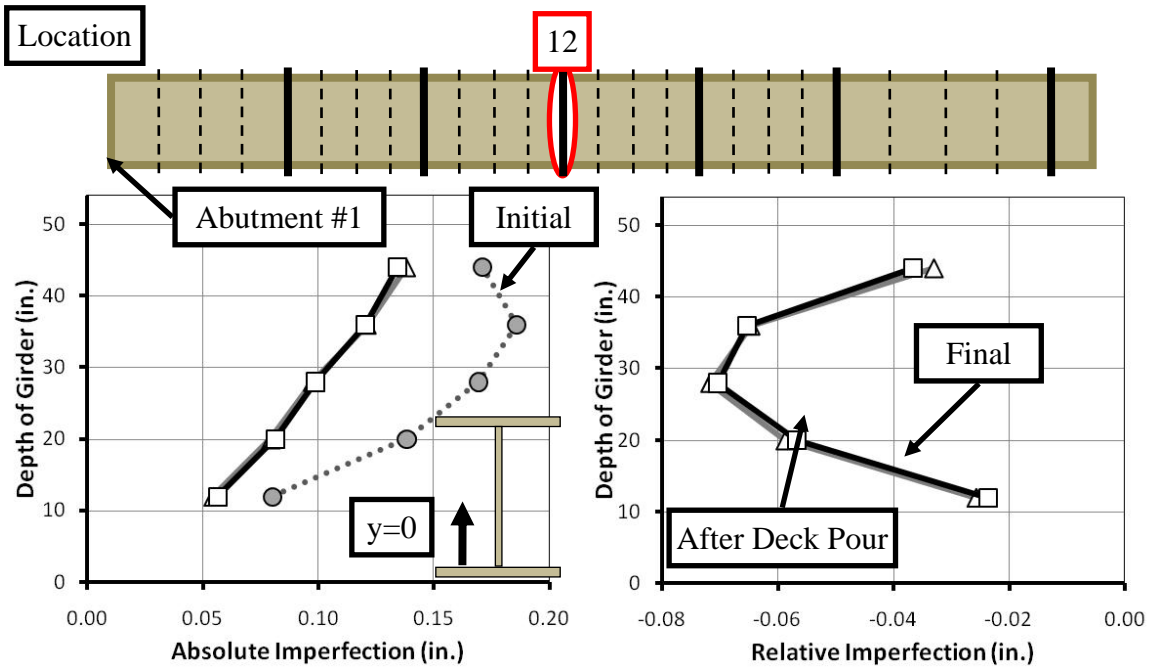
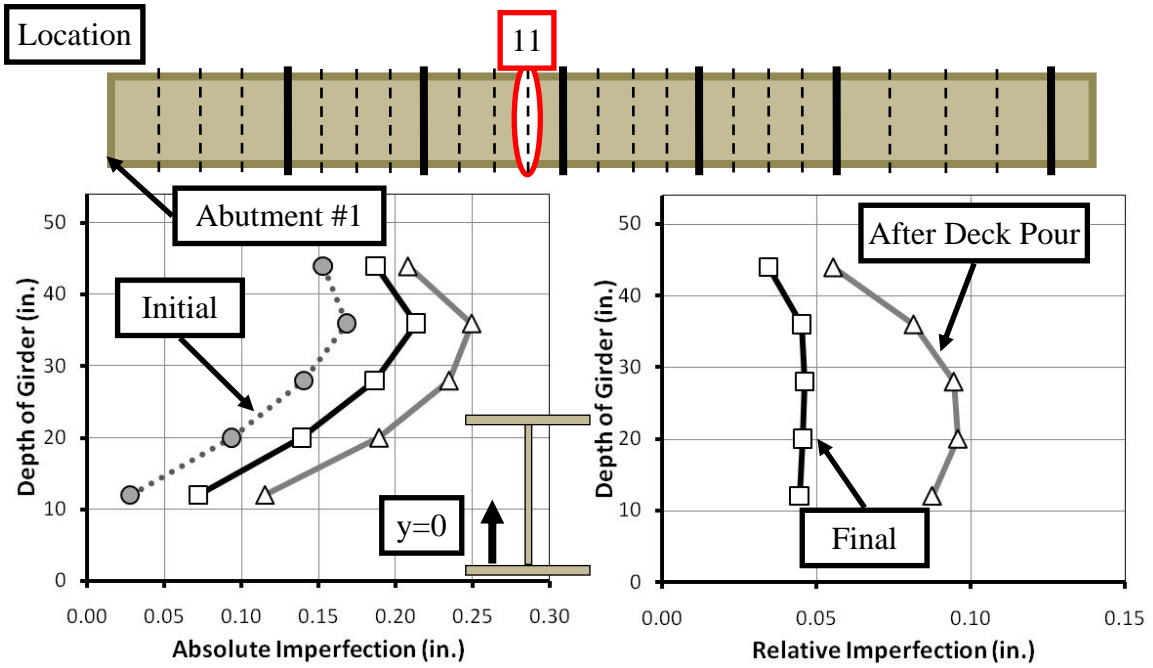


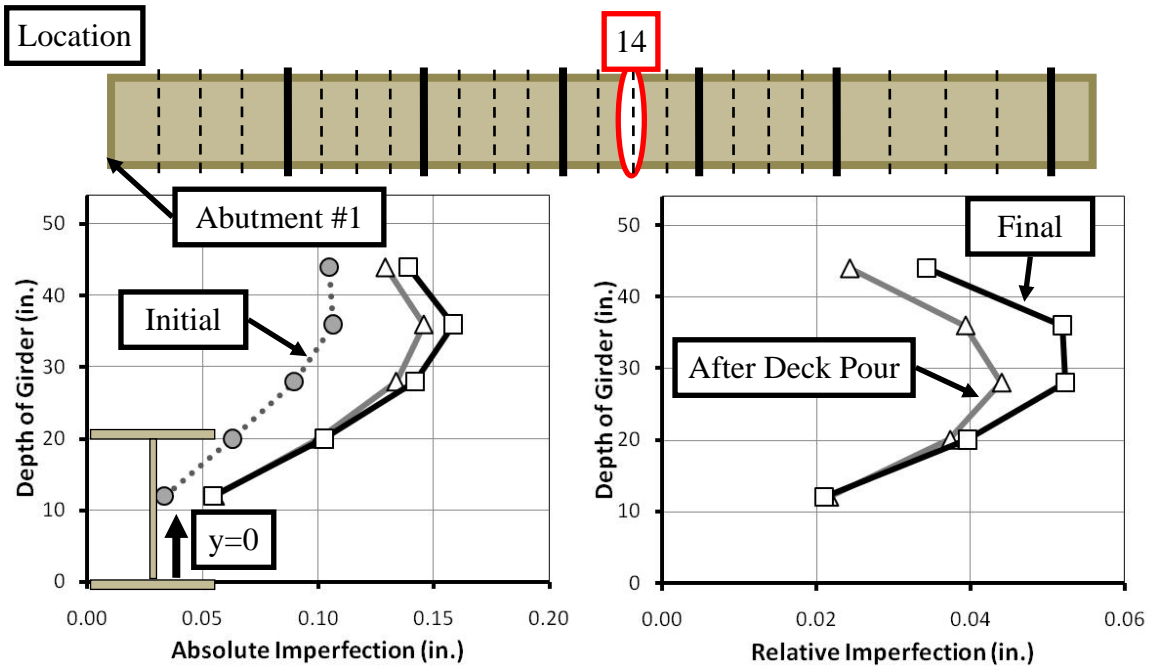
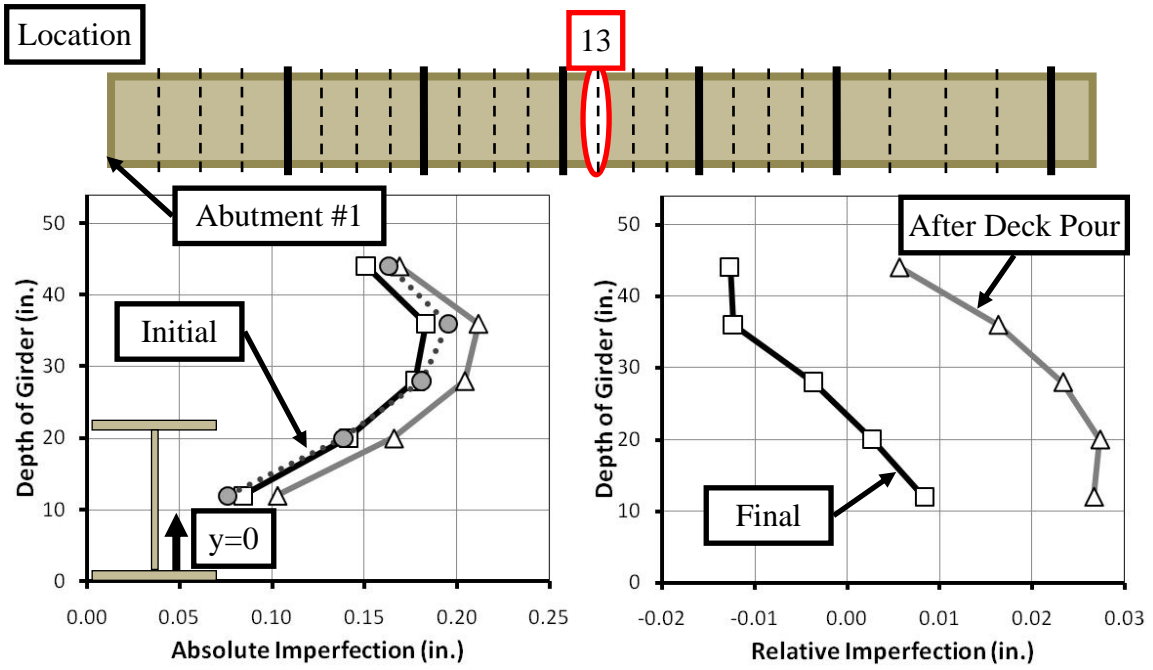


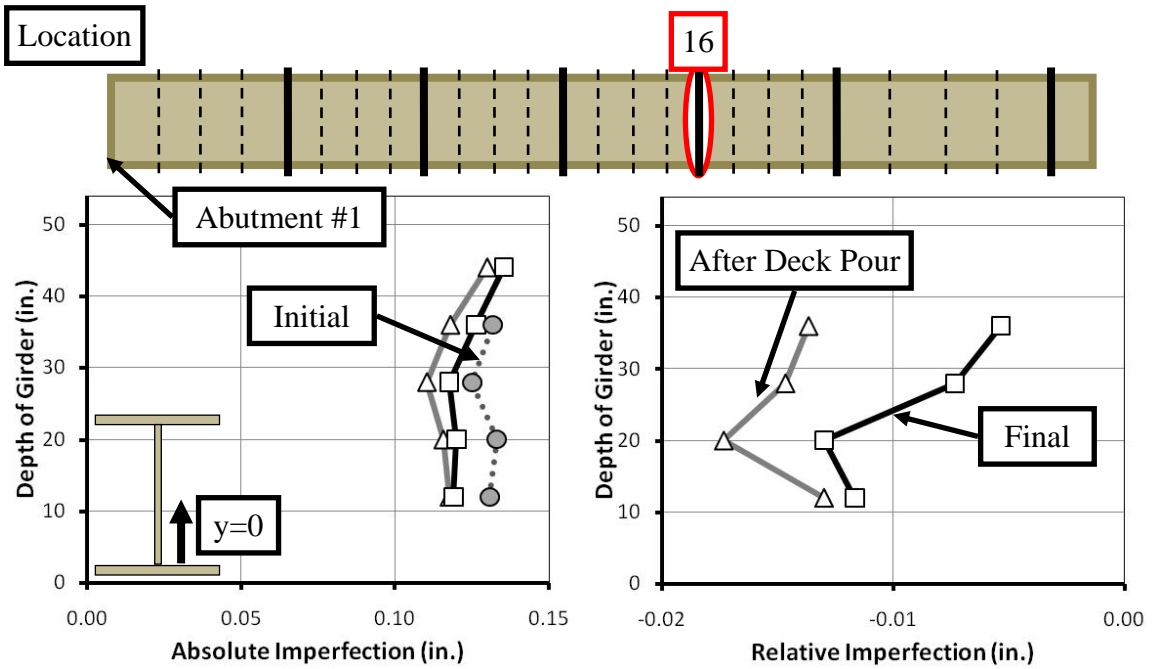
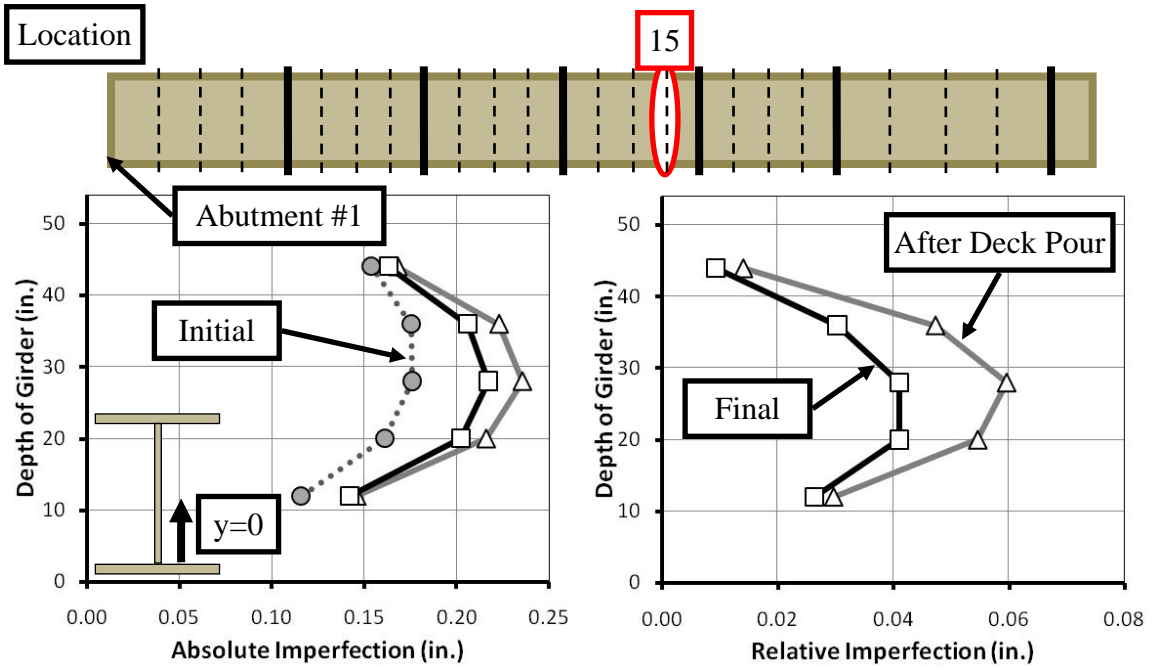


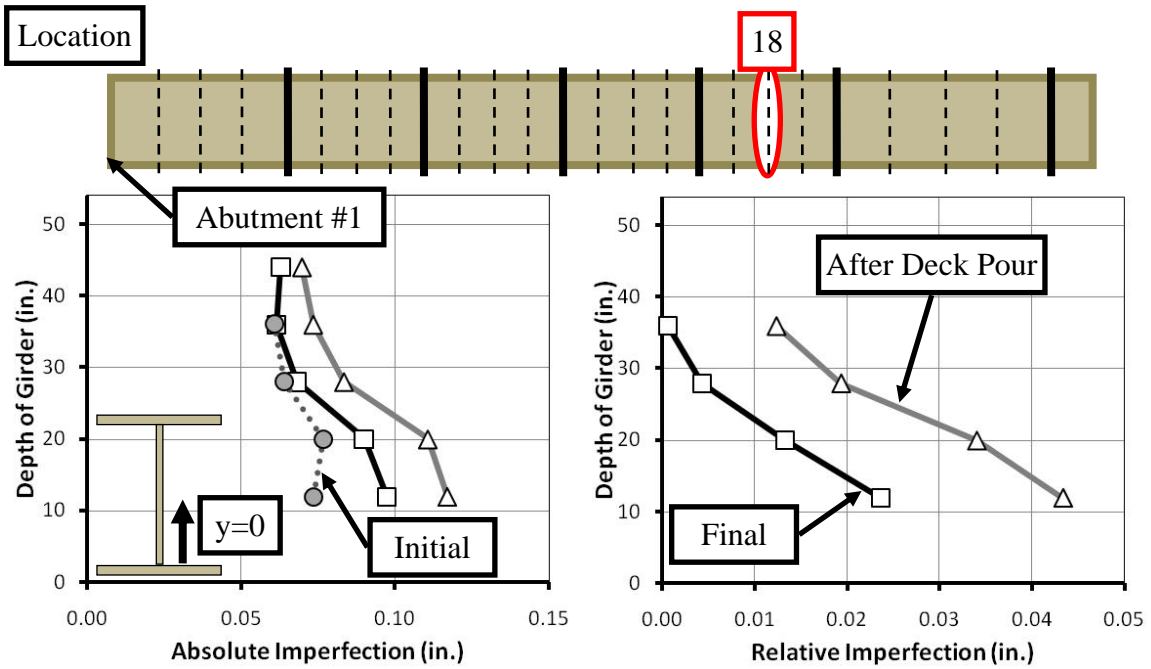
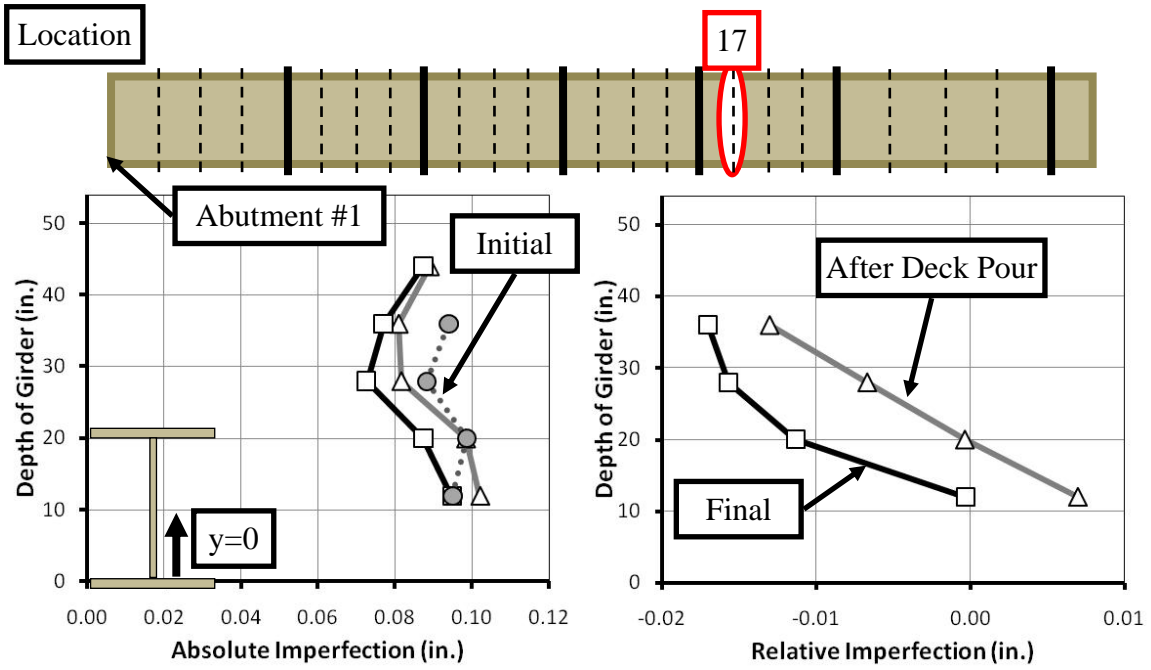


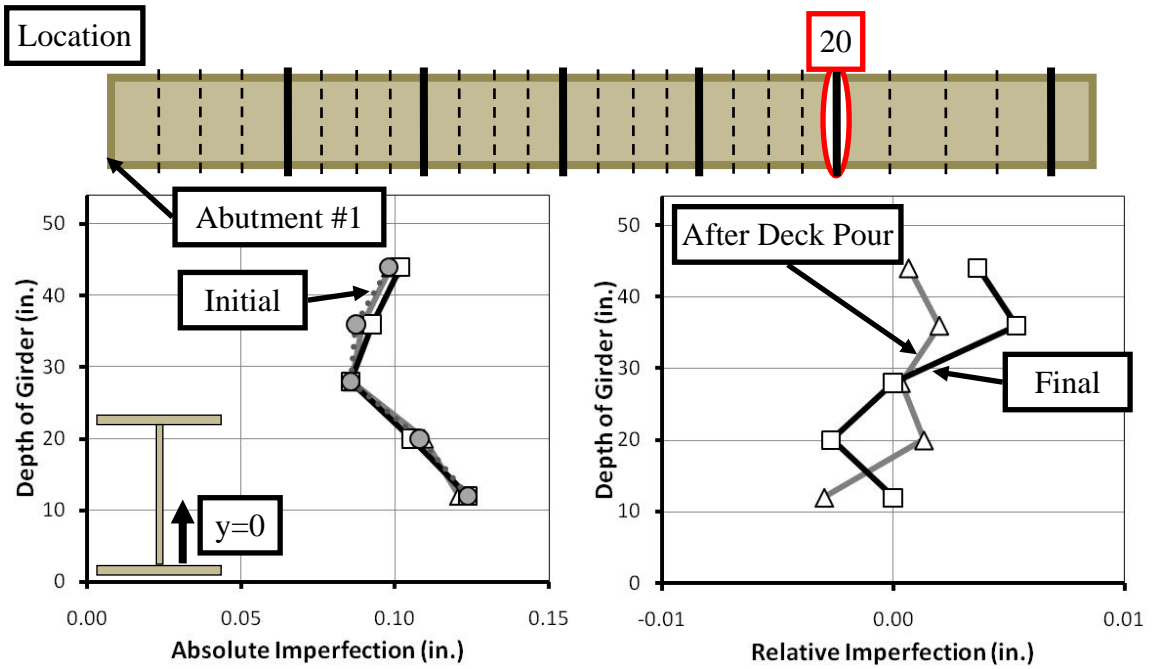
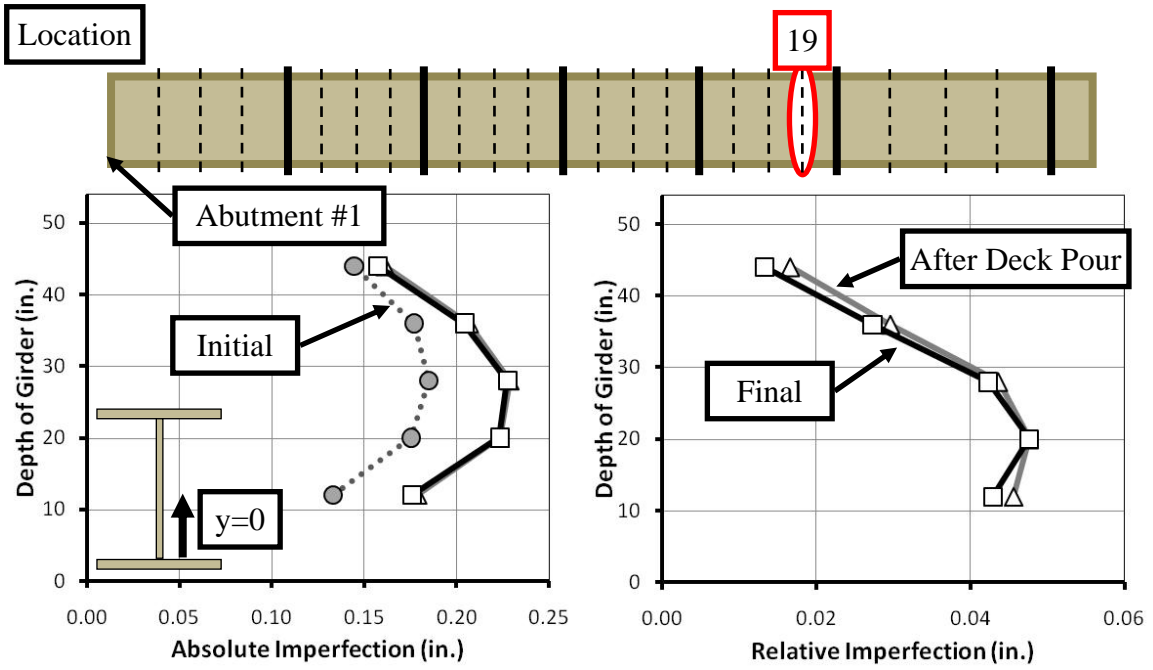


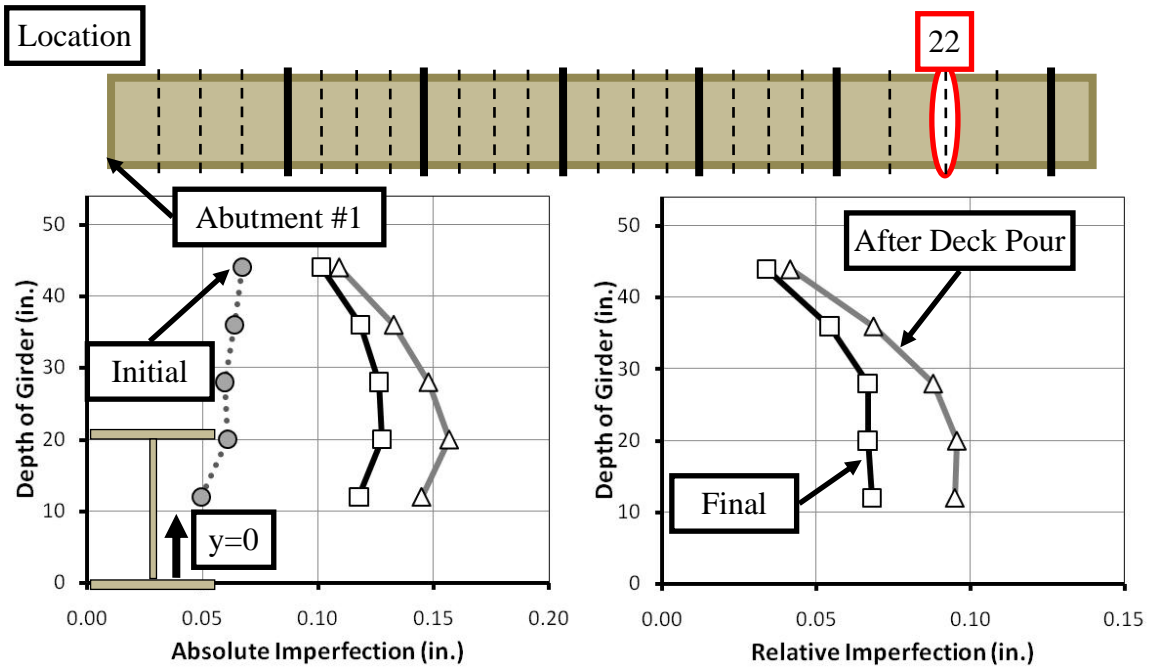
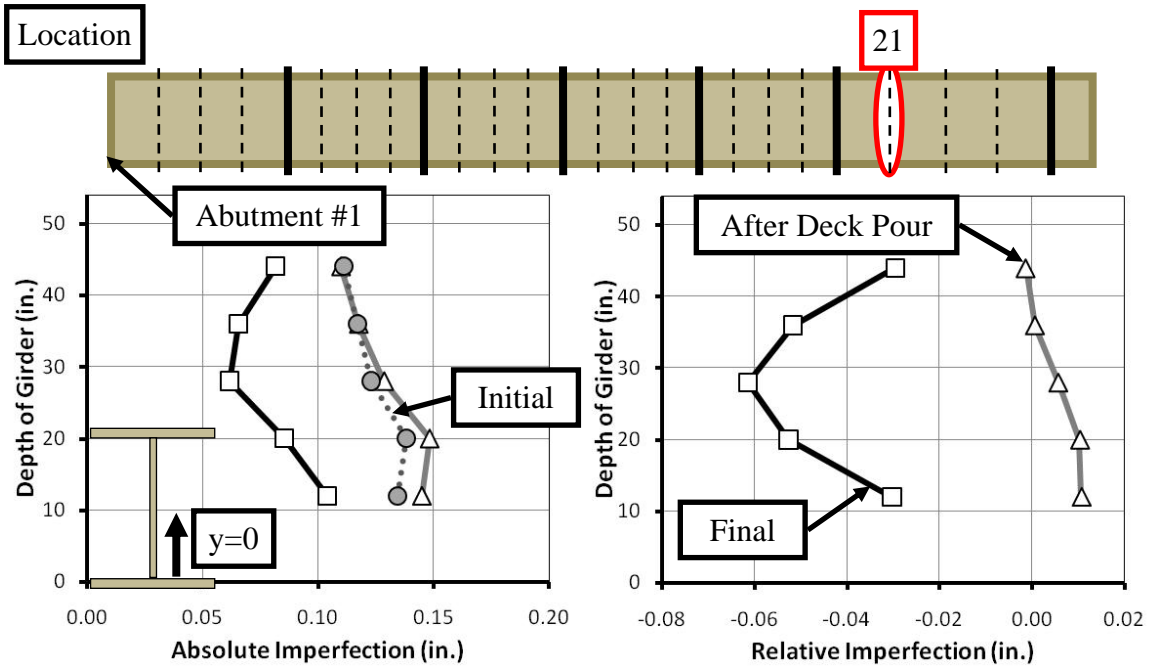


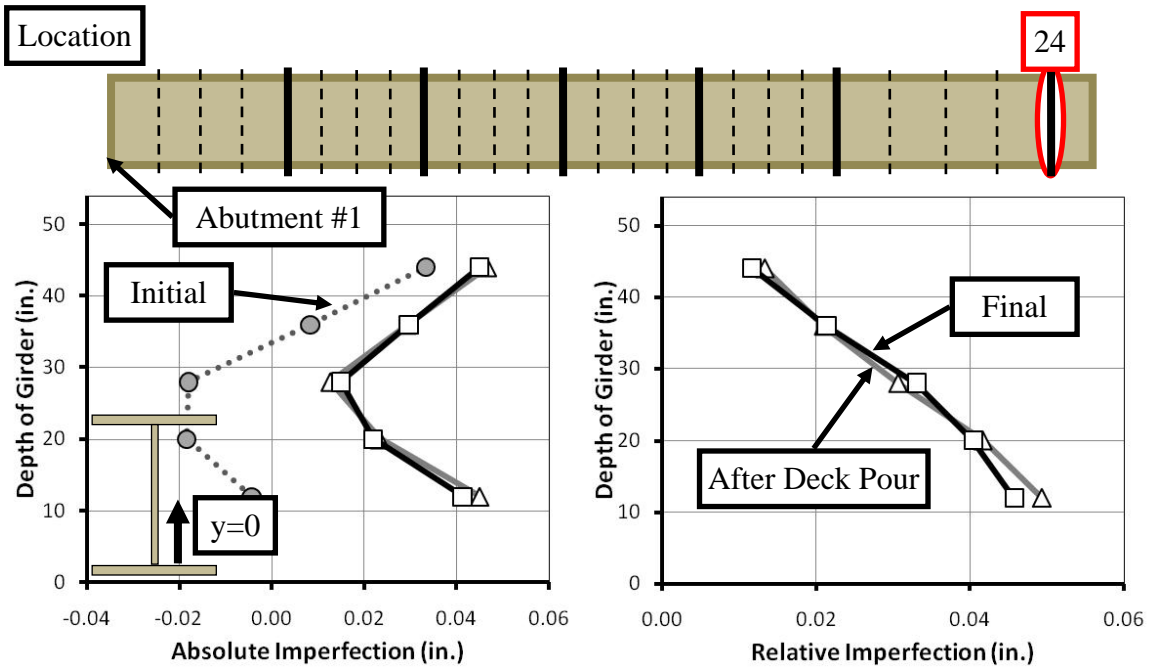
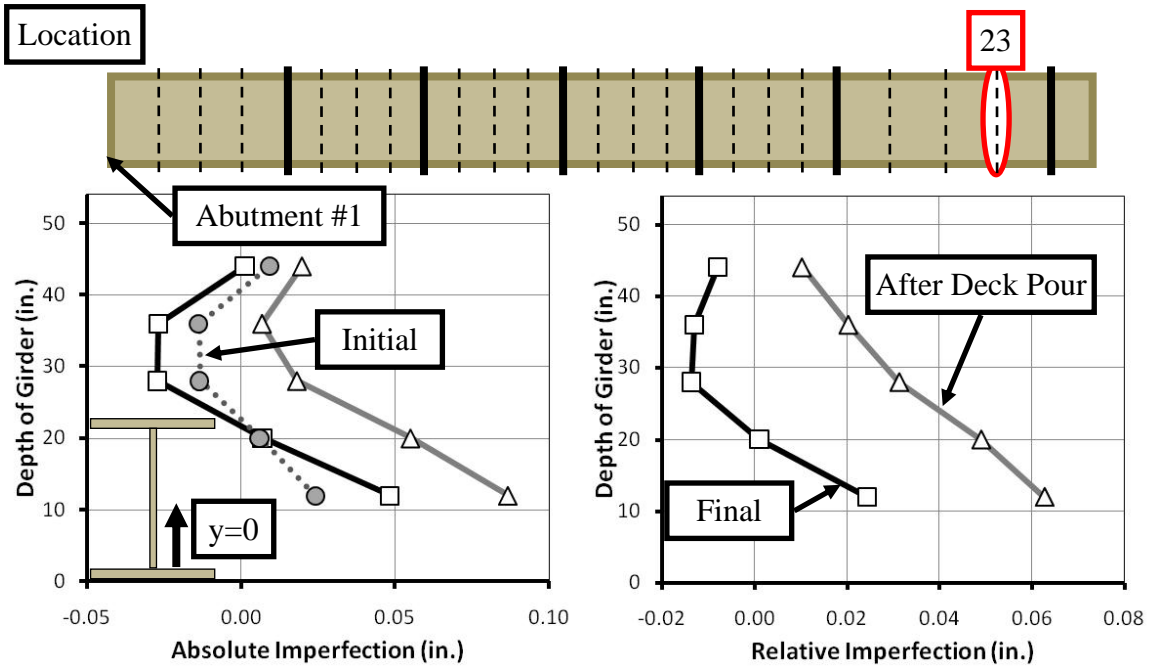






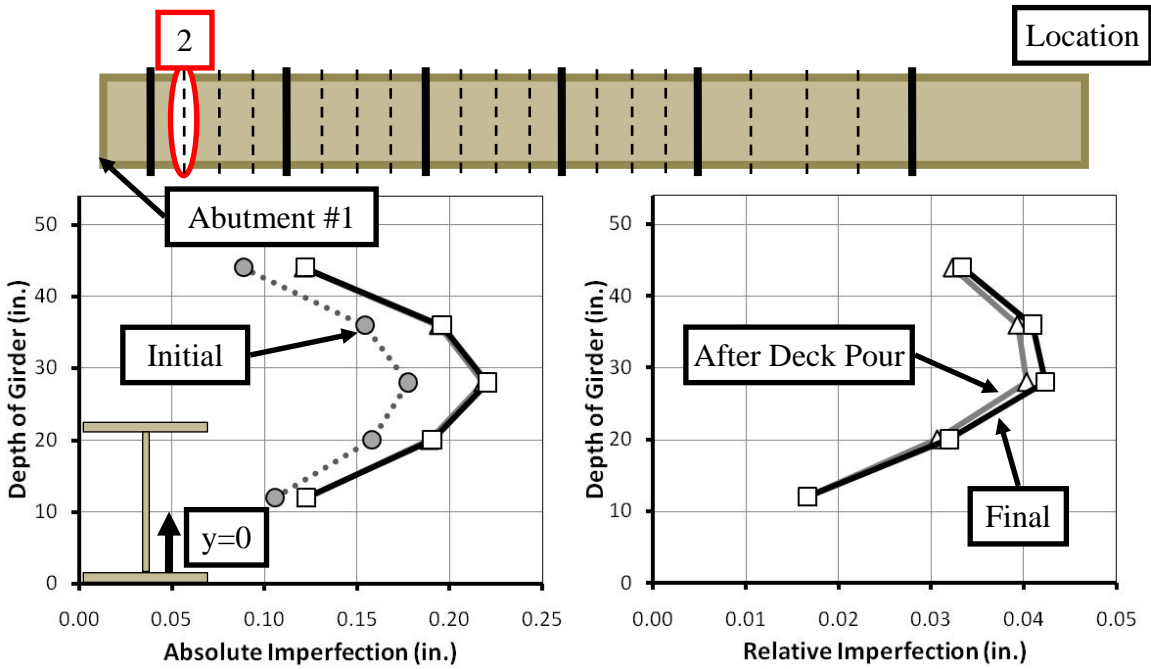
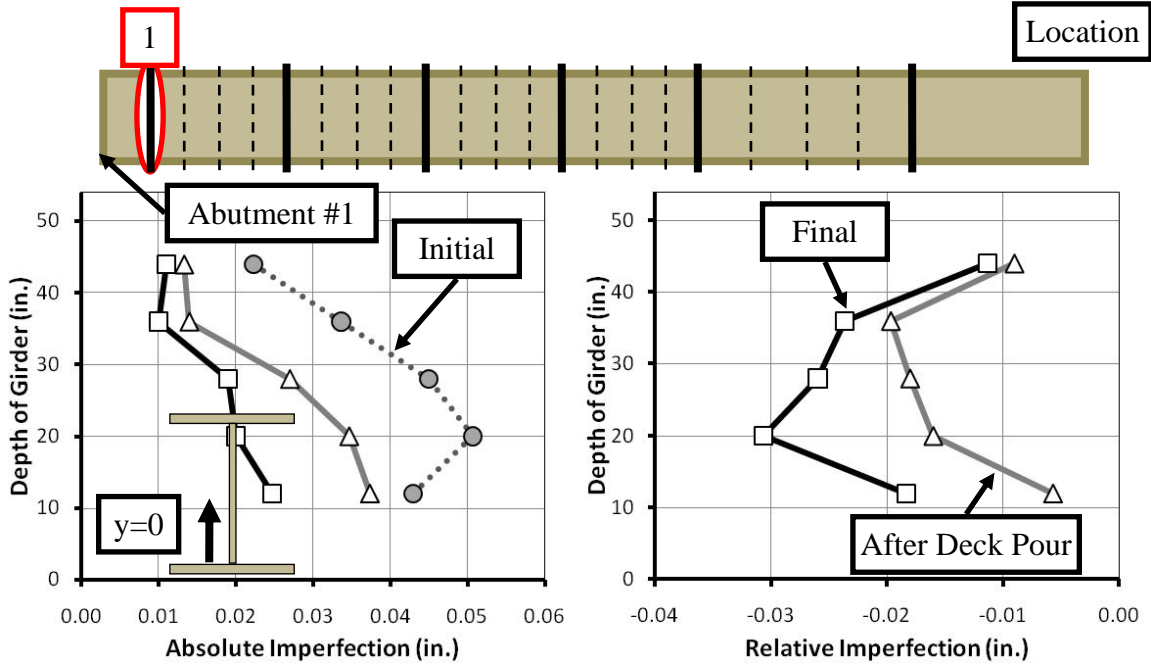


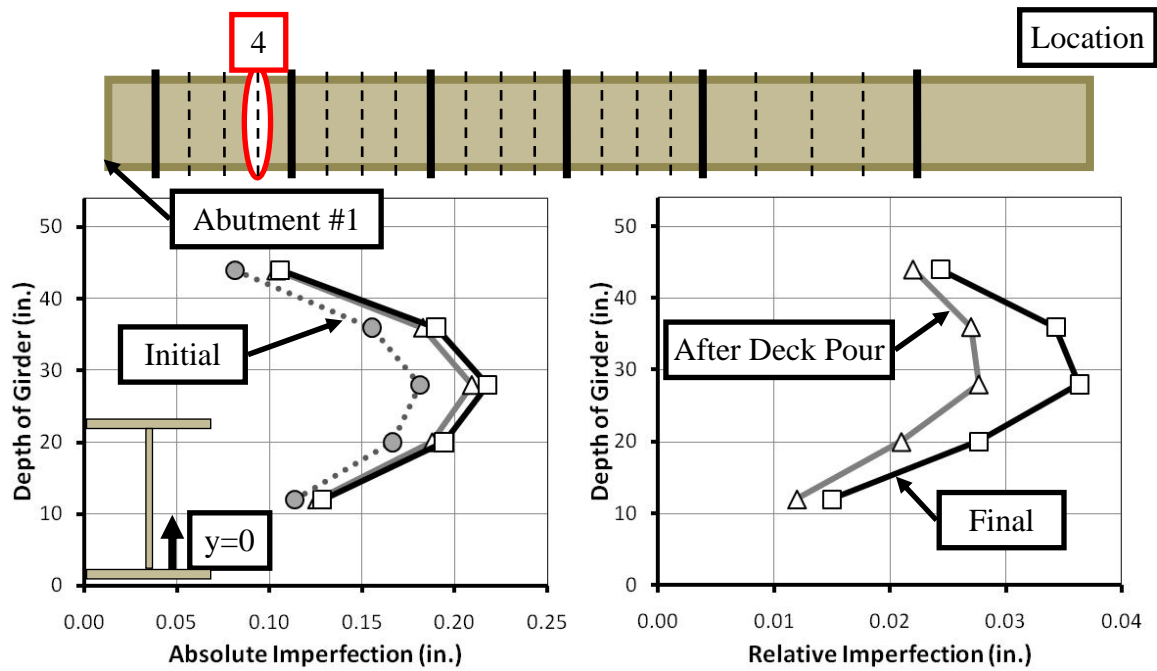
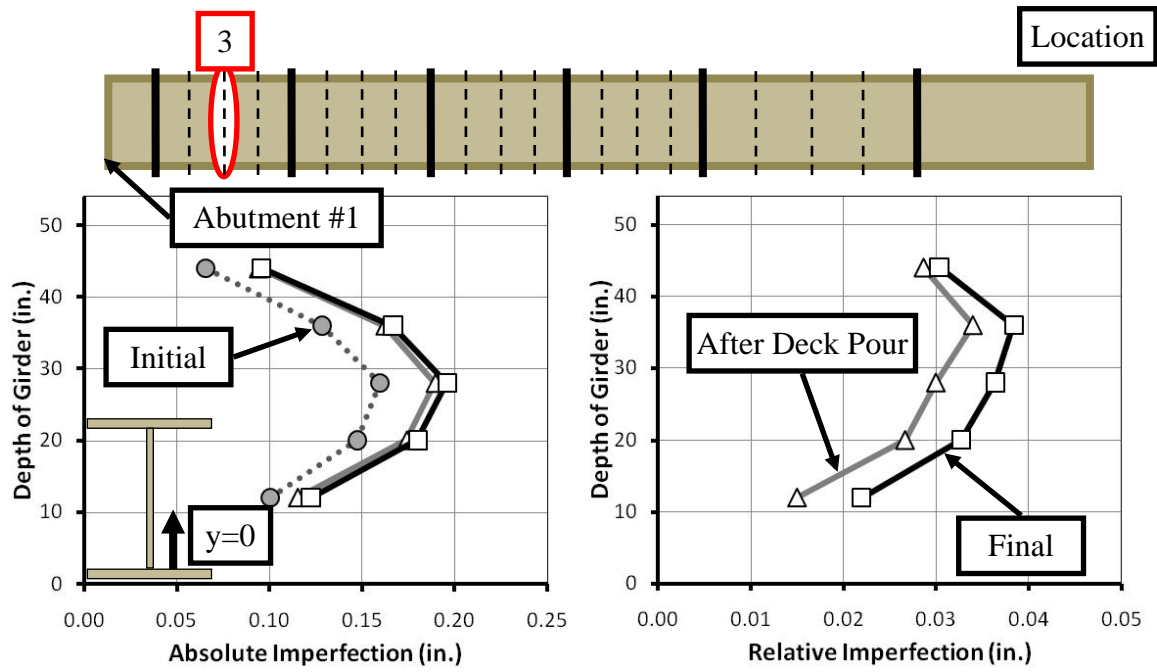


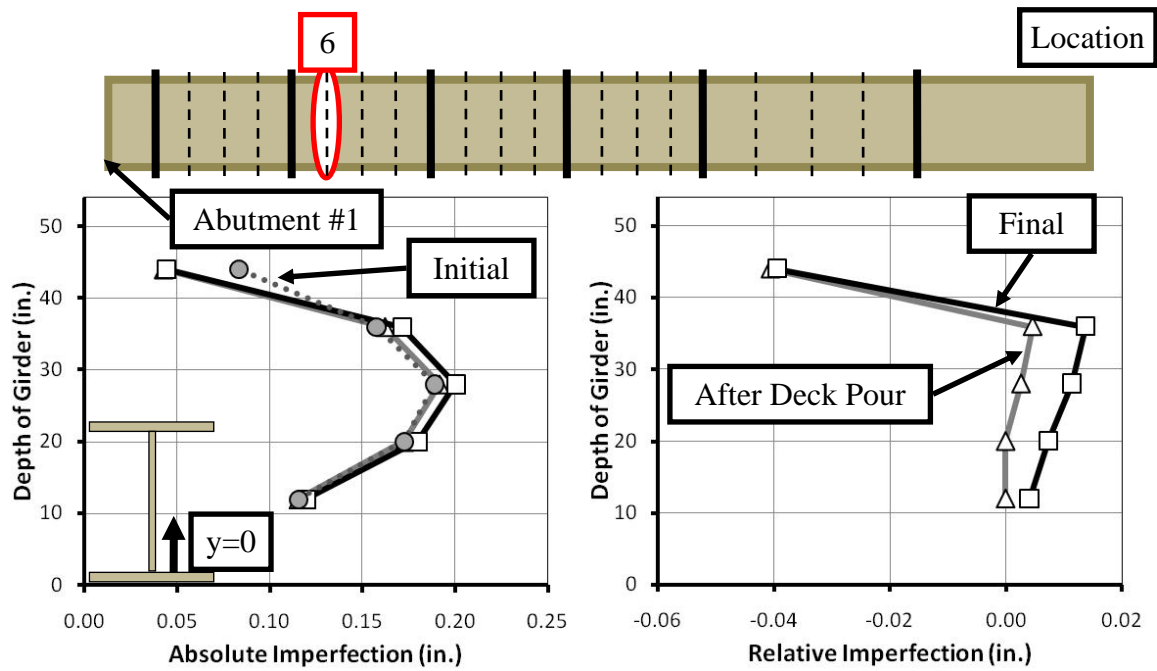
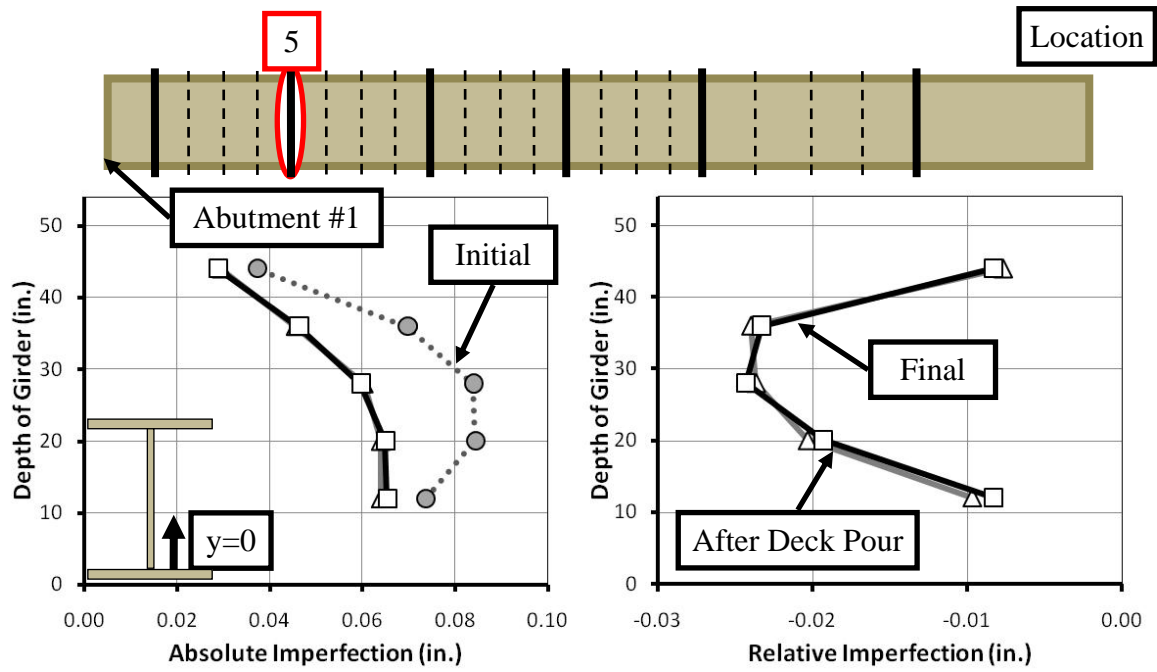


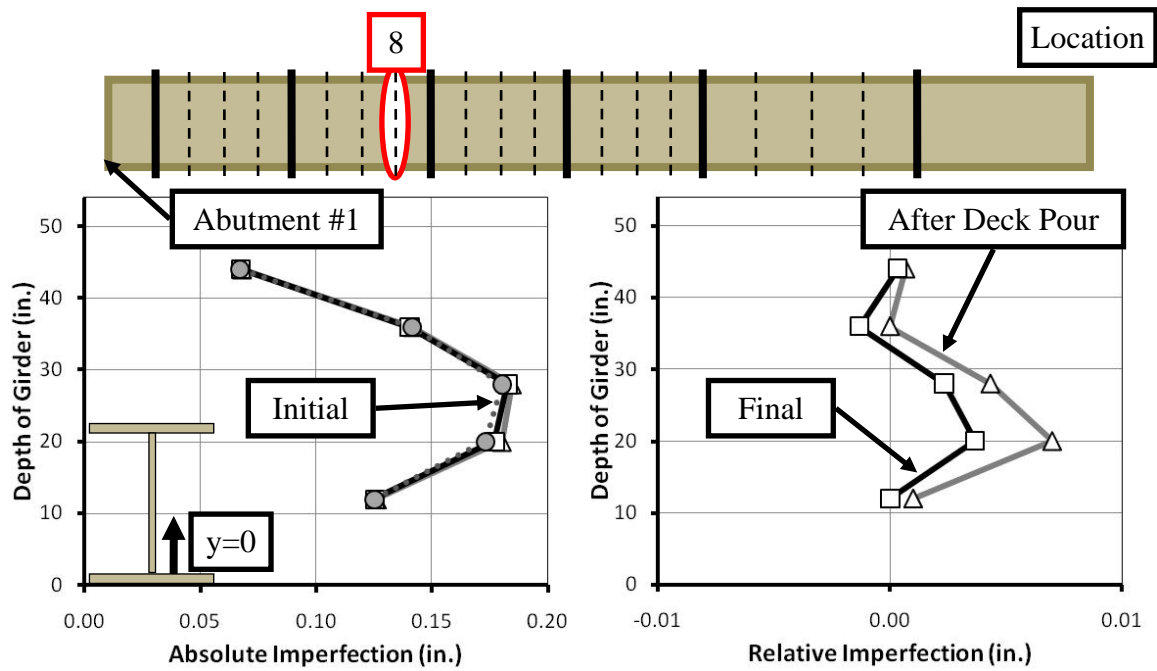
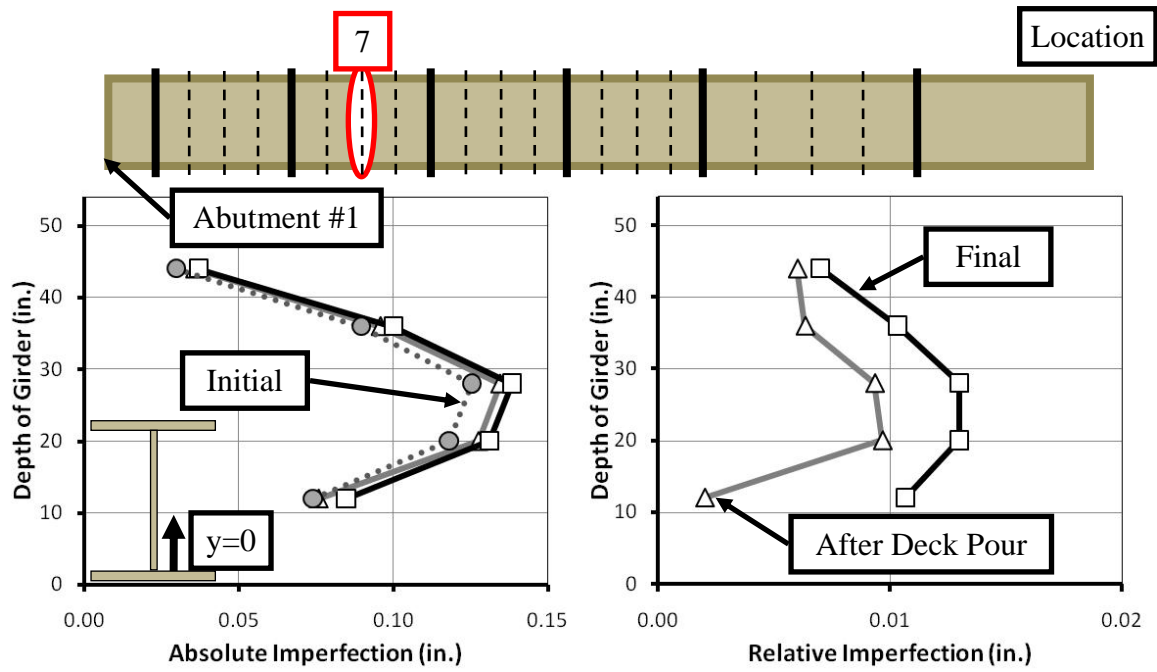
APPENDIX B

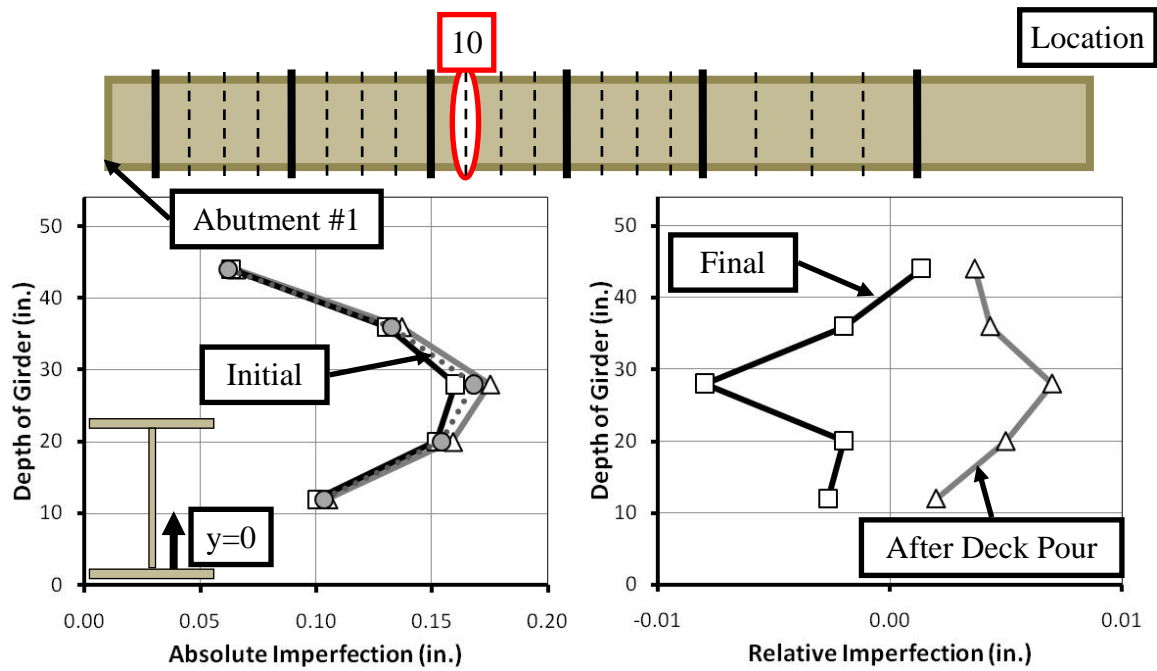
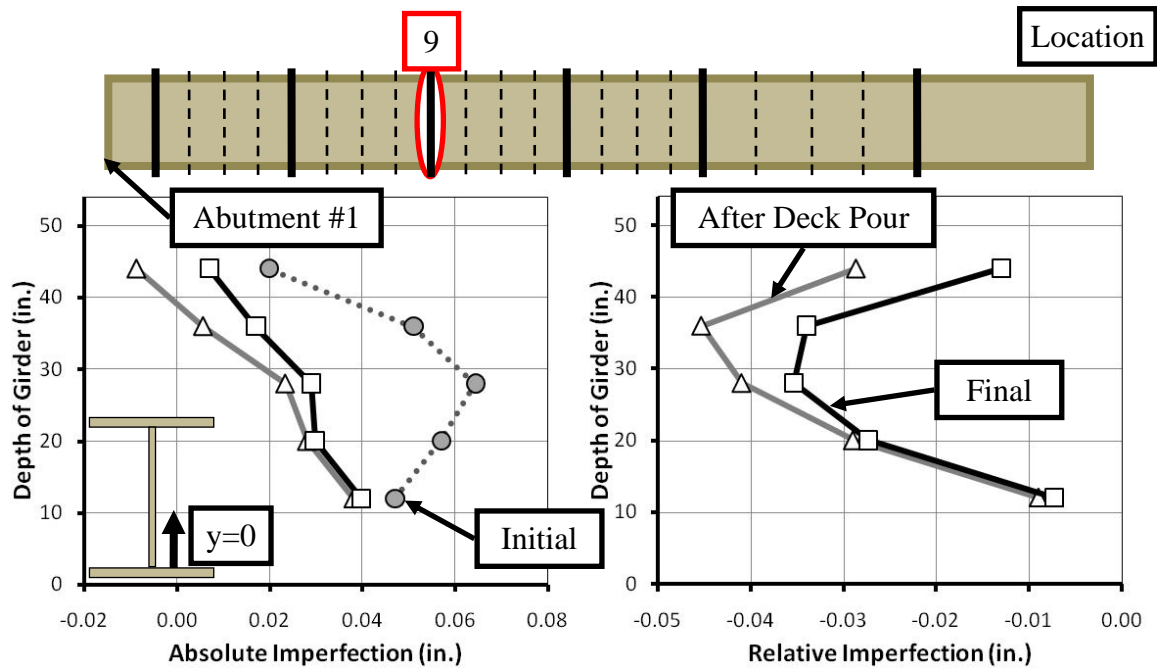
19th Street Bridge Web Imperfections: Interior Girder

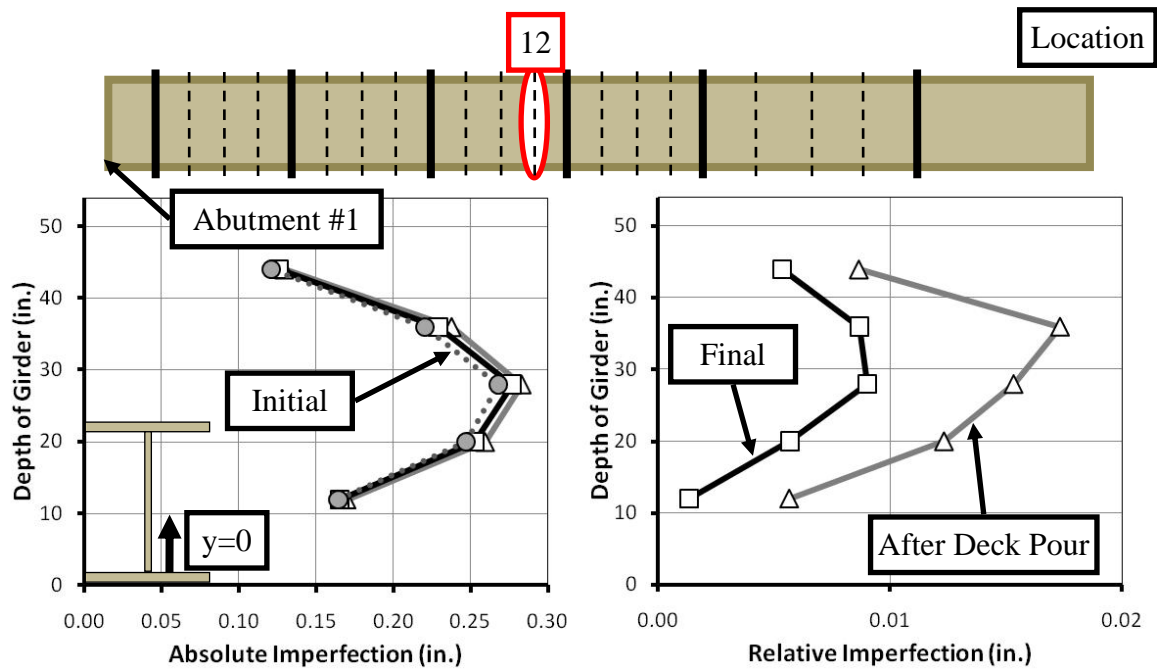
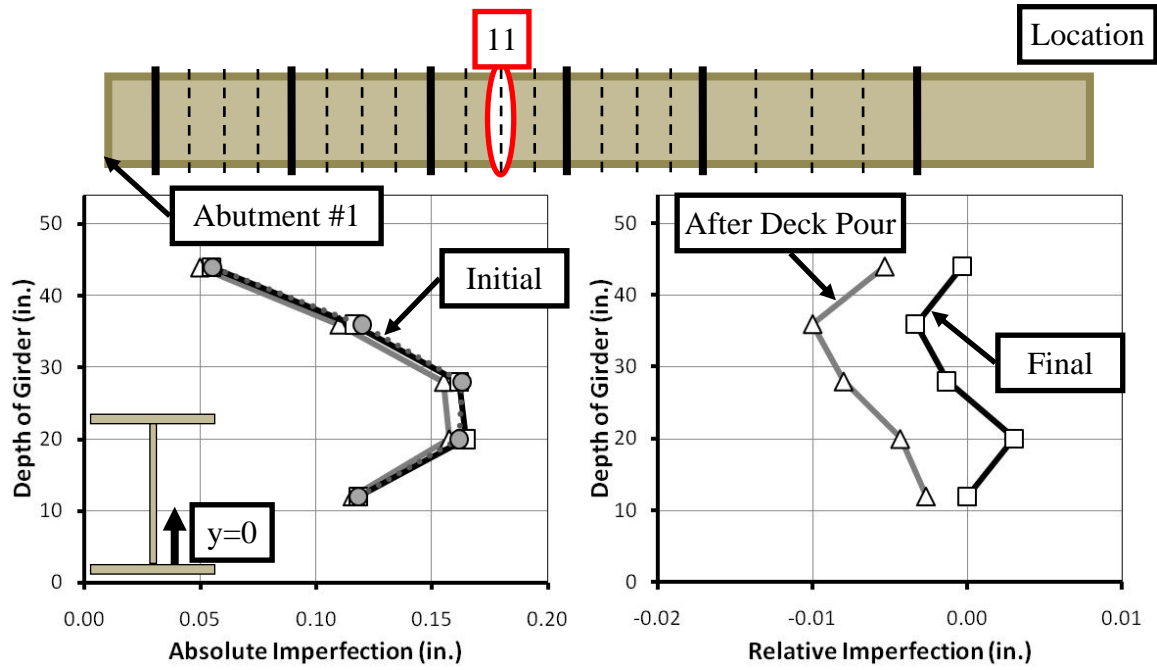


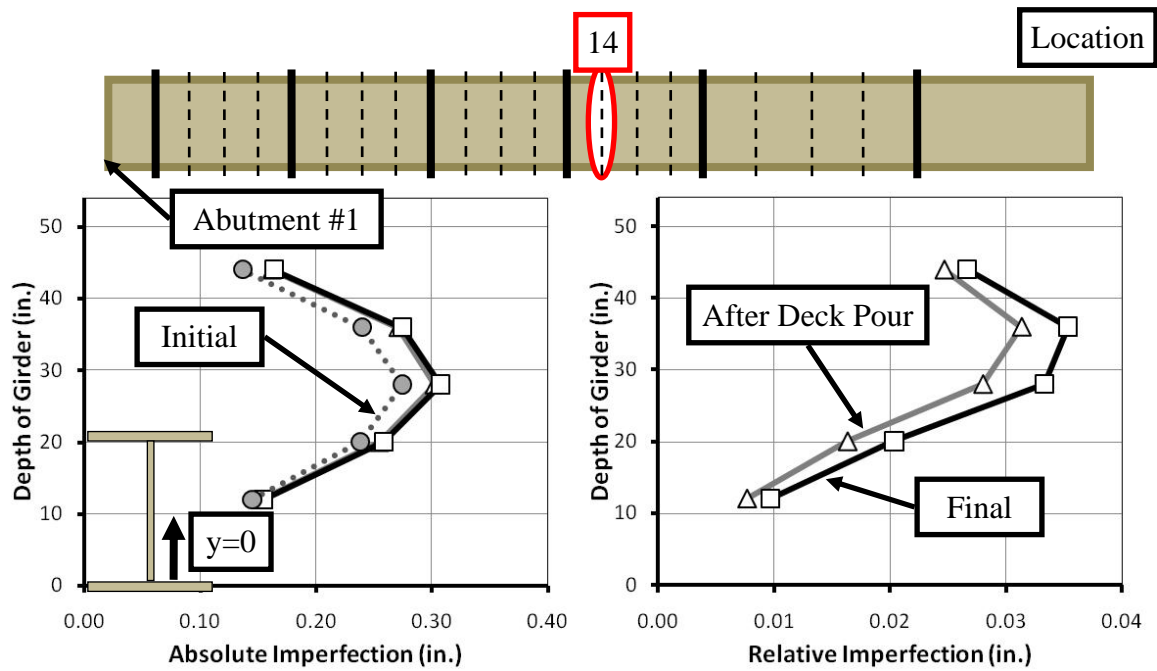
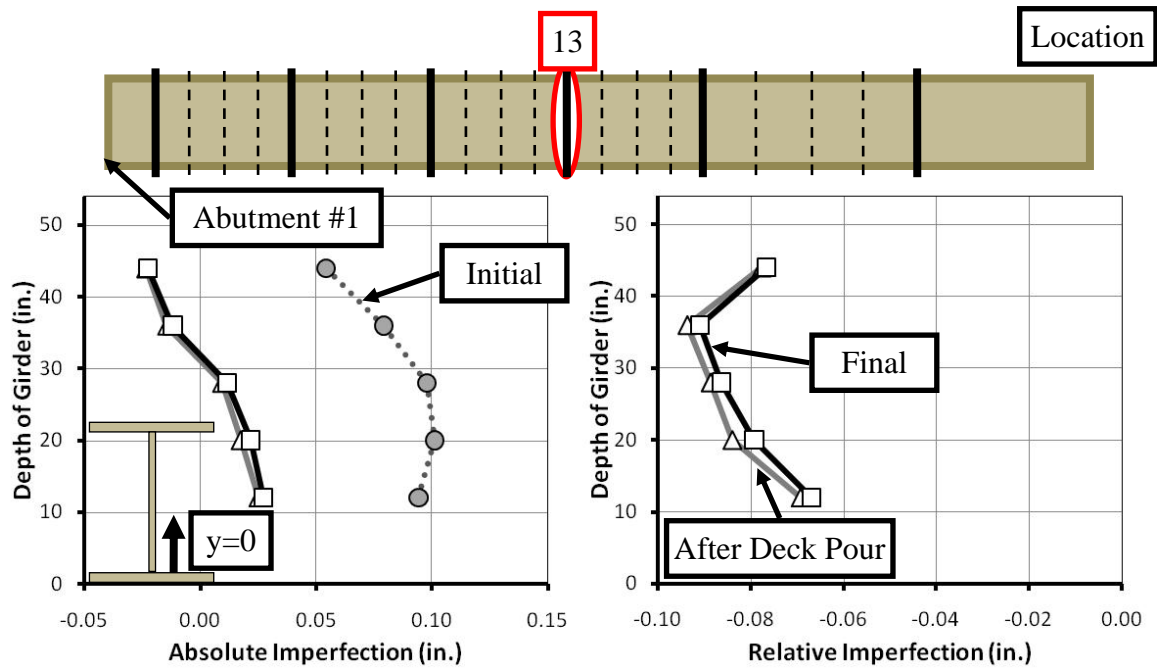


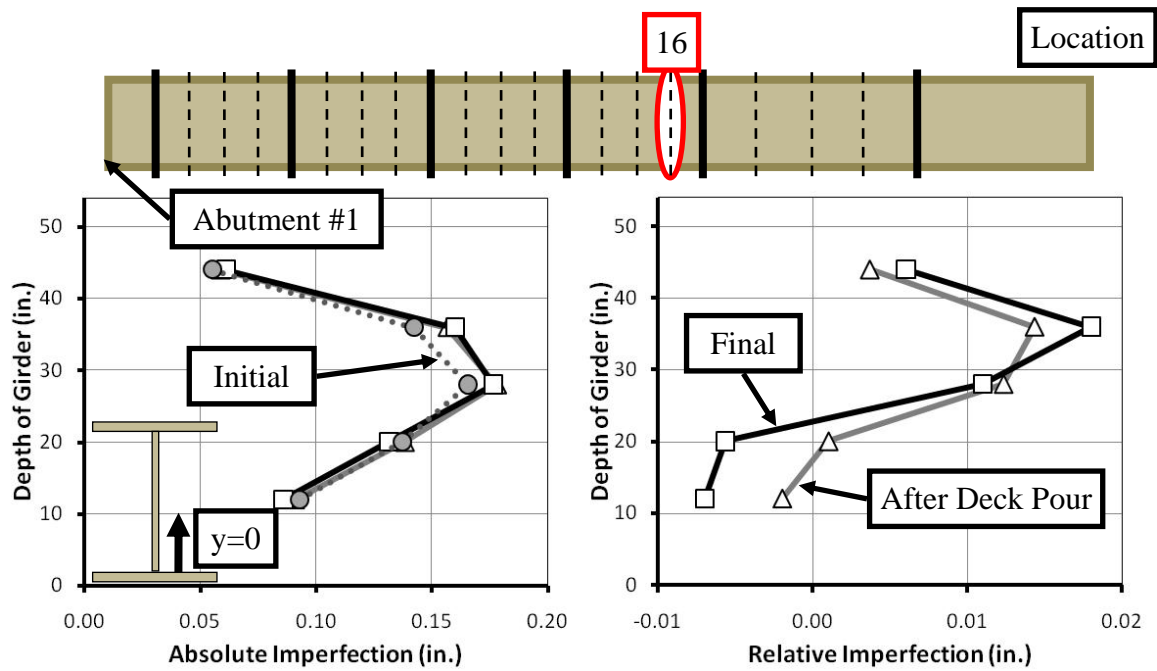
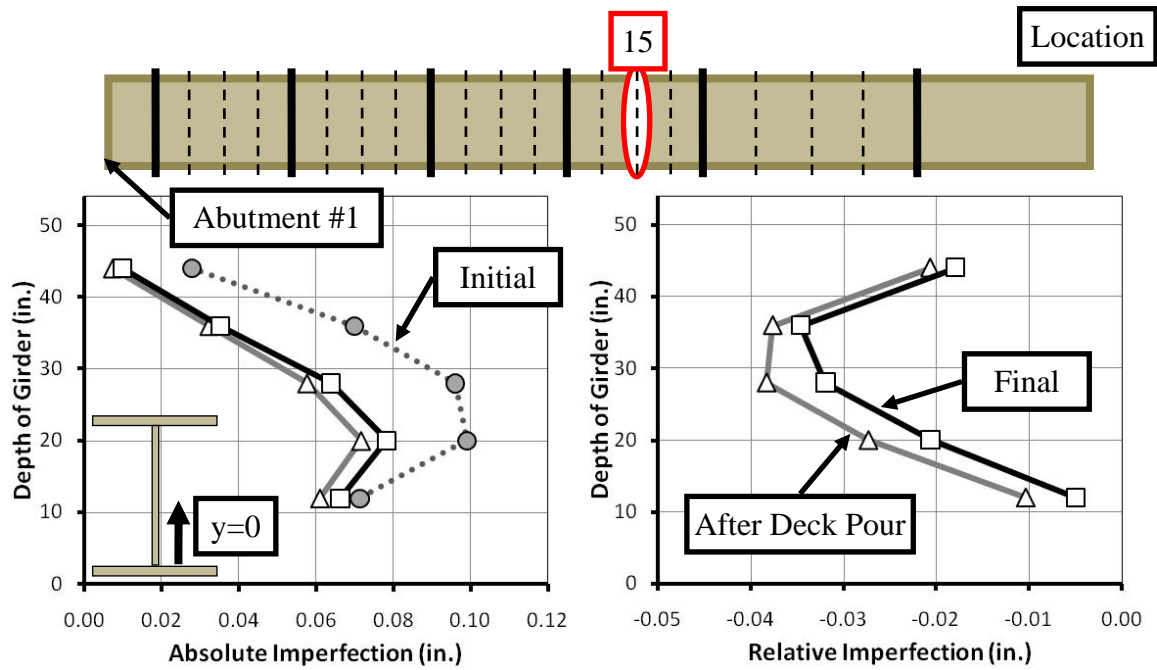


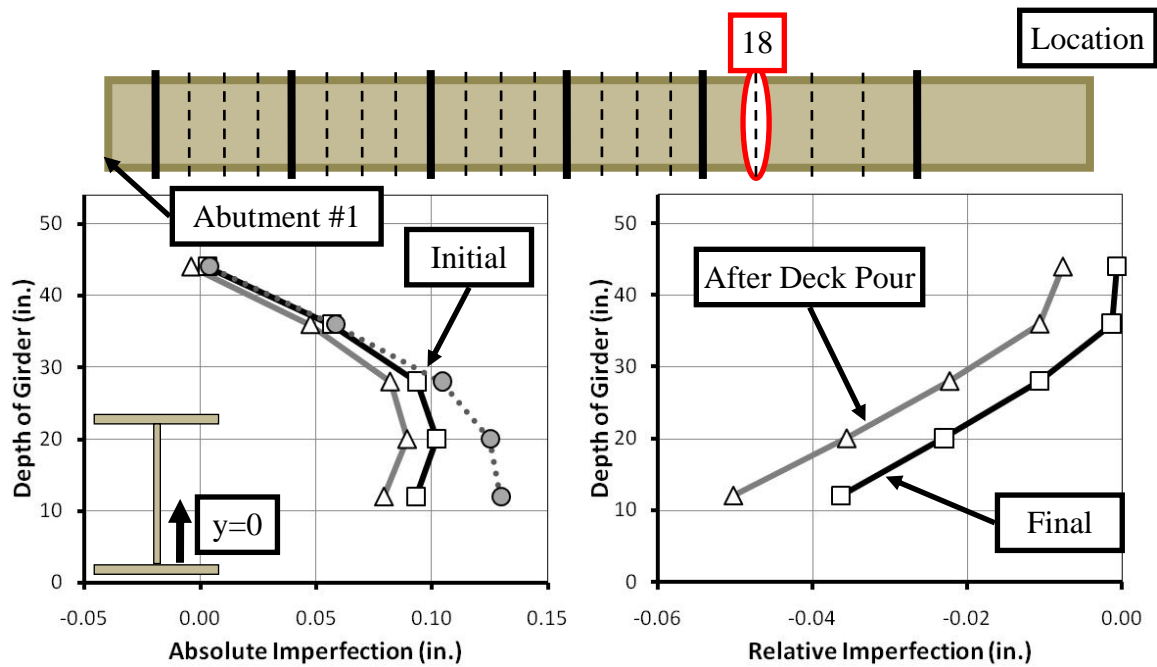
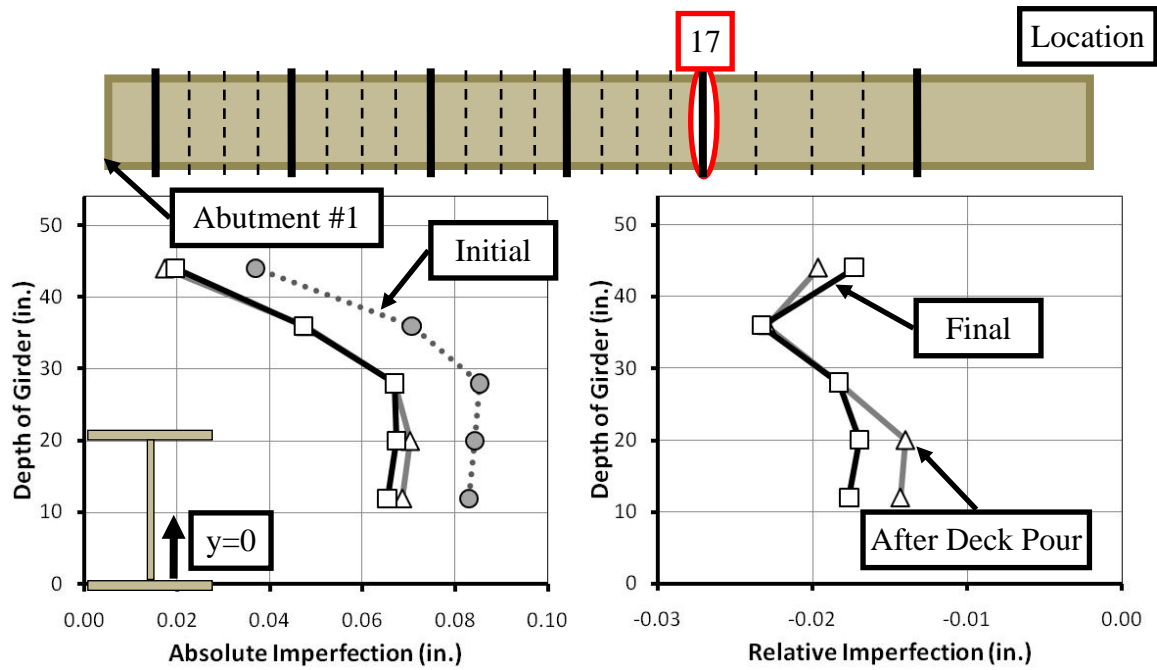


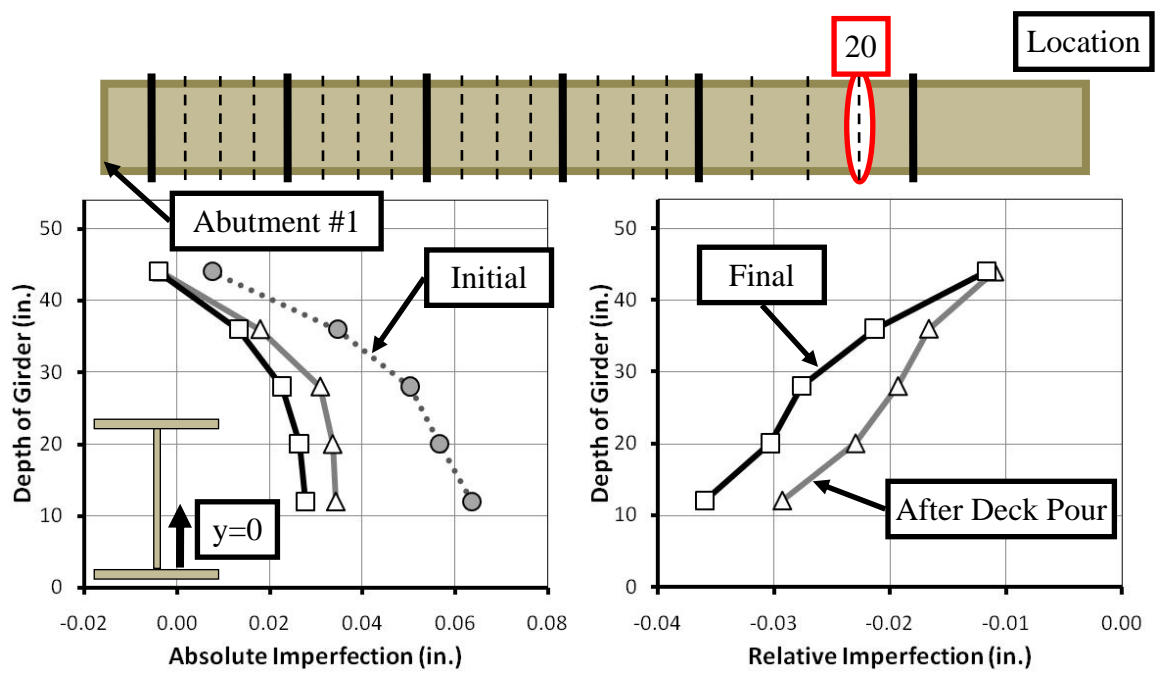
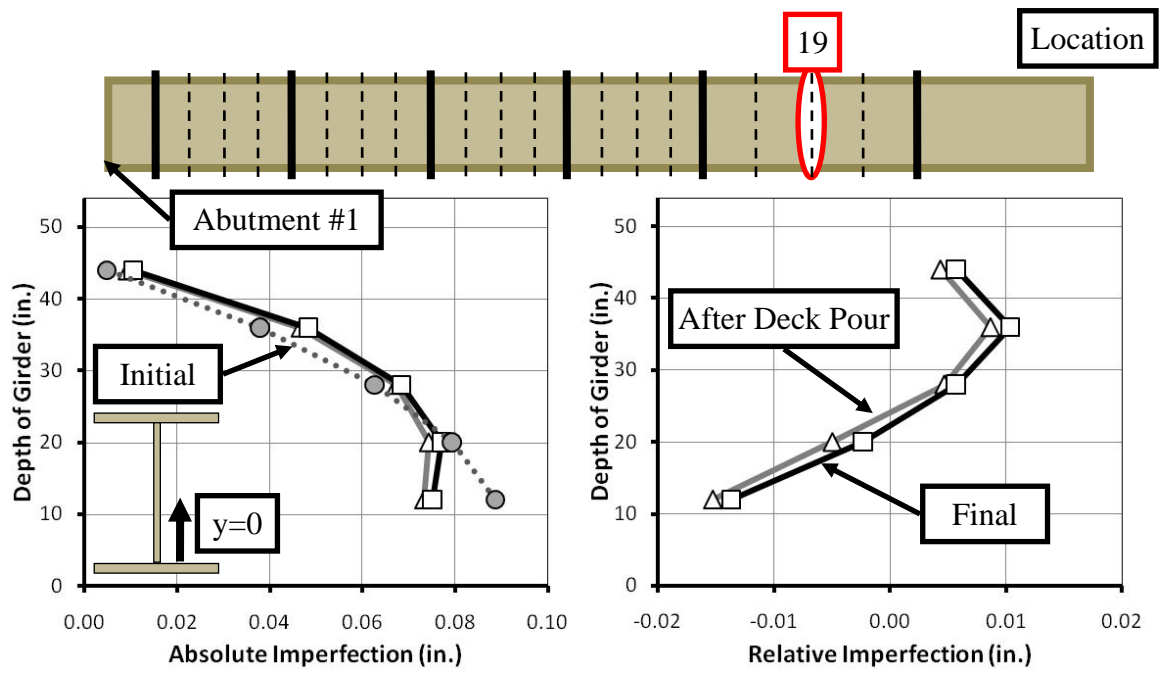


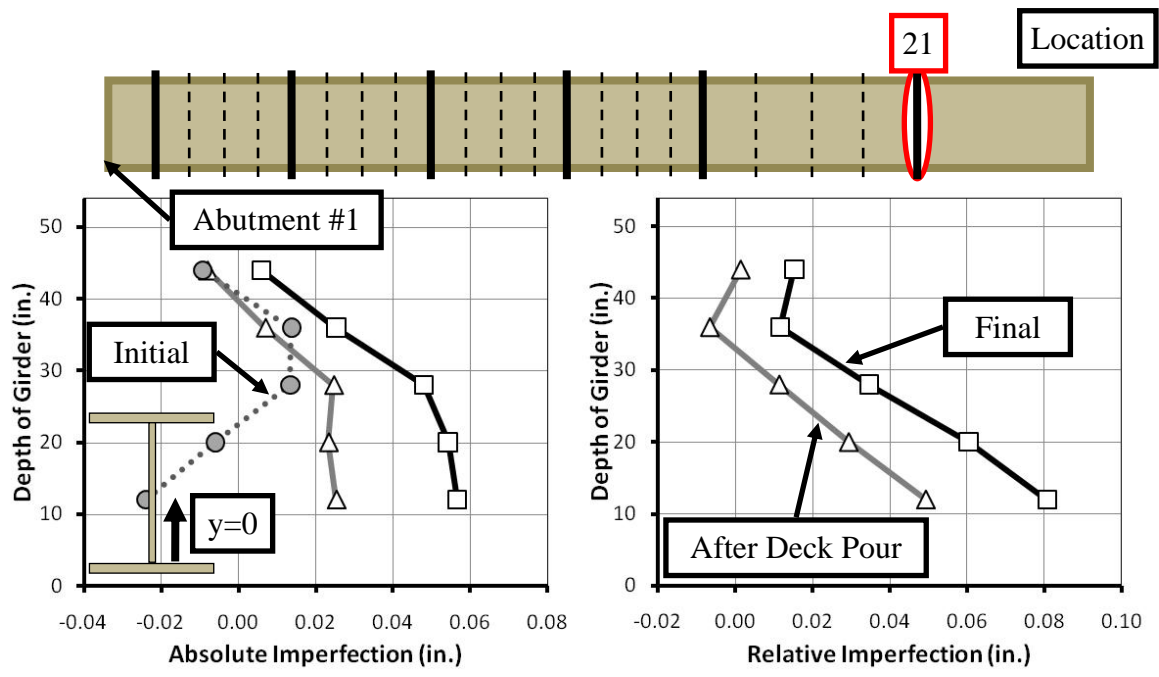






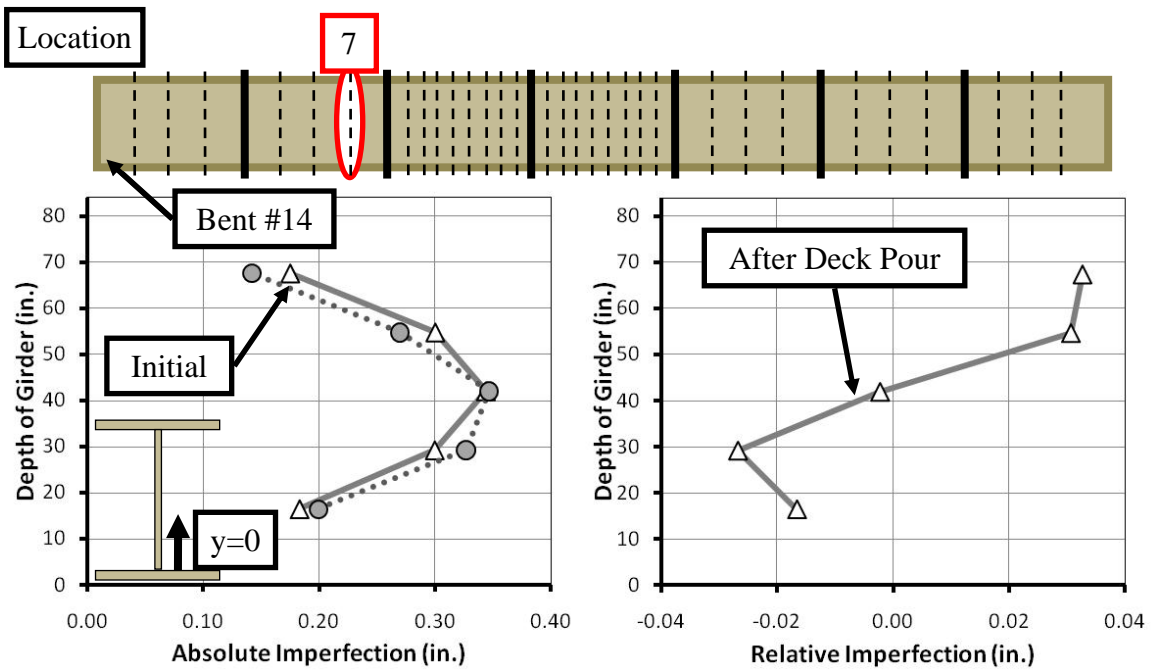
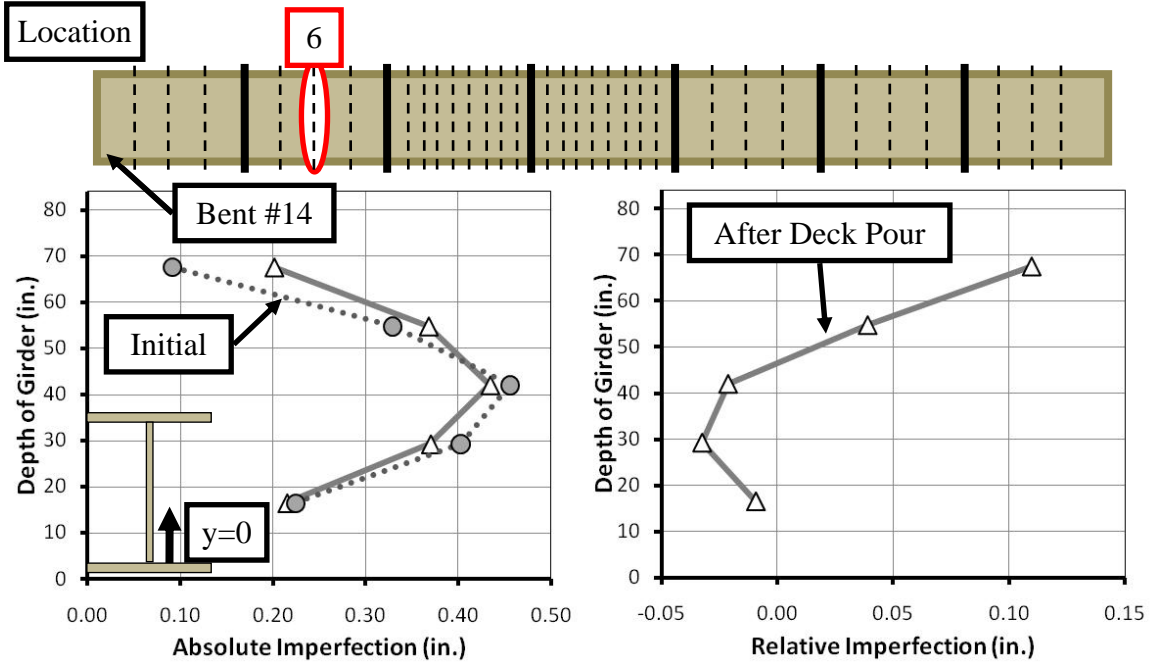


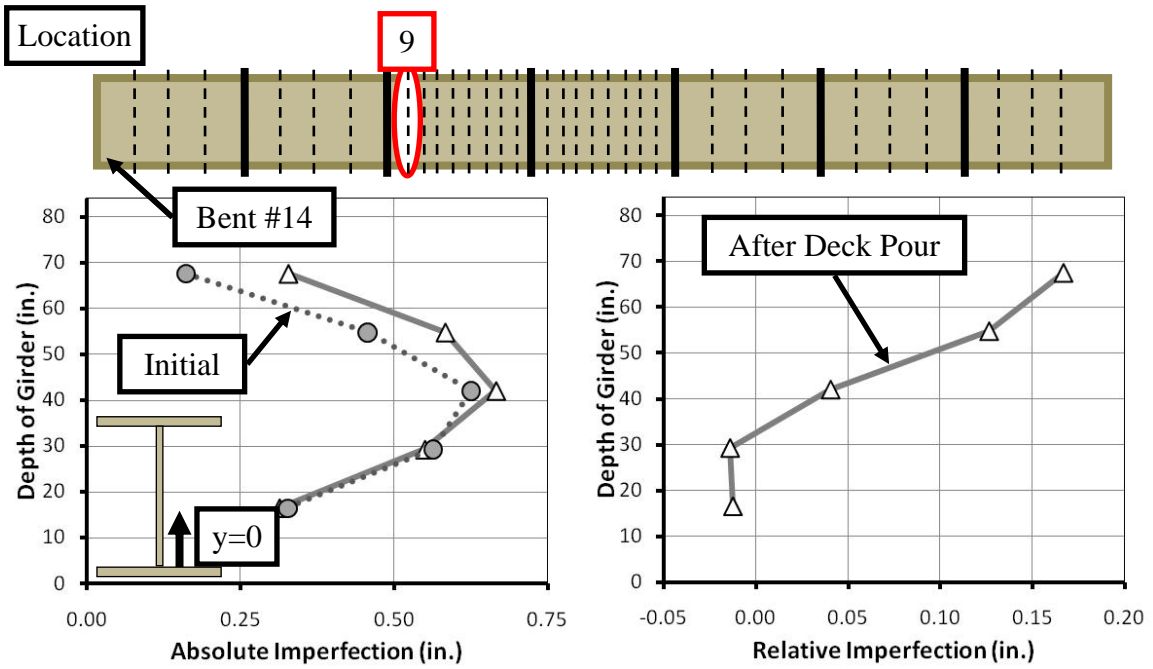
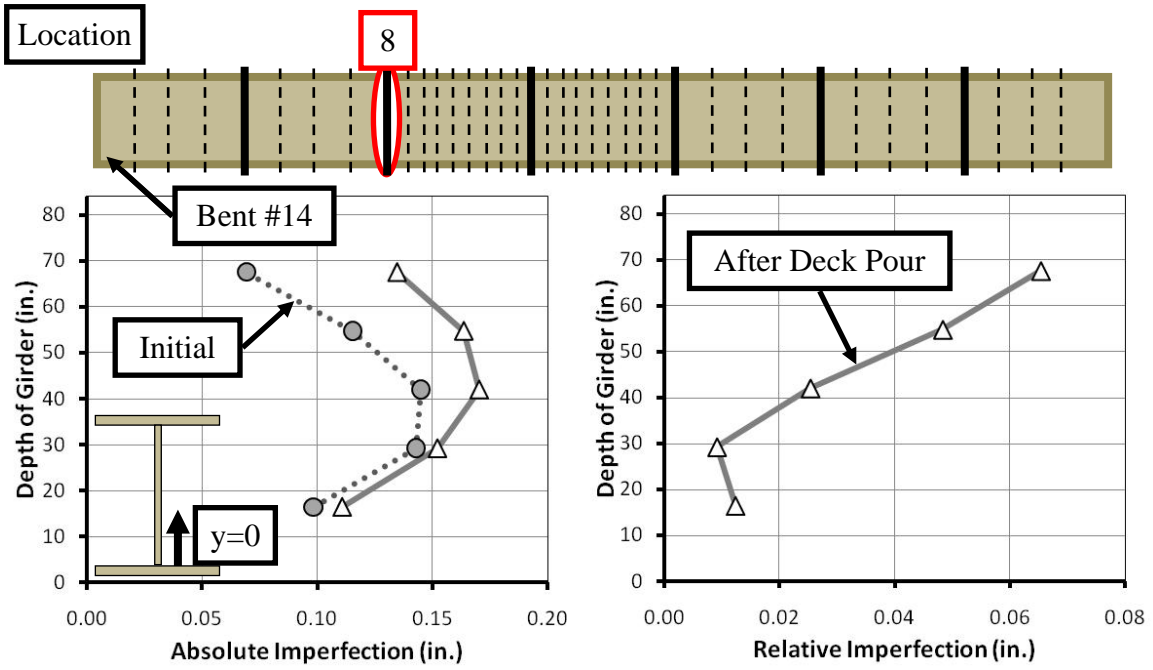


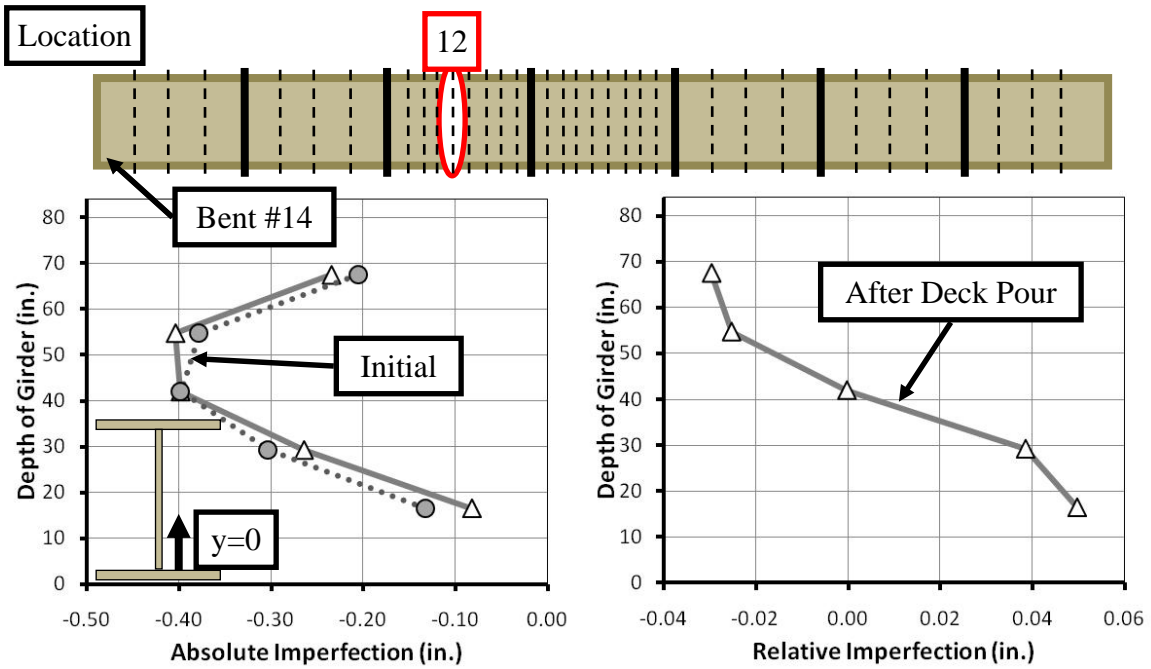
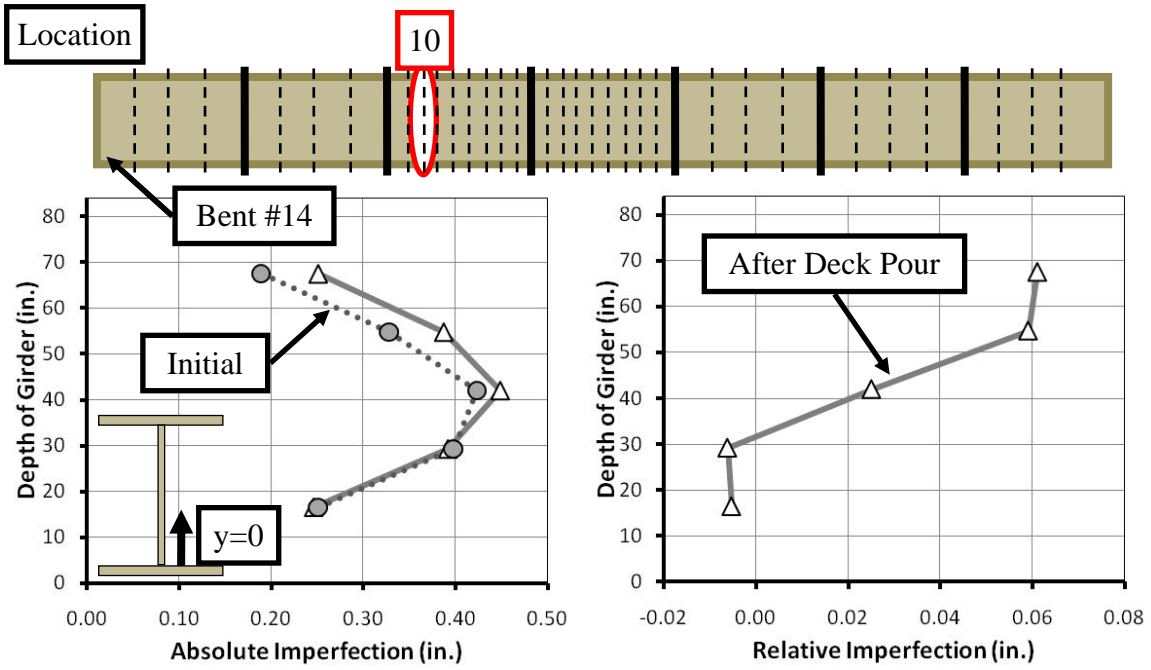


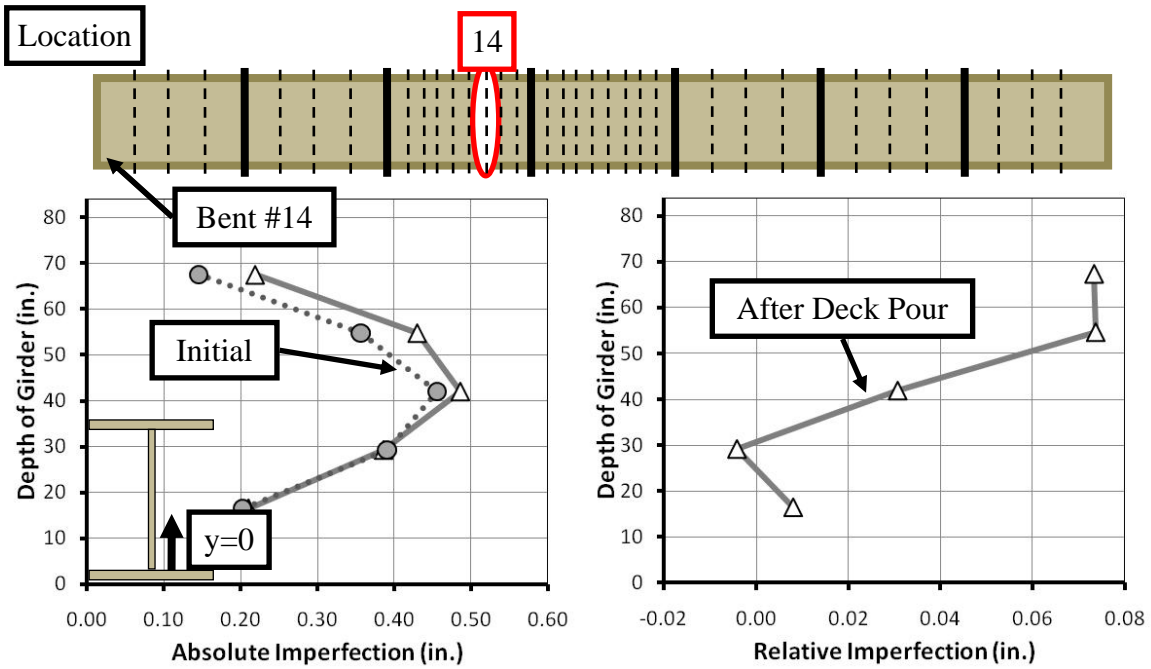
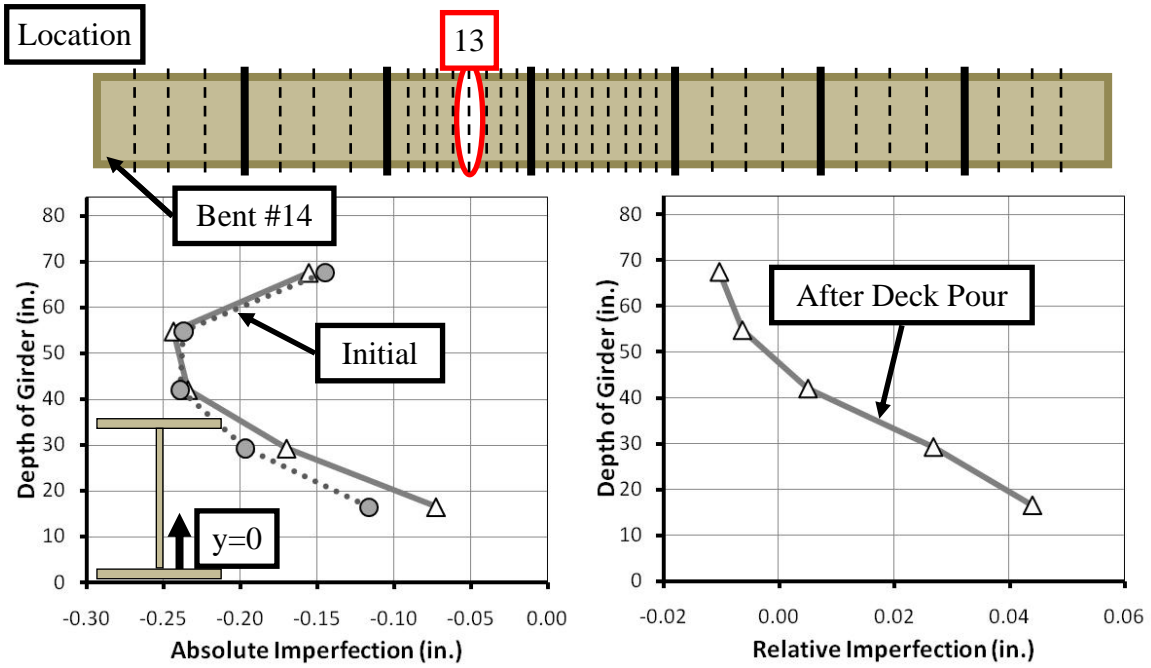
APPENDIX C

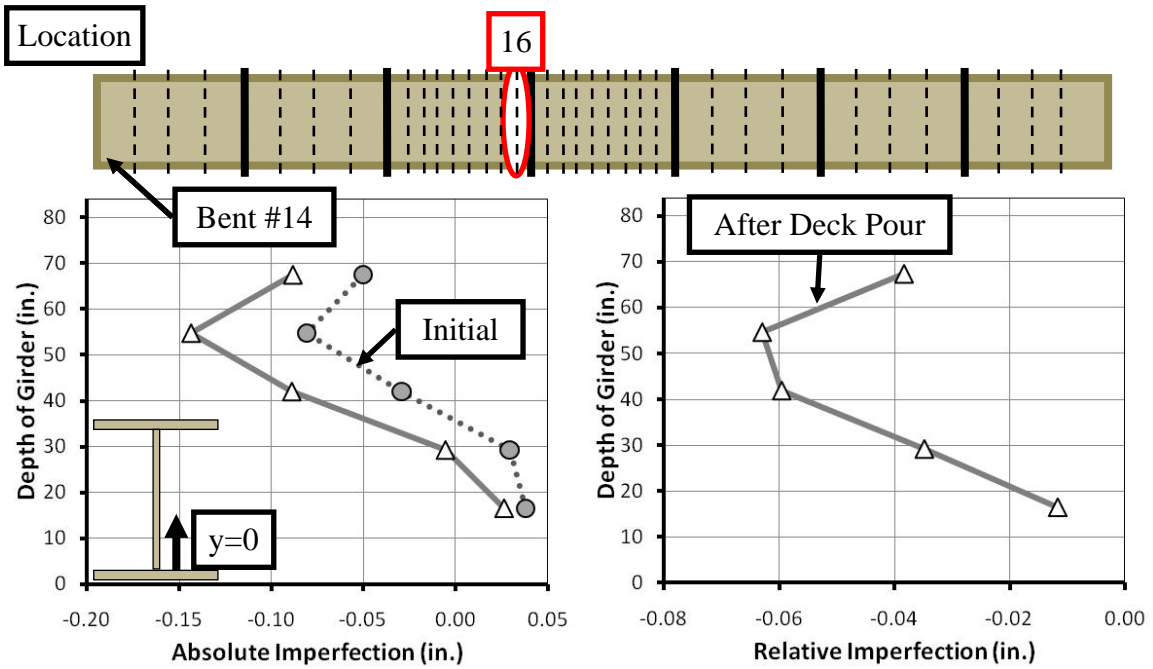
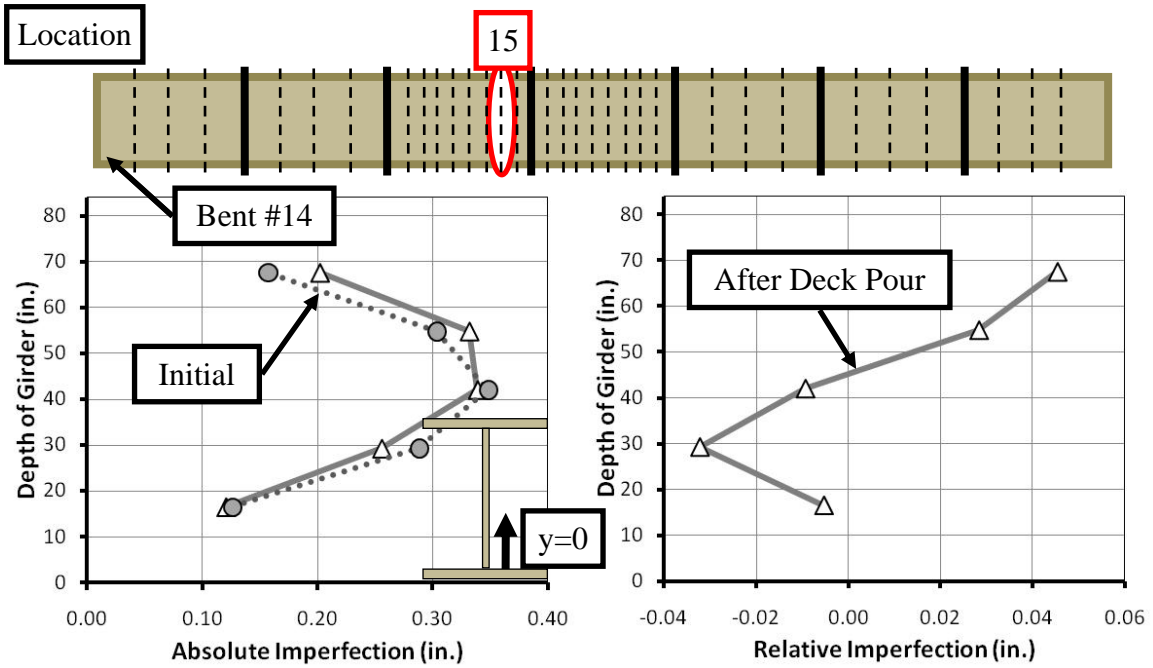
SH 71-SH 130 (Span 14): Fascia Girder

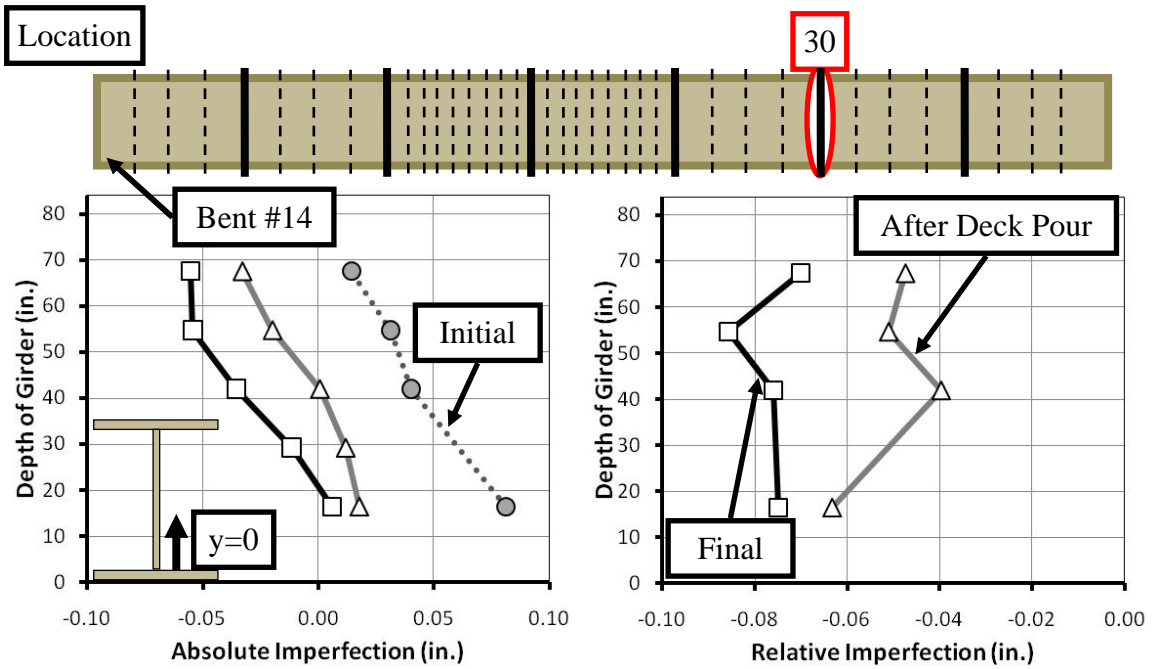
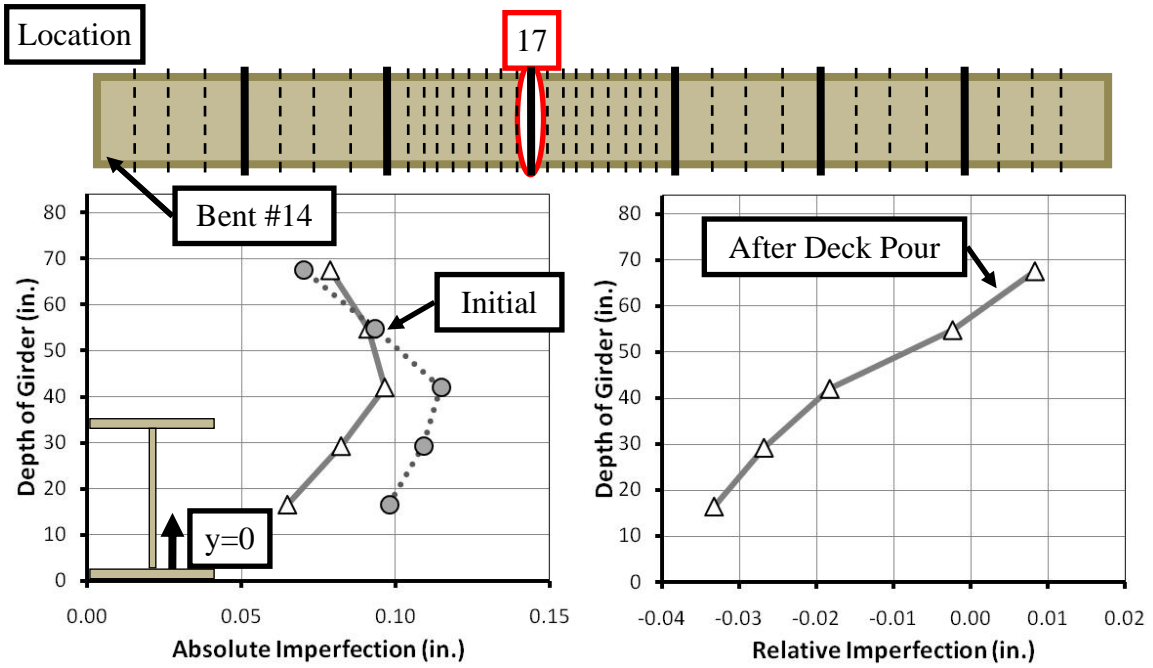


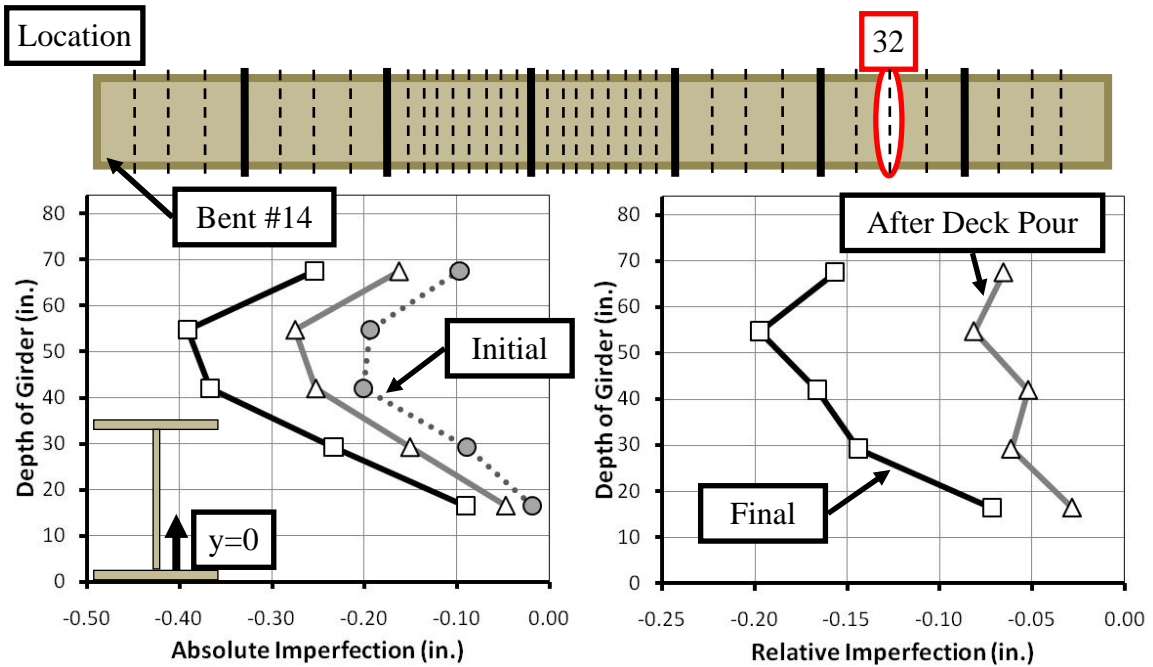
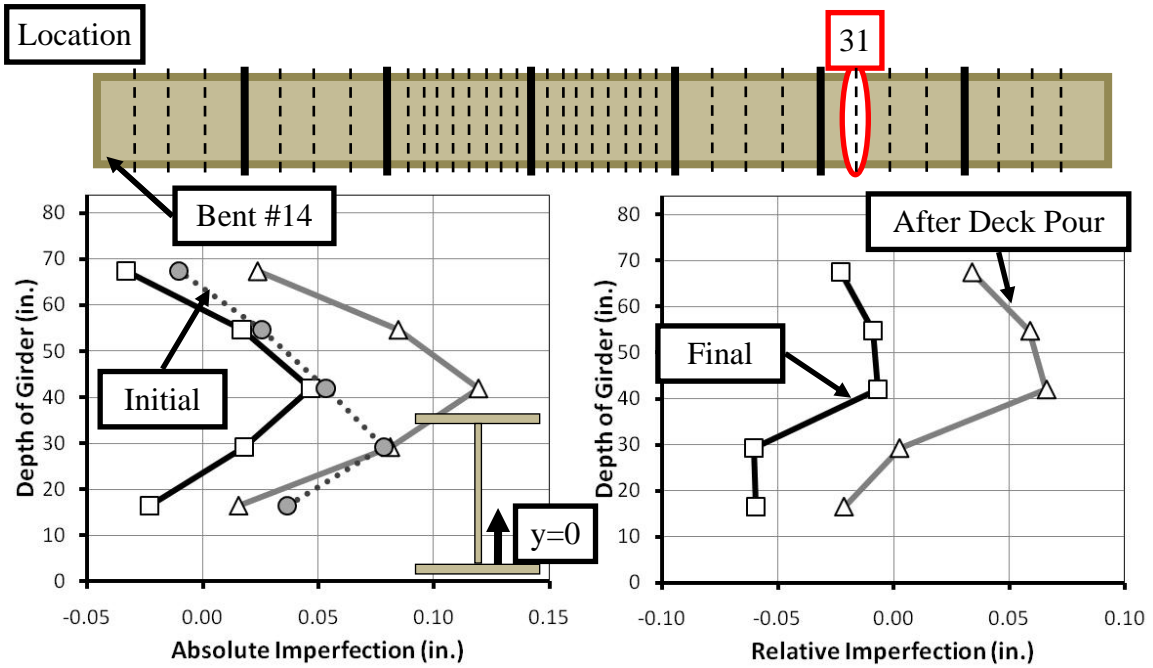


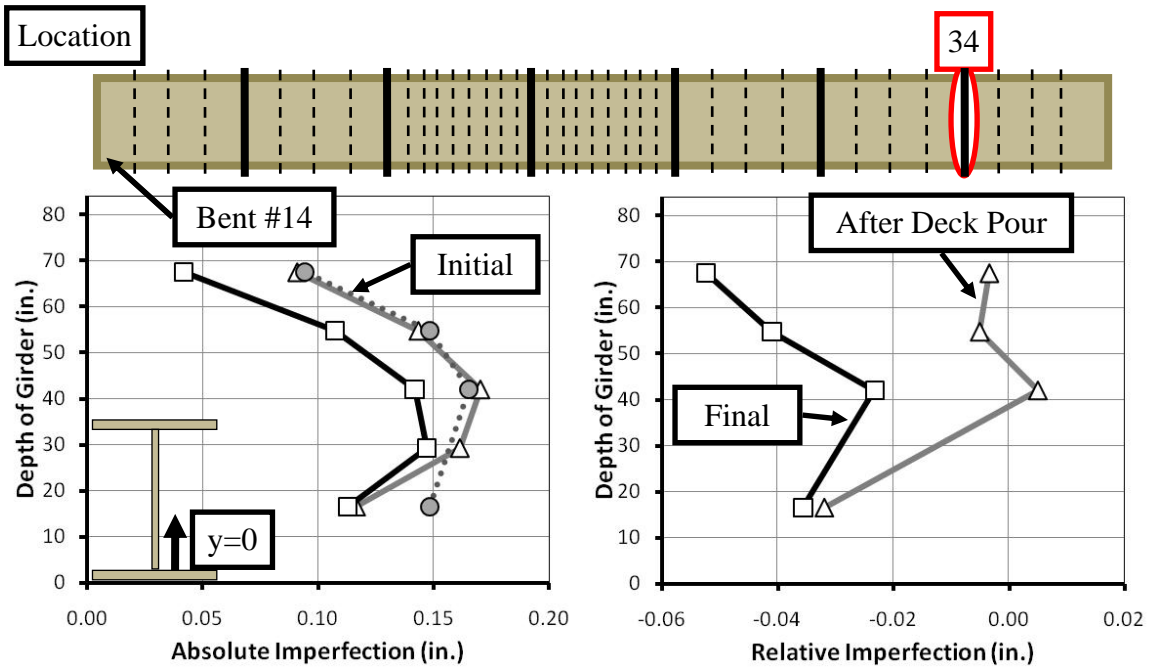
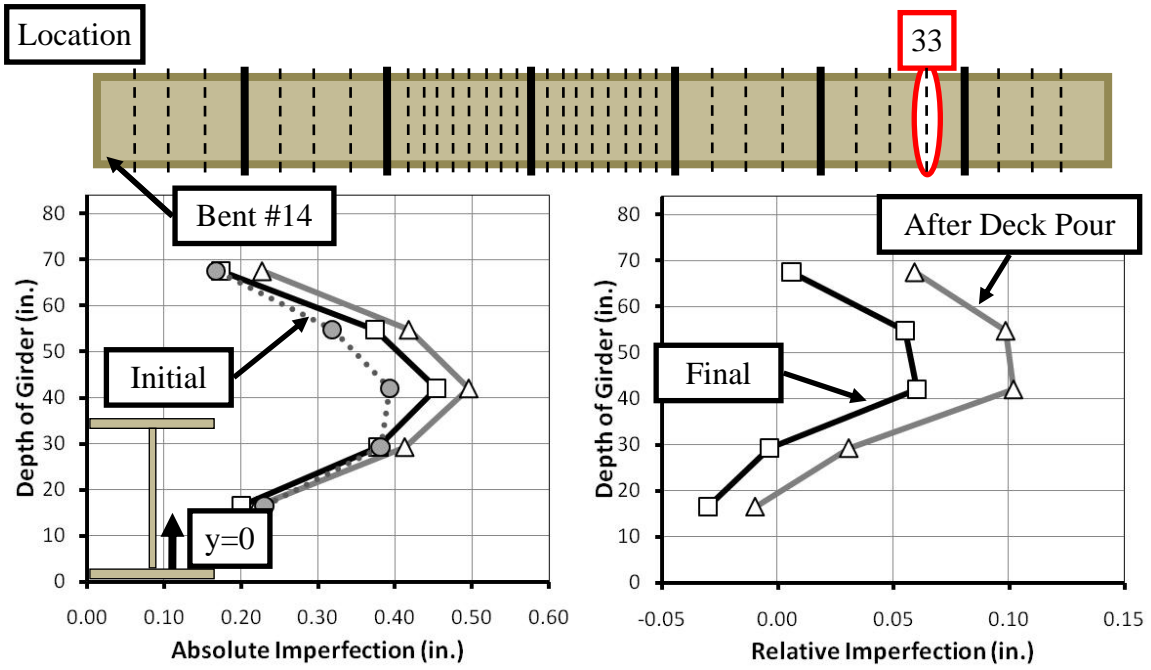






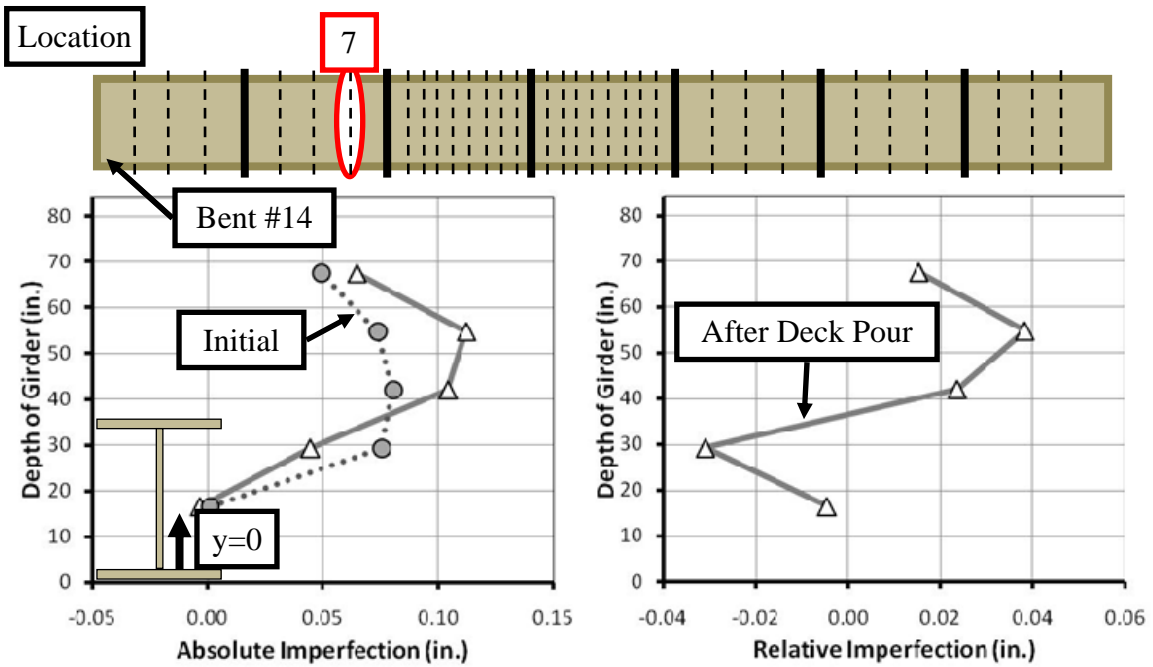
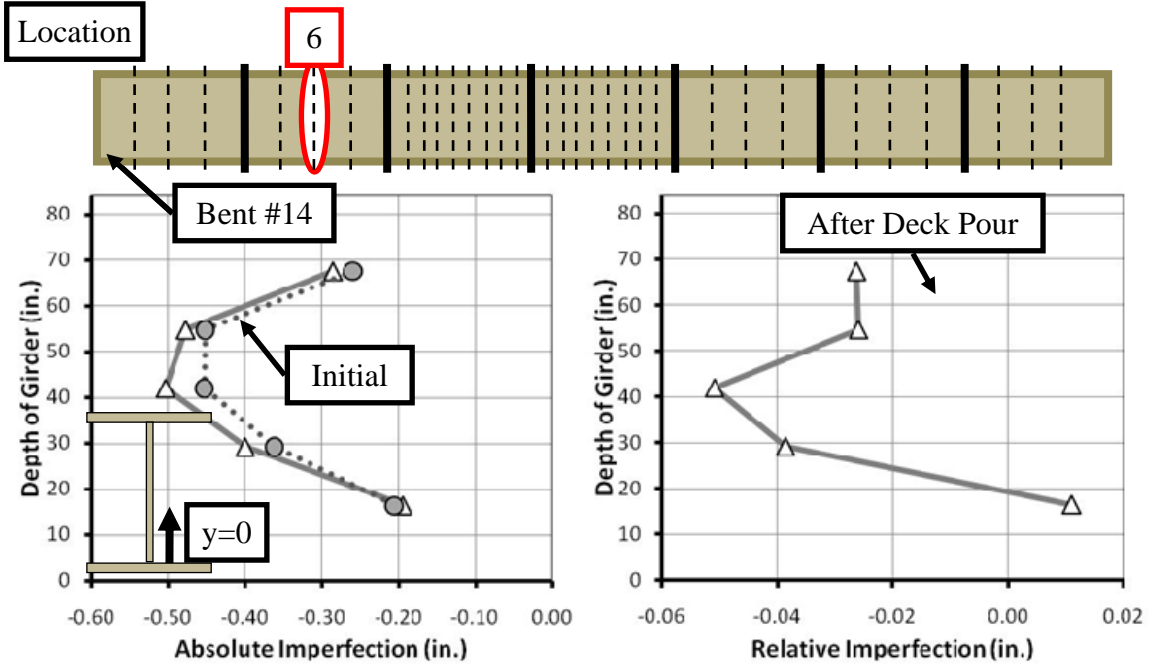


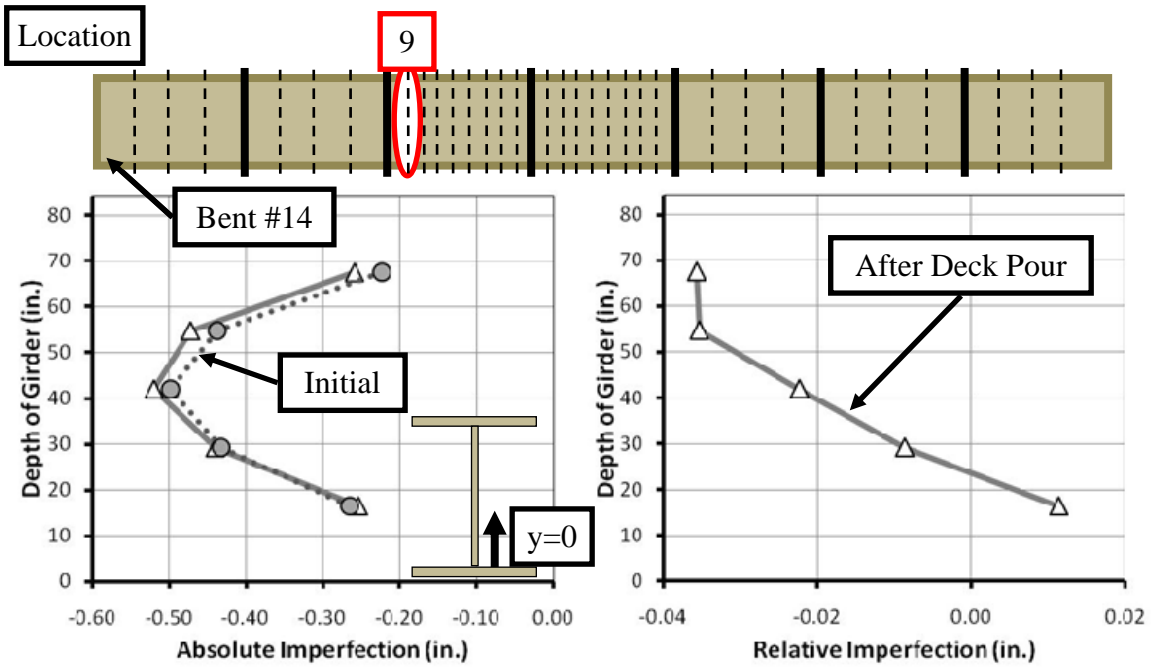
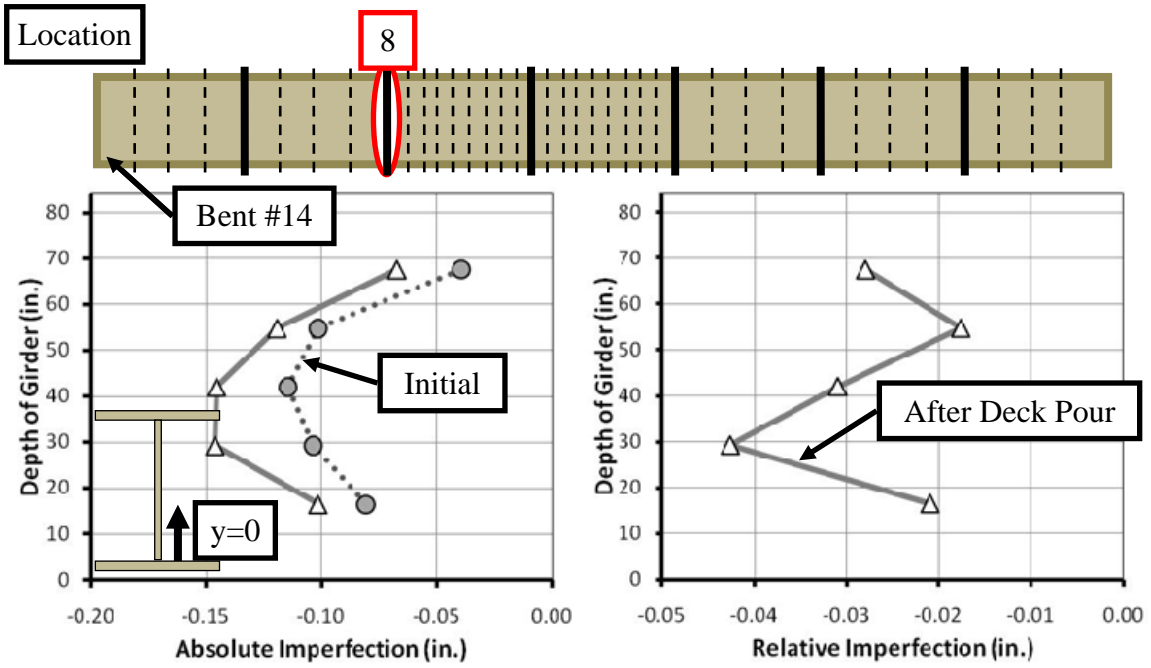


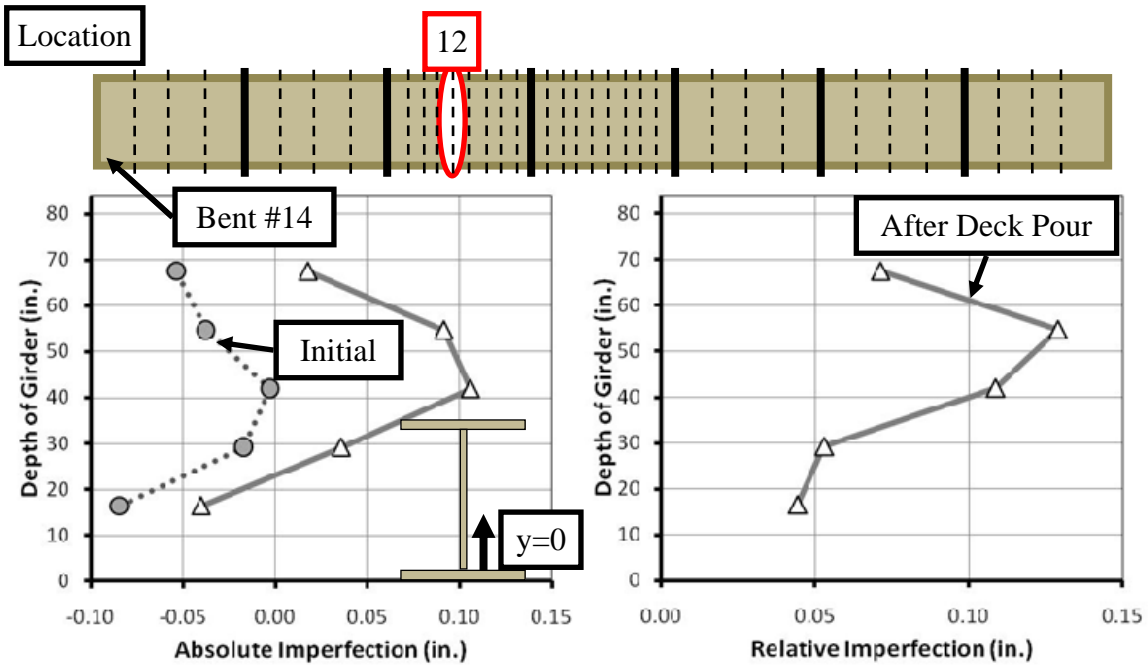
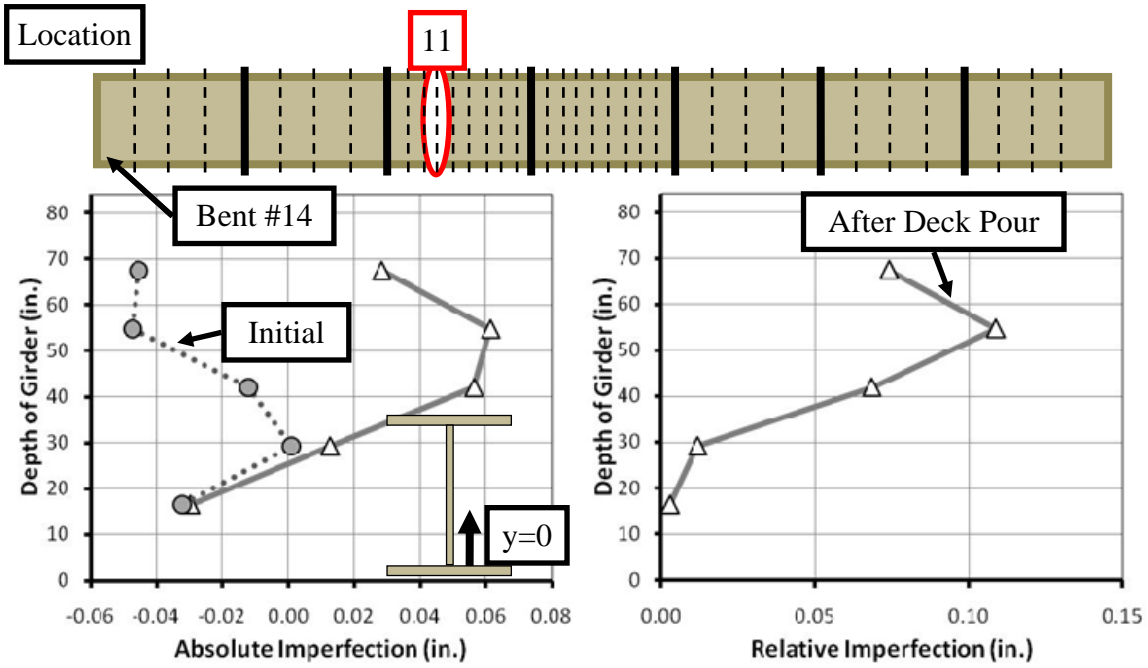


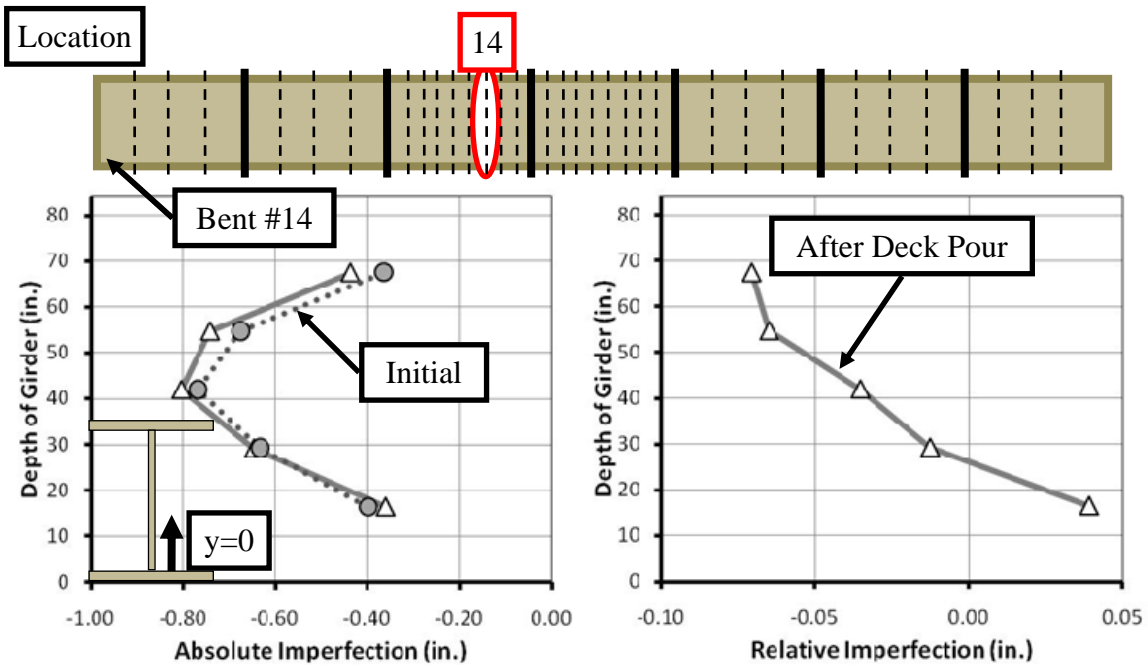
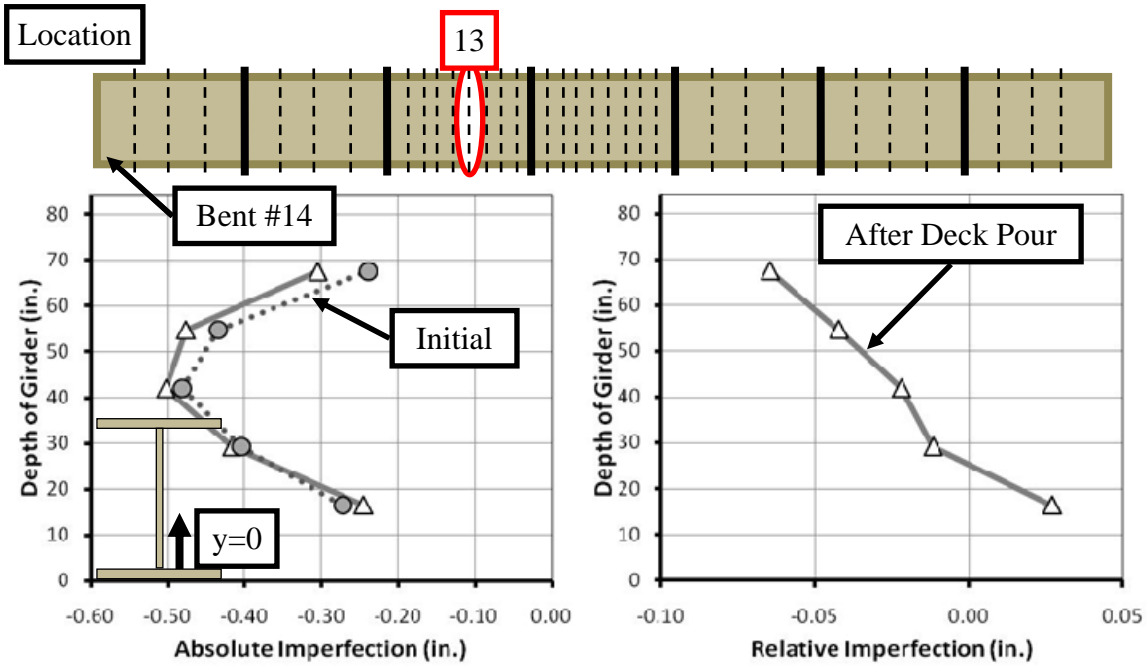
APPENDIX D

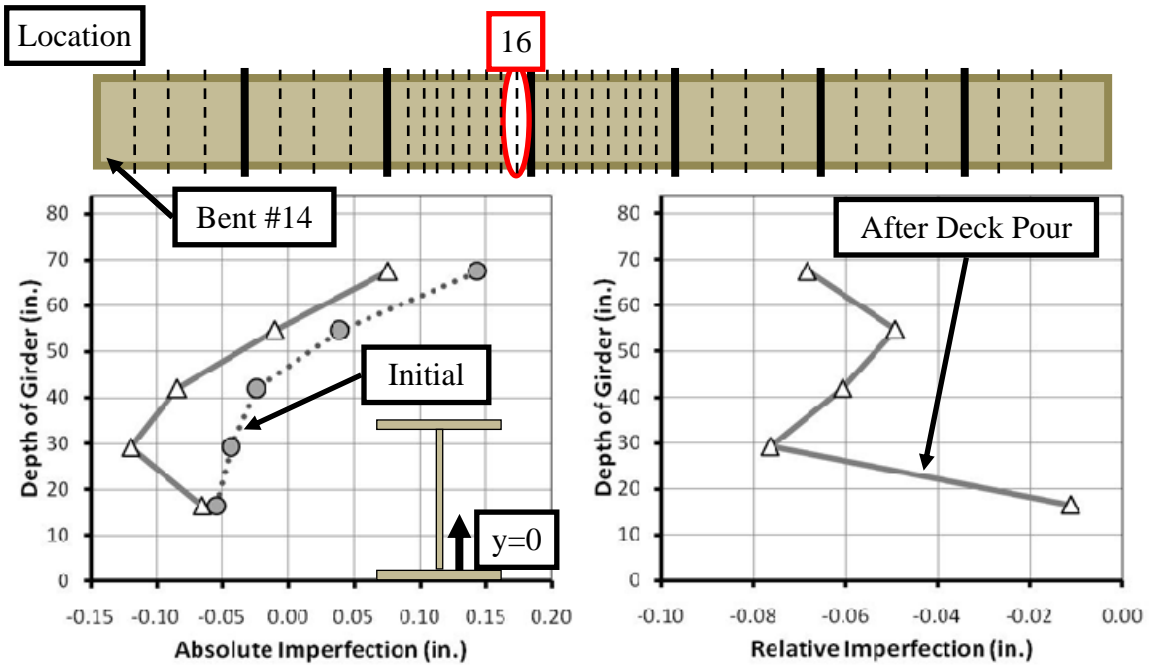
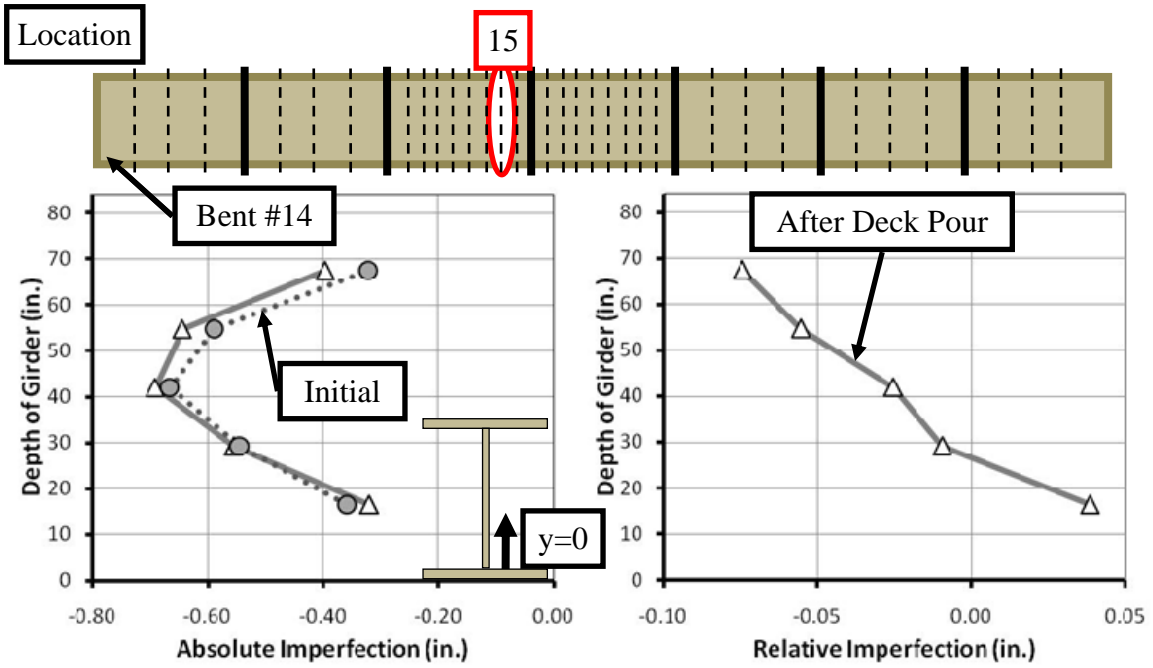
SH 71-SH 130 (Span 14): Interior Girder

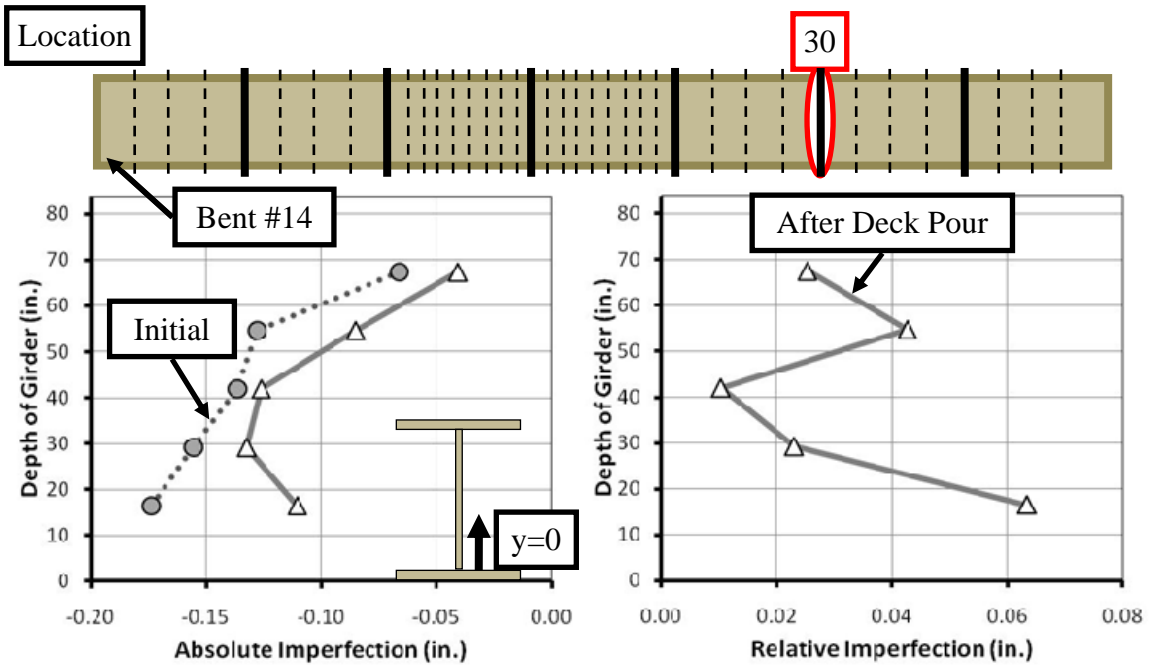
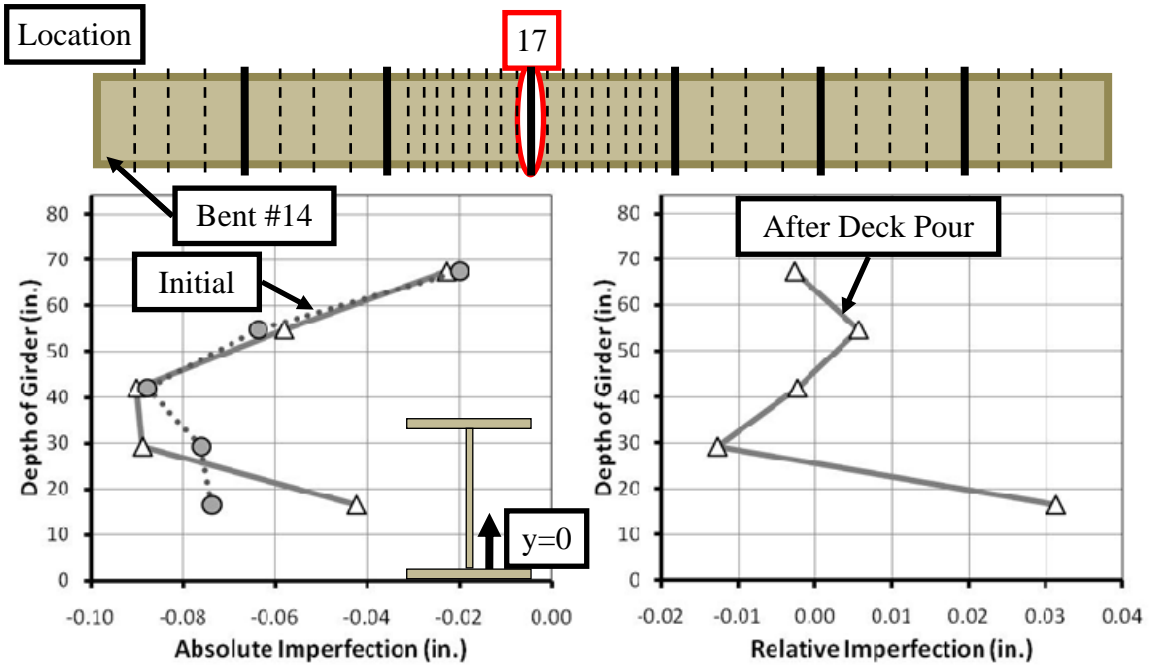


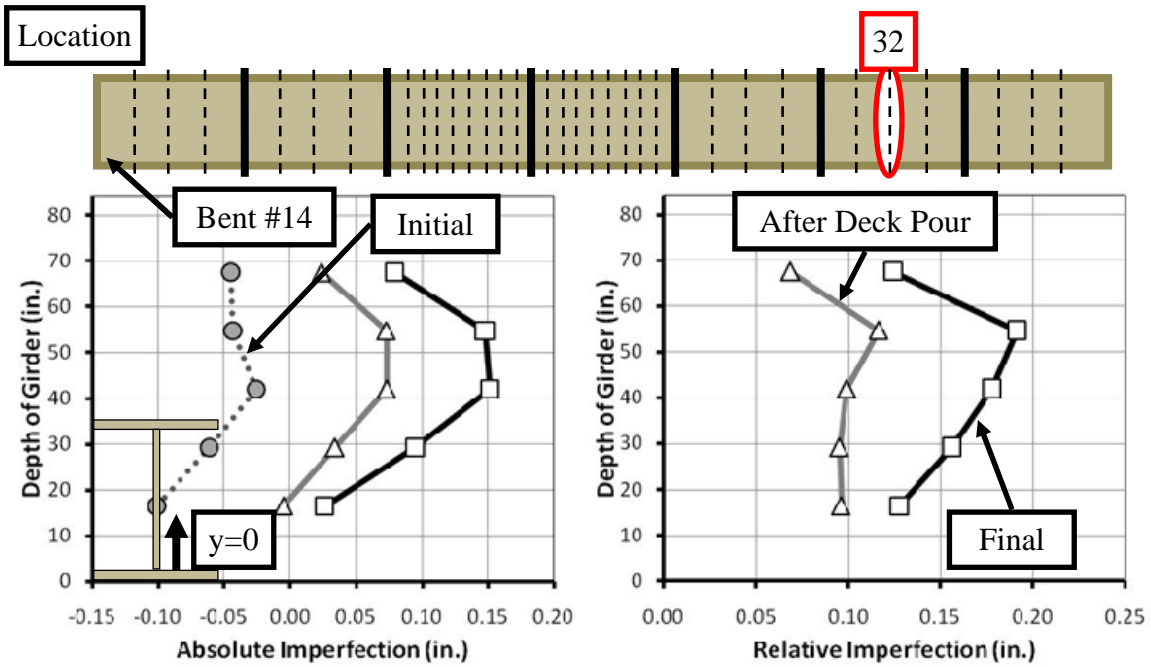
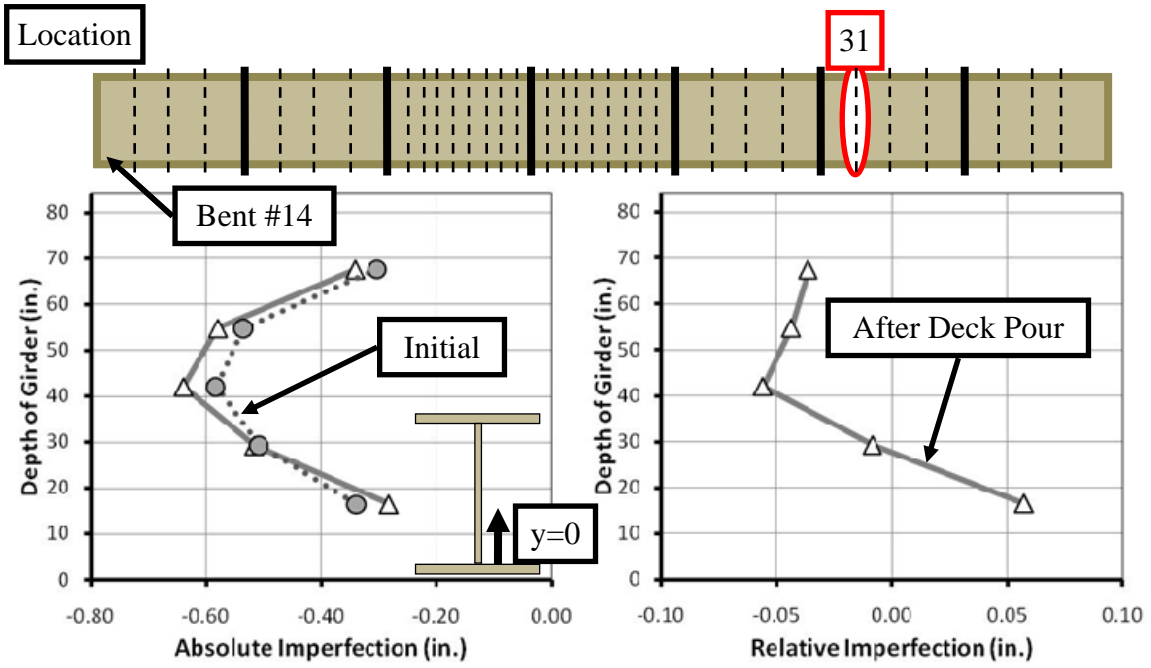


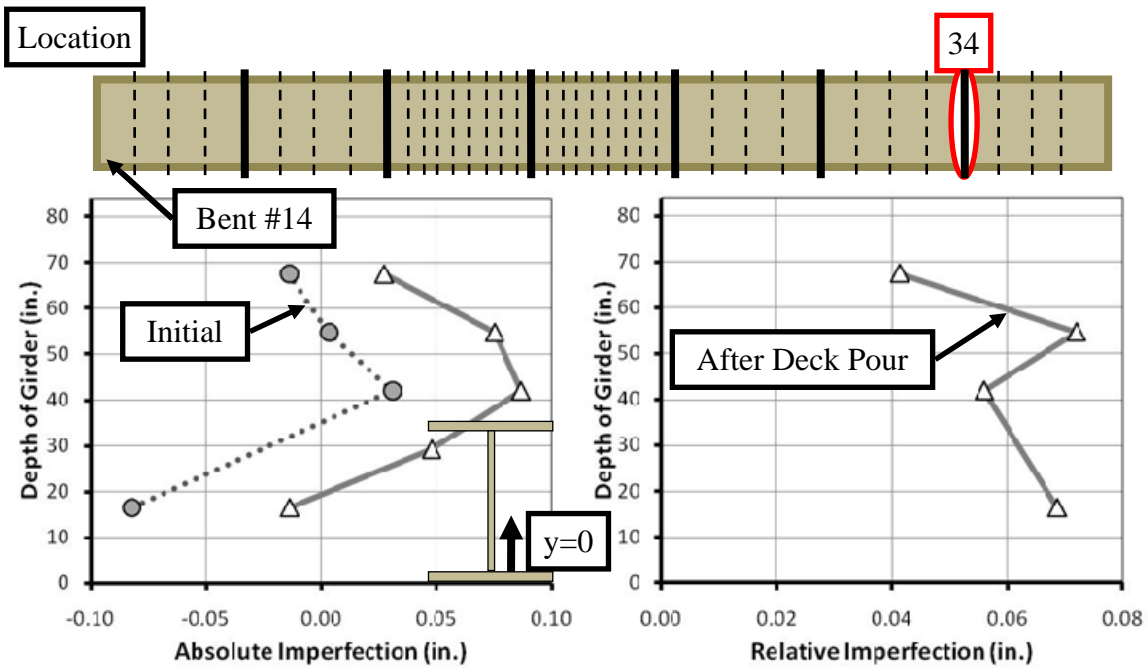
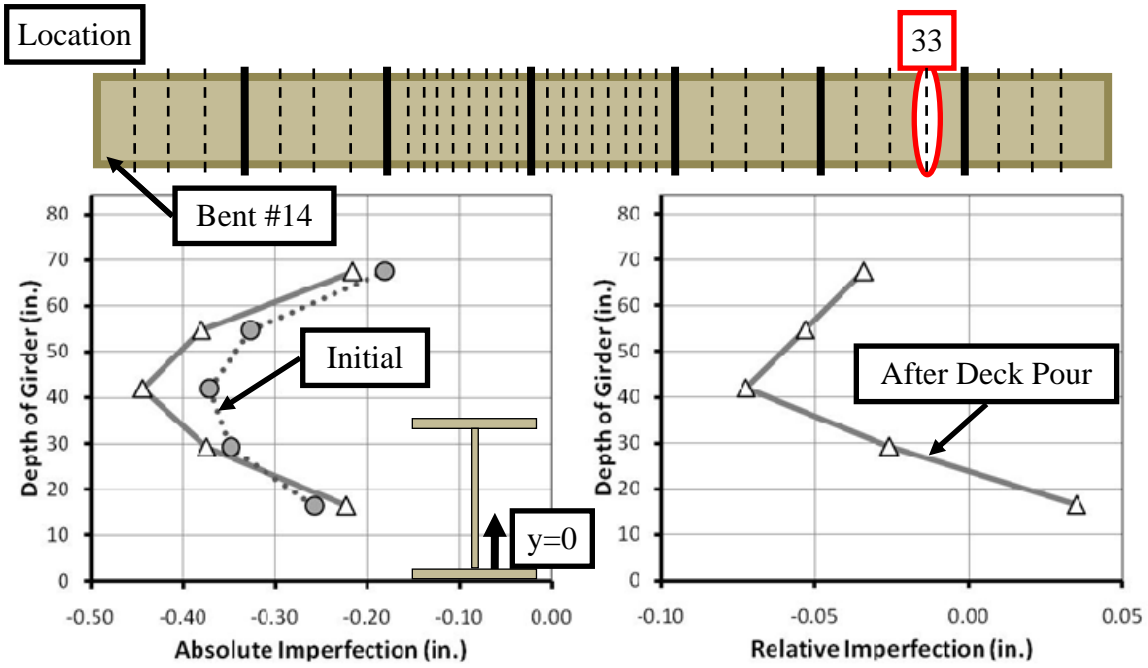












References

- American Welding Society (AWS). (2008). *D1.5M/D1.5 bridge welding code*. American Welding Society and American Association of State Highway and Transportation Officials.
- Ariyasajakorn, D. & Sumner, E. (2006). *Full scale testing of overhang falsework hangers on NCDOT modified bulb tee (MBT) girders*. North Carolina State University, Thesis.
- California Department of Transportation. (2004, February). Bridge design specifications. Retrieved September 19, 2006, from <http://www.dot.ca.gov/hq/esc/techpubs/manual/bridgemanuals/bridge-design-specifications/bds.html>.
- Campbell Scientific, Inc. (2001). *CR5000 measurement and control system operator's manual* (Revision 8/01). Logan, UT.
- Central Texas Turnpike System (CTTS). (2007, September). SH 130 general information. Retrieved June 3, 2007, from <http://www.centraltexasturnpike.org/sh130/>.
- Clifton, S. (2008, May). *Bridge deck overhang construction*. The University of Texas at Austin, Thesis.
- Colorado Department of Transportation. (1991, December). Bridge design manual. Retrieved September 19, 2006, from <http://www.dot.state.co.us/DesignSupport/>.
- Connecticut Department of Transportation. (2003). Bridge design manual (Revision 3/05). Retrieved September 19, 2006, from <http://www.ct.gov/dot/cwp/view.asp?a=1385&q=305506>.
- Crossbow Technology. (2006). CXTLA datasheet. Retrieved November 8, 2006, from: <http://www.xbow.com/>.
- Delaware Department of Transportation. (2005, May). Bridge design manual. Retrieved September 19, 2006, from http://www.deldot.gov/information/pubs_forms/.
- Florida Department of Transportation. (2008, January). Structures Manual, Volume 1. Retrieved August 06, 2008, from <http://www.dot.state.fl.us/structures/>.
- Grubb, M. (1990, June). *Design for concrete deck overhang loads* (Final Report). AISC Marketing INC.

- Illia, T. (2007, August 10). Arizona highway bridge falls during construction. *Engineering News-Record*. Retrieved August 20, 2007 from: <http://enr.construction.com/news/transportation/archives/070810.asp>.
- Kansas Department of Transportation. (2006, June). Bridge manual. Retrieved September 19, 2006, from <http://www.ksdot.org/burDesign/bridge/constructionmanual/bcm.asp>.
- Maine Department of Transportation. (2003, August). Bridge design manual. Retrieved September 19, 2006, from <http://www.maine.gov/mdot/technical-publications/brdesignguide.php>.
- Mercan, B. (2005, August). *Field measurements of plate imperfections in steel box girders*. University of Houston, Thesis.
- Michigan Department of Transportation. (2001). Bridge design guide. Retrieved September 16, 2006, from <http://mdotwas1.mdot.state.mi.us/public/design/englishbridgeguides/>.
- Montana Department of Transportation. (2002, August). Montana structures manual. Retrieved September 16, 2006, from <http://www.mdt.mt.gov/publications/manuals.shtml>.
- National Steel Bridge Alliance (NSBA). (2006). *Chapter 8: Stringer bridges – Making the right choices*. Steel Bridge Design Handbook.
- Nebraska Department of Roads. (2006). Bridge operations, policies & procedures. Retrieved September 16, 2006, from <http://www.dor.state.ne.us/design/bridge/>.
- Nevada Department of Transportation. (2001). Standard specifications for road and bridge construction. Retrieved September 16, 2006, from <http://www.nevadadot.com/business/contractor/Standards/>.
- New York State Department of Transportation. (2008, January). Bridge manual – US customary. Retrieved August 5, 2008, from <https://www.nysdot.gov/portal/page/portal/divisions/engineering/structures/manuals>.
- Ohio Department of Transportation. (2004). Bridge design manual. Retrieved September 16, 2006, from <http://www.dot.state.oh.us/Divisions/HighwayOps/Structures/standard/Bridge/Pages/BDM2004.aspx>.
- Oregon Department of Transportation. (2004). Bridge design & drafting manual. Retrieved September 16, 2006, from http://www.oregon.gov/ODOT/HWY/BRIDGE/standards_manuals.shtml.

- Roddis, K., Kriesten, M., & Liu, Z. (1999, April). *Torsional analysis for exterior girders*. The University of Kansas.
- Roddis, K., Kulseth, P., & Liu, Z. (2005, April 26). *TAEK 2.0*. The University of Kansas.
- Schuh, A. (2008, May). *Behavior of horizontally curved steel I-girders during lifting*. The University of Texas at Austin, Thesis.
- South Carolina Department of Transportation. (2006, April). Bridge design manual. Retrieved September 16, 2006, from http://www.scdot.org/doing/bridge/06design_manual.shtml.
- Texas Department of Transportation. (2001, December). Bridge design manual. Retrieved September 16, 2006, from <http://onlinemanuals.txdot.gov/txdotmanuals/des/index.htm>.
- Tremblay, R. & Mitchell, D. (2006, May). Collapse during construction of a precast girder bridge. *ASCE Journal of Performance of Constructed Facilities*. Vol. 20, No. 2, 113-125.
- Wang, L. & Helwig, T. (2005, June). Critical imperfections for beam bracing systems. *ASCE Journal of Structural Engineering*. Vol. 131, No. 6, 933-940.
- West Virginia Department of Transportation. (2004). Bridge design manual. Retrieved September 16, 2006, from http://www.wvdot.com/engineering/TOC_engineering.htm.
- Yura, J., Helwig, T., Herman, R., & Zhou, C. (2008, September). Global lateral buckling of I-shaped girder systems. *ASCE Journal of Structural Engineering*. Vol. 134, No. 9, To be published.

Vita

Jeremiah David Fasl, son of John and Kathy Fasl, was born in Kansas City, Missouri on May 20, 1984. Moving to Austin in 1992, he was homeschooled from second grade through high school and graduated in May 2002. He enrolled at The University of Texas at Austin in August 2002 and graduated with a Bachelor of Science in Civil Engineering in May 2006 with High Honors. Starting graduate school in August 2006, he worked as a research assistant at the Phil M. Ferguson Structural Engineering Laboratory. After graduating with a Master of Science degree, Jeremiah plans to continue at The University of Texas for a doctorate degree.

Permanent Address: 5713 Abilene Trail
Austin, TX 78749

This document was typed by the author.